PETROGENESIS OF HIGH-Mg ANDESITES

An experimental and geochemical study
with emphasis on high-Mg andesites
from Cape Vogel, PNG.

by

George Albert Jenner, B.Sc.(Hons.), M.Sc.

Submitted in fulfilment of the requirements
for the degree of Doctor of Philosophy.

University of Tasmania
HOBART

1982

(Conferred March 1983)

This thesis contains no material which has been accepted for the award of any other degree or diploma in any university, and to the best of my knowledge and belief, contains no copy or paraphrase of material previously published or written by another person, except where due reference is made in the text of this thesis.

G. A. Jenner

University of Tasmania
January, 1982.

CONTENTS

Contents cont.

Contents cont.

List of Figures

Contents cont.

List of Tables

Contents cont.

ABSTRACT

A detailed petrographic, geochemical and experimental study has been undertaken on selected high-Mg andesites from Cape Vogel, PNG, the Bonin Islands and the Mariana Trench. These rocks are chemically and mineralogically unusual; however, they are important to our understanding of the Earth's mantle since they represent primary magmas, and occur within an island-arc environment.

Mineralogically these volcanic rocks are characterized by very magnesian orthopyroxene (and/or clinoenstatite) (Mg_{80-92}), clinopyroxene, magnesian and chrome-rich spinel, and occasionally olivine (Mg_{85-92}). Petrographic and chemical criteria show that orthopyroxene is the major fractionating phase.

Comparison of pyroxene phenocryst composition with host magma composition demonstrates an extremely sensitive and regular relation. The occurrence of protoenstatite (now clinoenstatite) is limited to low pressures by the sensitivity of the pyroxene compositions to Ca-content of the melt (normative Di/Di+Hy) and the position of the appropriate orthoenstatite to protoenstatite inversion reaction.

Experimental studies were undertaken on selected compositions in the Mg-rich corner of the pyroxene quadrilateral. These studies were done in the hope that if the effects of Fe/Mg substitution and of $CaMgSi_2O_6$ solid solution on the protoenstatite to orthoenstatite inversion were more fully known it might be possible to limit the extrusion temperatures of clinoenstatite-bearing lavas. These studies did not closely constrain the conditions of origin of the high-Mg andesites, because the major determinant of protoenstatite appearance was found to be magma composition rather than magma temperature. The results of this study clarify our understanding of the pyroxene stability relations at low pressure. In particular, the demonstration that there is a high temperature stability field of orthoenstatite denies the existence of a stable invariant

point defined by the reactions OE ⇄ PE + DI, PE + DI ⇄ PI and OE + DI ⇄ PI, in the system $CaMgSi_2O_6$-$Mg_2Si_2O_6$. New phase relations, consistent with the experimental findings of this and other studies, for the Mg-rich corner of the pyroxene quadrilateral are presented.

Combination of experimental liquidus studies on high-Mg andesites and the controls on the occurrence of protoenstatite and olivine suggest conditions of origin of T > 1200°C and P < 5-10 kb. Water is essential to derive these melts from a peridotite source but the earlier view that water-saturated or near-saturated melting of peridotite is necessary is inconsistent with the observed mineralogy and results of the experimental studies.

Typically the high-Mg andesites (HMA) have SiO_2 ~ 56-58%, MgO ~ 11-16%, CaO/Al_2O_3 < 0.6, TiO_2 < 0.6%, Mg/Mg+Fe ~ 67-80, Ni ~ 200-400 ppm, and Cr ~ 600-1200 ppm. The incompatible element abundances in the HMA are generally less than 10x chondritic or primitive mantle values. The peridotite source region for these volcanics is refractory, as reflected in the Cr-rich compositions of the spinels, high Mg-numbers, low CaO/Al_2O_3 and low incompatible element abundances for the bulk rocks. However the incompatible trace element ratios and patterns are inconsistent with derivation from a refractory source and a complex series of enrichment events have been superimposed on the refractory source. These enrichment events have given the HMA a distinctive geochemical signature characterized by low Ti/Zr (<60) and light rare earth element enrichment. Two groups of high-Mg andesites are recognized on the basis of their rare earth patterns and the relationship between the rare earths and Ti, Zr, and Nb. Type-C HMA occur at all the localities studied and have a concave rare earth element pattern. There is no correlation of Ti/Zr and Zr/Nb ratios with La/Yb in type-C HMA. Type-E HMA are recognized only at Cape Vogel, PNG, and are characterized by light rare earth enrichment which has an inverse correlation with Ti/Zr and Zr/Nb ratios.

Detailed comparisons between high-Mg andesites and other high-SiO_2, high-MgO liquids demonstrates that these rocks define a petrogenetic group characterized by derivation from peridotite sources at $P < 15$ kb and $T \sim 1100\text{-}1400°C$. Of the group of high-$SiO_2$, high-MgO liquids for which experimental liquidus data are available only the HMA *require* water for derivation from a peridotite source. While the high-SiO_2, high-MgO liquids define a broad petrogenetic group there are nonetheless significant geochemical and petrographic differences between these rocks which preclude their derivation from a common peridotite source.

The location of known high-Mg andesites favours their origin in island-arc petrogenetic processes, although their place in the complex interactions of island-arc volcanism, back-arc basin creation, and trench formation remains uncertain.

ACKNOWLEDGEMENTS

Professor D.H. Green suggested that the HMA were a worthy project and throughout the course of this study his ideas and encouragement have been invaluable. I wish also to thank him for the good humour and tactfulness he maintained, at times I am sure it was an arduous task.

Drs Shiraki, Kuroda, Sato, Nesbitt and Jaques were instrumental in helping me obtain samples, as were Wally Dallwitz and other members of the Bureau of Mineral Resources, Australia.

Geochemical work on the HMA was facilitated by the help of S.R. Taylor, S. McLennan, P. Robinson, P. Muir, M. Shelley, B.J. Fryer, and N. Higgins.

I am indebted to Mr K.L. Harris for his instruction and assistance in the high-pressure laboratory. Brendon Griffin, R. Lincolne and R. Berry were an invaluable aid in obtaining good results from the microprobe.

I have benefited from discussions with many people on aspects of this project: Dr R.F. Berry, Dr J. Walshe, Dr R. Varne, Dr B. Duncan, Dr D. Ellis, Dr C Hatton, Dr L. Jaques, Dr S.S. Sun, Dr W. Cameron, Mr S. Harley, Mr B. Griffin, Mr A. Brown, and Mr W. Dallwitz.

I would also like to thank the many students and staff of the Geology Department for making the department an enjoyable place to work. In particular, Barbara, Virginia, Peter, Fred, Wayne and John have given invaluable aid.

This project was supported by a CFSP award.

Ms J. Pongratz did most of the hard work in producing this thesis; however, I cannot in all conscience allow her to accept the responsibility of its contents.

Finally I would like to thank Ron Berry and Simon Harley for putting up with me and providing friendship when it was most required; Brendon for fishing trips; Roz, Roz and Janine for distractions; Rick and Libby for

friendship, support and the opportunity to ride in an Alfa Romeo; all the others too numerous to mention who have had their ears bent in one of the diatribes; and lastly, Charlotte (and Imogen, Jeremy, Luke and Hercules) for their love and all that comes with it.

GLOSSARY OF ABBREVIATIONS AND SYMBOLS

Ab	albite
ALP	alpine peridotites
Amph	amphibole
An	anorthite
ANK	ankaramitic
AR	analytical reagent
B	basalt
BA	basaltic andesite
BI	Bonin Islands
C	concave
CAS	calk-alkaline series
CE	clinoenstatite
CFMS	CaO-FeO-MgO-SiO_2
CMS	CaO-MgO-SiO_2
cpx	clinopyroxene
Di	diopside
E	enriched
En	enstatite
EPMA	electron probe microanalysis
Fo	forsterite
gl	glass
HAP	hydroxyapatite
HFS	high field strength
HKCAS	high K CAS
HMA	high-Mg andesites
HMLA	high-Mg low-alkali liquids
HREE	heavy REE
Hy	hypersthene
IAB	island-arc basalt
IAT	island-arc tholeiite (series)
Ilm	ilmenite
Jd	jadeite
kb	kilobars
K_D	distribution coefficient
LFS	low field strength
Liq	liquid
LREE	light REE
M	microlite
MAR	mid-Atlantic Ridge
Mg, Mg-number	= molecular proportion 100 MgO/MgO + total Fe as FeO
mg	milligrams
MORB	mid-ocean ridge basalts
MP	microphyric
MT	Mariana Trench
Mt	magnetite

n	number of analyses
$(\ )_N$	normalized to chondritic values
nA	nannoamps
nd	not detectable
Ne	nepheline
NM	nepheline melelitites
N-MORB	normal-depleted-MORB
OE	orthoenstatite
OIB	ocean island basalt
ol	olivine
opx	orthopyroxene
Or	orthoclase
P	pressure (in kilobars)
PE	protoenstatite
Ph	phenocryst
PI	Mg-rich pigeonite
PNG	Papua New Guinea
PX	peridotite xenoliths
Qz	quartz
R	rim
REE	rare earth elements
RF	radio frequency
RNAA	radio chemical neutron activation
SC	stratiform complexes
SMA	sanukitoid magnesian andesites
SSMS	spark-source mass spectrography
Sp	spinel
STPK	spinifex textured peridotitic komatiite
T	temperature (°C)
TE	transition metals
THS	tholeiite series
Ts	Ca-Tschermak's
UN	ultramafic nodules
UPL	upper pillow lavas, Troodos
Xeno	xenolith
XRF	X-ray fluorescence

$$\Sigma Nd = \left(\frac{(^{143}Nd/^{144}Nd)}{(^{143}Nd/^{144}Nd)_{CHUR}} - 1 \right) \times 10^4$$

where CHUR = chondrite uniform reservoir,

$(^{143}Nd/^{144}Nd)_{CHUR} \equiv 0.511839$ $(^{146}Nd/^{142}Nd = 0.636155)$

or 0.51264 $(^{146}Nd/^{144}Nd = 0.72190)$.

Chapter 1

INTRODUCTION

1.1 PREAMBLE

Primary magmas, that is magmas of direct mantle derivation, are crucial to understanding the composition of the mantle and the evolutionary paths of related liquids. Only rarely, if ever, are primary magmas erupted at surface and we are usually obligated to look for the least evolved or fractionated lavas derived from them. Primary magmas and/or their least evolved derivatives are commonly recognized by their high Mg-numbers (65-80) and high Cr and Ni contents (Green, 1971; Sato, 1977; Roedder & Emslie, 1970). An additional criterion, the absence of phenocrysts (or an accumulative nature), is also important although Cox (1978) suggested that there may be "primitive porphyritic magmas", which though phenocryst-rich are representative of the compositions of primary magmas. It is not always easy to determine the nature of a primary magma from its fractionated derivatives. For example, Green *et al*. (1979) presented a detailed examination of the problems involved in determining the primary and/or parental magmas for mid-ocean ridge basalts.

Penultimately the proof that any composition is a primary magma relies on petrographic and experimental evidence that it can crystallize liquidus phases which are compatible with a peridotite source. Satisfaction of the criterion that a magma was derived by equilibrium partial melting of a peridotitic source under some pressure, temperature and $P_{volatile}$ conditions is a necessary but insufficient proof of it being a parental magma and it is important to show that it has phase relations which can account for the chemical and mineralogical features of the suite of rocks to which it is related.

It is now generally accepted that many basaltic and nephelinitic magmas can be derived by partial melting of a peridotitic mantle (Green & Ringwood, 1967; Green, 1971; Jaques & Green, 1980), i.e. these magmas may be primary ones. However few andesitic rocks meet the criteria usually used to recognize magmas (see for example Ewart, 1976; Whitford *et al.*, 1979). It may be possible to produce melts of andesitic composition (high SiO_2) by partial melting of peridotite under water-rich conditions at low pressures (Green, 1973; Nicholls, 1974).

Kushiro (1972) and Green (1973, 1976) drew attention to the siliceous, high-MgO, clinoenstatite-bearing volcanics from Cape Vogel, PNG as a possible example of a primary andesitic magma. Green (*ibid.*) suggested that these rocks may have been derived by water-saturated, or near-saturated, melting of a peridotite with melt segregation at pressures of 10 kb and at approximately 1100°C.

Rocks similar to those of the Cape Vogel siliceous, high-MgO, volcanics (Dallwitz *et al.*, 1966) have since been recognized in the Mariana island arc. In particular high-MgO andesites were "rediscovered" in the Bonin Islands by Kuroda & Shiraki (1975) and clinoenstatite-bearing varieties were recognized later (Shiraki *et al.*, 1980; Komatsu, 1980). Clinoenstatite-bearing high-MgO andesites dredged from the Mariana Trench near Guam were also described by Dietrich *et al.* (1978). The term "boninite" has been used to describe these rocks (Kuroda & Shiraki, 1975; Cameron *et al.*, 1979, 1980), however, as is discussed at some length in Chapter 6, this term has been misused and the nomenclature used to describe them here is high-Mg andesites (HMA) (Sun & Nesbitt, 1978; Jenner, 1981; Gill, 1981).

1.2 AIM OF THE PRESENT STUDY

The origin and significance of high-Mg andesites as possible primary magmas, perhaps formed in an island-arc environment could not be evaluated on the basis of previous work (cf. Jenner, 1981). The initial aims of the study were :

(i) to define the P, T, P_{H_2O} conditions under which these rocks may have been derived from a peridotitic source;

(ii) to document the chemical and mineralogic nature of high-Mg andesites; and

(iii) to comment on the nature of the source material.

To do this an integrated petrological and geochemical study was undertaken on selected samples, concentrating on the extensive suite of samples available from Cape Vogel, PNG.

As the thesis evolved it was necessary to use a variety of techniques and approaches to investigate the detailed petrogenesis of these rocks. To facilitate the reader's understanding of this work a brief outline is given below.

1.3 THESIS STRUCTURE

The thesis begins by presenting the petrographic and mineralogic characteristics of high-Mg andesites (Chapter 2). Particular attention has been paid to the relationship between pyroxene chemistry and magma chemistry.

Chapter 3 outlines the geochemistry of the high-Mg andesites with emphasis on the trace element characteristics and implications for the source.

Chapter 4 presents the results of experimental studies on pyroxene equilibria in the Mg-rich portion of the pyroxene quadrilateral. The aim of this study was to reach an understanding of the pyroxene phase relations sufficient to use them in limiting the temperature of extrusion of the clinoenstatite-bearing high-Mg andesites.

Chapter 5 addresses the question of what are the P, T and P_{H_2O} conditions of origin of the high-Mg andesites. The liquidus studies were done on selected compositions to reproduce the crystallization sequence documented in Chapter 2, and determine the nature of the parental magma(s) to high-Mg andesite suites.

During the course of this study a great deal of literature concerning possible inter-relationships between various high-SiO_2, high-MgO volcanics was published. The nature of the relationship between the high-Mg andesites of this study and sanukitoids, komatiites and boninites is reviewed and discussed in some detail in Chapter 6. The tectonic environment of formation of the high-Mg andesites is also discussed.

Chapter 7 presents a summary of the conclusions and findings of this study.

Additional data collected on related rocks is given in Appendices 1 and 2. A description of a rare earth element analytical technique developed during the course of this study is given in Appendix 3. The low abundances of rare earth elements in high-Mg andesites made it necessary to do the bulk of analyses for these elements by other techniques, however results are presented for some associated volcanics and for standards.

Chapter 2

PETROGRAPHY AND MINERALOGY

2.1 INTRODUCTION

The general geologic setting and petrographic descriptions of the high-Mg andesite samples used in this study are presented in this chapter. Four samples (V1-V4) were selected for detailed petrography from the range of rocks available from Cape Vogel. The Bonin Islands are represented by seven samples (B1-B5, 60144, 60145) which span the petrographic varieties reported for this area. Only one sample (M1) from the Mariana Trench area was available for this study. Major element analyses along with selected trace elements, normative compositions and some important ratios are given in Table 2.1 for all of the above mentioned rocks, excluding 60144 and 60145 for which there was insufficient sample. Figure 2.1 shows the geographic location of the areas studied.

2.2 GEOLOGIC SETTING

2.2.1 Cape Vogel, PNG

The geology of the Cape Vogel area was described by Dallwitz *et al.* (1966), Dallwitz (1968) and Smith & Davis (1976). The occurrence of high-Mg andesites can be summarized as follows: (i) they are found in association with tholeiitic volcanics of the Dabi Volcanics but form only a small proportion of this formation; (ii) little outcrop has been observed and specimens were collected from residual boulders. Reliable field relationships between varieties of clinoenstatite-bearing high-Mg andesites and associated volcanics are thus unknown; and (iii) the age of the volcanism is poorly known. A minimum age of early Miocene is indicated by sedimentary rocks unconformably overlying the formation.

Table 2.1

Chemical compositions, calculated on an anhydrous and reduced basis, for rocks described in this study.

	Marianas Trench	Bonin Islands					Cape Vogel, PNG			
	M1**	B1**	B2**	B3**	B4†	B5†	V1*	V2*	V3*	V4*
SiO_2	57.33	58.46	57.23	58.43	59.69	69.56	56.80	57.80	57.60	57.60
TiO_2	0.14	0.10	0.12	0.12	0.29	0.33	0.30	0.40	0.30	0.20
Al_2O_3	9.75	13.37	10.61	11.35	14.44	13.26	11.80	11.50	9.10	8.50
FeO	9.06	8.27	8.80	8.57	8.24	5.94	8.63	9.46	9.34	9.83
MnO	0.13	0.14	0.12	0.12	0.23	0.12	0.20	0.20	0.20	0.26
MgO	15.19	9.39	12.27	11.40	5.71	1.65	12.60	12.60	16.80	17.10
CaO	5.86	8.11	9.69	7.76	8.38	4.80	7.90	6.00	4.90	5.10
Na_2O	1.59	1.59	0.87	1.74	2.28	3.27	1.10	1.30	1.10	0.60
K_2O	0.93	0.70	0.30	0.51	0.51	0.95	0.40	0.40	0.20	0.40
Mg #	74.92	66.92	71.30	70.33	55.25	33.11	72.24	70.36	76.22	75.61
Ni	258	140	111	205	80		154	199	534	334
Cr	685	405	560	445	155	5	560	545	1050	960
CIPW norms (calculated with $Fe^{2+}/Fe^{2+}+Fe^{3+} = 0.9$)										
Q=	5.66	12.03	10.86	10.5	15.18	31.18	9.91	11.65	9.46	10.53
Or	5.50	4.14	1.77	3.0	3.01	5.61	2.36	2.36	1.18	2.36
Ab	13.45	13.45	7.37	14.6	19.29	27.67	9.31	11.00	9.31	5.08
An	16.72	27.28	24.16	21.8	27.66	18.70	26.08	24.37	19.30	19.32
Di	9.50	10.52	19.31	13.5	11.47	4.34	10.57	4.36	4.01	4.28
Hy	47.41	31.27	35.00	35.2	21.36	10.86	39.64	43.74	54.22	56.04
Mt	1.46	1.33	1.42	1.4	1.33	0.96	1.39	1.52	1.49	1.58
Il	0.27	0.19	0.23	0.2	0.55	0.63	0.57	0.76	0.57	0.38
Di/Di+Hy	0.167	0.252	0.356	0.277	0.349	0.286	0.210	0.091	0.069	0.071

** new analyses - microprobe analyses of fused glass beads. * analyses from Dallwitz (1968).
† analyses from Shiraki & Kuroda (1977).

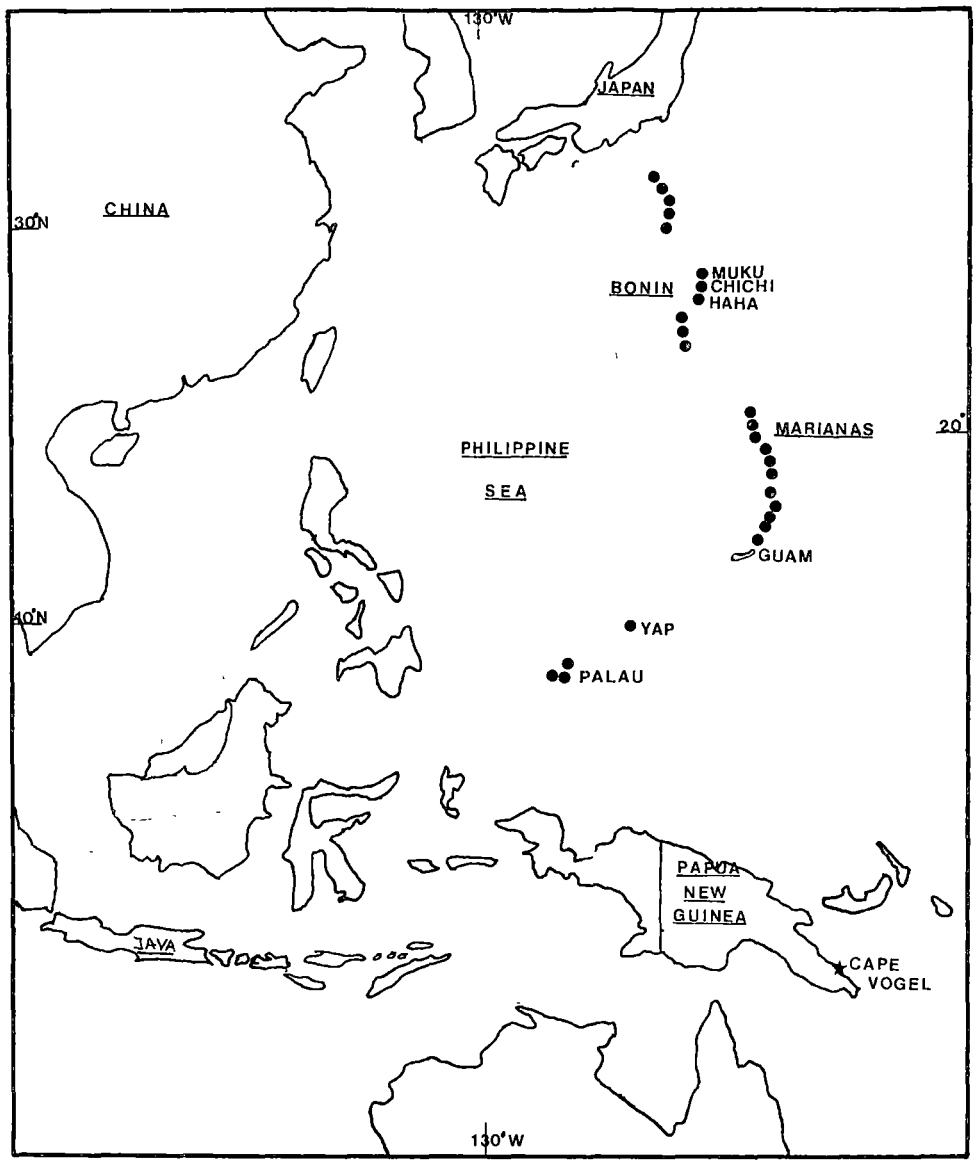

Figure 2.1 Generalized location map of the west and south-west Pacific area. Sample localities were from Cape Vogel, PNG, Chichi-jima, Bonin Islands, and from slightly south-east of Guam in the Mariana Trench.

However, the Dabi Volcanics are probably considerably older as indicated by a minimum K-Ar age of 28 ± 1 m.y. on a clinoenstatite-bearing rock (Dallwitz, 1968) and an Ar-Ar age of 58 m.y. obtained by David Walker of the Australian National University (W. Cameron, pers. comm., 1981).

Smith (1976) and Smith & Davies (1976) have shown that the Dabi Volcanics, excluding the high-Mg andesites, range from basalt through dacite and have a tholeiitic nature. The data from this study and that of Smith (1976) and Smith & Davies (1976) also define tholeiitic trends on FeO^t and TiO_2 versus FeO^t/MgO (after Miyashiro, 1974) and SiO_2 versus K_2O plots (after Whitford *et al.*, 1979). The trace element characteristics of these volcanics are poorly known, the only available data being given in Appendix 1. Their abundances of Cr, Ni, Y, Zr and Nb, and relationships between these elements, TiO_2 and Mg-number are consistent with variations observed in the island-arc tholeiite (IAT) series (Gill, 1979). The alumina content of a given compositional group, i.e., basalt, andesite, dacite, is lower than those normally found (Dallwitz, 1968).

2.2.2 Bonin Islands

The Bonin (Ogasawara) Islands, part of the outer arc of the Izu-Mariana Arc, form an emergent section along the trench slope break (Kuroda & Shiraki, 1975; Karig & Moore, 1975). There are three major island groups: Chichi-jima, Haha-jima and Muko-jima. Chichi-jima, source of the samples used in this study, is the central group with Haha-jima lying some 50 km south and Muko-jima approximately 70 km north.

Chichi-jima consists predominantly of boninite; which occurs as; vesicular pillow lavas; occasional hyaloclastites; and feeder dykes (Shiraki *et al.*, 1978; Kuroda & Shiraki, 1975). The term *boninite* is used to describe glassy, feldspar-free, olivine-bronzite andesites

(Shiraki & Kuroda, 1977) and more recently (Shiraki *et al.*, 1980; Komatsu, 1980) clinoenstatite-bearing varieties have been recognized. Bronzite andesites, hypersthene andesites and dacite lavas and pyroclastics form the remaining volcanics (Kuroda & Shiraki, 1975). Limestone overlying volcanic lavas and breccias contains fossils of Oligocene to Early Miocene age, and a K-Ar age of 26 m.y. has been obtained from a volcanic rock (Shiraki *et al.*, 1978).

Haha-jima is composed of a sequence of lavas, pyroclastics and volcaniclastic sediments. Fossiliferous beds containing Middle Eocene foraminifera are intercalated with other units and there is a K-Ar age of 40 m.y. reported from a volcanic rock (Shiraki *et al.*, 1978). The lavas are described as: pyroxene andesite - the dominant rock type - which is strongly porphyritic with plagioclase, augite and hypersthene; olivine-bearing pyroxene andesite; and quartz-bearing pyroxene andesite (Shiraki *et al.*, 1978). The lavas range in composition from basalt to dacite and are said to be similar to the island-arc tholeiite series of volcanics (Shiraki *et al.*, 1978). Primitive varieties (in terms of Mg-number, and Cr and Ni contents) are lacking and boninites are not present (Shiraki *et al.*, 1978).

According to Shiraki *et al.* (1980) Muko-jima is made up largely of boninite pillow lavas and breccias, some of which contain clinoenstatite (see also Komatsu, 1980).

2.2.3 Mariana Trench

M1 is a piece of one of many fragments of clinoenstatite-bearing volcanics recovered in dredge 1403 from the island-arc slope of the Mariana Trench at 12°N (near Guam) (Dietrich *et al.*, 1978; Sharaskin *et al.*, 1980). The dredge haul also contained serpentinized and partly

mylonitized peridotites, troctolite, gabbro and basaltic rocks, the latter with typical ocean-floor chemistry (Dietrich *et al.*, 1978). Sharaskin *et al.* (1980) suggested an age greater than 33 m.y., while Crawford *et al.* (1981) indicated an age of 28-36 m.y. for samples from this locality.

Bloomer *et al.* (1979) and Hawkins *et al.* (1979) described volcanics dredged at three sites between 11-18°N, from the inner wall of the Mariana Trench, which appear to have chemical and petrographic similarities to those discussed above. No clinoenstatite is reported.

2.3 PETROGRAPHY

2.3.1 Cape Vogel (V1-V4)

Detailed petrographic descriptions of clinoenstatite-bearing lavas are given by Dallwitz *et al.* (1966). One specimen (V4) in this study is from the same sample as their LB107, and results from the earlier study are included below.

The rocks consist of clinoenstatite and bronzite phenocrysts, abundant pyroxene microlites, altered and unaltered glass, zeolites (in vesicles), and rare Cr-spinel. A single occurrence of olivine (Fo_{90}) completely rimmed by clinoenstatite (En_{90}) was found in V3. Dallwitz (1968) reported other possible occurrences of olivine, now pseudomorphed by hydrous minerals.

The major variation between samples is in the proportion of clinoenstatite to bronzite phenocrysts. Clinoenstatite accounts for 80% of the phenocrysts in V4 but bronzite forms 70-90% of the phenocrysts in V2 and V3, and only one clinoenstatite crystal was found in V1. Sample V2 is texturally distinct from the other samples in its fine grain size; consisting predominantly of microlites with rare scattered

phenocrysts. Glomeroporphyritic texture is commonly developed in the other samples. Rare rounded clots (5-10 mm) of crystals (0.1-0.2 mm) occur in V3 and V4. These clots consist of a murky core area (reacting pyroxene and glass ?) surrounded radially by equant bronzite crystals. Clinoenstatite does not appear to be present in these areas.

Glass accounts for approximately 30-40% of each sample but the ratio of unaltered to altered glass shows considerable variation in all samples.

Chrome spinels generally occur as small inclusions (0.01 mm) in phenocryst phases. *Clinoenstatite* phenocrysts are commonly euhedral and range in length from 0.3-20 mm, averaging about 1 mm. They are characterized by multiple twinning and by closely spaced cracks, cleavage, partings and, in some cases, by high concentrations of minute, globular, fluid inclusions. Narrow (0.01 mm) rims of clinopyroxene are found on the clinoenstatite phenocrysts. Clinoenstatite also occurs as quench crystals, as inclusions within bronzite, and as part of composite bronzite/clinoenstatite phenocrysts (see Fig. 5, Plate 2, Dallwitz *et al.*, 1966; Fig. 1, Nakamura, 1971). *Bronzite* phenocrysts are colourless, euhedral to subhedral, show simple zoning and range in length from 0.3-2 mm, averaging 0.6 mm. Bronzite also occurs as quench crystals and in both forms is rimmed by clinopyroxene. *Clinopyroxene* occurs as very narrow rims or microlites. The largest acicular microlites are 0.3 mm x 0.035 mm and are best developed in V1.

2.3.2 Mariana Trench (M1)

This sample consists of clinoenstatite, bronzite and clinopyroxene phenocrysts in a groundmass of variably altered glass (30-40% of the sample). Zeolites (in vesicles) and feathery clinopyroxene-amphibole (?)

microlites also occur in the glass. Spinel occurs as inclusions in the clinoenstatite and bronzite phenocrysts. Clinoenstatite and bronzite phenocrysts are subhedral to euhedral and range in length from 0.2-0.7 mm. Clinoenstatite occurs as cores in bronzites and as rims to bronzite.

Clinopyroxene occurs as rims to clinoenstatite and bronzite phenocrysts and as discrete phenocrysts. The occurrence of clinopyroxene as a distinct phenocryst phase and the lack of pyroxene quench crystals distinguish the Mariana Trench samples from Cape Vogel rocks.

While no olivine was found in this sample, similar rocks from the same dredge haul contain rare olivine (Dietrich *et al.*, 1978; Sharaskin *et al.*, 1980). Olivines in sample 1403-45 (*ibid.*) range from a phenocryst (xenocryst ?) Fo_{92} (NiO = 0.40 wt.%) to microphenocryst olivines of Fo_{88-89} (NiO = 0.31-0.35 wt.%) (W. Cameron, pers. comm.).

2.3.3 Bonin Islands (B1-B5, 60144, 60145)

Samples B1, B2 and B3 are "boninites" (see Kuroda & Shiraki, 1975) which occur as pillow lavas. Sample 60144 is a dyke which cuts a boninite breccia and 60145 is a fragment from a breccia. Samples B4 and B5 are the bronzite andesite (NK741129-4) and perlitic dacite (NK741127-5) described by Shiraki & Kuroda (1977).

Samples B1, B2 and B3 consist of subhedral to euhedral phenocrysts of orthopyroxene in a matrix of variably altered glass and pyroxene quench crystals. Zeolite (in vesicles) and feathery clinopyroxene-amphibole (?) microlites occur in the glass. Spinel occurs as inclusions in the pyroxenes. Olivine [not present except as pseudomorphs in our samples] has been reported by Kuroda & Shiraki (1975) and Shiraki & Kuroda (1977) for rocks of similar composition and from the same localities. It occurs as phenocrysts and microphenocrysts varying in composition from Fo_{83-90}. The mantling of some grains by orthopyroxene

is taken as evidence of a reaction relationship, with olivine reacting with liquid to produce orthopyroxene. A minor role for olivine as a fractionating phase is also indicated by the major element data. Least squares modelling of bulk compositions shows that derivation of boninite 741127-4 (Mg_{70}) from Og-44 (Mg_{77}) (Shiraki & Kuroda, 1977) requires 15.4% orthopyroxene, 0.8% clinopyroxene and only 1.05% olivine (sum of squared residuals = 0.001). The predominance of orthopyroxene in explaining the compositional variation is similar to that seen in the Cape Vogel rocks (Chapter 3; Dallwitz, 1968).

Orthopyroxene phenocrysts in B1-B3 range in length from 0.1-0.7 mm and may have "swallow-tail" quench growths. Some of the orthopyroxenes have resorbed or reacted cores. Clinopyroxene may be present as small inclusions in these reacting orthopyroxenes. Obvious zoning is restricted to a few crystals. Orthopyroxene also occurs as quench crystals which are generally acicular (0.15 mm x 0.02 mm).

Clinopyroxene occurs as quench crystals or as rims to orthopyroxene phenocrysts in samples B1 and B2. It also appears as microphenocrysts in sample B3.

Glass accounts for 20-30% of the sample in B1 and B3, and 40-50% in B2.

Sample B1 contains a xenolith (?) consisting of 0.1-0.4 mm, tightly packed, equant orthopyroxene and clinopyroxene in a matrix of glass. Poikilitic clinopyroxene is also present. Orthopyroxene laths (0.07 mm wide) separated by equally wide zones of glass occur at the edge of the xenolith. The aggregate of equant orthopyroxene and poikilitic clinopyroxene rimmed by orthopyroxene and glass is suggestive of replacement of an earlier phase (? olivine) or phases (? olivine, clinopyroxene).

Sample 60145 is similar in most respects to the "boninites" B1-B3, but lacks some of the quench crystal forms and has less textural evidence for the (past) occurrence of olivine. The rock consists of ~40% glass, ~40% very fine grained pyroxene microlites, and 20% medium grained orthopyroxene phenocrysts. The orthopyroxene phenocrysts are predominantly subhedral-euhedral and show minor zoning. Clinopyroxene occurs as a very rare component in glomeroporphyritic accumulations of predominantly orthopyroxene.

Sample 60144 is unique among the samples studied here from the Bonin Islands in containing both fresh olivine and clinoenstatite. In general the rock consists of 40-50% phenocrysts (medium-coarse grained) which are predominantly orthopyroxene with rare olivine and clinoenstatite in a matrix composed equally of glass and fine grained pyroxene microlites. The orthopyroxene phenocrysts are generally subhedral-euhedral, but minor resorption textures are shown in some grains. The clinoenstatite occurs as subhedral phenocrysts and as cores to orthopyroxenes. The olivine is subhedral to euhedral and one crystal appears to have a reaction rim of clinoenstatite. Spinels occur both as inclusions and as phenocryst phases.

Bronzite andesite (B4) consists of subhedral-euhedral phenocrysts of orthopyroxene, clinopyroxene and plagioclase in a groundmass of highly altered glass (~ 40%). The phenocrysts range in length from 0.1-0.3 mm. Xenocrysts of bronzite (2-3 mm in length), showing a narrow reaction rim, also occur. A single xenocryst of Cr-spinel is also present.

The perlitic dacite (B5) is 70% glass (with perlitic texture), 23% microlites (plagioclase, clinopyroxene, orthopyroxene) and 7% plagioclase, clinopyroxene, orthopyroxene and magnetite phenocrysts.

The phenocrysts (excluding magnetite) are generally 0.2 mm x 0.7 mm and tend to occur in crystal clots. The glass is mainly unaltered.

2.4 MINERAL CHEMISTRY

2.4.1 Clinoenstatites

Analyses of clinoenstatite from M1, V2-V4, and 60144 are shown in Figure 2.2 and selected analyses are given in Table 2.2.

Clinoenstatites in Cape Vogel rocks range in Mg-number from 88 to 93, in the Bonin Islands rocks from 88 to 92.4 (including Shiraki *et al.*, 1980), while the Mariana sample varies little (~ 90 to 91) (see also Shiraki *et al.*, 1980). Calcium and alumina contents from the localities overlap, ranging from 0.1-0.67 wt.% CaO and 0.12-1.0 wt.% Al_2O_3. Cr contents of Mariana Trench clinoenstatites average 0.33 wt.% Cr_2O_3, while those in Cape Vogel rocks are generally higher and range from 0.32-0.86 wt.% Cr_2O_3. A range of 0.21-0.78 wt.% Cr_2O_3 is reported by Shiraki *et al.* (1980) and Komatsu (1980), for clinoenstatites from the Bonin Islands.

Generally, the multiply twinned clinoenstatites are more magnesian than orthopyroxenes, with an apparent limiting Mg-number for clinoenstatite of approximately 88. There are exceptions to this rule in Cape Vogel rocks, and, as discussed by Dallwitz *et al.* (1966), the chemistry of the two pyroxene types seems to converge, especially where (?) untwinned clinoenstatite occurs. Nakamura (1971) determined a partition coefficient [$K_{D_{OE}}^{PE} = (Mg/Fe)^{PE}/(Mg/Fe)^{OE}$]* of 1.12 for coexisting (in contact) clinoenstatite and orthopyroxene. Similar values

---

* PE = protoenstatite and OE = orthoenstatite. See Chapter 4 for a more detailed discussion of pyroxene nomenclature.

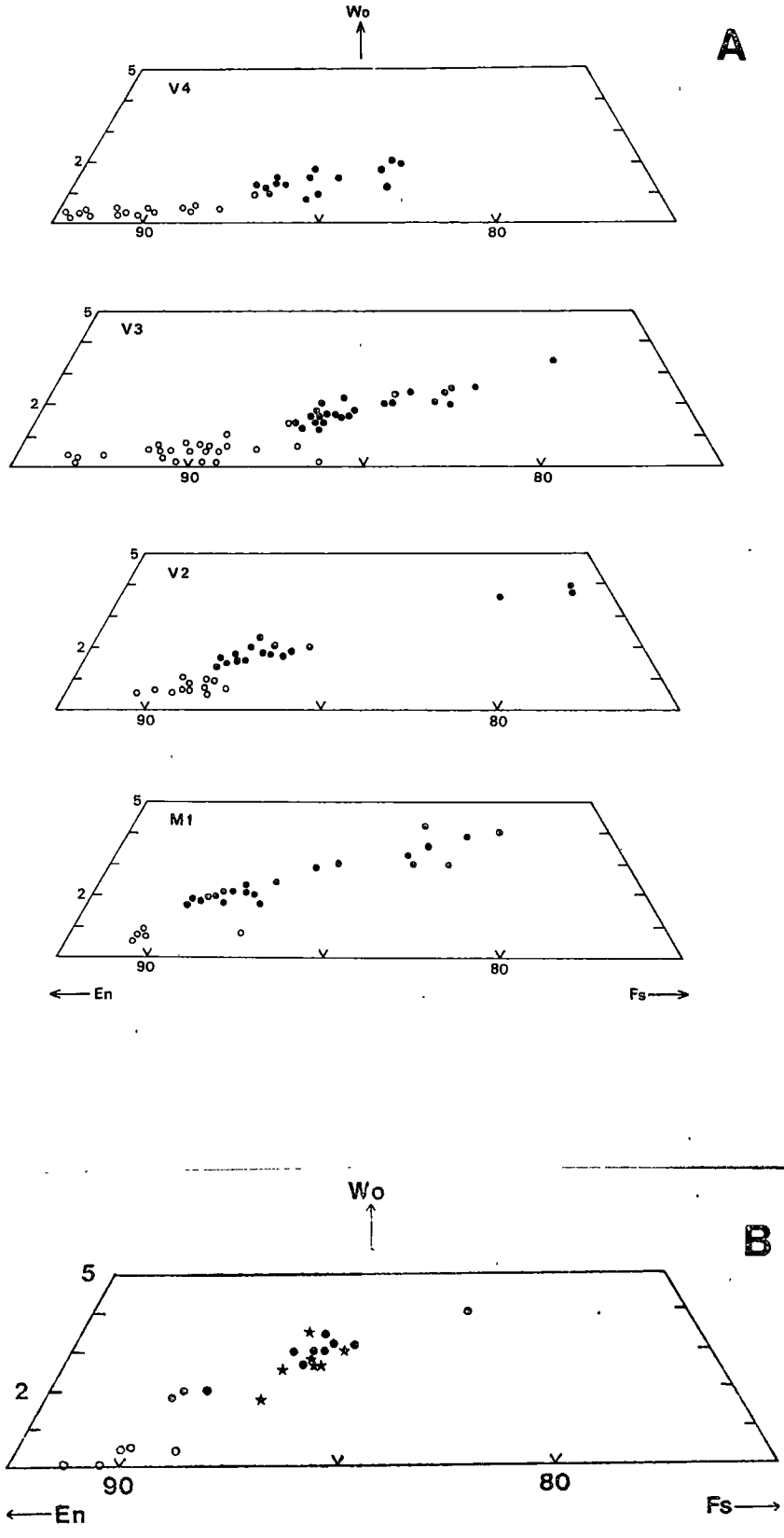

Figure 2.2 Ca-poor pyroxenes from clinoenstatite-bearing volcanics.
(A) M1 (Mariana Trench) and V2-V4 (Cape Vogel.
(B) 60144 and 60145 (Bonin Islands).
Open circles: clinoenstatite. Solid dots: orthopyroxene.
Stars: orthopyroxene in 60145.

Table 2.2

Selected clinoenstatite analyses.*

	M1	M1	V2	V3	V3	V4
SiO_2	58.00	57.69	58.07	56.99	57.12	58.19
TiO_2					0.08	
Al_2O_3	0.45	0.93	0.62	0.57	0.28	
Cr_2O_3	0.23		0.51	0.47	0.41	
FeO	6.63	6.42	7.87	7.95	7.19	5.48
MgO	34.44	34.59	33.64	33.73	34.61	35.87
CaO	0.28	0.39	0.28	0.29	0.32	0.10
Mg #	90.25	90.57	88.38	88.32	89.56	92.10
Si	1.997	1.985	1.981	1.979	1.978	1.995
Ti						
Al	0.018	0.037	0.026	0.023	0.012	
Cr	0.006		0.014	0.013	0.011	0.010
Fe	0.191	0.184	0.229	0.231	0.208	0.157
Mg	1.768	1.774	1.741	1.746	1.786	1.833
Ca	0.01	0.014	0.01	0.011	0.012	0.004
Total	3.99	3.997	4.001	4.003	4.007	3.999

* Note: mineral analyses normalized to 100%.

were found in this study, and those of Shiraki *et al.* (1980) and Komatsu (1980); however, some Cape Vogel samples have higher values ranging from 1.28-1.52. The significance of this is discussed later.

Zoning in the clinoenstatite is slight except in Cape Vogel samples where the Mg-number may increase (see Dallwitz *et al.*, 1966) towards the margins of crystals.

2.4.2 Orthopyroxenes

Compositional variation in the orthopyroxenes is shown in Figures 2.2, 2.3 and 2.4, and Tables 2.3 and 2.4.

Bronzites in all samples have higher Ca contents and are more Fe-rich than clinoenstatite from the same rock. Al_2O_3 and Cr_2O_3 contents overlap but there is a bias towards higher Al_2O_3 and Cr_2O_3 contents in orthopyroxene and lower values in clinoenstatite (see Tables 2.2, 2.3 and 2.4).

The variation of bronzite composition in high-Mg andesites shows the following features (see Table 2.4 and Figures 2.2 and 2.3):

(1) Calcium increases with decreasing Mg-number except in sample B1.

(2) There are small but consistent differences in Ca content of bronzite in different rocks. At a given Mg-number, bronzites in V2, V3, V4 are virtually indistinguishable but lower in Ca content than M1, V1 (similar) which are in turn lower than B2 and B3. The trend of *decreasing* Ca content with decreasing Mg-number of B1 is quite distinctive. The differences in Ca content at a given Mg-number, excluding B1, correlate very well with the normative Di/Di+Hy ratios of the rocks (Table 2.1).

(3) Alumina increases with decreasing Mg-number in B2, B3 and V1; shows a similar but less well developed trend in M1, V3 and V4, and shows no correlation in B1 and V2. While differences are small

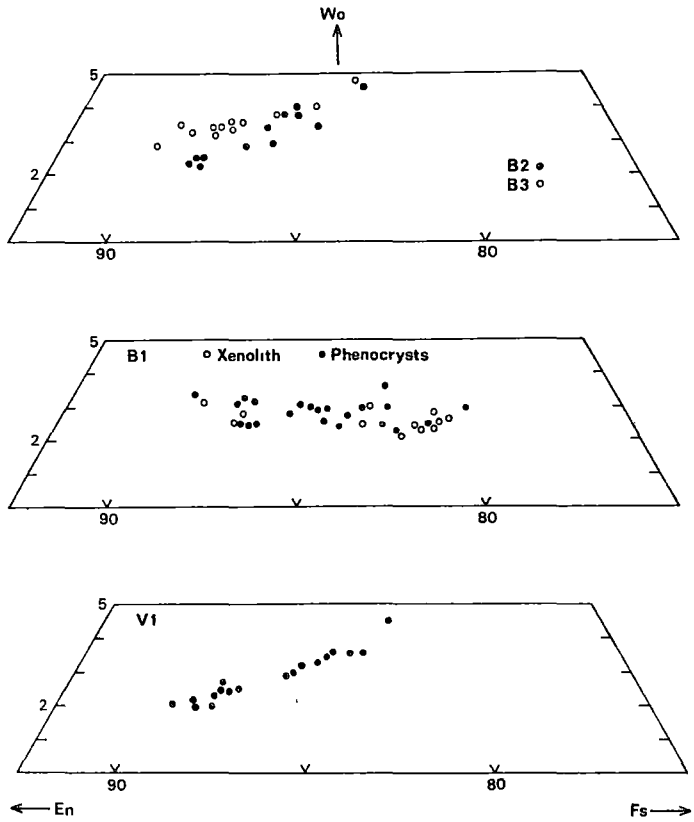

Figure 2.3 Ca-poor compositions from B1-B3 (Bonin Islands), and V1 (Cape Vogel).

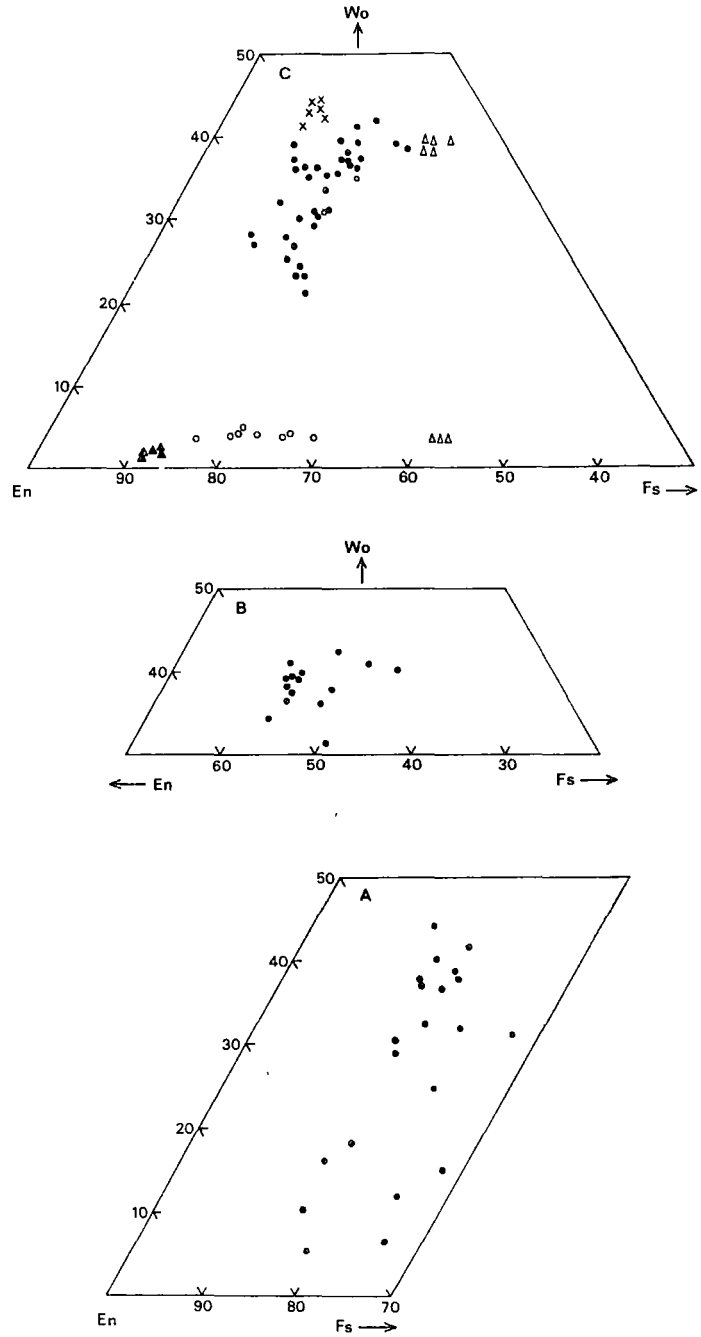

Figure 2.4 Compositional variation in clinopyroxenes from (A) Cape Vogel and (B) Mariana Trench (M1).
(C) Clinopyroxene compositions in B1-B4 (solid dots); orthopyroxene in B4 (open circles); xenocryst + orthopyroxene B4 (solid triangle); pyroxenes in B5 (open triangles); and clinopyroxenes in xenolith of B1 (crosses).

Table 2.3 Selected orthopyroxene analyses.*

	M1 Ph	M1 R	B1 Xeno	B1 Ph	B2 Ph	B4 Xeno	B4 Ph	B4 Ph	B5 Ph	V1 Ph	V1 M	V2 Ph	V3 Ph	V3 Ph	V4 Ph
SiO_2	57.42	56.18	56.43	55.88	55.90	56.82	53.65	54.46	52.24	57.07	54.46	56.41	56.00	54.57	56.56
TiO_2					0.15	0.12		0.18			0.10			0.28	
Al_2O_3	0.51	0.74	0.93	1.28	0.79	0.36	1.72	1.17	0.94	0.70	1.51	0.96	1.04	2.00	0.60
Cr_2O_3	0.29		1.02	0.50	0.45	0.50		0.25		0.39	0.37	0.66	0.56	0.32	0.37
FeO	7.29	10.56	7.08	9.13	8.40	8.08	18.06	14.24	24.70	7.28	11.27	7.87	8.84	13.04	8.58
MnO							0.25	0.25	0.58			0.26	0.31	0.41	0.31
MgO	33.49	30.71	32.73	31.57	32.30	33.18	24.44	27.38	19.83	33.48	26.99	33.06	32.37	26.86	32.93
CaO	0.99	1.83	1.80	1.64	1.51	1.34	1.87	1.97	1.71	1.05	5.27	0.77	0.88	2.49	0.66
Mg no.	89.13	83.84	89.18	86.03	87.30	88.00	70.70	77.41	58.87	89.13	81.02	88.23	86.70	78.59	87.23
Ca:Mg:Fe	2/87/11	3.5/81/15.5	3/86/11	3/83/14	3/85/12	3/86/11	4/68/28	4/74/22	4/57/39	2/87/11	10/73/17	2/87/11	2/85/13	5/75/20	1/86/13
Si	1.989	1.98	1.964	1.96	1.964	1.974	0.962	1.96	1.975	0.979	0.951	1.965	0.961	1.955	1.975
Ti					0.004	0.003		0.005			0.003			0.008	
Al	0.021	0.031	0.038	0.053	0.033	0.015	0.074	0.050	0.042	0.029	0.064	0.040	0.043	0.085	0.025
Cr	0.008		0.028	0.014	0.013	0.014		0.007		0.011	0.010	0.018	0.015	0.009	0.010
Fe	0.211	0.311	2.060	0.268	0.247	0.235	0.552	0.429	0.781	0.211	0.338	0.229	0.259	0.391	0.251
Mn							0.008	0.011	0.019			0.008	0.009	0.013	0.009
Mg	1.730	1.614	1.698	1.651	1.692	1.718	1.332	1.469	1.118	1.731	1.441	1.717	1.689	1.435	1.714
Ca	0.037	0.069	0.067	0.062	0.057	0.050	0.073	0.076	0.069	0.039	0.202	0.029	0.003	0.096	0.025
Total	3.996	4.005	4.001	4.008	4.009	4.008	4.001	4.007	4.004	4.000	4.009	4.006	4.009	3.992	4.009

Ph = phenocryst, Xeno = occurring in xenolith, M = microlite, R - rim to clinoenstatite.

* Analyses normalized to 100%

Table 2.4

Ranges of selected elements in orthopyroxenes.

	CaO	Al_2O_3	Cr_2O_3	Mg #	n
M1	0.92-2.18	0.45-1.68	nd-0.64	82.3-89.8	23
B1**	1.08-1.85	0.34-2.57	0.31-1.20	78-87.7	24
B1†	1.13-1.80	0.42-1.25	0.31-1.02	81.5-89.2	10
B2	1.25-3.09	0.30-1.63	0.42-0.88	84.1-88.5	13
B3	1.53-3.01	0.40-1.17	0.31-1.02	84.8-89.8	12
B4*	1.87-2.57	0.93-2.46	nd - 0.41	70.7-83.6	9
B5	1.71-1.79	0.68-1.00	nd	57.5-58.9	6
V1	1.02-5.27	0.36-1.89	0.26-0.92	80.8-89.1	29
V2	0.73-2.67	0.34-1.83	0.25-1.13	78.1-88.6	17
V3	0.69-2.90	0.43-2.51	0.34-0.75	77.5-87.4	26
V4	0.56-1.08	0.26-1.04	0.35-0.72	83.4-87.0	11

* excluding xenocrysts

n number of analyses

** phenocryst phase

† occurring in xenolith (?)

nd not detectable

alumina contents at a given Mg-number decrease in the order M1 > (B2, B3, V1) > V3, V4.

(4) Orthopyroxenes occurring as phenocrysts and in the xenolith of B1 are very similar in composition.

(5) Orthopyroxene in the crystal clots of V4 generally have the highest Mg-numbers and lowest Ca content of those in the rock.

(6) Strong compositional zoning is not generally present, but increases in Mg-number towards phenocryst margins occur in some crystals.

Orthopyroxene compositions in the andesite B4 and dacite B5 are shown in Figure 2.4c. The more magnesian orthopyroxenes in B4 are identical to those in B2 or V1 and show increasing Ca content with decreasing Mg-number to near Mg_{80}. For bronzite $<Mg_{80}$, Ca content decreases with decreasing Mg-number as in B1. The change in Ca-Mg-Fe trend may be attributed to the appearance of coexisting Ca-rich clinopyroxene at $\sim Mg_{80}$ in the bronzite andesite composition.

2.4.3 Clinopyroxene

Representative clinopyroxene analyses are given in Table 2.5 and the data are shown in Figure 2.3. Clinopyroxenes occurring in the xenolith of B1, in M1, and in the dacite B5 have small compositional variations and appear to represent equilibrium compositions and near-liquidus pyroxenes. Clinopyroxenes occurring in the remaining samples show a wide range of sub-calcic composition, spread across the pyroxene composition gap (Figure 2.4) and are interpreted as quench or non-equilibrium compositions. Sub-calcic quench clinopyroxenes are not restricted to obvious quench crystals, and some cores of phenocrysts are sub-calcic while the rim has a higher calcium content.

Alumina contents (wt.%) of the clinopyroxenes vary as follows:

Table 2.5 Selected clinopyroxene analyses.*

	M1 R	M1 Ph	B1 M	B1 P	B2 R	B3 M	B4 R	B4 Ph	B5 Ph	V1 M	60145 Ph
SiO_2	52.68	52.30	49.37	53.42	49.31	47.30	52.90	50.27	51.96	50.68	51.74
TiO_2			0.28		0.37	0.25	0.18		0.33		
Al_2O_3	2.19	3.31	7.31	1.34	6.52	9.79	2.51	3.72	1.38	4.89	2.76
Cr_2O_3				0.76	0.23	0.26	0.31				0.30
FeO	8.41	7.47	9.74	5.44	11.71	12.34	8.53	14.05	14.36	7.78	8.51
MnO									0.36		
MgO	17.00	16.70	13.96	17.46	13.78	13.00	16.38	13.20	13.03	14.94	17.19
CaO	19.53	20.22	19.32	21.58	18.09	17.06	19.18	18.75	18.90	21.35	19.14
Mg no.	78.27	79.93	71.88	85.09	67.72	65.30	77.39	62.63	61.80	77.37	78.24
Ca:Mg:Fe	39/48/13	41/47/12	42/42/16	43/49/8	39/41/20	38/40/22	39/47/14	39/38/23	39/38/23	44/43/13	38.5/48/13.5
Si	1.947	1.922	1.831	1.957	1.841	1.767	1.947	1.901	1.969	1.875	
Ti			0.008		0.010	0.007	0.005			0.009	
Al	0.095	0.143	0.32	0.058	0.287	0.431	0.109	0.166	0.062	0.213	
Cr				0.022	0.007	0.008	0.009				
Fe	0.259	0.229	0.302	0.167	0.366	0.386	0.263	0.444	0.455	0.241	
Mg	0.933	0.914	0.772	0.953	0.767	0.724	0.899	0.744	0.736	0.824	
Ca	0.771	0.796	0.768	0.847	0.724	0.683	0.757	0.760	0.767	0.846	
Total	4.005	4.006	4.001	4.004	4.002	4.006	3.989	4.015	4.001	4.008	

M = microlite, P = poikilitic, R = rim to opx, Ph = phenocryst.

* Analyses normalized to 100%.

M1: 2.83 to 8.50

B1 (microlites or phenocrysts): 2.97 to 7.31

B1 (xenolith): 1.32 to 1.85

B2: 1.74 to 9.11

B3: 0.87 to 9.79

B4: 1.44 to 3.72

B5: 1.25 to 1.49

V1: 3.44 to 6.27

V2, V3, and V4: 1.72 to 5.08.

2.4.4 Feldspars

Plagioclase occurring as phenocrysts in the bronzite andesite (B4) ranges from An_{71-73}, and in the perlitic dacite (B5) it occurs as a bimodal population of An_{71} and An_{82}.

2.4.5 Spinels

Compositional variation for the spinels is shown in Figures 2.5 and 2.6 and recorded in Tables 2.6 and 2.7. Fe^{3+} comprises 2-13% of the trivalent cations, overlapping the fields of spinel in mid-Atlantic Ridge basalts and alpine peridotites (Sigurdsson & Schilling, 1976). There are no real differences between spinels from the Cape Vogel, Mariana Trench or Bonin Islands high-Mg andesites, and the spinels in the bronzite andesite (B4) occurring within bronzite phenocrysts (xenocrysts) are similarly picrochromites.

In general the spinels are characterized by greater than 55% Cr_2O_3, less than 8.5% Al_2O_3, $Fe^{3+}/Fe^{3+}+Al+Cr$ less than 0.1, and Cr/Cr+Al greater than 0.80. On the Cr/Cr+Al versus $Mg/Mg+Fe^{2+}$ plot (Figure 2.5), some analyses plot in the fields for alpine type and stratiform complexes, however a significant number of analyses plot outside these fields due to their high Cr content.

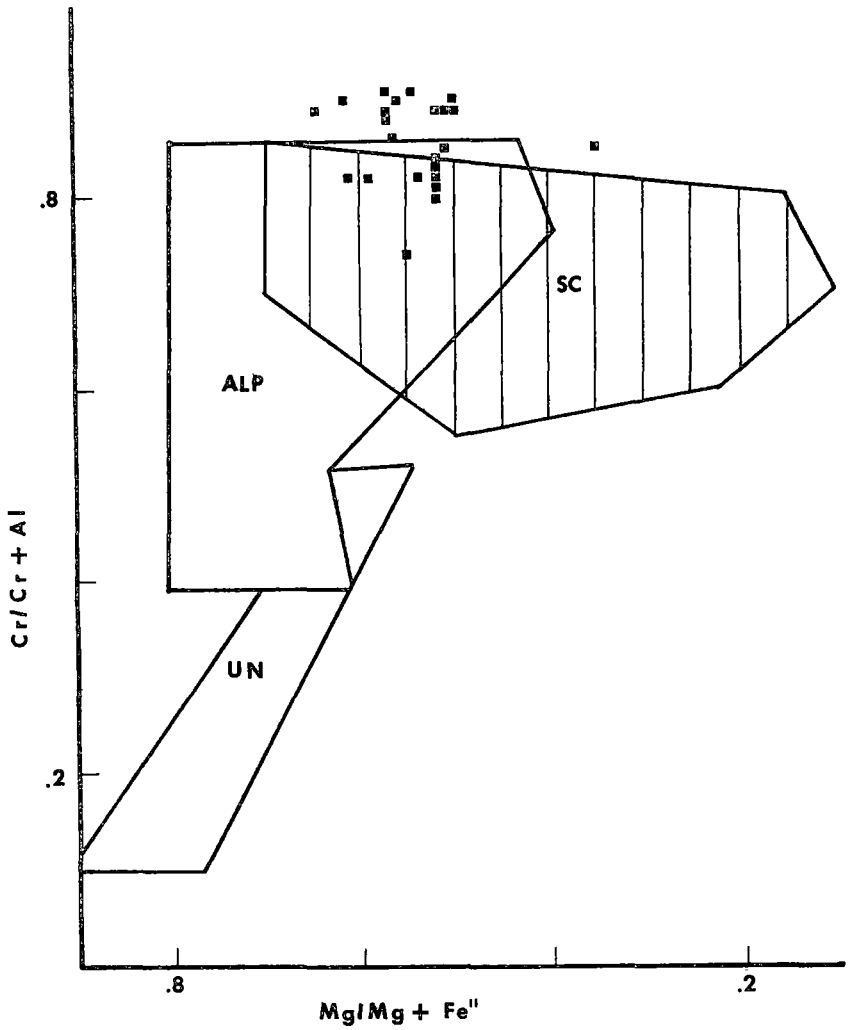

Figure 2.5 Comparison of Cr/Cr+Al versus Mg/Mg+Fe^{2+} in spinels from high-Mg andesites (solid squares) with fields for alpine peridotites (ALP), stratiform complexes (SC), and ultramafic nodules (UN). (After Rodgers, 1973.)

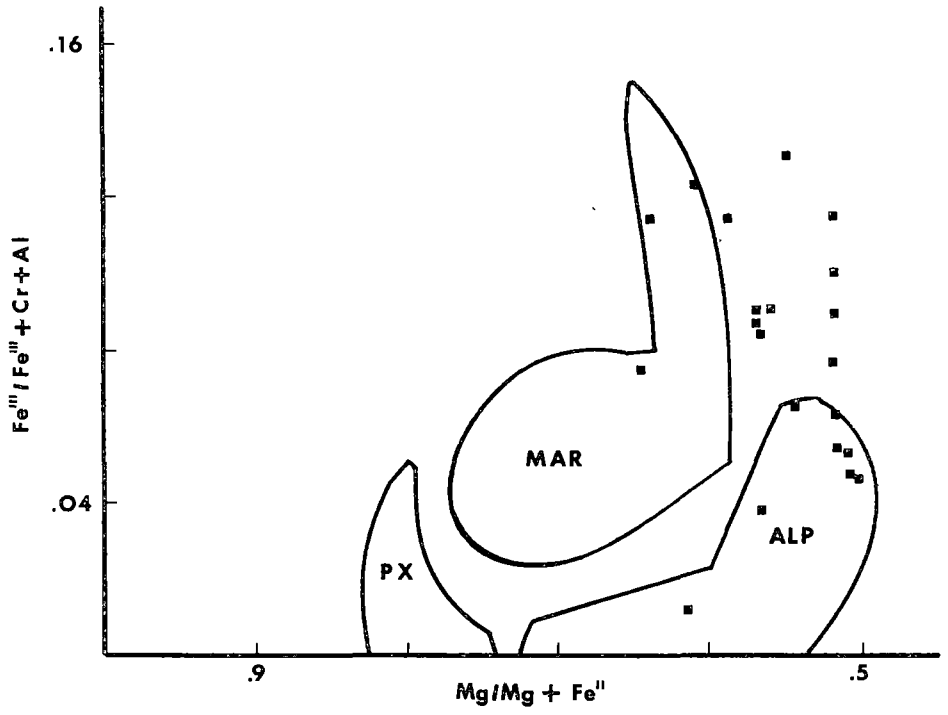

Figure 2.6 Range of $Fe^{3+}/Fe^{3+}+Cr+Al$ versus $Mg/Mg+Fe^{2+}$ in spinels from high-Mg andesites (solid squares). For comparison are fields for spinels from mid-Atlantic Ridge basalts (MAR), peridotite xenoliths (PX), and alpine peridotites (ALP). (After Sigurdsson & Schilling, 1976.)

Table 2.6

Selected chrome spinel analyses.ŧ

	1	2	3	4
Sample	V4	V3	V2	B4
MgO	13.17	7.59	9.72	10.26
Al_2O_3	5.12	6.80	4.86	6.99
TiO_2		0.33	0.18	
Cr_2O_3	63.39	57.15	64.63	61.34
FeO	12.84	21.55	17.97	17.55
Fe_2O_3†	6.09	7.30	2.93	4.27
Mg	5.170	3.071	3.917	4.081
Al	1.590	2.176	1.549	2.199
Ti		0.067	0.037	
Cr	13.202	12.267	13.818	12.944
Fe^{2+}	2.830	4.893	4.064	3.917
Fe^{3+}	1.208	1.491	0.596	0.858
Total	24.0	23.97	23.98	24
$Mg/Mg+Fe^{2+}$	0.65	0.39	0.49	0.51
Cr/Cr+Al	0.89	0.85	0.90	0.85
$Fe^{2+}/Fe^{2+}+Fe^{3+}$	0.701	0.766	0.872	0.82
$Fe^{3+}/Fe^{3+}+Cr+Al$	0.076	0.094	0.037	0.054
Mg-number silicate	91*	83.87**		88**

* clinoenstatite

** bronzite

† Fe^{3+} calculated from structural formula (after Rodgers, 1973).

ŧ Analyses normalized to 100%.

Table 2.7

Range of chrome spinel compositions.*

	Og-44 (4)**	V2 (2)††	V3 (8)	V4 (6)	V4 (4)	B4 (3)	60144	Marianas (3)†
Cr_2O_3	54.49-64.29	59.91-64.63	54.57-63.87	61.19-64.07	54.88-56.02	50-67.8	64.1	51-62
Al_2O_3	5.59-8.80	4.86-7.97	5.16-9.30	4.04-5.12	7.92-8.58	5-11.94	6	5-9.8
$Mg/Mg+Fe^{2+}$	0.55-0.64	0.49-0.52	0.39-0.57	0.54-0.69	0.52-0.61	0.51-0.62	0.68	0.34-0.62
Cr/Cr+Al	0.81-0.89	0.83-0.90	0.80-0.89	0.88-0.91	0.82	0.74-0.90	0.88	0.78-0.89
$Fe^{3+}/Fe^{3+}+Al+Cr$	0.040-0.098	0.037-0.055	0.047-0.107	0.066-0.092	0.115-0.124	0.012-0.132	0.037	0.063-0.11
$Fe^{2+}/Fe^{2+}+Fe^{3+}$		0.813-0.872	0.691-0.849	0.701-0.775	0.612-6.78	0.631-0.941	0.80	0.65-0.79

* Fe^{3+} calculated from structural formula (after Rodgers, 1973)

** from Shiraki & Kuroda (1977)

† from Sharaskin *et al.* (1980)

†† numbers in brackets refer to number of analyses

Based on the work of Irvine (1967), Jaques & Green (1980), and Crawford (1980) some inter-dependence of the spinel Cr/Cr+Al with its $Mg/Mg+Fe^{2+}$ or spinel Mg-number with the host silicate Mg-number could be expected to occur. The lack of any such trends in the analysed Cr-spinels and host phases may reflect, either singularly or in combination, subsolidus re-equilibration or alteration of original oxidation state of the spinels.

2.5 DISCUSSION AND SUMMARY

The high-Mg andesites of Cape Vogel, Bonin Islands and Mariana Trench are predominantly clinoenstatite and/or orthopyroxene phyric. The importance of low-Ca pyroxenes in these rocks is reflected in their bulk compositions which show very little variation in silica content over a wide range of Mg-numbers (Chapter 3; Dietrich *et al.*, 1978; Sharaskin *et al.*, 1980; Dallwitz, 1968). Consequently changes in high-Mg andesite composition are best modelled by fractionation of these phases as pointed out in this chapter, Shiraki & Kuroda (1977), Chapter 3, and Dallwitz (1968).

The Ca-poor pyroxenes in the high-Mg andesites reflect the calcium content and normative Di/Di+Hy of the melt. Referring to Table 2.1 and the previous discussion, we can generalize that highly magnesian, silica-rich lavas (Mg_{70-80}) with compositions appropriate to precipitation of Ca-poor pyroxene of Mg_{85-95} composition may crystallize protoenstatite only if they have normative Di/Di+Hy ratios of < 0.2. This suggestion is applicable not only to the rocks described here but also to those in Shiraki *et al.* (1980) and Komatsu (1980). Komatsu (1980) concluded that there was no significant chemical differences between clinoenstatite-bearing and clinoenstatite-free lavas.

This conclusion was based on a very limited data base and includes the only known exception to this generalization (the M-1 composition of Komatsu, 1980). The CaO/Al_2O_3 ratio (0.93) of the unusual clinoenstatite-bearing high-Mg andesite of Komatsu (1980) is high for these rocks (see Chapter 3), and based on the petrographic description given in Komatsu (*ibid.*) it is possible that this may be due to analysis of a clinopyroxene-rich portion of the rock. The Ca content of the orthopyroxenes also reflects the normative Di/Di+Hy ratio of the melt. In general the Cape Vogel orthopyroxenes from samples V2-V4 (Di/Di+Hy = 0.069-0.091) are lower in Ca than M1 (Di/Di+Hy = 0.167), which are lower than the Bonin Island samples (B1-B3) (Di/Di+Hy = 0.252-0.356) and Cape Vogel (V1) (Di/Di+Hy = 0.210). Komatsu (1980) also noted that the changes in pyroxene composition in the rocks he studied may have been partly due to bulk rock compositional differences, particularly Ca content.

The crystallization of clinoenstatite from a melt is discussed in more detail in Chapter 5, however one aspect noted earlier can be discussed here. The $K_{D_{OE}}^{PE} = (Mg/Fe)^{PE}/(Mg/Fe)^{OE}$ would appear to have a value of ~1.1-1.2 for equilibrium crystallization of bronzite and protoenstatite. The occurrence of values for this ratio of 1.28-1.52 in some Cape Vogel lavas, along with petrographic evidence for the crystallization of protoenstatite around bronzites indicates that a simple cooling path is inadequate. This suggests the possibility of convective motion in a magma chamber and/or magma mixing.

The increase in Ca (and generally Al) contents with decreasing Mg-number in the orthopyroxenes up to approximately Mg_{80} is attributed to the absence of coexisting Ca-rich pyroxene. This interpretation is consistent with the decrease or levelling-off of Ca (and Al) contents after the appearance of a stable Ca-rich pyroxene, with $<Mg_{80}$ in both the

high-Mg andesites and their less primitive differentiates (cf. Komatsu, 1980). The pattern of decreasing or non-increasing Ca content in the orthopyroxenes of B1 is evidence for at least local saturation in diopside with Mg/Mg+Fe >80, as is witnessed by the occurrence of Mg_{85} clinopyroxene (see Table 2.5). This could, for example, result from resorption of either a xenolith enriched in calcic clinopyroxene or a xenocryst of clinopyroxene.

Olivine crystals in high-Mg andesites are often rimmed by clinoenstatite and/or orthopyroxene (this chapter; Kuroda & Shiraki, 1975; Komatsu, 1980) and it would appear that olivine has a reaction relationship with liquid. The occurrence of a range of olivine compositions suggests that the reaction relationship is a sliding reaction in which early formed magnesian olivine reacts over a small temperature interval, becoming more Fe-rich and less abundant as it is replaced by Ca-poor pyroxene. Fe-rich olivine microphenocrysts (Kuroda & Shiraki, 1975) may be a reflection of the sliding nature of the reaction relationship and/or be metastable quench products. The occurrence of euhedral Mg_{85} olivine crystals in glass in 60144, which also has Mg_{92} olivines exhibiting replacement textures (i.e. rimmed by orthopyroxene and rounded shapes), suggests this olivine is possibly a xenocryst. There is insufficient evidence to evaluate that magma mixing has occurred; however, this is one possible interpretation. It is also suggestive of re-equilibration of non-included olivine, and armouring of included olivine.

The glass occurring in these rocks is variably altered, with microprobe analyses totals ranging from 85-95%. The Mg-numbers of the glass are low (25-35) and suggest that the glass compositions are residual from crystallization which includes the quench overgrowths and microlites. Glass compositions are thus not particularly

significant in discussing crystal fractionation trends as they are determined by quench crystallization. There are also uncertainties in interpreting water contents of glasses (Carmichael, 1979; cf. Cameron *et al.*, 1979, 1980). The occurrence of feathery clinopyroxene-amphibole microlites in the glasses of HMA has received some attention (Cameron *et al.*, 1979), but is is not possible to quantify the water content of a liquid on the basis of the presence of quench amphibole and absence of information on pressure and temperature cooling rate.

The mineralogy and texture of the high-Mg andesites is not conducive to the use of clinopyroxene-orthopyroxene (e.g. Wells, 1977) or olivine-spinel (e.g. Roeder *et al.*, 1979) geothermometers. However, coexisting pyroxenes in the xenolith of B1, the bronzite andesite (B4) and perlitic dacite (B5) have been used to determine temperatures, using the equation developed by Wells (1977). A poikiolitic clinopyroxene (Mg_{85}) enclosing orthopyroxene (Mg_{82}) in the xenolith of B1 gave a temperature of ~1050°C. This temperature is a minimum temperature for crystallization of the magmas as the orthopyroxene-clinopyroxene pair probably formed during the equilibration process taking place between the cooling melt and a xenolith or xenocryst. An intergrown orthopyroxene (Mg_{72})-clinopyroxene (Mg_{76}) pair in B4 gave a temperature of 1120°C, while orthopyroxenes and clinopyroxenes (both cores and rims) give temperatures of 1120°C and 1120-1180°C respectively (for orthopyroxene Mg_{74-77} and clinopyroxene of Mg_{77-78}). These temperatures are virtually indistinguishable and are probably the minimum (quenching in) temperature of formation of the clinopyroxene. A temperature of 1045°C was calculated on an Mg_{59} clinopyroxene-Mg_{56} orthopyroxene pair in the perlitic dacite (B5).

If the temperature of ~1150°C for B4 is accepted, then either HMA were at T > 1150°C (which implies low water contents in the magma series) or alternatively a temperature as low as ~1150°C for HMA is possible, with the necessary corollary that these HMA began crystallizing at higher P_{H_2O} than the andesite B4.

Chapter 3

GEOCHEMISTRY

3.1 INTRODUCTION

Previous studies of high-Mg andesites had shown that these rocks were unusual in major element composition and some trace element patterns, e.g. Sun & Nesbitt (1978), Dietrich *et al*. (1978), Nesbitt & Sun (1980). However, a detailed study of HMA from one locality and a comprehensive study of the trace element characteristics of these rocks was lacking. In this study, 21 samples from Cape Vogel have been analysed, along with six other samples from the Bonin Islands and Mariana Trench, for up to 37 major and trace elements. The results from the Cape Vogel area have been presented in Jenner (1981).

Selected samples from this study were given for isotopic analysis and preliminary results were published by Hickey *et al*. (1980). Although detailed discussion of the Sm/Nd isotopics in HMA is therefore not presented in this thesis, some essential and inter-related aspects of the results are discussed.

The data and discussion are presented in the following manner. First, the chemistry of the HMA from the different localities is presented and comparisons between HMA are made. Some detailed discussion of the Cape Vogel rocks is presented. Secondly, the HMA are compared briefly with island-arc and other primitive or primary volcanics, so as to outline major differences. Thirdly, a detailed comparison of trace element patterns for HMA and a variety of other rocks is presented. The purpose of this section is to elucidate the origin of the trace element characteristics of HMA and to present a detailed comparison with other volcanics.

3.2 RESULTS

3.2.1 Analytical Techniques

Major elements were determined by X-ray fluorescence (XRF), using the heavy-absorber technique of Norrish & Hutton (1969). Ba, Rb, Sr, Y, Zr, Nb, Cr, Ni, Sc, and V, on most samples, were determined by XRF on pressed powder pellets. Pure element standards in silica or kaolin and mass absorption coefficients calculated from major element composition were used for calibration and determinations of trace elements (cf. Norrish & Chappell, 1977). Excellent agreement with international standards is found (Table 3.1). Rare-earth elements (REE) were determined by either spark source mass spectrography (SSMS) by the author or radiochemical neutron activation (RNAA) by F. Frey and R. Hickey. Analytical uncertainty in SSMS is reported in Taylor & Gorton (1977); that for RNAA is given by Frey *et al.* (1974). All REE (excluding Lu) and commonly, Cs, Th, U, Hf, Zr, Nb, and Y, were determined for each sample by SSMS whereas only eight REE are reported for RNAA. Nb determinations on SSMS are accurate to ~ lower levels than those determined by XRF and thus long counting times and internal calibration with SSMS values have been used to determine Nb by XRF. Errors involved in this method are difficult to estimate but Nb values to 1 ppm (± 25-50%) are reported. All distinctions between HMA groups based on Zr/Nb ratios are made solely on SSMS data.

3.2.2 Trace Element Nomenclature

The following nomenclature for trace element groups has been adopted in this thesis (modified from Saunders *et al.*, 1980): low field strength (LFS) - Cs, Rb, K, Ba, Sr, Th, and U; high field strength (HFS) - Zr, Hf, Ti, P, and Nb; rare earth elements (REE) - light REE

Table 3.1

Chemical data for standard rocks.

	BCR-1	AGV-1	JB-1	PCC-1	DL
No.†	[2]	[1]	[1]	[1]	[2]
SiO_2	54.53				
TiO_2	2.30				
Al_2O_3	13.67				
Fe_2O_3*	13.52				
MnO	0.19				
MgO	3.56				
CaO	7.06				
Na_2O	3.53				
K_2O	1.72				
P_2O_5	0.34				
Ba	746	1221			3
Rb	48	69			1
Sr	330	654			4
Y	45	22			1
Zr	187	227			4
Nb	14	14			1
Cr	15	10	442	2626	3
Ni	11	19	131	2312	3
Sc	28	14			1
V	409	124			3

Major elements: wt.%

Trace elements: ppm

* total Fe as Fe_2O_3

DL: calculated detection limit (3δ) for standards matrix (silica or kaolin).

No.† – number of determinations

(LREE) = La-Sm; heavy REE (HREE) = Er-Lu, including Y; and transition metals (TE) = Cr, Ni, Sc, and V.

Reasons for these subdivisions, excluding the last group, are discussed in Saunders *et al.* (1980) (see also Pearce & Norry, 1979). The transition elements are grouped together based on their similar behaviour and more compatible nature (distribution coefficients for crystal/liquid > 0.3, Frey *et al.*, 1978).

3.2.3 Alteration

Petrographically the rocks are relatively free of secondary alteration, e.g. glass is preserved, however this does not ensure that some elements have retained their primary igneous abundances. As a first approximation it is assumed that all HFS and HREE have been immobile as elements in these groups are the least susceptible to effects of post-magmatic alteration processes (Pearce, 1975; Coish, 1977; Pearce & Norry, 1979; Saunders *et al.*, 1980). In addition, an element is assumed to be immobile if it behaves in a linear, or predictable manner, relative to an element of accepted high immobility (e.g. Zr) or relative to a ratio of immobile or relatively immobile major elements (e.g. Mg-number) (cf. Coish, 1977; Hellmann *et al.*, 1979; Jenner & Fryer, 1981).

3.2.3.1 Major elements

In large part, the major element chemistry of the HMA appears to reflect primary igneous variation. This is apparent in terms of the correlation between petrography, mineral chemistry, and major element composition discussed in Chapter 2. Some mobility of selected major elements is however indicated by both the petrography and geochemistry. In some Cape Vogel samples silica-replacement or addition textures can be observed in thin section and although rocks obviously affected by this process have not been included in the results, some scatter in

SiO_2 contents may be due to secondary processes. Na_2O and K_2O show no predictable trends against Mg-number or HFS element contents in Cape Vogel rocks and are considered mobile elements in the sense of secondary addition or removal. Na_2O and K_2O abundances are also erratic in some Mariana Trench and Bonin Island samples (see below) and it is difficult to determine what the primary abundances were and if the differences in abundances between the three HMA localities reflect original differences. At least some of the scatter in alkali element abundances is attributable to the amygdaloidal nature of HMA.

3.2.3.2 Trace elements

Hart (1969, 1971) and others have emphasized the mobility of some members of the LFS group at extremely low grades of alteration. As noted earlier, K appears to have been mobile and Rb which shows considerable scatter versus Zr (Figure 3.1) is likewise interpreted as a mobile element. Note that this is based primarily on the Cape Vogel samples, since there is insufficient data available from the other localities. The limited number of Cs analyses makes it difficult to establish its behaviour. Sample I (Table 3.2), from a subgroup of the HMA (see below), has a reasonably high Cs content (0.7 ppm) compared to other Cape Vogel HMA; however, these HMA are from a different subgroup, and other HMA in the same grouping as sample 1 also have higher Cs abundances. It is possible that this is an original feature of the group (type-C, see below). The Cs content in sample 18 (Table 3.2) is 1.3 ppm and this correlates with anomalous Ba and Sr (Figure 3.1; Table 3.2). This is thought to reflect mobility of these elements, in this instance. The behaviour of Ba is enigmatic. Ba is resistant to hydrothermal alteration up to greenschist facies in oceanic basalts (Humphris & Thompson, 1978). These are more severe conditions of metamorphism than the HMA of this study undergone, yet Ba in Cape Vogel samples do not correlate well

Table 3.2 ANALYSES OF HIGH Mg ANDESITES FROM CAPE VOGEL, PNG

Sample No.	1	2	3	4	5	6	7	8	9	10	11	12	13	14	15	16	17	18	19	20	21	
Coll. No.*	47799	47810	47811	47816	47786	47787	47788	47789	47790	47792	47793	47795	47796	47797	47804	47805	47806	47807	47809	47812	47815	
SiO_2	56.80	57.80	57.60	57.60	57.32	58.36	58.08	56.86	56.80	57.44	58.07	57.26	57.49	57.51	55.55	59.11	56.96	57.10	57.08	57.79	58.42	
TiO_2	.30	.46	.34	.27	.36	.42	.15	.13	.21	.28	.31	.20	.25	.22	.09	.15	.14	.23	.16	.29	.27	
Al_2O_3	11.80	11.50	9.10	8.50	9.86	11.42	7.73	5.35	7.77	8.50	9.34	7.45	8.99	7.56	5.07	8.09	5.39	7.87	6.01	9.34	9.32	
FeO^T	8.63	9.46	9.34	9.83	9.24	9.46	9.95	9.50	9.88	9.21	9.57	9.73	10.21	9.80	9.75	9.70	9.49	10.19	9.46	9.62	9.17	
MnO	.20	.20	.20	.26	.16	.18	.21	.22	.21	.17	.18	.20	.26	.20	.20	.19	.21	.22	.20	.19	.17	
MgO	12.60	12.60	16.80	17.10	14.73	12.02	18.54	24.55	19.62	17.27	15.11	19.62	16.48	19.01	24.29	17.40	23.61	17.64	23.31	15.77	16.14	
CaO	7.90	6.00	4.90	5.10	5.89	6.66	4.21	2.95	4.59	6.05	6.01	4.37	5.29	4.38	2.74	4.62	3.18	4.22	3.34	5.65	5.37	
Na_2O	1.10	1.30	1.10	.60	.81	1.07	.85	.27	.61	.36	.99	.94	.62	1.05	.29	.69	.87	2.05	.05	1.15	.81	
K_2O	.40	.40	.20	.40	.73	.38	.24	.16	.24	.67	.35	.21	.43	.21	.29	.23	.12	.46	.36	.27	.26	
P_2O_5					.04	.04	.03	.03	.03	.04	.06	.02	.04	.03	.01	.02	.03	.03	.01	.04	.06	
$Mg(Mg+Fe^t)$	72.2	70.4	76.2	75.6	74	69.4	76.9	82.2	78	77	73.8	78.2	74.2	77.6	81.6	76.2	81.6	75.5	81.5	74.5	75.8	
CaO/Al_2O_3	.67	.52	.54	.60	.60	.58	.54	.55	.59	.71	.64	.59	.59	.58	.54	.57	.59	.54	.56	.60	.58	
Cs	.66					.30	.17		.16							.15		1.27				
Rb	8	7	5	6	14	9	6	3	4	10	7	1	6	4	5	1	3	11	2	6	5	
Ba	39				106	34	31	20	25	65	48	59	115	64	30	32	22	68	36	42	39	
Sr	274	91	78	83	339	96	69	33	63	209	110	57	102	56	42	59	34	110	33	85	73	
Th	.40					.85	.52		.50							.77		.42				
U	.12					.23	.12		.14							.17		.11				
Zr	30	55	49	36	53	62	32	19	28	41	42	34	40	35	14	42	22	24	23	47	53	
Hf	.79					1.50	.70		.81							.98		.66				
Nb	.88				1.8	3.2	1.7	.9	1.32	3.6	.9	1.6		1.9		2.2	2.8	1.3	2.3	1.6	1.4	
Cr	715	664	1790	1615	1193	735	2225	2868	2191	1396	1414	2105	1386	2003	2976	2178	2885	1831	2586	1660	847	
V	187	165	132	145	171	211	158	111	149	153	177	155	183	159	125	163	118	164	118	175	164	
Sc	35	34	28	31	29	36	29	21	28	32	33	28	34	30	26	30	24	28	24	32	28	
Ni	154	189	334	334	264	212	415	657	574	316	310	445	292	416	596	415	603	288	558	393	163	
La	1.47	4.80	4.57	3.11		4.06	2.88		2.03							3.25		2.10				.367 X
Ce	3.51	9.47	9.16	6.48		9.74	5.35		4.35							6.45		4.30				.957
Pr						1.07	.62		.55							.74		.53				.137
Nd	2.09	4.72	4.44	2.95		4.64	2.38		2.45							3.00		2.35				.711
Sm	.602	1.127	.972	.689		1.19	.56		.60							.69		.58				.231
Eu	.210	.392	.326	.234		.39	.17		.21							.22		.18				.087
Gd						1.16	.50		.63							.61		.57				.306
Tb	.144	.221	.178	.130		.22	.09		.12							.11		.10				.058
Dy						1.33	.57		.76							.69		.64				.381
Ho						.29	.11		.17							.15		.13				.085
Er						.84	.28		.48							.43		.35				.249
Yb	.809	.820	.653	.521		.72	.29		.42							.41		.37				.248
Lu	.133	.131	.108	.087																		.042
Y	7	7	6	3	8	9	3	2	4	7	6	4	4	5	2	4	3	3		6	6	2.0

* University of Tasmania, Geology Department collection numbers

T Total Fe as FeO

t total Fe as Fe^{+2}

X Chondrite normalizing values for REE plots (from Taylor, pers. comm. 1979).

with Zr (Figure 3.1). This variability may be partly due to source heterogeneity and while this is a subjective interpretation, I suggest that Ba contents are a fairly reliable indicator of the original abundances. The Sr, Th, and U contents of Cape Vogel HMA appear to have been relatively immobile (Figure 3.1; Table 3.2) and are interpreted as reflecting original variations in the HMA.

LREE may be mobile under some circumstances (Hellmann *et al.*, 1979). The correlation of La with Zr in Cape Vogel samples (Figure 3.2) and the observation that significant changes in other elements usually accompany LREE mobility (Jenner & Fryer, 1981), suggest the LREE are immobile in HMA.

Behaviour of the TE during alteration is less certain than that of the HFS, but Cr, Ni, V, and Sc appear to be relatively immobile (Hart *et al.*, 1974; Pearce, 1975; Coish, 1977; Humphris & Thompson, 1978). For this reason and the consistent trends followed by these elements (Figure 3.3), their abundances are thought not to have changed significantly due to alteration.

3.2.4 Major Elements

Major element analyses for Cape Vogel HMA are given in Table 3.2 and those for Mariana Trench and Bonin Island samples are in Table 3.3. Analyses have been recalculated on an anhydrous basis with total Fe as FeO. Loss on ignition mostly ranged from 2-6% except for one sample (Table 3.2, no. 10) which has a loss of 10%. Major element analyses for 61496-61499 (M1, B1-B3) (Table 3.3) are microprobe analyses of fused glasses, while 61500-61501 (B4, B5) are from Shiraki & Kuroda (1977). Averages from other studies are also included in Table 3.3.

In general the HMA are characterized by SiO_2 contents of 56-59 wt.%, low TiO_2 (0.10-0.46 wt.%), high Mg-numbers [mol. prop. $100\ MgO/(MgO+FeO^t)$] (67-82), and CaO/Al_2O_3 ratios generally less than 0.60.

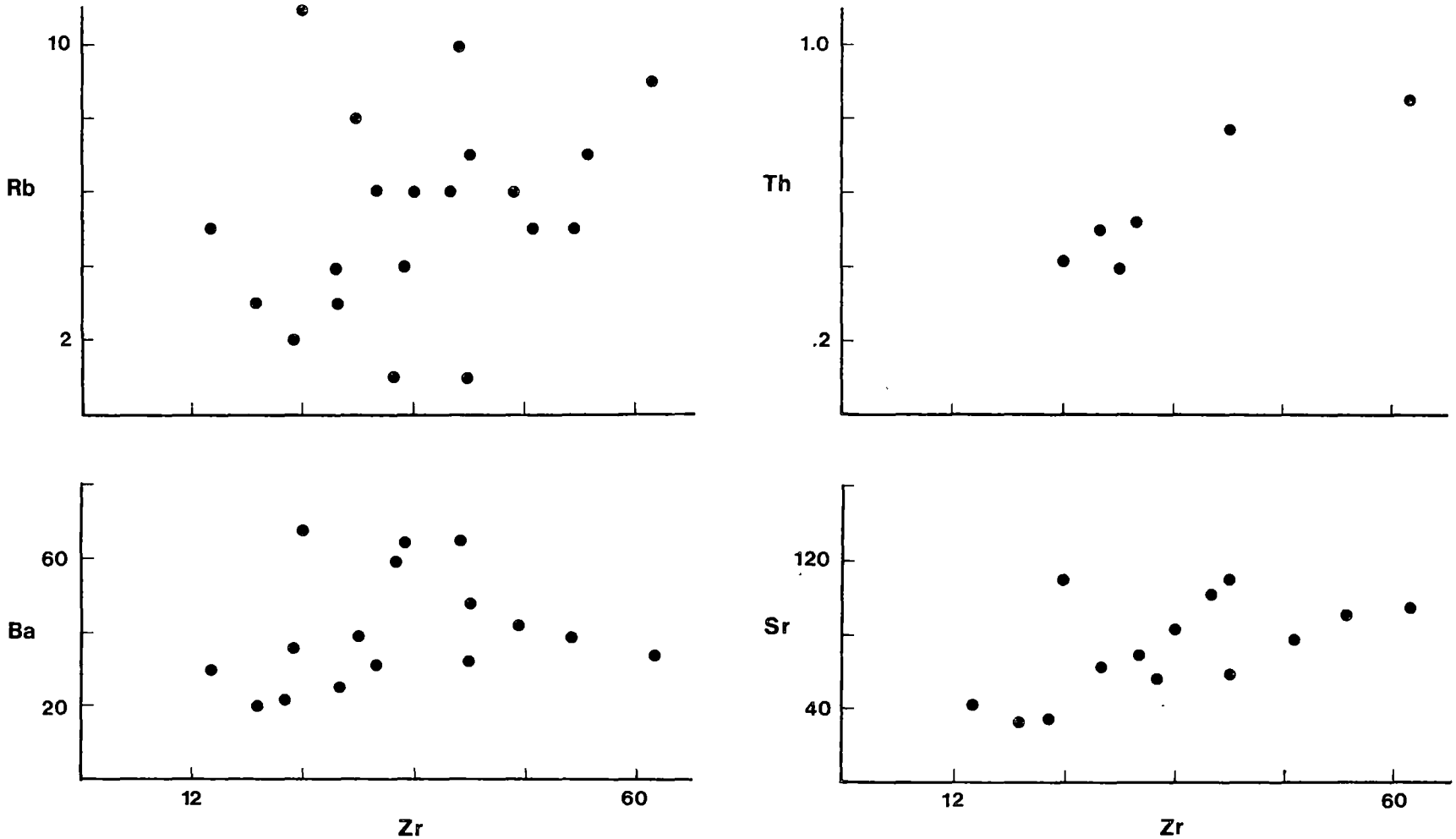

Figure 3 1 LFS elements vs Zr for Cape Vogel HMA X-axis (Zr) common to all plots.

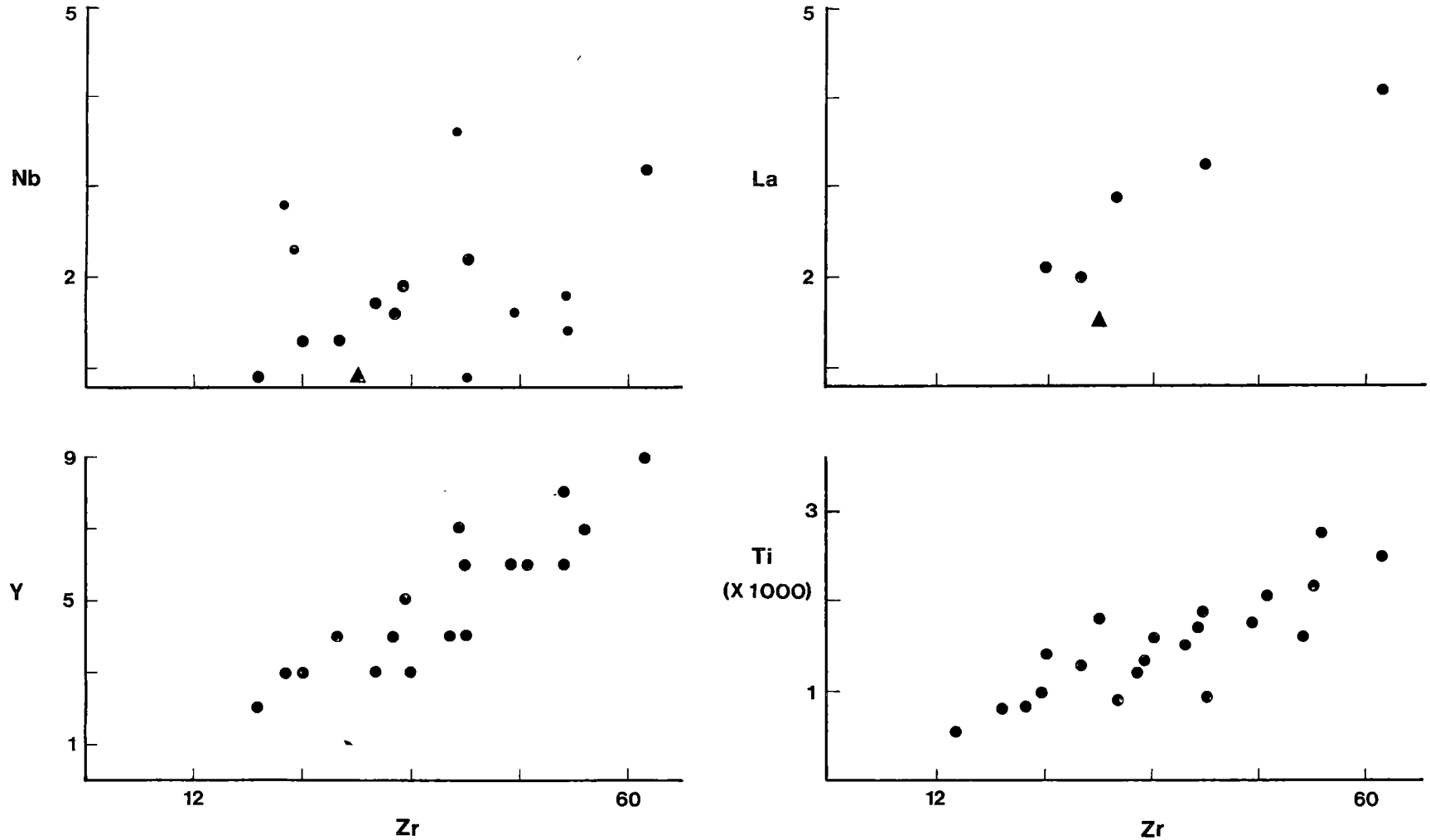

Figure 3 2 Selected HFS elements and REE vs Zr, Cape Vogel HMA X-axis (Zr) common to all plots In Nb vs Zr large solid dots SMSS and coherent XRF analyses, small dots for anomalous values (see text for discussion) Triangle in Nb and La vs Zr is for sample 1, Table 3 2 (type-C HMA, see text for discussion)

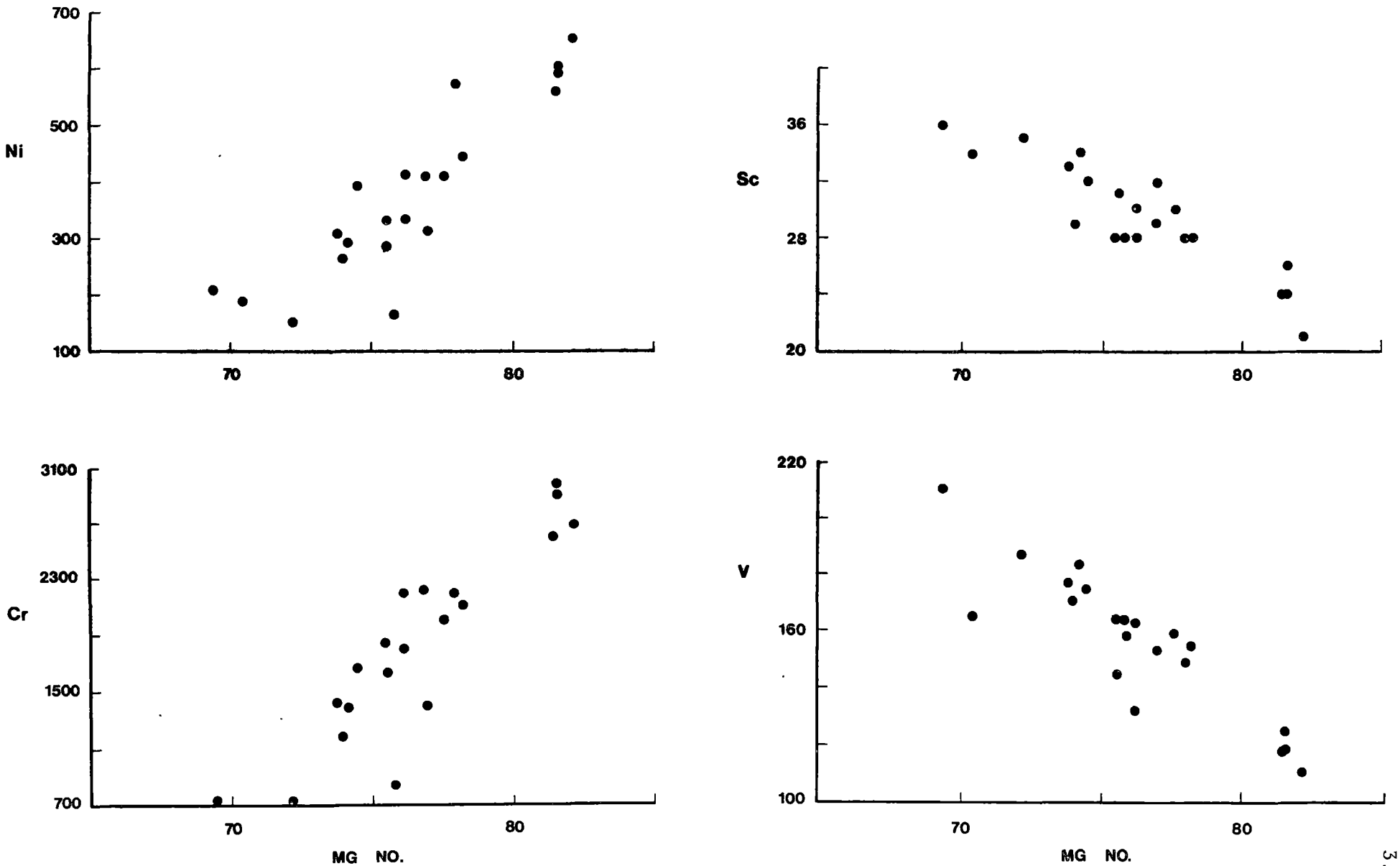

Fig. 3.3 Trace element vs Mg-number for Cape Vogel HMA.

Table 3.5 Analyses of HMA from the Mariana Trench, Bonin Islands and Cape Vogel

	Mariana	Bonin Islands					Mariana		PNG	Bonin		Cape Vogel
Sample	M1	B1	B2	B3	B4	B5	Av. M*	M**	P**	1	2	CV74-77
UTGD no	61496	61497	61499	61500	61501	61502						
SiO_2	57.33	58.46	57.25	58 43	59 69	69 56	57 68	57 42	56.04	56.90	58 70	57.80
TiO_2	0.14	0.10	0 12	0 17	0.27	0 25	0.19	0 19	0 24	0.22	0.20	0.26
Al_2O_3	9 75	13 37	10 61	11 35	14 44	13.26	10 55	10 73	8 02	11 96	10 56	8 73
FeO†	9 06	8 27	8.80	8.57	8.24	5 94	8.76	8 25	10 49	8.34	8.59	9 65
MnO	0.13	0.14	0.12	0 12	0.23	0.12	0 17	0.18	0.20	0.18	0.21	0 20
MgO	15 19	9 39	12.27	11 40	5.71	1 65	14.25	15.82	19.29	13 19	12 02	16.79
CaO	5.86	8.11	9.69	7 76	8.38	4 80	5 76	5.63	4.82	7.18	7.60	5.13
Na_2O	1.59	1.59	0 87	1.74	2 28	3 27	1.79	1.70	0.37	1.46	1.48	0.90
K_2O	0.93	0 70	0.30	0 51	0.51	0 95	0 80	0 80	0 49	0 42	0 62	0.39
P_2O_5	0.08						0.03	0.03	0 04	0.02	0 01	
$Mg/(Mg+Fe^t)$	74.92	66.92	71.30	70 33	55.25	33 11	74.35	74 91	76.62	73.81	71.40	
CaO/Al_2O_3	0.60	0.61	0.91	0.68	0.58	0.36	0.55	0 52	0 60	0.60	0 72	0.59
Cs	0.43	0.33										
Rb	14	17	7	10	12	21		13	5.1			
Ba	24	25						27	34			62
Sr	100	101	59	71	88	111	116	103	90			120
Th	0.50											0.57
U	0.12											0.13
Zr	36	25	11	19	30	44	31	28	40			42
Hf	0.93	0.55					0.73					0.78
Nb	0.72	0.44							2			1.94
Cr	1386	538	888	832			798	1420	1460			1612
V	132	174	145	164			163	145	172			161
Sc	31	36	45	37	32	24	30	30	34			30
Ni	258	140	111	205			276	234	328			321
La	1.27	1.27	0.713	0 967	1.13	1 82		0 978	2 91			3 18
Ce	2.93	2 57	1.62	2 15	2 69	3.96		2 14	6.52			
Nd	1 85	1.65	0 97	1.44	1 95	2 69		1 51	3.08			
Sm	0.528	0.426	0 266	0.43	0 623	0 769		0 454	0 745			0 70
Eu	0 171	0.146	0 107	0 149	0 231	0 268		0.170	0.293			
Gd								0.590	0 844			
Tb	0.115	0 099	0.078	0.111	0 160	0 188						
Dy								0.761	0.854			
Er								0.544	0 541			
Yb	0.602	0 591	0 480	0.665	0 894	1 08		0 634	0 561			
Lu	0.104	0 103	0 084	0 116	0 149	0 186		0 104	0 094			0.45
Y	5	5	2	5	8	7		5	3			5

* Mean from Dietrich *et al* (1978) ** From Sun & Nesbitt (1978)
Bonin 1 and 2 from Komatsu (1980), Shiraki *et al* (1980) CV74-77 - this study
† - total Fe as FeO

Comparison of Mariana Trench (MT) HMA with an average of ten HMA from Cape Vogel (CV) (of similar Mg-numbers) shows the following: (i) CaO/Al_2O_3 ratios in the two areas are very similar [0.55 (MT) vs. 0.59 (CV)]; (ii) TiO_2 contents are marginally higher in MT rocks; (iii) MgO contents are higher at a given Mg-number in CV; and (iv) Na_2O and K_2O are on average about twice as high in MT HMA.

HMA from the Bonin Islands are divisible into two groups (see Table 3.3) based on Mg-number and CaO/Al_2O_3 ratio. The high-Mg group (Mg-numbers 73-76) has consistently low CaO/Al_2O_3 ratios (< 0.60) while the low-Mg group has Mg-numbers of 66-72 and variable CaO/Al_2O_3 ratios (ranging from 0.53-0.93). The origin of the CaO/Al_2O_3 ratio variation in the latter group is unknown, however it may in part correlate with occurrence of clinopyroxene phenocrysts (< Mg_{80}) (see Chapter 2). The most magnesian Bonin Islands HMA have higher CaO and Al_2O_3 but almost identical CaO/Al_2O_3 ratios; slightly lower TiO_2, lower SiO_2 and MgO and higher (~ 1.5x) Na_2O contents; when compared to Cape Vogel rocks of similar Mg-number. The less magnesian "boninites" or Bonin Islands HMA are higher in SiO_2, Al_2O_3, Na_2O, and K_2O, and lower in TiO_2 and CaO, and have a higher average CaO/Al_2O_3 ratio (0.72) than Cape Vogel HMA of similar Mg-number (see Table 3.2, columns 1, 2, and 6).

As noted earlier, the Bonin Islands are unique amongst occurrences of HMA in having associated more fractionated volcanics which are probably related by fractional crystallization (Shiraki & Kuroda, 1977; Shiraki *et al.*, 1978). Analyses for a bronzite andesite (61501/B4) and a perlitic dacite (61502/B5) from Chichi-jima are given in Table 3.3.

3.2.5 Trace Elements

Trace element abundances and patterns are given in Tables 3.2 to 3.5, and Figures 3.1 to 3.7. Many of the plots contain data from Cape Vogel alone, the reason for this is two-fold: first, there is a much larger data base for Cape Vogel samples, and secondly, as will be shown later, plotting all the samples together would involve mixing of two different groups.

The HMA are characterized by high Ni and Cr contents ranging from 111-657 and 538-2976 ppm, respectively. Cr/Ni ratios (Table 3.4) overlap widely although on average the Mariana Trench HMA may have a lower value. The abundance of V and Sc is similar in all areas, however on average, Ti/V, Ti/Sc, and V/Sc ratios decrease from Cape Vogel to Mariana Trench to Bonin Islands. Note the large range in values for Ti/V and Ti/Sc in Cape Vogel, this is discussed in Section 3.2.8.

Excluding Sr, Cs, Th, and U, the HMA are characterized by abundances of incompatible elements less than 10x chondritic and/or primitive mantle (Figure 3.7). The overall abundance of incompatible elements appears to decrease from Cape Vogel to Mariana Trench to Bonin Islands.

Two distinct REE and trace element patterns occur in the HMA (Figures 3.4, 3.5, 3.7). The Mariana Trench and Bonin Islands HMA and one sample from Cape Vogel (Table 3.2, column 1) are characterized by a concave or dish REE pattern and a positive, normalized, Sr anomaly. HMA with these characteristics have been termed *type-C* ("concave") HMA (Jenner, 1981). The majority of the Cape Vogel HMA have a marked REE enrichment; which is accompanied by a loss, or decrease in size, of the positive, normalized, Sr anomaly. These HMA are termed *type-E* ("enriched") HMA (Jenner, 1981), and have as yet been recognized only at Cape Vogel.

Selected trace element ratios are given in Table 3.5 and there is an overall similarity between type-C HMA from the different localities,

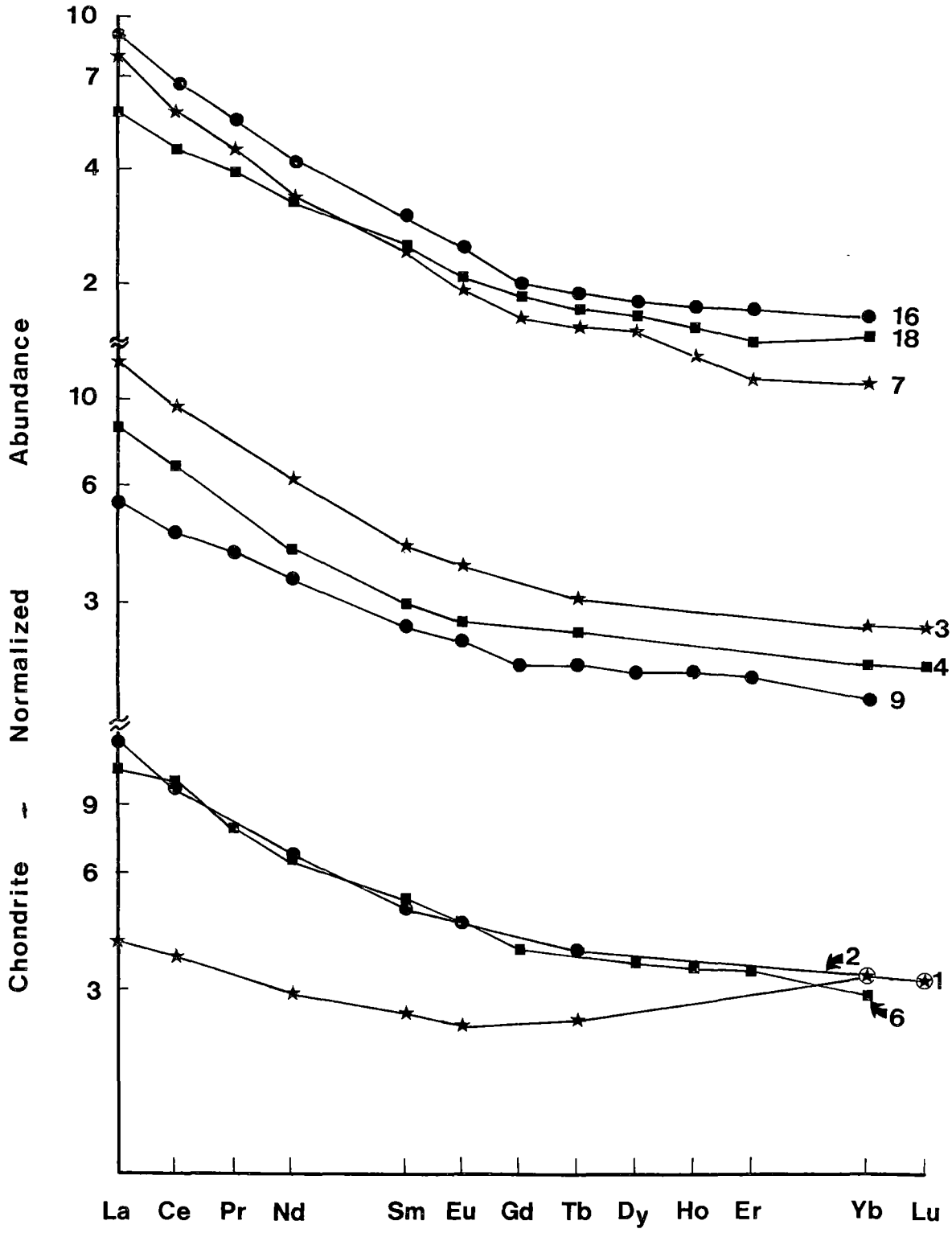

Figure 3.4 Chondrite-normalized REE plot for Cape Vogel HMA. Numbers on right-hand side are sample numbers from Table 3.2. Chondrite-normalizing values given in Table 3.2.

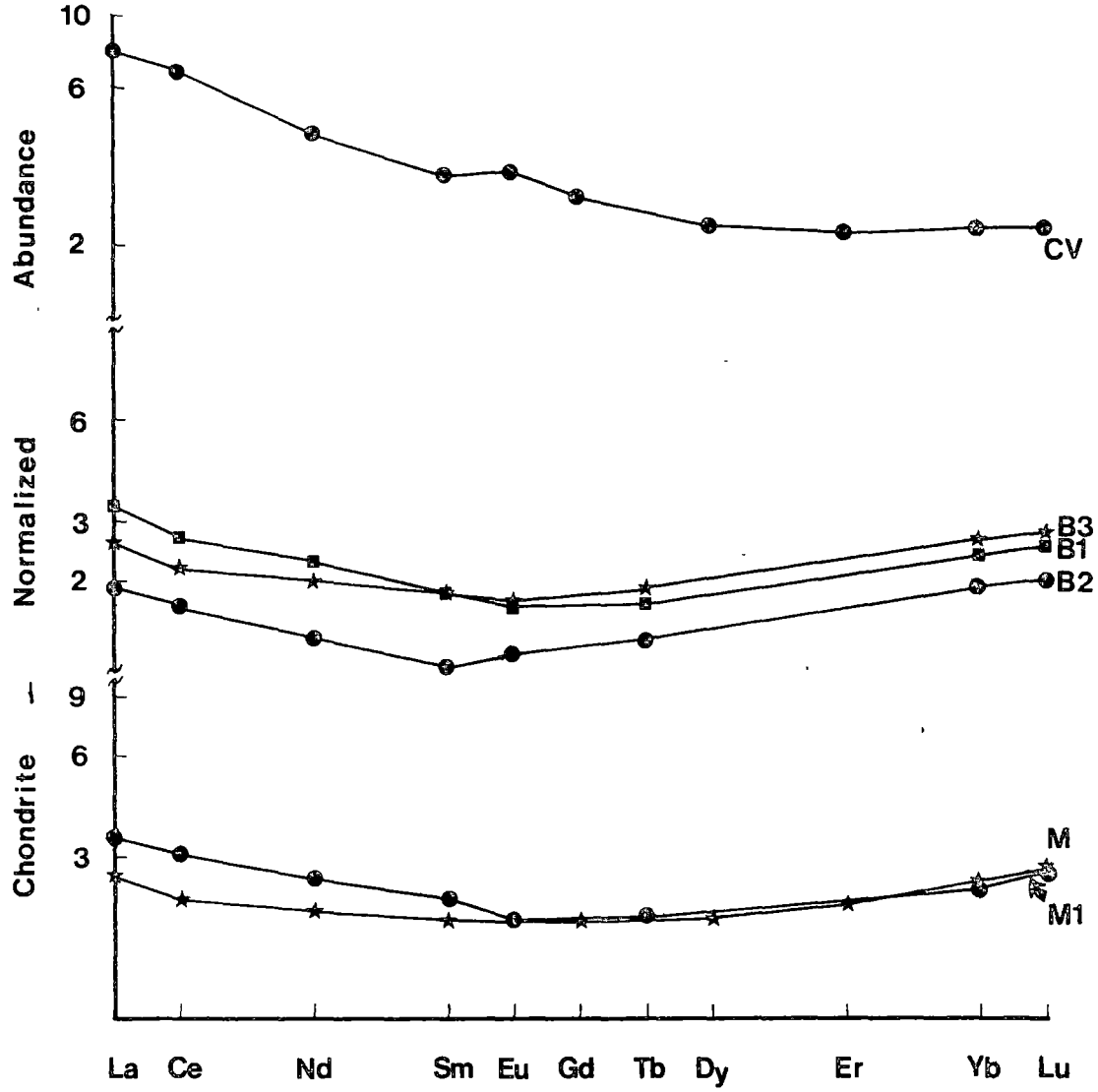

Figure 3.5 REE plot for Mariana and Bonin Islands HMA. Initials refer to Table 3.3. Note difference between Cape Vogel (type-E HMA) and others (type-C HMA). See text for further discussion.

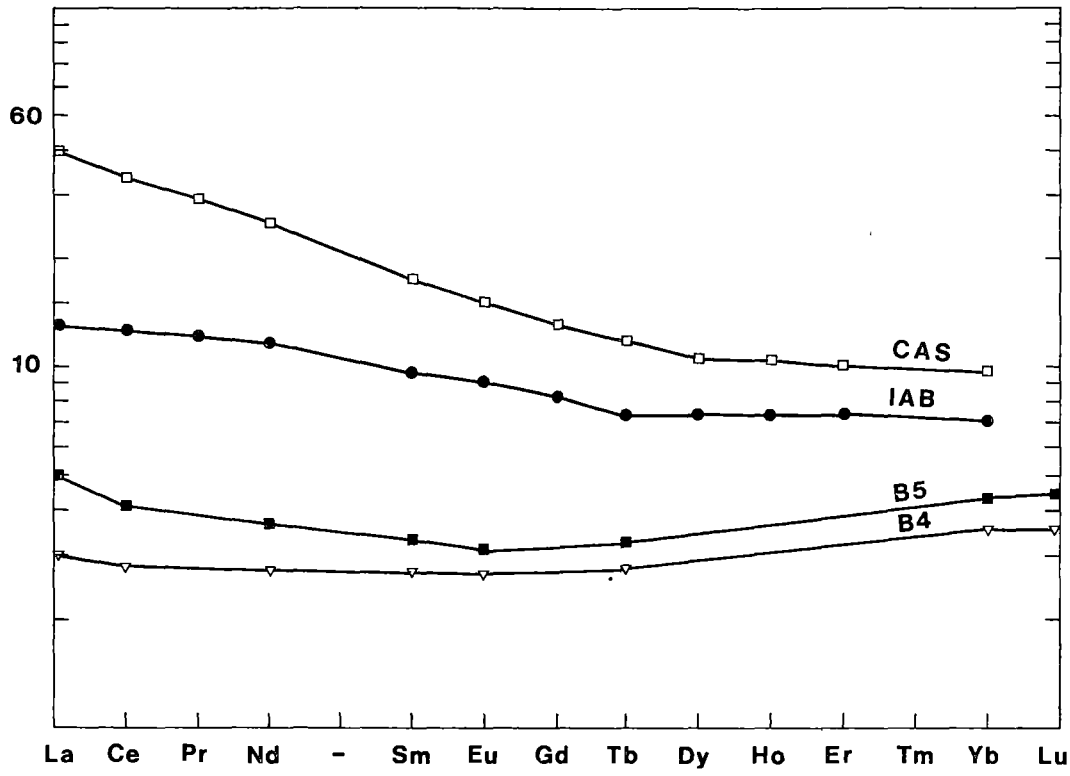

Figure 3.6 REE in bronzite andesite (B4) and dacite (B5) from Bonin Islands. IAB (island-arc basalt, Sun, 1980) and CAS (calc-alkaline basalts, Whitford *et al.*, 1979) shown for comparison. Chondrite-normalized plot.

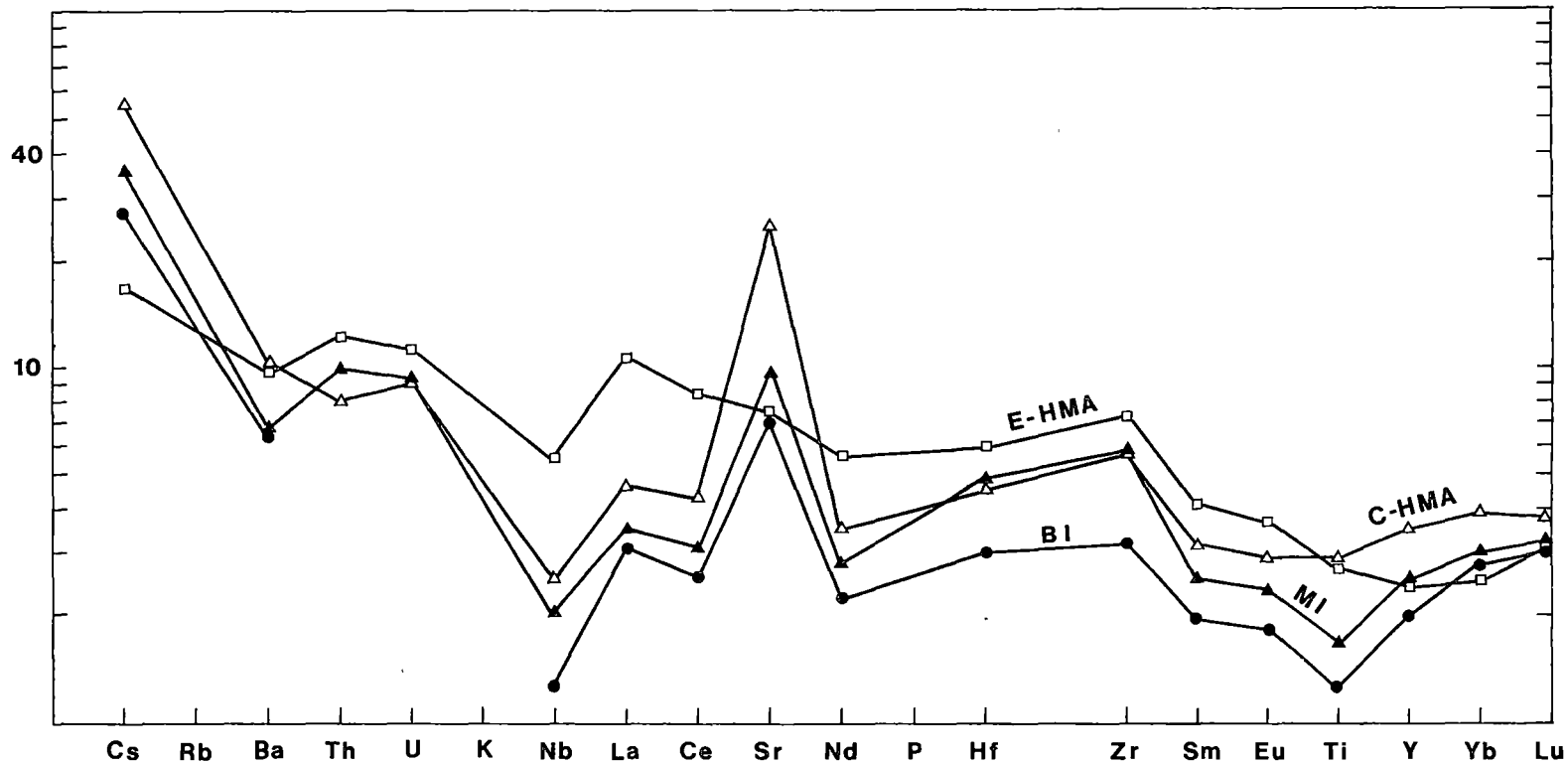

Figure 3.7 Normalized incompatible element plot (after Sun *et al.*, 1979). E-HMA = type-E HMA, Cape Vogel; C-HMA = type-C HMA, Cape Vogel; MI = type-C HMA, Mariana Trench, BI = type-C HMA, Bonin Islands. Data is from this study. See Figure 3.11 for further normalization details.

Table 3.4

Transition metal ratios in HMA and selected volcanics.

	MT	BI	CV	MORB	STPK
Ti/Sc	27-38	16-27.5	53(30-81)	110	78
Ti/V	6.4-8	3.5-6.2	9.4(4.3-16.7)	22	14
V/Sc	4.3-5.4	3.2-4.8	5.3	6	5.6
Cr/Ni	2.9-6.1	3.8-8	4-8	1-3	1-3

Data Sources:

MT = Mariana Trench - Dietrich *et al.* (1978); Sun & Nesbitt (1978); this study.

BI = Bonin Islands - this study.

CV = Cape Vogel - this study (bracketed values are ranges).

MORB = Mid ocean ridge basalts
STPK = Spinifex textured peridotitic komatiites
} Nesbitt & Sun (1980); Kay & Hubbard (1978); Nisbett *et al.* (1979).

Table 3.5

High-Mg andesites: selected trace element ratios.

	1	2	3	4	5	6	7
Ti/Zr	41.7	60	39	0.38	0.55	0.36	0.65
Ti/Y	218	257	316	0.68	0.80	0.98	1.23
Zr/Y	5.4	4.3	8.9	1.84	1.47	3.04	2.07
Ba/Zr	0.88	1.3	0.8	6.24	9.22	5.67	0.62
La/Zr	0.047	0.049	0.078	1.31	1.36	2.17	1.59
Sr/Zr	3.91	9.13	2.11	2.68	6.25	1.46	0.23
Sr/Ba	4.21	7.03	2.15	0.41	0.68	0.21	0.31
La/Rb	1.75	1.82	6.8	1.92	2	7.5	3.74
$(La/Sm)_N$*	1.56	1.54	2.63	2.31	2.28	3.90	1.71
$(La/Yb)_N$	1.18	1.23	4.31				3.50
Zr/Nb	54	33.5	19.4	1.97	1.22	0.71	0.58
La/Nb	2.33	1.67	1.5	2.40	1.72	1.55	0.90
La/Sr	0.012	0.005	0.036	0.50	0.21	1.50	7.20

1 - Average HMA from Bonin Islands and Mariana Trench from Hickey & Frey (1981), Sun & Nesbitt (1978), Jenner (1981), and this study.

2 - Cape Vogel type-C HMA (Jenner, 1981; this study).

3 - Cape Vogel type-E HMA (Jenner, 1981; this study).

4 - column 1 normalized to N-MORB of Sun (1980).

5 - column 2 normalized to N-MORB of Sun (1980).

6 - column 3 normalized to N-MORB of Sun (1980).

7 - column 3 normalized to column 2.

* chondrite-normalized ratios, values given in Table 3.2.

excluding ratios involving Sr. The change from type-C to type-E at Cape Vogel is accompanied by a decrease in Zr/Nb, Ti/Zr, Ba/Zr, Sr/Zr, Sr/Ba, and (?)La/Nb, and an increase in Ti/Y, Zr/Y, La/Zr, La/Yb, $(La/Yb)_N$, $(La/Sm)_N$ and La/Sr ratios. If type-C HMA from other localities are compared to the type-E HMA the changes noted above are also, for the most part, observed.

REE patterns for the bronzite andesite (B4) and perlitic dacite (B5) are shown in Figure 3.6. The REE and trace element ratios in B5 are similar to those in type-C HMA. B4 is less LREE enriched than type-C HMA although again there is an overall similarity with type-C HMA.

3.2.6 Isotopic Characteristics

$^{143}Nd/^{144}Nd$ ratios have been measured in nine HMA which are part of this study. The values given in Table 3.6 are from Hickey & Frey (1981). ΣNd ranges from -0.3 to +5.6 in the Bonin Islands and shows a positive correlation with Sm/Nd and a poorly defined trend with Ti/Zr (Figure 3.8) (Hickey & Frey, 1981). The HMA from Cape Vogel show a much smaller range in ΣNd, and similarly show a poor correlation between Sm/Nd versus Ti/Zr (Figure 3.8) (cf. Hickey & Frey, 1981). If the type-C HMA from Cape Vogel is plotted in conjunction with the type-E HMA there is a suggestion of a positive trend of ΣNd with Sm/Nd; however, as discussed later this may be an "artificial" trend. For a given Sm/Nd ratio the ΣNd is higher in Cape Vogel rocks, than it is in either the Bonin Islands or Mariana Trench HMA.

An extremely high $^{87}Sr/^{86}Sr$ ratio (0.7052), for volcanic rocks from the Izu, Bonin, Mariana, Yap and Palau Islands, was reported by Matsuda *et al.* (1977) for an andesite from Chichi-jima, Bonin Islands. The locality of this sample makes it highly likely that it is a type-C HMA differentiate.

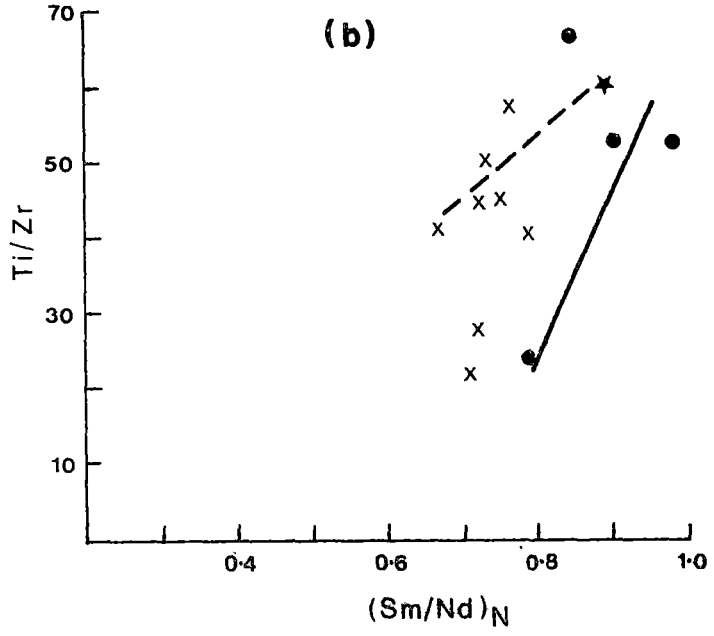

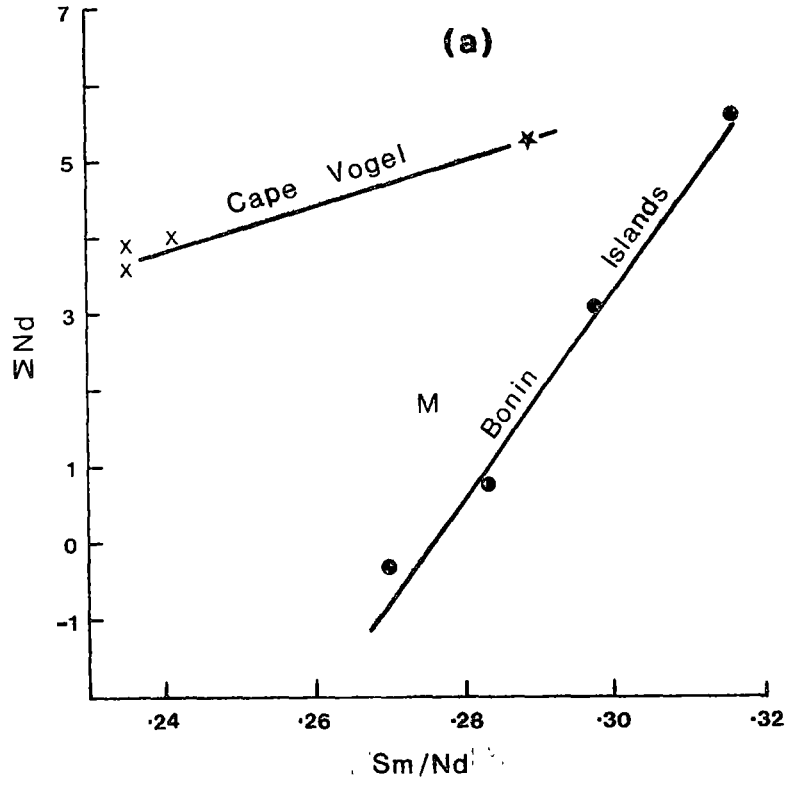

Figure 3.8 (a) ΣNd vs Sm/Nd in selected HMA. Solid dots - Bonin Islands; asterisk - type-C HMA, Cape Vogel; crosses - type-E HMA, Cape Vogel; M - Mariana Trench. See Table 3.6. Lines show positive trend between ΣNd and Sm/Nd, after Hickey & Frey (1981).

(b) Ti/Zr vs chondrite-normalized Sm/Nd. Symbols as for Figure 3.8(a). Dashed line is trend from Hickey & Frey (1981) for Cape Vogel HMA. Solid line is trend for Bonin Islands HMA (*ibid.*).

Table 3.6

Sm/Nd isotope results on HMA.

	Sm/Nd	$^{143}Nd/^{144}Nd$*	εNd†
Bonin Islands (refer to Table 3.3)			
61497 (B1)	0.270	0.512619	-0.3
61498 (B2)	0.283	0.512677	+0.8
61499 (B3)	0.298	0.512798	+3.1
61500 (B4)	0.316	0.512926	+5.6
61501 (B5)	0.290		
Cape Vogel (refer to Table 3.2)			
47799 (1)	0.289	0.512908	+5.3
47810 (2)	0.241	0.512837	+4.0
47811 (3)	0.235	0.512815	+3.6
47816 (4)	0.235	0.512832	+3.9
47787 (6)	0.256		
47788 (7)	0.235		
47790 (9)	0.245		
47805 (16)	0.230		
47807 (18)	0.247		
Mariana (refer to Table 3.3)			
61496 (M1)	0.275	0.512731	+1.9

* $^{143}Nd/^{144}Nd$ normalized to $^{146}Nd/^{144}Nd = 0.7219$

† εNd value calculated using a present day chondritic $^{143}Nd/^{144}Nd$ ratio of 0.51264 and approximate 30 m.y. age for all samples.

Bloomer *et al.* (1979) and Poreda & Craig (1979) reported a Sr-isotope and He-isotope value on a Mariana Trench dredge sample, which based on the data given by Bloomer *et al.* (*ibid.*) is a type-C HMA. The $^{87}Sr/^{86}Sr$ ratio was 0.70337 and $^{3}He/^{4}He$ was 1.6 x atmospheric.

Pb isotopic analyses on Bonin Island samples (Meijer & Hanan, 1981), have not yet been reported in full but the authors indicate the Pb isotopic compositions are unusual and could contain a sedimentary component.

3.2.7 Major Element Modelling, Cape Vogel

The porphyritic nature of the Cape Vogel HMA makes it difficult to establish the parental liquid composition for the series. However, to satisfy constraints from experimental studies and natural mineral compositions, i.e. pyroxenes and olivines of Mg-numbers 90-93, a parental liquid of Mg-number 76-79 is required (see Chapter 5). Some portion of the compositional variation within the Cape Vogel Suite of HMA should be explicable in terms of fractional crystallization or accumulation of clinoenstatite, orthopyroxene and (?) olivine from the parental composition selected. Sample 9 (Table 3.2) was selected as an appropriate parental composition based on its fine grained nature and Mg-number of 78, and attempts were made to model fractionation using a least-squares mixing program (Wright & Doherty, 1970). Elements modelled were restricted to SiO_2, CaO, Al_2O_3, FeO, and MgO. TiO_2 and P_2O_5 were excluded because the former is treated as a trace element and analytical uncertainty excludes the latter. Na_2O and K_2O were excluded because they may have been affected by post-magmatic alteration.

Results of the modelling indicate that samples 4 (and 6), 11 and 16 would be derived by 35, 25 and 15% fractional crystallization of Ca-poor pyroxene from sample 9. The sum of squares of residuals for the modelling is not entirely satisfactory (ranging from 0.1 to 1), but,

in general, the results support the earlier conclusions of Dallwitz (1968) that Ca-poor pyroxene fractionation and accumulation accounts for most of the observed major element variation. The poor fits in the modelling are due in part to the limited compositional range of pyroxene selected, i.e., for large degrees of fractionation it would be better to select a more fractionated pyroxene composition after a set increment of crystallization, for example 5%. Another aspect which must be considered is the nature of the program itself. Because SiO_2 is the largest component the relative errors are reduced if the best fit is produced for this element. This feature gave rise to errors in two ways, first because some of the SiO_2 variation may reflect alteration and secondly because combination of small differences in SiO_2 content of bronzite and clinoenstatite, and the above-noted feature of the program, lead to petrographically unreasonable solutions in many cases where the two Ca-poor pyroxenes were modelled as fractionating simultaneously.

It was clear from the modelling that within the limits imposed by the analyses and techniques that Ca-poor pyroxene was the most important fractionating phase. Small amounts of olivine fractionation could not be excluded by either the modelling or petrography. As an approximation, it is suggested that low-pressure olivine fractionation within the series represented in Table 3.2 was less than 3-5%.

3.2.8 Modelling of Trace Element Variations, Cape Vogel

There are two aspects of the trace element modelling to be considered in HMA in general and at Cape Vogel. The first aspect is the origin of the two groups, i.e. type-C HMA and type-E HMA. The second aspect is the origin of the variation within a group, for which there is sufficient data only for type-E HMA from Cape Vogel.

The differences and similarities between type-C and type-E HMA are more fully developed later; however, the following points can be made here. The differences in incompatible element contents in the two types of HMA can occur at the same Mg-number, or degree of fractionation. Fractional crystallization of olivine or low-Ca pyroxene will not account for the loss of the normalized Sr-anomaly or the increased LREE enrichment. Similarly fractional crystallization cannot account for changes in the trace element ratios between the two groups.

The inability of fractional crystallization to account for the changes between type-C and type-E HMA suggests that another explanation should be sought. Some of the trace element ratios of type-C HMA are unexpected or atypical in relation to the major and trace element abundances and it has been proposed that an enrichment in certain elements has taken place (Sun & Nesbitt, 1978; Nesbitt & Sun, 1980). The details of this enrichment event for type-C HMA are discussed more fully below; however, this interpretation suggested that a similar type of process may be important in generating type-E HMA. The enriching fluid for type-E HMA must be different from that for type-C HMA in order to account for the changes in incompatible element patterns. To check on the nature of the enrichment in type-E HMA ratios of selected HFS elements were plotted versus $(La/Yb)_N$, shown in Figure 3.9. Note that the increase in $(La/Yb)_N$ is not correlated with Mg-number or Ti content, and most likely reflects source heterogeneity. The trends shown in Figure 3.9 were analysed qualitatively by considering that type-E HMA characteristics were imposed on a type-C HMA characterized source. [Note: only Cape Vogel rocks are considered.] Mixing of trace element characteristics were analysed qualitatively, using as a guide the equations developed in Langmuir *et al.* (1977). The trend shown by Zr/Hf versus $(La/Yb)_N$ suggests that this ratio remains relatively constant during the event which leads to LREE

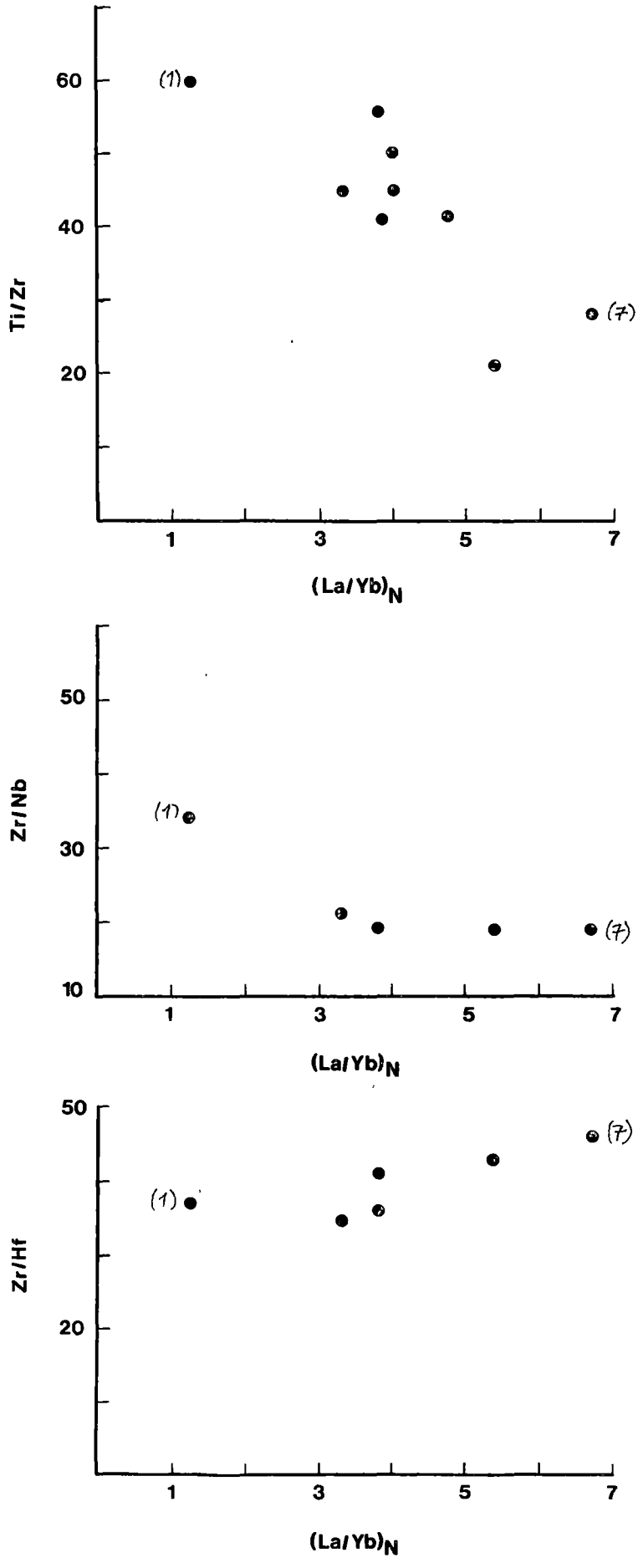

Figure 3.9 Selected HFS element ratios vs chondrite-normalized La/Yb ratio for Cape Vogel HMA See text for discussion
Numbers in brackets refer to analyses in Table 3.2.

enrichment. The decrease in Zr/Nb versus $(La/Yb)_N$ is consistent with relatively simple mixing of two end-member components, represented by analysis 1, of Table 3.2, and analysis 7 of Table 3.2. The trend shown in Ti/Zr versus $(La/Yb)_N$ is not interpreted simply in terms of the mixing of the two above end members. Ti/Zr ratios scatter off between analyses 1 and 7 (Table 3.2) a potential mixing line and suggest, if interpreted in conjunction with the trend in Zr/Nb, that Ti distribution is either heterogeneous in the source material or in the enriching fluid. The trends while not necessarily simply interpreted suggest that the enriching fluid had a Ti/Zr ratio < 20 and a $(La/Yb)_N$ ratio > 7.

To study the origin of the variation within the type-E HMA at Cape Vogel, samples 2, 3, 4, 6, 9, 11, and 16 were selected for trace element modelling. This was done on the basis of complete analyses, large range in Mg-numbers, and the previous demonstration, on the basis of major element compositions, that samples 4, 6, 11, and 16 could be related to sample 9 by pyroxene (protoenstatite-bronzite) fractionation. Ti, Zr, Y, Nb, La, Sm, Yb, Ni, Cr, V, and Sc abundances were modelled. Calculations were done in the following manner: (i) surface equilibrium (Rayleigh fractionation) equations from Arth (1976) were used; (ii) the majority of computer runs were made assuming magnesium-rich Ca-poor pyroxene was the sole fractionating phase. This assumption is justified in light of the petrography, major element modelling and the fact that for almost all elements considered, olivine would have similar distribution coefficients; and (iii) partition coefficients were adopted from Frey *et al.* (1978) (values for REE are from Set 1 and, initially, intermediate values from the range given for other elements were chosen). The unique chemical composition of HMA makes selection of appropriate distribution coefficients difficult.

It was assumed that HMA, with their distinctive mineralogy, high magnesian contents, and perhaps high crystallization temperatures can be modelled more accurately using distribution coefficients from basalts rather than "normal" intermediate volcanics. An example of the results from the modelling is given in Table 3.7.

In general, the abundances for the HFS elements and REE are low by 10-30% at the degree of fractionation predicted from the major element modelling. It is not possible to predict the behaviour of these elements in a simple manner for all samples and some degree of fractionation and/or heterogeneity in the source may be an additional factor. TE abundances agree more closely with the degree of fractionation implied by major element modelling. While recognizing that some latitude is given by uncertainty in the distribution coefficients used, it seems that the HFS and LFS elements, and REE, are decoupled from the major elements while TE are not. Decoupling of major and trace elements has been previously noted and one possible explanation for this may be magma mixing (Rhodes & Dungan, 1979). Some petrographic features in HMA (Chapter 2) support the possibility of magma maxing.

Of particular note are the Sc abundances which do not decrease with fractionation. The observed variation requires that the distribution coefficient for $Sc^{opx/l}$ must be less than 1 (< 0.8). It is unlikely that this apparently low value is due to a lowering of the bulk distribution coefficient by the presence of another phase, e.g. olivine.

A large range in Ti/Sc and Ti/V ratios was noted earlier (Section 3.2.5) and these ratios have a positive correlation with increasing Ti. This reflects the higher degree of incompatibility of Ti. Variation in the amount of Ti due to source heterogeneity; phenocryst accumulation; or some other process; introduces some scatter

Table 3.7

Example of trace-element modelling.*

	Parent (obs.)	Daughter (obs.)	Orthopyroxene Fractionation (calc.)		Distribution Coefficient
Ti	1259	2518	2583	(55)**	0.10
Zr	28	62	61	(55)	0.03
Y	4	9	9	(55)	0.02
Nb	1.32	3.2	2.7	(55)	0.10
La	2.03	4.06	4.06	(50)	0.00
Sm	0.60	1.19	1.20	(50)	0.00
Yb	0.42	0.72	0.82	(50)	0.03
Sc	28	36	32	(30)	0.80
V	149	211	191	(30)	0.30
Ni	574	212	197	(30)	4.00
Cr	2191	735	752	(30)	4.00

* Assuming orthopyroxene is sole fractionating phase.

** Value in brackets is the degree of fractionation.

obs. - observed values
calc. - calculated values

in the trends. However; recognition of these trends points out the necessity of recognizing the residual or fractionating phases present, even in apparently primitive liquids, if one is trying to ascertain trace element ratios in the source (cf. Nesbitt & Sun, 1980).

It was previously noted that some olivine fractionation was allowable based on major element modelling; similarly some olivine fractionation is permitted by the trend shown in Ni (Figure 3.3.). The only requirement necessary to explain the Ni trend illustrated is a bulk distribution coefficient of ~3. $Ni^{opx/l}$ can be 3 (Frey *et al.*, 1978) and orthopyroxene alone can provide a satisfactory solution. However, olivine and orthopyroxene fractionation (1:9 ratio) with distribution coefficients of 20 and 1 respectively, also provides a satisfactory solution. Larger proportions of olivine fractionation with a K_D of 20 are prohibited, but if lower values for $D_{Ni}^{ol/l}$ are accepted then a greater proportion of olivine fractionation is feasible. For example, based on the experimental studies of Hart & Davis (1978) and data of Chapter 5, a value of 6 may be applicable. However, the petrographic evidence does not support the extensive olivine fractionation permitted by the use of lower K_D's.

Fortuitously, the samples selected for SSMS analysis define a linear trend for Nb versus Zr (Figure 3.2) which is also adhered to by some samples with XRF analysis. The origin of the anomalous values (samples 10, 11, 17, 19, and 21) is unknown. Some of the lower values may reflect the presence of additional type-C HMA at Cape Vogel but better analytical data for Nb and values for REE would be needed to substantiate this.

3.3 COMPARISON OF HMA WITH ISLAND-ARC AND HIGH-MAGNESIAN LOW-ALKALI (HMLA) VOLCANICS

The occurrence of high-Mg andesites in an island-arc environment (Chapter 2; Chapter 6) and their high SiO_2 contents leads one to compare them with island-arc andesites. Significant differences in chemistry are found; however, of particular importance in the HMA are the high Mg-numbers (66-82), these are considerably higher than those in most andesites, e.g. 47 at Bagana Volcano (column 2, Table 3.8). The high Mg-numbers in HMA are characteristic of magmas which may represent "primary" magmas, in the sense of equilibration with mantle peridotite compositions (D.H. Green, 1971, 1973, 1976).

The low abundances of TiO_2, Al_2O_3, Na_2O, K_2O, and P_2O_5 in HMA compared to most andesites (see Table 3.8) are not solely attributable to the primitive nature of HMA but reflect inherent differences in the source compositions. The bronzite andesite and perlitic dacite compositions from Chichi-jima, Bonin Islands best illustrate this aspect of the geochemistry of HMA. These rocks (Table 3.3, B4 and B5) are differentiates from HMA (Shiraki & Kuroda, 1977) and have Mg-numbers similar to those of many andesite-dacite compositions (Table 3.8), nonetheless they retain distinctive major element compositions.

Kuroda *et al.* (1978) have suggested that the Bonin Islands HMA are a primary calc-alkaline magma. They based their definition of calc-alkaline on two points: (i) the HMA plot in the calc-alkaline field on a SiO_2 versus FeO^t/MgO plot (after Miyashiro, 1974); and (ii) there is a reaction relation between olivine and orthopyroxene. They noted however that the more fractionated rocks plot in the tholeiitic field in the SiO_2 versus FeO^t/MgO plot. In terms of major element chemistry (and trace elements, see below) it is difficult to accept the HMA as a parental calc-alkaline lava. The trend of FeO^t versus FeO^t/MgO (also

Table 3.8

Island-arc andesite compositions.

	1	2	3	4	5
SiO_2	59.70	55.5	59.0	65.6	57.40
TiO_2	0.77	0.81	0.74	0.64	1.25
Al_2O_3	16.96	17.7	18.1	16.1	15.60
FeO^t	7.11	7.94	6.8	5.3	8.14
MnO	0.14	0.18	0.10	0.09	
MgO	3.23	3.38	2.9	1.6	3.38
CaO	6.94	8.01	6.7	4.1	6.14
Na_2O	3.33	3.95	3.5	4.2	4.20
K_2O	1.31	1.61	1.84	2.47	0.43
P_2O_5	0.17	0.35	0.22	0.17	0.44
$Mg/(Mg+Fe^t)$	44.74	43.14	47	38	42.52
Cs		0.26	4.4	9.4	
Rb		25	62	81	6
Ba		250	420	450	100
Sr		810	360	240	220
Th		1.3	6.7	13	0.31
U		0.55	1.6	2.6	0.34
Zr		81	151	195	70
Hf		2.2	3.6	4.7	1.0
Nb		4	9.4	6.1	
Cr		9	19	3.4	15
V		178	130	50	175
Sc		16	16	12	
Ni		6	8	<2	20
La		11	19.4	30.9	2.4
Ce		24	40.9	58.9	
Pr		2.9	4.9	8.4	
Nd		13	19.4	28.8	
Sm		2.9	3.5	5.0	
Eu		0.93	1.0	0.97	
Gd		2.9	3.3	3.7	
Tb		0.47	0.53	0.68	
Dy		2.9	3.3	4.0	
Ho		0.64	0.73	0.86	
Er		1.8	2.2	2.5	
Yb		1.7	2.1	2.4	2.4
Lu		0.27			
Y		17	28	39	

1. "Island-arc" pyroxene andesite - Ewart (1976).
2. Bagana andesite, PNG - Bultitude *et al.* (1978).
3. Average calc-alkaline andesite from Java and Bali - Whitford *et al.* (1979).
4. Average calc-alkaline dacite from Java and Bali - Whitford *et al.* (1979).
5. Island-arc tholeiite series andesite - Jakes & White (1972).

Miyashiro, 1974) has been used to define calc-alkaline versus tholeiitic volcanics and on this plot the HMA show little evidence of belonging to either suite. Hickey & Frey (1981) similarly concluded that the Fe-fractionation trend in HMA was neither calc-alkaline nor tholeiitic.

The Cr and Ni contents of HMA are, as would be expected, substantially higher than those of island-arc volcanics in general (Gill, 1979; T.H. Green, 1980) (see also Table 3.8).

REE and incompatible element patterns in island-arc volcanics and HMA are shown in Figures 3.6 and 3.11. The concave REE pattern of type-C HMA is distinctly different from that found in other volcanics. The REE pattern in type-E HMA is somewhat similar to that in some island-arc volcanics. However, as will be shown later, there are differences in the LFS elements and the overall nature of the incompatible element trends.

The primary or primitive nature of HMA suggests that their geochemical features relate in some way to their parental material. This is particularly true if the constraints imposed by P/T conditions of origin and the residual phases of the parental material (see Chapter 5) are considered. The experimental petrology and petrography of HMA (Chapter 2 and Chapter 5) indicate that olivine, low-alumina enstatite and Cr-rich spinel are the liquidus or near-liquidus phases for HMA, and thus most of the major and incompatible trace element ratios and patterns are directly comparable to that in their source peridotite. Comparison of HMA and other high-magnesian low-alkali liquids (HMLA), which likewise reflect their mantle source compositions (Nesbitt & Sun, 1980), gives us information on the nature of the mantle.

Nesbitt & Sun (1980) have compiled the characteristics of a variety of HMLA and the present comparison is primarily based on this work.

It should be pointed out that the comparison with some HMLA is further developed in Chapter 6 when the inter-relationship between komatiites, HMA and "boninites" is more carefully explored.

In general, the HMA are distinctive in major elements among HMLA for their high SiO_2 contents and fractionated CaO/Al_2O_3 ratio (~ 0.60). Most HMLA volcanics have CaO/Al_2O_3 ratios of 0.8-1.0, close to that for many natural and most model mantle compositions (Ringwood, 1966; Maaloe & Aoki, 1977; D.H. Green *et al.*, 1979).

Cr and Ni contents in HMA are similar to those in HMLA (Nesbitt & Sun, 1980), however Ni values are lower relative to Cr in HMA. This feature is illustrated in Table 3.4, HMA have Cr/Ni ratios of 3-8 while MORB and STPK are 1-3. Olivines on the liquidi of HMA and MORB are about the same in Ni content (Kuroda *et al.*, 1978; Sato, 1977) however the Cr-spinel on the liquidi varies from greater than 60% Cr_2O_3 in HMA to less than 45% Cr_2O_3 in MORB (Green *et al.*, 1979; Sigurdsson & Schilling, 1976) (see also Figures 2.5 and 2.6). This testifies to the reality of the differences in Cr/Ni ratio of the liquids.

V and Sc contents in HMA are similar to those in HMLA (Nesbitt & Sun, 1980; Hickey & Frey, 1981), however Sc may be enriched in HMA as V/Sc values as low as 3.2 are reported, while V/Sc ratios in STPK and MORB are 5.6 and 6. The Ti/V and Ti/Sc ratios in HMA are lower than those reported for most HMLA, however some caution is needed in interpreting these ratios, as was discussed earlier.

Ti/Zr ratios in most HMLA are near chondritic, i.e. 110, although values up to 220 are found in some low-Ti basalts associated with ophiolites (Nesbitt & Sun, 1980). The Ti/Zr ratios in HMA are < 60 and this is a very distinctive characteristic of these rocks (see below).

The REE pattern in HMLA ranges from LREE depleted to enriched (Nesbitt & Sun, 1978; Green, 1980), however patterns like those observed in type-C HMA are not known from other areas. The type-E HMA REE pattern is not as distinctive as that for type-C HMA, however only the Archaean Negri volcanics have a REE pattern which is not only similar to type-E HMA but is accompanied by other characteristics of HMA (Nesbitt & Sun, 1980; Sun & Nesbitt, 1978b). The relationship to these volcanics is discussed in Chapter 6.

3.4 NATURE OF THE ENRICHMENT PROCESSES

It is obvious from the previous sections in this chapter and that of Chapter 3 that the HMA are mineralogically and chemically unusual. Four features of these rocks suggest that they are derived from a peridotite source which has been previously depleted by prior melting events, i.e. the overall low abundances of incompatible elements, the low CaO/Al_2O_3 ratio, the refractory spinel and primitive pyroxene compositions, and the high Cr/Ni ratio. However the variable LREE enrichment and existence of two distinct groups of HMA suggest that prior to their derivation the mantle source underwent enrichment events. It is the superposition of enrichment events on a highly depleted source which determines the unusual trace element characteristics of HMA. In order to understand the nature of the enrichment processes, it is necessary to adopt some set of characteristics for the depleted source.

3.4.1 Nature of the Depleted Source

There are two approaches which can be made to delimit the nature of the depleted source and the nature of the enrichment processes. The first of these is the empirical approach, which depends on comparison

with other rocks, and makes, in essence, an educated guess at the nature of the depleted source. The second approach is more quantitative in nature and involves a series of calculations based on the chemistry of the rocks being studied. Both approaches have been utilized in studies on the HMA, the first by Jenner (1981) and the second by Hickey & Frey (1981). Before presenting and extending the model developed in Jenner (1981), it is worth considering the approach used by Hickey & Frey (1981).

3.4.1.1 Quantitative model

Hickey & Frey (1981) proposed that the positive correlation between $^{143}Nd/^{144}Nd$, Ti/Zr, and other geochemical parameters, and Sm/Nd could be used to infer several compositional characteristics of the end members responsible for the chemistry of HMA. Interpreting the trends on plots of $(La/Nd)_N$, $(Ti/Nd)_N$, and $(Yb/Nd)_N$ as mixing lines (see Figure 3.10) they were able, by a series of extrapolations and iterations, to calculate depleted and enriched end members for Cape Vogel and Bonin Islands HMA.

There are a number of criticisms which can be made of this approach to determining end-member characteristics in HMA:

1. In the Cape Vogel rocks it is clear that there is no correlation between Ti/Zr and Sm/Nd. Ti behaves in a non-predictable fashion (see Section 3.2.8) and was probably heterogeneous either in the original source or in the enriching fluid. The trends of Ti/Zr against Sm/Nd are also not well developed for Bonin Islands HMA.
2. The model of Hickey & Frey (1981) does not take into account the differences between type-C and type-E HMA. Differences between these groups are not explicable by an enrichment *event* during which the composition of the enriching "fluid" remains constant, as is implicit

in their model. Thus the positive correlation between Nd and Sm/Nd in Cape Vogel HMA may not have any direct significance, since the correlation is a function of the separation between type-E and type-C HMA.

3. Even if it were possible to ignore the difficulties differences between type-C and type-E HMA pose in this type of modelling, it is nonetheless apparent that if the additional data from Cape Vogel are used then significant errors are introduced in extrapolating end-member compositions (see Figure 3.10). Without the type-E HMA the spread of compositions within type-C HMA is too small to establish a reliable mixing line.

The approach used by Hickey & Frey (1981) is useful in some circumstances, however with the present data base for HMA its use is inappropriate.

3.4.1.2 Empirical approach

A survey of the current literature concerning models of continental crust development and mantle evolution (cf. Sun & Nesbitt, 1977; Jacobsen & Wasserburg, 1979a; O'Nions *et al.*, 1979; Sun, 1980; Allègre *et al.*, 1980; De Paolo, 1980) suggests that there are a number of arguments to support the existence of a depleted upper mantle, characterized by N-MORB (Sun *et al.*, 1979) trace element ratios. In particular, Nd/Sm and Rb/Sr studies indicate that the source for many oceanic basalts has had a time-integrated depletion in LREE, Rb/Sr and, by implication, most highly incompatible elements (cf. Gast, 1968; De Paolo & Wasserburg, 1976; O'Nions *et al.*, 1977; Carlson *et al.*, 1978; Jacobsen & Wasserburg, 1979b; Dupré & Allegrè, 1980). Basaltic volcanics in oceanic settings with enriched isotopic and trace element abundances have been derived from a source characterized by N-MORB-type trace element characteristics upon which enrichment events have been

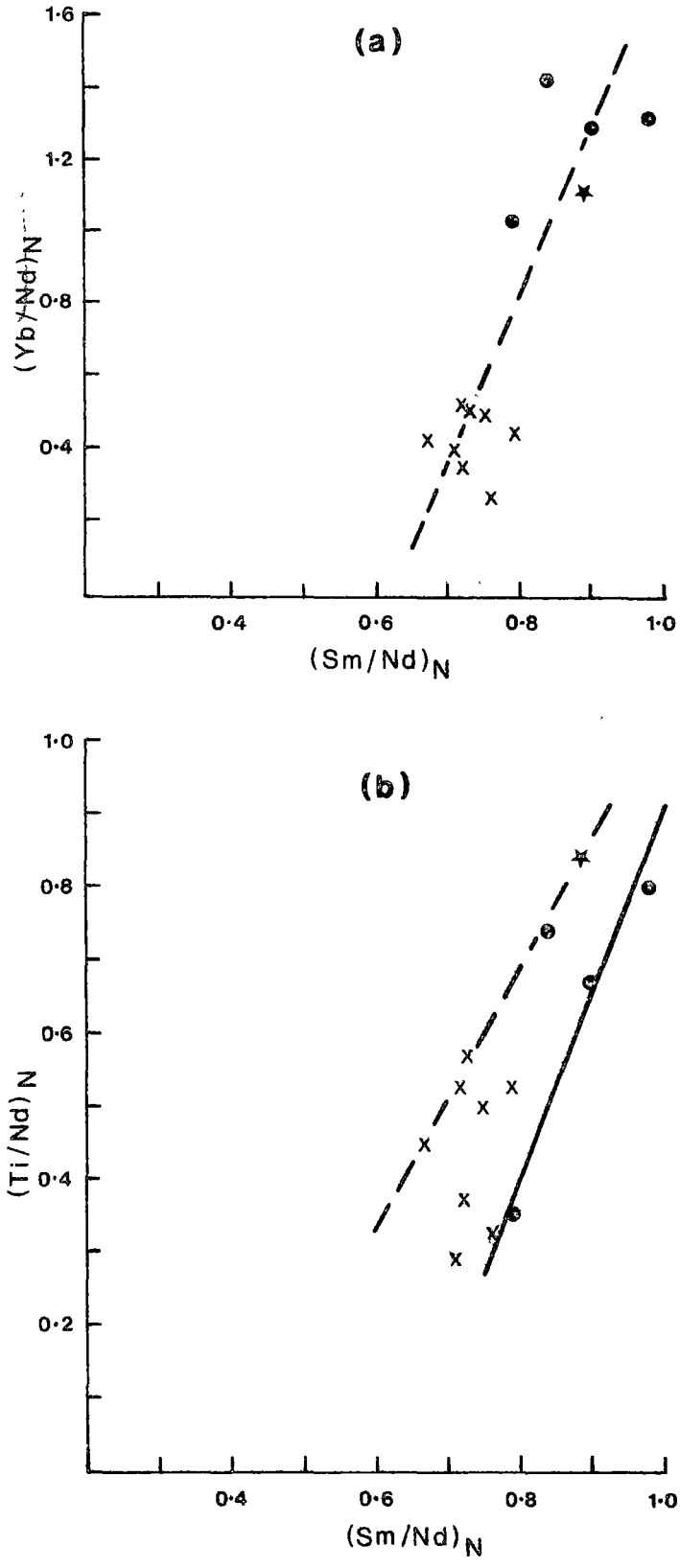

Figure 3.10 (a) $(Yb/Nd)_N$ vs $(Sm/Nd)_N$. Symbols as for Figure 3.8. Dashed line is from Hickey & Frey (1981) and is one of their modelling regression lines. Note that the line is drawn between two groups of data, corresponding to type-C and type-E HMA. (b) $(Ti/Nd)_N$ vs $(Sm/Nd)_N$. Symbols as for Figure 3.8. Dashed line is regression line for Cape Vogel HMA, solid line is regression line for Bonin Islands HMA, after Hickey & Frey (1981). Note how the additional data for type-E HMA scatter off the "mixing" line of Hickey & Frey (1981).

superimposed. The enrichment fluids may be in the form of silicate melts, e.g. undersaturated nephelinitic or kimberlitic liquids (Frey & Green, 1974; Green, 1971; O'Nions *et al.*, 1977; Frey *et al.*, 1978; Wood, 1979). The enrichment event took place only in the last few hundred million years (Sun, 1980).

Let us accept that an island-arc situation is one of geochemical mobility accompanying the dynamic processes, whether these be subduction and/or mantle diapirism. This milieu is one in which mixing of different chemical signatures may occur. Assume, however, that the precursor mantle source for intra-oceanic island arcs may be represented by N-MORB trace element ratios. IAT, which represent the earliest volcanism in models of island-arc volcanism (T.H. Green, 1980) are depleted in HFS elements relative to N-MORB but do not exhibit major differences in HFS element ratios (see Table 1.20; also Jakes & Gill, 1970; T.H. Green, 1980; Perfit *et al.*, 1980; Saunders *et al.*, 1980). Addition of LFS and LREE elements in island arcs is a comparatively recent event and a time-integrated depletion in LREE is indicated by Nd/Sm studies (De Paolo & Wasserburg, 1977; De Paolo & Johnson, 1979).

In view of the possible widespread occurrence of mantle characterized by N-MORB trace element ratios (and in some cases abundances), enrichment events in oceanic settings may be studied by normalizing trace element ratios in (enriched) volcanics to those found in N-MORB. This is a reasonable assumption for many of the volcanics listed in Tables 3.9 to 3.12, but is less justified for HMA. The difficulty in applying this technique to HMA is the possibility that the source is more severely depleted than N-MORB, as is implied by the fractionated CaO/Al_2O_3 ratio , and high Cr/Ni ratio in HMA, and that this has affected the trace element ratios. Low-Ti basalts associated with some ophiolites may represent a second-stage melt derived from an

N-MORB type peridotite source (Duncan & Green, 1980). These rocks, which may not come from as depleted a source as that of HMA, nonetheless provide an opportunity to test the hypothesis that trace element ratios are affected by previous partial melting (depletion) events.

Data from the occurrence of low-Ti basalts associated with ophiolites were taken from Kay & Senechal (1976), Simonian & Gass (1978), Sun & Nesbitt (1978), Coish & Church (1979), and G.A. Jenner (unpublished data, 1977). Unfortunately, many of the analyses are not complete, in the sense that the full range of incompatible elements (see Figure 3.11) are not reported. La/Yb ratios in these rocks average 0.3, Ti/Zr ratios scatter above and below the chondritic ratio of 110 (~ 80-220) but average 120, Ti/Y averages 254 and Zr/Y is ~2. These values, compared to those for N-MORB (see Table 3.9) support the hypothesis that these rocks are derived from a more depleted source.

Results from the low-Ti basalts associated with ophiolites suggest that if HMA are derived from a more depleted source than N-MORB then it may be appropriate to use more fractionated (in the sence of more refractory) trace element characteristics for the source. If sufficient data from low-Ti basalts were available then adoption of their trace element characteristics would be a method of circumventing some of the complications of having a more depleted source; however, this is not the case and the problem has been dealt with in two alternative ways.

First, type-C HMA have been normalized to N-MORB. Using the information from the low-Ti basalts and the degree of incompatibility of the elements shown in Figure 3.11, it can be argued that many of the *differences* in enrichment patterns between HMA and other oceanic volcanics will be strengthened if a more depleted source is applicable. For example, ratios of Ba/Zr, La/Zr, and La/Yb could well be lower in a depleted source since the denominator is the more compatible element.

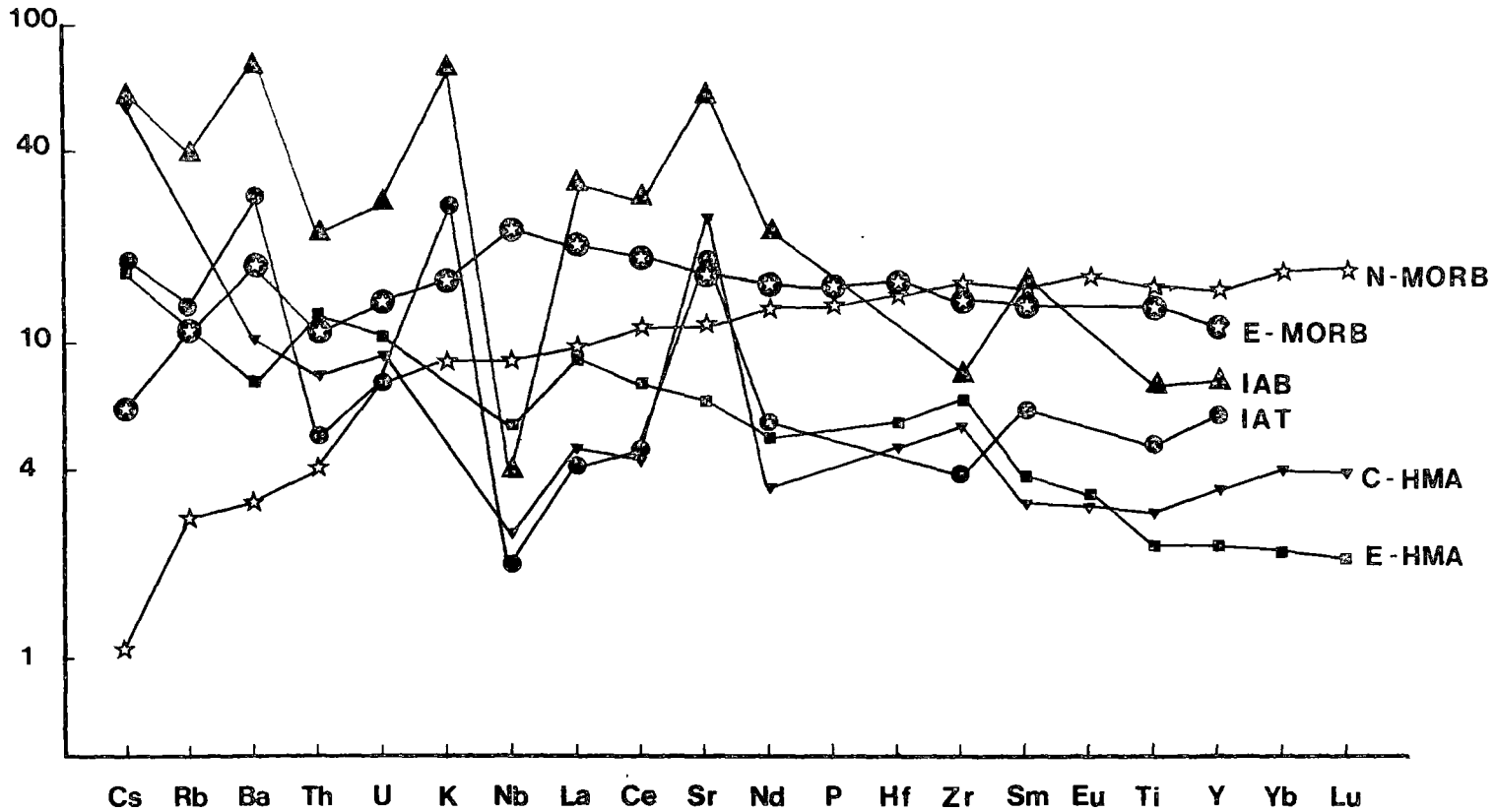

Figure 3.11 Normalized incompatible element plot. Elements increase in compatibility from Cs to Lu. Normalizing values after Sun (1980) and Haskin *et al.* (1968). Data sources and definition of terms are given in the text and Tables 3.2, 3.3 and 3.9.

Table 3.9

Trace element ratios in selected oceanic volcanics.

	N-MORB	E-MORB	OIB	NM	E-MORB/ N-MORB	OIB/ N-MORB	NM/ N-MORB
Ti/Zr	109	92-107	91-108	75	0.84-1	0.84-1	0.69
Ti/Y	321	366	667	523	1.15	2.1	1.63
Zr/Y	2.93	3.4-4.2	7.3	7	1.2-1.5	2.5	2.4
Ba/Zr	0.141	0.42-0.91	1.73-3.53	4.9	3-8.7	12-34	35
La/Zr	0.036	0.084	0.159	0.46	2.3	4.4	13
Sr/Zr	1.46	2.40	3.64	8.42	1.64	2.49	5.77
Sr/Ba	10.3	2.65	2.06	1.75	0.26	0.20	0.17
K/Rb	1060	488	435	318	0.46	0.41	0.30
La/Yb	0.91	2.9	17	51	3.2	18.7	56
$(La/Sm)_N$	0.67	1.57	1.70	3.83	2.35	2.53	5.72
Zr/Nb	27.4	9.3-16	4.2	3.8	0.34-0.58	0.15	0.14
La/Nb	0.97	0.78-0.92	0.66-0.92	1.74	0.80-0.95	0.68-0.95	1.79
La/Sr	0.024				1.46	1.83	2.25

N-MORB, E-MORB = depleted and enriched mid-ocean ridge basalts

OIB = ocean island alkali basalt

NM = nepheline melilitite

Data sources: Clague & Frey (1980); Sun (1980); Wood (1979).

Lower values for these ratios will accentuate the differences seen relative to N-MORB. Note that greater similarity is to be expected for ratios between more closely compatible elements, e.g. Zr/Hf, La/Nb, and Ti/Y.

Secondly, the enrichment pattern for type-E HMA has been normalized to type-C HMA (Table 3.5). There are a number of reasons for treating type-E HMA as if they had a source characterized by type-C HMA trace element ratios. Among these are: (i) type-C and type-E HMA are found together at Cape Vogel; (ii) the isotopic studies of Hickey *et al.* (1980) and Hickey & Frey (1981) do not preclude the imposition of type-E characteristics on a type-C source; and (iii) since the trace element differences between type-C and type-E HMA cannot be explained in terms of an enrichment event having a constant composition enriching "fluid", it is conceptually easier to consider the enrichment process as a sequence of events.

3.4.2 Nature of the Enriching Event in Type-C HMA

N-MORB normalized ratios for selected trace element ratios in type-C HMA are given in Table 3.5. Compared to an original N-MORB type source the LREE enrichment in type-C HMA is accompanied by: (i) a marked decrease in Ti/Zr, Sr/Ba, and La/Sr; (ii) a slight decrease in Ti/Y; and (iii) increases in Zr/Y, Ba/Zr, La/Zr, Sr/Zr, Zr/Nb, and La/Nb. The Sm/Nd studies indicate there is a marked decrease in the ΣNd from that of an N-MORB type source ($\sim$ +10, De Paolo, 1981).

Compared to oceanic island or E-MORB volcanics (Table 3.9; Figure 3.11), the LREE enrichment in type-C HMA differs in the following manner: (i) it is accompanied by a marked decrease in Ti/Zr, Ti/Y, and La/Sr; and (ii) Zr/Nb and La/Nb increase. Oceanic island volcanics often show a decrease in ΣNd with LREE enrichment (De Paolo, 1981) and

Hickey & Frey (1981) have noted that the range of values observed in type-C HMA is comparable to that in oceanic islands.

Compared to island-arc tholeiites (Table 3.10) type-C HMA differ as follows: (i) they exhibit chondrite-normalized LREE enrichment; (ii) they are depleted in Ti/Zr and Ba/Zr; and (iii) they are enriched in Ti/Y, Zr/Y, La/Zr, Sr/Zr, Sr/Ba, Zr/Nb(?) and La/Nb(?). The ΣNd of island-arc tholeiites is depleted relative to N-MORB by only a small amount (+8.3-9) (De Paolo, 1981).

Trace element characteristics of a variety of island-arc volcanics are given in Tables 3.11 and 3.12. The volcanics used in this compilation are predominantly basalts but they are more fractionated than HMA and some ratios have undoubtedly been changed relative to that in their source. This problem may have been circumvented to a certain extent by using the island-arc basalts (IAB) of Sun (1980).

Compared to IAB and an average of THS and CAS from Java and Bali, Papua, Lau and Dominica, type-C HMA are characterized by (i) lower Ti/Zr and possibly Ti/Y ratios; (ii) higher Zr/Y and Zr/Nb ratios, (iii) lower Ba/Zr, La/Zr, La/Nb, La/Sr and (excluding Cape Vogel) Sr/Zr; and (iv) Sr/Ba ratios are higher. ΣNd values is island arcs are highly variable. De Paolo (1981), De Paolo & Johnson (1979) and De Paolo & Wasserburg (1977) reported values ranging from +6 to 10, with an average of +8 suggested for magmatic arcs. However, Hawkesworth (1979) and Hawkesworth *et al.* (1979) reported values ranging from -0.4 to +6.2 in microphyric basalts on Grenada. Some of these values overlap those reported in type-C HMA (Table 3.6).

Table 3.10

Island-arc tholeiites: selected trace element abundances and ratios.

	Range*	IAT/N-MORB†	Prim IAT§/ N-MORB
Ti/Zr	80-136	0.73-1.25	1.25
Ti/Y	180-270	0.56-0.84	0.78
Zr/Y	1.8-3.5	0.61-1.19	0.62
Ba/Zr	1.03-5.0	7.3-35.5	35.5
La/Zr	0.031-0.059	0.86-1.64	1.64
Sr/Zr	1.93-9.09	1.3-6.23	6.23
Sr/Ba	1.72-2.66	0.17-0.26	0.18
K/Rb	527-1138	0.50-1.07	0.66
La/Yb	0.96-1.38	1.05-1.52	
$(La/Sm)_N$	0.43-0.83	0.64-1.24	0.74
$(La/Yb)_N$	0.65-0.94		
Zr/Nb	31-44	1.13-1.61	1.13
La/Nb	1.64-1.86	1.69-1.92	1.92
La/Sr	0.007-0.018	0.29-0.75	0.29
$^{87}Sr/^{86}Sr$	0.7037-0.7039		
ΣNd	+8.3-9		
La (ppm)	1.3-2.7 ×	0.43-0.90 ℓ	0.43 ℓ
Sr	129-290 ×	1.04-2.40	1.61
Ba	67-126 ×	5.6-10.5	9.17
Zr	22-77 ×	0.26-0.91	0.26
Y	12-30 ×	0.41-1.03	0.41

* Based on data selected from: Hawkesworth *et al.* (1977), McReath (1972), Brown *et al.* (1977), Hawkesworth & Powell (1980), Sun (1980), Gill (1970, 1976).

† N-MORB from Sun (1980).

§ Primitive IAT from Sun (1980).

× abundances in ppm.

ℓ ratio of ppm abundances in IAT/N-MORB and primitive IAT/N-MORB.

Table 3.11

Selected trace element ratios and abundances in island-arc volcanics.

	Java and Bali			Papua	Lau		Dominica	Grenada	
	THS(B)	CAS(B)	HKCAS(B)	CAS(BA)	CAS(BA)	IAB	THS(B)	MP(B)	ANK(B)
Ti/Zr	78	59	61	60	90	116	116	53	35
Ti/Y	240	272	246	286	143	310	392	286	243
Zr/Y	3.08	4.61	4.04	4.76	2.49	2.66	3.38	5.4	7
Ba/Zr	1.62	2.64	4.25	3.09	3.15	7.50	2.39	2.59	3.72
La/Zr	0.070	0.113	0.204	0.44	0.103	0.25	0.127	0.255	0.131
Sr/Zr	4.19	3.10	4.78	10	3.15	7.50	7.05	5.98	14.25
Sr/Ba	2.58	1.18	1.13	3.24	2.08	1.83	2.95	2.30	3.82
K/Rb	392	377	297	535	587	617	254	330	690
La/Yb	2.5	6.1	15	6.5	2.94		3.09	15.5	11.42
$(La/SM)_N$	0.77	2.30	3.54	2.39	1.50	2.17	1.47	2.88	2.36
$(La/Yb)_N$	1.03	4.11	10.41	4.37	1.99		2.09	10.50	7.72
Zr/Nb	27	22	10	20	37	29	15	12	15
La/Nb	1.93	2.52	2.1	2.8	3.85	7.14	1.86	2.92	2.02
La/Sr	0.017	0.037	0.043	0.014	0.033	0.018	0.018	0.042	0.009
$^{87}Sr/^{86}Sr$					0.7033		0.7044		
ΣNd							+3.9-4.7	-0.4-+6.2	+6.1-8.6
La	5.2	14.6	23.1	36	10	10	5.6	27.5	20.2
Sr	310	400	540	810	306	550	310	646	2194
Ba	120	340	480	250	147	300	105	280	574
Zr	74	129	113	81	97	40	44	108	154
Y	24	28	28	17	39	15	13	20	22

THS = tholeiitic series, CAS = calcalkaline series, HKCAS = high K calcalkaline series, from Whitford *et al.* (1979). B = basalt (<52% SiO_2), BA = basaltic andesite (52-57% SiO_2) (see Whitford *et al.* (1979). MP = microphyric, ANK = ankaramitic (see Hawkesworth *et al.*, 1979; Arculus, 1978).
Sources: Java and Bali - Whitford *et al.* (1979); Papua - Bultitude *et al.* (1978); Lau - Gill (1976); IAB - Sun (1980); Dominica and Grenada - Brown *et al.* (1977), Arculus (1976, 1978), Hawkesworth *et al.* (1979), Hawkesworth & Powell (1980).

Table 3.12

Selected trace element ratios and abundances in island-arc volcanics: normalized to N-MORB.

	Java and Bali			Papua	Lau		Dominica	Grenada		St.Kitts
	THS	CAS	HKCAS	CAS	CAS	IAB	THS	MP	ANK	IAT
Ti/Zr	0.72	0.54	0.56	0.55	0.83	1.06	1.06	0.49	0.32	0.83
Ti/Y	0.75	0.85	0.77	0.89	0.45	0.97	1.22	0.89	0.76	0.83
Zr/Y	1.05	1.57	1.38	1.62	0.85	0.91	1.15	1.84	2.39	1.02
Ba/Zr	11.49	18.72	30.14	21.91	22.34	53.19	16.95	18.37	26.38	13.76
La/Zr	1.94	3.14	5.67	12.22	2.86	6.94	3.53	7.08	3.61	1.39
Sr/Zr	2.87	2.12	3.27	6.85	2.16	5.14	4.83	4.10	9.76	3.05
Sr/Ba	0.25	0.11	0.11	0.31	0.20	0.18	0.29	0.22	0.37	0.22
K/Rb	0.37	0.36	0.28	0.50	0.55	0.58	0.24	0.31	0.65	0.57
La/Yb	2.75	6.70	16.50	7.14	3.23		3.40	17.03	12.55	1.53
$(La/Sm)_N$	1.15	3.43	5.28	3.57	2.24	3.24	2.19	4.30	3.52	1.23
Zr/Nb	0.99	0.80	0.36	0.73	1.35	1.06	0.55	0.44	0.55	1.26
La/Nb	1.99	2.60	2.16	2.89	3.97	7.36	1.92	3.01	2.08	1.69
La/Sr	0.71	1.54	1.79	0.58	1.38	0.75	0.75	1.75	0.38	0.46
La	1.73	4.87	7.7	12	3.3	3.3	1.87	9.17	6.73	1.09
Sr	2.5	3.23	4.35	6.5	2.5	4.4	2.50	5.21	17.70	2.34
Ba	10	28.33	40	20.8	12.3	25	8.76	23.33	47.83	10.5
Zr	0.87	1.52	1.33	0.95	1.14	0.47	0.52	1.27	1.81	0.76
Y	0.83	0.97	0.97	0.59	1.35	0.52	0.45	0.69	0.76	0.76

Data sources given in Table 3.11.

3.4.3 Nature of the Enriching Event in Type-E HMA

Type-E HMA normalized to a type-C HMA from Cape Vogel is given in Table 3.5. The low Ti/Zr ratio in HMA is accentuated during this enrichment and this remains a distinctive feature of these rocks. Changes in Ti/Y, Zr/Y, La/Zr, Sr/Ba, Zr/Nb, and La/Nb are common to the enrichment from type-C to type-E HMA and also N-MORB to E-MORB, OIB and NM. Of particular note is the decrease in Zr/Nb. Most island-arc volcanics (Table 3.12) do not show a decrease in Zr/Nb relative to N-MORB, except in highly potassic calc-alkaline sequences or in the case of Dominica and Grenada. The enrichment in the latter case and for E-MORB, OIB and NM relative to N-MORB is accompanied by markedly higher Ba/Zr, La/Zr, Sr/Zr, La/Yb $(La/Sm)_N$, La/Nb, and La/Sr compared to type-E HMA.

3.4.4 Discussion

The enrichment patterns observed in HMA appear to differ from those found in most volcanics and it is difficult to determine what processes may have been responsible. The occurrence of HMA in an island-arc environment allows a wide possible range of processes which may have affected their source area. These include mantle metasomatism such as that encountered in ocean islands, sediment subduction, dehydration of subducted oceanic crust, and partial melting of subducted oceanic crust (cf. T.H. Green, 1980; Perfit *et al.*, 1980). Certainly if these or a combination of these processes did affect the mantle source for HMA, they have done so in a seemingly unique manner.

The low ΣNd ratios found in HMA suggested to Hickey & Frey (1981) that it was either sediment subduction or mantle metasomatism from an ocean island type source. These authors dismissed sediment subduction on the basis of K/La and Rb/La ratios. These ratios are high in type-C HMA; however, it is possible this is due to alteration (see above).

Interestingly, if the K/La and Rb/La ratios are compared to those in kimberlites, nephelinites and ocean-island basalts then using the argument of Hickey & Frey (1981) these sources could as well be excluded. Comparing the *trends* predicted from mixing upper continental crust (Taylor, 1977) with N-MORB, then at least in a relative sense they show the same pattern as indicated by type-C HMA (again excluding Zr/Nb). This approach is undoubtedly too simplistic since it views the sediment involvement in a purely mechanical mixing method, whereas they may be involved in generating a dehydrating fluid or have residual phases present which alter the trace element pattern. Nonetheless the present isotopic data, including the Pb isotopic data from the Bonin Islands, do not preclude a sedimentary component in explaining the trace element characteristics of HMA.

During the subduction of ocean crust it is inevitable that dehydration of hydrous phases in the ocean crust will occur (Delaney & Helgeson, 1978; Anderson *et al.*, 1976). Unfortunately we have, as yet, poor constraints on the nature of the phases involved, P/T conditions of dehydration or nature of the resultant fluids and the manner of their interaction with the overlying mantle wedge (Delany & Helgeson, 1978; Fyfe & McBirney, 1975). As a consequence, one can generally attribute to the fluid evolved by dehydration the characteristics needed to explain many aspects of the various island-arc volcanics (Anderson *et al.*, 1978). Saunders *et al.* (1980b) argued that the LFS and perhaps LREE will be released during dehydration, along with silica and the alkalis. Hawkesworth (1979) however suggested that significant quantities of REE may not be released and therefore the Nd-isotope composition may reflect pre-subduction evolution of the over-riding lithosphere.

The high volatile contents, crystal-rich nature, vesicularity and the petrogenetic constraints from experimental work (Chapter 5) suggest water plays an important role in the genesis of HMA. This water may be derived from a subduction zone, as the $^3He/^4He$ data of Bloomer *et al.* (1979) and Poreda & Craig (1979) suggested, at least in some HMA. If the H_2O is derived from the slab we could expect to find LFS and other alkali elements, and possibly REE, accompanying it. However a quantitative assessment for the role of dehydration is difficult since other enrichment processes carry these elements as well. Perhaps the lower LFS/HFS and LREE/LFS elements in HMA compared to island-arc volcanics reflect a lesser role for dehydration in explaining the chemistry of HMA.

Mantle metasomatism in the form of a silicate melt, e.g. undersaturated nephelenitic or kimberlitic liquids (O'Nions *et al.*, 1979; Frey *et al.*, 1978; Wood, 1979) is called on to explain the chemistry of enriched oceanic volcanics. If a melt phase is responsible for the chemistry of HMA, then it must have a Ti-bearing mineral left in the residue to account for the low Ti/Zr ratios. While it is unclear in type-C HMA, for type-E HMA it is likely that garnet would have also to be a residual phase since a $(La/Yb)_N$ ratio of >7 is indicated for EF2 (see above).

3.5 SUMMARY

High-magnesian andesites are characterized by ~56-59% SiO_2 high Mg-numbers (66-82), low TiO_2 contents (< 0.5%), low Ti/Zr (<60), low CaO/Al_2O_3 ratios (~<0.6), high Cr/Ni ratios (~>3), and low incompatible trace element abundances (generally less than 10x chondritic). Two groups of HMA, type-C and type-E, are recognized, based primarily on

REE patterns and also on Zr/Nb ratios. Both these groups show LREE enrichment. The origin of the trace element characteristics in these rocks is due to at least a two-stage enrichment event superimposed on a previously depleted source.

These enrichment processes appear to be unique to HMA as there are no close analogies to be found in either oceanic-island or island-arc volcanics. It is unclear what possible combination of processes may have given rise to the enrichment events. Certainly a sedimentary component can not be ruled out and it seems almost certain that dehydration of oceanic crust must play a part. Regardless of the processes occurring, it seems certain that a Ti-bearing phase, capable of fractionating Ti, Zr, and probably Y, is required at some stage.

The isotopic studies on HMA are as yet too restricted to delimit the origin of the enriching events. Further work on Sm/Nd, Rb/Sr, and Pb, on the same sample, is clearly required. Nonetheless, the Sm/Nd data are very informative since they indicate a long-term enriched mantle source for the Bonin Islands HMA, a more recently enriched mantle source for Cape Vogel HMA, or a sedimentary component.

Chapter 4

EQUILIBRIA IN THE Mg-RICH PART OF THE PYROXENE QUADRILATERAL

4.1 INTRODUCTION

A thorough understanding of the phase relationships of pyroxenes is essential to the interpretation of many igneous (and other) rocks. Establishing the equilibrium phase relations in pyroxenes involves not only experimental work but careful observation of the natural phase assemblages (Huebner, 1980). The occurrence of clinoenstatite in some high-Mg andesites is an excellent example of the interplay necessary between experimental and natural pyroxene studies. The distinctive crystallization of protoenstatite (clinoenstatite precursor - Tilley *et al.*, 1964; Dallwitz *et al.*, 1966; Nakamura, 1971; Huebner, 1980) over a limited compositional range, and its replacement by orthopyroxene at a particular composition, suggests that it may be possible to constrain the extrusion temperatures, and to limit the conditions of origin of parental magmas of the high-Mg andesites using knowledge of the stability relations of protoenstatite and orthopyroxene. Conversely, observed phase relations in HMA have been important in deducing possible equilibrium phase relations in the pyroxene quadrilateral (Nakamura, 1971).

Recent controversy concerning the nature of the phase relations in the Mg-rich portion of the pyroxene quadrilateral (Huebner, 1980; Longhi & Boudreau, 1980), and the limited amount of data available on protoenstatite stability, has necessitated a re-examination of phase relations on the join $Mg_2Si_2O_6$-$CaMgSi_2O_6$ and in the system CaO-FeO-MgO-SiO_2 (CFMS).

4.1.1 Previous Work and Nature of the Controversy

Atlas (1952) studied phase equilibria in the system $MgSiO_3$-$CaMgSi_2O_6$ and also the polymorphism of $MgSiO_3$. Much of his work in the system $MgSiO_3$-$CaMgSi_2O_6$ was redone as part of a more comprehensive study by Boyd & Schairer (1964); however, his determination of the orthopyroxene-protopyroxene transition temperature (985 ± 10°C) in the pure $MgSiO_3$ system has been confirmed by Anastasiou & Seifert (1972) and Smyth (1974).

The stability fields of calcium-poor pyroxenes in the system $Mg_2Si_2O_6$-$CaMgSi_2O_6$ are limited by the reactions schematically presented in Figure 4.1 (Warner, 1975; Mori & Green, 1975) and are related to the stability fields of orthoenstatite, protoenstatite and Ca-free high temperature clinopyroxene ("pigeonite") in the system $Mg_2Si_2O_6$. The position of the invariant point A in $CaMgSi_2O_6$-$Mg_2Si_2O_6$ is estimated as 1.6 kb and 1280°C (Warner, 1975; Mori & Green, 1975). This P-T location is subject to considerable uncertainty arising chiefly from inadequacies in conventional experimental techniques at low pressures and high temperatures. The location of invariant point A' is not well constrained. The univariant reaction OE $\leftrightarrows$ PE ($Mg_2Si_2O_6$) passes through 1 bar, 985°C (see above) and the PE $\leftrightarrows$ PI may pass through 1 bar, 1400°C if the experiments in the $Mg_2Si_2O_6$-$LiScSi_2O_6$ system can be extrapolated to pure $Mg_2Si_2O_6$ (Takeuchi, 1978).

Phase relations in the pyroxene quadrilateral presented by Nakamura (1971) (see Figure 4.2) are consistent with the phase relations depicted in Figure 4.1, assuming the 1 atm. P-axis passes below invariant point A. That the 1 atm. P-axis would pass below A is inherent in the interpretation of experimental results by Warner (1975) and is consistent with the relations on the $Mg_2Si_2O_6$-$CaMgSi_2O_6$ join as depicted

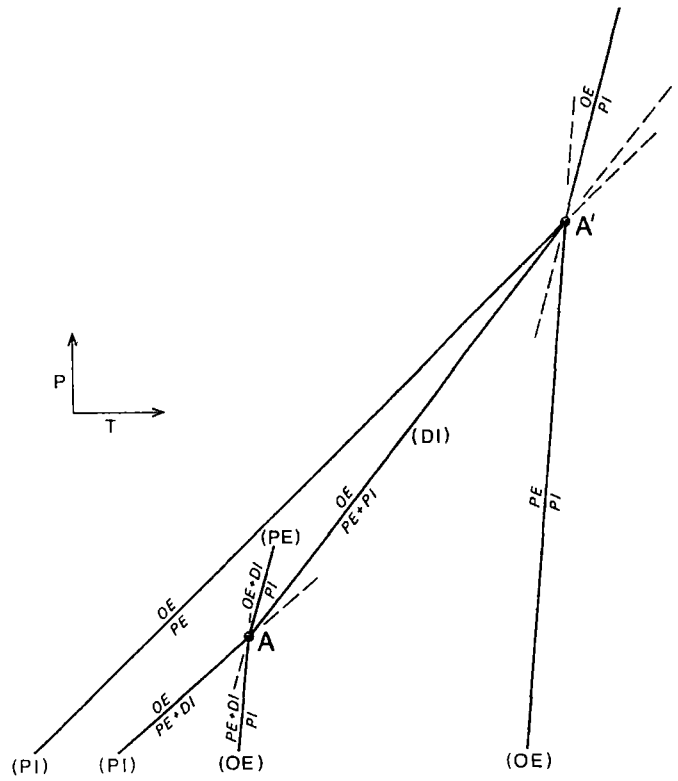

Figure 4.1 Schematic P-T projection of inferred invariant and univariant pyroxene phase equilibrium relationships for the systems $Mg_2Si_2O_6$ and $Mg_2Si_2O_6$-$CaMgSi_2O_6$ (after Warner, 1975).

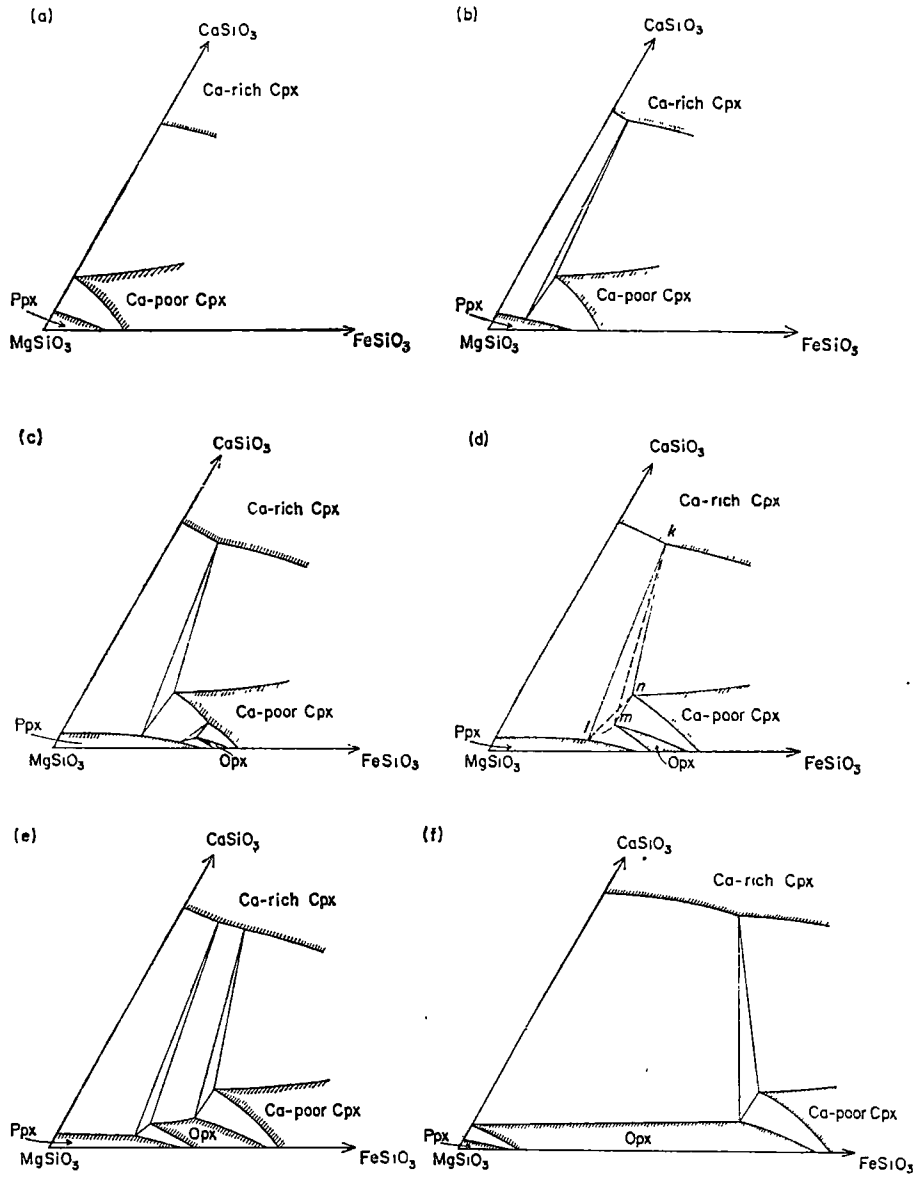

Figure 4.2 Possible isothermal sections on the Mg-rich part of the pyroxene quadrilateral. Temperature falls successively from (a) to (f). From Nakamura (1971).

by Boyd & Schairer (1964), Kushiro (1972b), and Warner (1975; for $P < 1.5$ kb).

Longhi & Boudreau (1980) re-investigated the system forsterite (Fo)-diopside (Di)-silica (SiO_2) at one atmosphere and suggested that there is an orthoenstatite liquidus field in this system. Foster & Lin (1975) had also noted the existence of an OE liquidus field in the same system. Longhi & Boudreau (1980) and Huebner (1980) presented reviews of the work by Yang & Foster (1972), Yang (1973) and Kushiro (1972b), and concluded that these authors had also found evidence for the existence of an OE liquidus field, however misidentification of the low-Ca pyroxene phases had led to this field being overlooked.

Based on the interpretation of results from the liquidus studies Longhi & Boudreau (1980) and Huebner (1980) have suggested that the topology of the $Mg_2Si_2O_6$-$CaMgSi_2O_6$ join at 1 atm. should be that shown in Figure 4.3. Longhi and Boudreau (1980) interpreted the OE field to extend from the liquidus to 1375°C (see Figure 4.3A), and to account for the existence of a high and low temperature OE field proposed that there was a bow-like shape for the PE+OE two-phase fields. Huebner (1980) proposed that two lines of evidence suggested that at low pressure OE is continuously stable from low temperature (< 1000°C) to the solidus (see Figure 4.3B). These are (i) PE does not appear to be stable in the presence of augite at pressures > 2 kb, and (ii) when natural magnesian orthopyroxenes are heated in the presence of augite, no protopyroxene was detected.

The topology of the $Mg_2Si_2O_6$-$CaMgSi_2O_6$ join at 1 atm. as depicted in Figure 4.3A is inconsistent with a Schreinemakers' analysis of the pyroxene relations presented in Figure 4.1. The topology depicted in Figure 4.3B is inconsistent with a Schreinemakers' analysis of the pyroxene relations presented in Figure 4.1, if the invariant point A

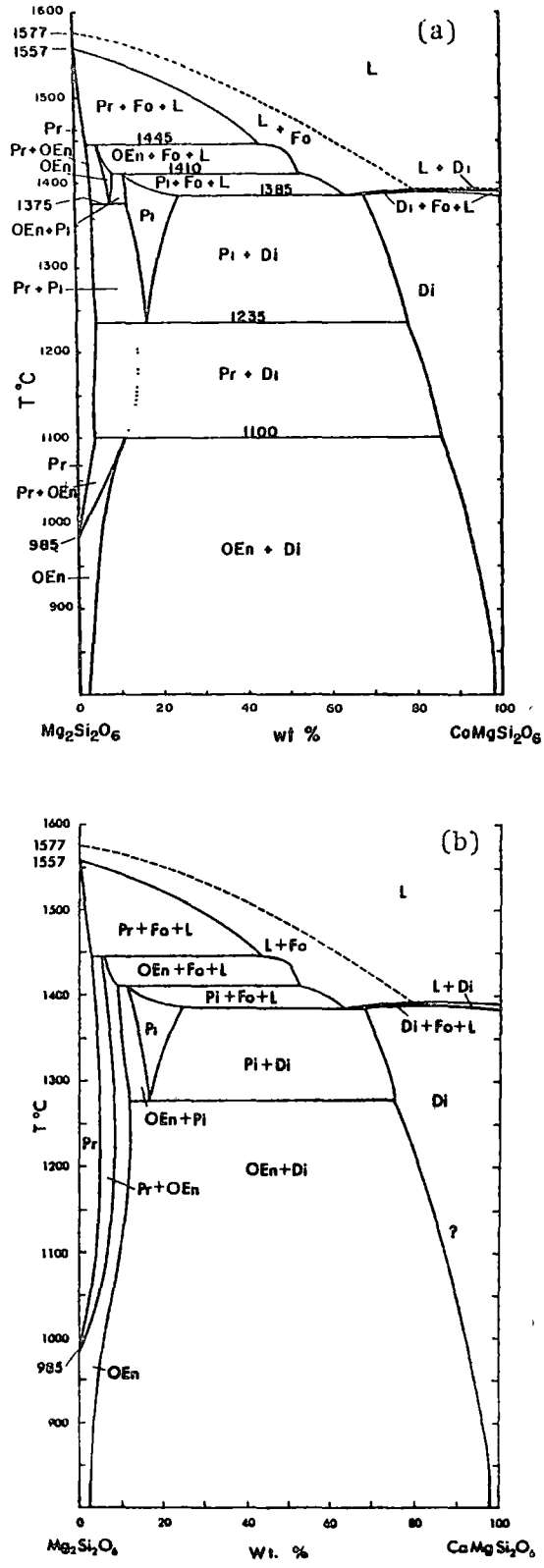

Figure 4.5 Temperature-composition diagram for the system $Mg_2Si_2O_6$-$CaMgSi_2O_6$ at 1 bar. (a) Phase topology depicted by Longhi & Boudreau (1980). (b) Phase topology suggested by Huebner (1980) based on same data as above. After Huebner (1980).

is real. However, if the invariant point A is metastable or unreal the phase relations at pressure >A and <A' are consistent with the topology of the $Mg_2Si_2O_6$-$CaMgSi_2O_6$ join as depicted in Figure 4.3B (cf. Warner, 1975; for P > 1.5 kb).

4.2 PRESENT STUDY

4.2.1 Experimental Techniques

Sixteen mixes were prepared by mechanical mixing of clinoenstatite (CE), enstatite (OE), diopside (DI) and hypersthene (HY) Mg_{52} . Proportions of the end members were selected to produce (i) mixes of Mg-numbers 85, 90, 95 with 0, 1, 4 wt.% CaO; (ii) mixes of Mg-number 98 with 1, 2, 6 wt.% CaO; and (iii) mixes of Mg_{100} with 4, 6, 8, 15 wt.% Di. Note that 1 wt.% CaO is equivalent to approximately 4 wt.% Di. During all stages of preparation mixes were ground to dryness under acetone a minimum of three times, in an agate mortar. Particle size in the resulting mixes was generally less than 10 microns, with 10-20 micron-sized particles forming less than 5-20% of the mix.

Prior to the preparation of the above mixes the pure phases were prepared from oxides, carbonate or metal AR grade reagents. Details of the synthesis of the pure phases are given below.

Clinoenstatite was prepared by sintering a 1 gram pellet of $MgSiO_3$ at 1300°C/1 atm. in a Pt crucible, for 48 hours. Minor amounts of quartz and olivine were present, as indicated by a routine X-ray diffractometer tracing. 300 mg of pure orthoenstatite was made by running CE at 15 kb/1150°C for 6 hours in large capacity $Ag_{50}Pd_{50}$ capsules (3 mm diameter).

Diopside was prepared by sintering a pellet at 1300°C/1 atm. in a Pt crucible for 48 hours. The mix was well crystallized and no other

phases were observed in the X-ray diffraction pattern. 300 mg of this DI was run at 10 kb/1150°C for 5 hours in a large capacity $Ag_{50}Pd_{50}$ capsule to provide material for seeds, chemical analysis and as a check on the 1 atm. product.

Hypersthene was prepared using a three-stage procedure. Firstly, MgO, Fe_2O_3 and SiO_2 were dried for 3 hours at 600°C. Fe metal was then mixed in and a pellet made. The resultant mix was run in an evacuated SiO_2 tube for 3 days at 1000°C, along with a pellet of 1.5 grams of Fe-metal to ensure no oxidation took place. The resulting product was poorly crystalline and very fine grained. 300 mg of well crystallized hypersthene was made at 20 kb/1050°C by running the 1 atm. HY for 4.5 hours in $Ag_{50}Pd_{50}$ capsules.

Seeds of high pressure OE and HY were added to the Mg_{85-95} mixes in amounts such that the seeds were 10% OE and 30% HY of the total OE and HY contents respectively of the mixes. In the Mg_{85-95} runs all DI was from the high pressure synthesis. The remainder of the components in the Mg_{85-95} compositions and all components in other compositions were from 1 atm. sintered oxide mixes.

4.2.1.1 Run conditions

Fe-bearing runs were performed in spec-pure Fe capsules sealed in evacuated SiO_2 tubes. CE-DI mixes were run in Pt capsules, which had been sealed by welding at the base and crimping at the top, in open SiO_2 tubes. Runs were made in either a one-inch or three-quarter inch 1 atm. furnace. A harness of Pt wire capable of holding three SiO_2 tubes, each containing up to three capsules, made it possible to run up to nine mixes at a time. The position of the hot "spot" was checked before each run and temperature variation due to thermal gradients in the assembly and calibration is within ± 5°C. The runs were drop quenched into a beaker of water.

4.2.1.2 Examination of run products

Each run was examined using three techniques: the optical microscope, SEM-microprobe, and X-ray powder camera. Optical mounts were made of crushed run products placed in refractive index oil. Emphasis in the optical work was on the detection of twinning, cracking, crystal morphology and overall texture.

X-ray camera patterns were obtained on needles made up finely ground run products and gum tragacanth. An 11.54 cm Straumanis camera and Fe-tube were used. Identification of the phases was achieved in large part by comparison with films run on standards of known composition. Standards used were: (a) natural CE separated from a high-Mg andesite from Cape Vogel, PNG; (b) synthetic OE and DI (conditions of origin described above); (c) natural OE and DI (Mg_{92}) from a spinel lherzolite xenolith from Mt Porndon, Victoria (N. Ortez, pers. comm., 1980). CE and Mg-rich pigeonite (PI) have indistinguishable X-ray powder patterns. PE was identified on the basis of the pattern given in Atlas (1952).

Probe mounts of run products were made either of small fragments, or in the case of some CaO-poor runs a slurry of powder in resin had to be prepared first. A JEOL 50X-A SEM-microprobe with an EDAX energy dispersive system was used. Calibration of the system is described by Griffin (1979). High pressure DI, OE and HY were used to double check the calibration.

PE is recognized by either the presence of its distinctive X-ray pattern or in the more general case by the presence of its lower temperature multiply-twinned inversion product CE. As noted, CE and PI have identical powder X-ray patterns (at least in the lines observable with our concentrations and techniques), therefore a combination of microprobe and XRD techniques is required. Thus observations and interpretations are related as follows:

a) very low CaO phase (CE or PI) + 1-2% CaO phase OE (EPMA) (X-ray)		CE + OE
b) 1-2% CaO phase OE + 2% CaO phase (CE or PI) (EPMA) (X-ray)		PI + OE

In (a) CE is interpreted to be present and implies that PE+OE were originally present. PE+OE assemblages may also be identified by the presence of a very low CaO-bearing phase plus a PE X-ray pattern.

4.2.2 Results

4.2.2.1 Attainment of equilibrium

One of the major difficulties hampering interpretation of the pyroxene phase relations in the Mg-rich portion of the pyroxene quadrilateral is that of knowing when equilibrium has been attained (Huebner, 1980). Subsolidus runs are particularly notorious for their slow reaction rates (Huebner & Turnock, 1980; Boyd & Schairer, 1964). Internal consistency, phase homogeneity and results consistent with our knowledge of crystal chemistry are the major criteria which have been adopted in this study in recognising or presuming the attainment of equilibrium (see also Huebner & Turnock, 1980). Run times for experiments were selected on the basis of previous experience in subsolidus (metamorphic) phase equilibrium studies (S. Harley, pers. comm., 1980). Experiments at 1300°C were run for 4 and 7 days with identical results being obtained.

Two series of Fe-bearing runs failed to meet the equilibrium requirements noted above. One series at 1100°C was run for 4 weeks, however original mix heterogeneities were present and these led to the development of quartz and olivine. These products were larger than anything in the original mix and presumably they grew at the expense of the poorly crystalline hypersthene. Pure diopside and enstatite seeds were also noted.

A series of runs at 1200°C (2 weeks run time) showed phase homogeneity however the results were inconsistent with those from higher temperature experiments in this study (see below) and also with the experiments of Longhi & Boudreau (1980), and the interpretation of Huebner (1980) (see above). In particular the three-phase assemblage PI - OE-PE was suggested to be present, based on X-ray, optical and probe examination of the run products. This association would mark the reaction OE + DI $\rightleftarrows$ PE + PI and thus define the upper stability field of orthopyroxene. The existence of orthopyroxene in the 1300°, 1370° and 1400°C experiments shows that the above reaction cannot limit the stability field of orthopyroxene and the 1200°C runs were therefore interpreted as non-equilibrium runs.

Interpretation of the 1370° and 1400°C experiments in the pure Mg system was hampered by the presence of disequilibrium assemblages in some runs. For example, the 4% and 6% Di runs at 1400°C contain the assemblage CE (inverted PE) + OE, which with the increasing Di content would be expected to give way to OE and/or OE+PI. The 8% Di (1400°C) run however contains OE+CE+PI. A possible interpretation of this observation is that CE persists metastably in the presence of a high-Ca-bearing phase, i.e. PI. This is consistent with the observation that OE increases in abundance from the 4% to 6% Di run and then decreases abruptly in the 8% Di run.

An attempt was made to reverse the reaction PI $\rightleftarrows$ DI + OE. Some of the run product from the 1370°C 15% Di run, which was homogeneous PI, was loaded in another capsule and run at 1280°C for 4 days along with an equivalent composition made up from 1 atm. sintered oxide mixes. Conditions for the run were estimated from our work and that of Warner (1975). The PI from the 1370°C run remained "stable" at the lower temperature, while the sintered oxide mix showed signs of obvious

disequilibrium, i.e. unreacted DI seeds remained and olivine and quartz appeared. According to Huebner (1980) (see also Figure 4.3B) the reaction PI $\rightleftarrows$ DI + OE occurs at about 1270 ± 10°C and the close proximity of our runs to this reaction position may account in part for the lack of success.

4.2.2.2 Bulk composition

It was difficult to check the bulk composition of an individual run because of the disaggregated texture of most of the runs. Fe-loss to Pt capsules was a minor problem (see also Chapter 5) as indicated in Table 4.1. Ca-content of the mixes was dependent on the thorough mixing and reaction of the diopside component of the mix. In general Ca-contents appear to be slightly lower than expected in almost all runs, and observation attributed to persistence of diopside seeds. The difficulties in knowing the reacting composition of the mix would be a problem if we were dependent on only X-ray and optical analysis. However, with use of the microprobe we can determine the phase compositions and use these results to plot in the quadrilateral, rather than having to rely on an assumed bulk composition.

4.2.2.3 Results

Results from experiments which met the criteria for having attained equilibrium are given in Table 4.1 and selected analyses of products are given in Table 4.2. Details for specific run compositions or temperatures are given below.

Mg_{100} - 1400°C The 4% and 8% Di runs were characterized by 20-30 micron sized crystals. Orthopyroxene in the 6% Di run however ranged from 60-120 microns and may enclose low-Ca (PE or CE) crystals. The orthopyroxene X-ray pattern is clearly developed in the 6% Di run, while intensity differences in the 2.93-3.02 and 3.27-3.35d (Å) lines point to its presence in the 4% and 8% Di runs. The X-ray patterns

Table 4.1

Results of "equilibrium" 1 atmosphere pyroxene experiments.

T(°C)	Mix (wt.%)	Products†		Composition*		
				CaO	(range)	n
1400	96EN-4DI	CE		0.62	(0.48-0.82)	27
(96 hours)		OE		1.21	(1.20-1.22)	3
	94EN-6DI	CE		0.64	(0.51-0.83)	17
		OE		1.54	(1.27-1.68)	17
	92EN-8DI	CE		0.66	(0.56-0.77)	26
		OE		1.40	(0.93-1.87)	5
		PI		2.30	(2.0-2.6)	14
1370	94EN-6DI	OE		0.97	(0.83-1.17)	12
(96 hours)		PI		2.91	(2.68-3.24)	21
	92EN-8DI	OE		0.94	(0.73-1.20)	9
		PI		3.03	(2.58-3.25)	21
	85EN-15DI	PI		4.07	(3.78-4.38)	10
	Mg_{98}-4DI	CE	Mg_{95}	0.73	(0.68-0.80)	5
		OE	$Mg_{94.5}$	1.50	(1.38-1.68)	12
	Mg_{98}-8DI	OE	Mg_{95}	1.66	(1.64-1.72)	8
		PI	$Mg_{94.6}$	2.23	(2.18-2.30)	11
	Mg_{98}-24DI	PI	Mg_{95}	5.11	(4.68-5.65)	12
1300	Mg_{95}-0% CaO	PE	Mg_{92}			10
(168 hours)	1% CaO	OE	Mg_{92}	1.1	(0.96-1.15)	14
	4% CaO	PI	Mg_{92}	3.60	(3.32-4.16)	30
	Mg_{90}-0% CaO	PE	Mg_{87}			10
	1% CaO	OE	Mg_{87}	0.9	(0.74-1.18)	39
	4% CaO	PI	Mg_{87}	3.57	(3.4-3.82)	19
	Mg_{85}-1% CaO	OE	$Mg_{84.3}$	0.86	(0.74-1.12)	11
	4% CaO	PI	$Mg_{83.5}$	3.50	(3.34-3.77)	8

† identification based on X-ray, probe and optical examination.
* average CaO in wt.%
n = number of analyses.

Table 4.2

Representative analyses of pyroxenes from 1 atm. CMS and CFMS experiments.

T, °C	1300	1300	1300	1300	1300	1300	1370	1370
CaO%(mix)	1	4	1	4	1	4	1	1
Mg no.	85	85	90	90	95	95	98	98
SiO_2	55.58	56.03	57.07	56.49	58.21	57.37	59.25	59.25
FeO	10.65	10.21	8.51	8.19	5.38	5.29	3.51	3.72
MgO	31.82	29.68	33.15	31.21	34.83	33.21	36.57	35.57
CaO	0.84	3.46	0.89	3.59	1.14	3.57	0.68	1.46
Mg no.	84.19	83.83	87.4	87.19	92	91.81	94.87	94.46
Ca:Mg:Fe	1.6/82.9/15.6	6.6/78.3/15.1	1.7/86,12.4	6.7/81.4/12	2.1,90.1,7.8	6.6/85.7/7.7	1.3/93.7/5.1	2.7/91.9/5.4
T, °C	1370	1370	1370	1370	1370	1370	1370	1370
CaO%(mix)	2	2	6	1.5	1.5	2	2	3.75
Mg no.	98	98	98	100	100	100	100	100
SiO_2	58.95	58.87	58.57	60.18	59.87	60.28	59.27	59.89
FeO	3.56	3.48	3.06					
MgO	35.87	35.41	33.44	38.77	37.27	38.50	36.72	36.27
CaO	1.62	2.23	4.93	0.83	2.86	0.95	2.93	3.84
Mg no.	94.75	94.79	95.11	100	100	100	100	100
Ca:Mg:Fe	3/92/5	4.1/90.9/5	9.1/86.4/4.4	1.5/98.5	5.2/94.8	1.7/98.3	5.4/94.6	7.1/92.9
T, °C	1400	1400	1400	1400	1400	1400	1400	
CaO%(mix)	1	1	1.5	1.5	2	2	2	
Mg no.	100	100	100	100	100	100	100	
SiO_2	59.9	59.75	60.05	60.11	59.97	59.48	59.62	
MgO	39.46	38.72	38.52	39.27	39.42	37.82	38.76	
CaO	0.64	1.22	1.42	0.63	0.61	2.39	1.62	
Mg no.	100	100	100	100	100	100	100	
Ca:Mg:Fe	1.2/98.8	2.2/97.8	2.6/97.4	1.1/98.9	1.1/98.9	4.3/95.7	2.9/97.1	

confirm the existence of the CE/PI phase in addition to OE and do not show PE. Microprobe analyses combined with the XRD data thus indicate the presence of OE+CE (after PE). The CE in these runs does not show transverse cracks or well-developed multiple twinning.

Mg_{100} - 1370°C Grain size in the 6% Di run is predominantly less than 10 microns; however, orthopyroxenes form approximately 20 micron sized prismatic crystals with parallel extinction. The 8% and 15% Di runs have an overall grain size of 10-20 microns. Pigeonite grains appear to have a more regular or less diffuse multiple and simple twinning than clinoenstatite.

Mg_{98} - 1370°C Average grain size increases from 10-20 microns in 4% Di runs through 20 microns in 8% Di to 40-50 microns in the 24% Di run. Twinning is not well developed in any of the runs and many grains have indeterminate extinction. The orthopyroxene is somewhat lath-shaped.

1300°C In general grain size increases from 10-20 microns in Ca-free runs to 30-50 microns in 4% CaO runs. Protoenstatite is the low Ca-bearing phase, as determined by the X-ray pattern and lack of twinning. The orthopyroxene is equigranular and has a well defined X-ray pattern. Orthopyroxene is not obvious in the optical mounts having no distinctive morphology. Pigeonites have well developed twinning.

4.3 DISCUSSION

The results of the 1300-1400°C experiments of this study in the systems CMS and CFMS indicate that *orthopyroxene is a stable phase in this temperature range* and that its stability field extends from the $Mg_2Si_2O_6$-$CaMgSi_2O_6$ join (CMS) into the CFMS pyroxene quadrilateral. The phase relations schematically given in Figure 4.4 are consistent with the experimental results and with the interpretation that the P = 1 atm. axis passes above the invariant point A in Figure 4.1. Referring to Figure 4.4, the temperature for the change from T1 to T2, i.e. the intersection of the PI stability field with the CMS boundary, is not fixed in this study since the three-phase assemblage OE+DI+PI was not encountered. Results from the study of Huebner & Turnock (1980) indicate that the change from phase relations in T1 to those in T2 may take place at temperatures of 1230-1300°C and a temperature of 1275°C is indicated in Figure 4.3B. The reaction OE $\rightleftarrows$ PE + PI (Figure 4.1) will not be reached before melting takes place in either CMS or CFMS, thus this reaction cannot be used to construct possible phase relations beyond T2 (Huebner & Turnock, 1980; Longhi & Boudreau, 1980).

The experimental results and interpretation offered here are in agreement with those suggested by Huebner (1980) both for the $CaMgSi_2O_6$-$Mg_2Si_2O_6$ join (Figure 4.3B) and the solidus phase topology in the Mg-rich portion of the pyroxene quadrilateral (see his Figure 21a). This interpretation implies that invariant point A in Figure 4.1 is imaginary and hence also the reactions, among others, PE + DI $\rightleftarrows$ PI (Nakamura, 1971; Mori & Green, 1975) and OE $\rightleftarrows$ PE + DI (Atlas, 1952), do not occur in real P,T space.

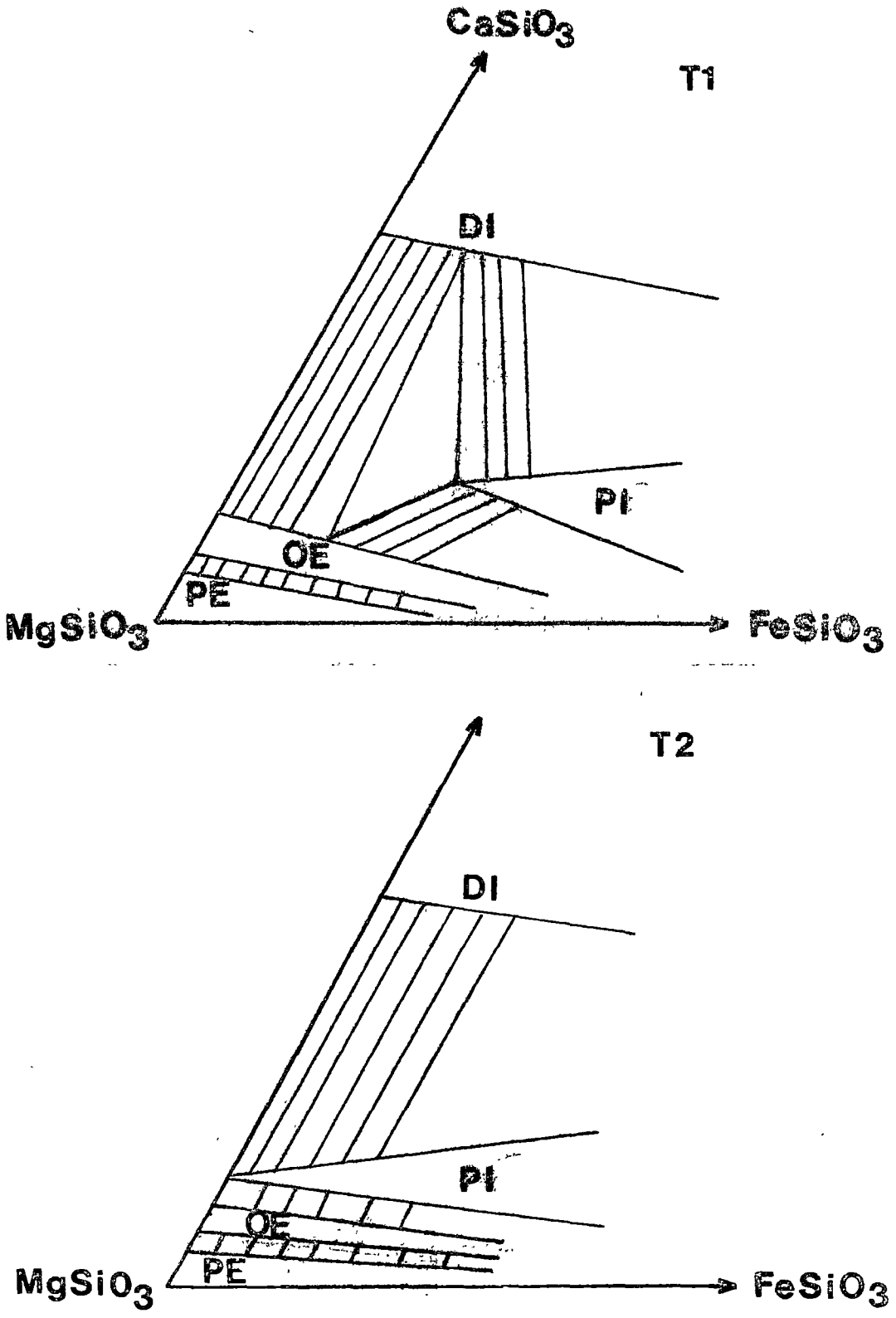

Figure 4.4 Probable isothermal sections in the Mg-rich part of the pyroxene quadrilateral, based on results of this study. Temperatures in T2 higher than T1. In T2, OE+PI and DI+PI stable. In T1, PI $\leftrightharpoons$ OE+DI (univariant in CMS) and PI $\leftrightharpoons$ OE+DI+PI (3-phase field). Temperature of transition from T1 $\rightarrow$ T2 approximately 1230-1250°C (see text).

Experimental evidence for the existence of the reaction OE ⇄ PE + DI comes from three studies, those of Atlas (1952), Boyd & Schairer (1964), and Warner (1975). Warner (1975) investigated the position of the invariant line OE ⇄ PE + DI at 1 kb and 1240°C, however he noted that the results are difficult to interpret since the assemblages he obtained in different runs are incompatible. Boyd & Schairer (1964) failed to locate the solvus boundary in the OE-rich side of the system OE+DI at temperatures of 100-1250°C because of reaction rates. Hydrothermal runs in the lower part of this temperature range were unsuccessful and they noted that the presence of a flux in dry runs created problems. Atlas (1952) did a number of runs using LiF flux and glasses on the OE-rich side of the OE+DI join. His results are equivocal in many respects, for instance, he reported CE+DI+OE at 12.5% Di and 1135°C in an experiment for 12 days, however a run at 15% Di/1130°C for 7 days gave CE+PE+DI and at 20% Di/1140°C for 12 days only CE+DI are reported. Atlas (1952) noted a slight inflection in the OE-DI solvus at 1050-1100°C and he suggested that along with his experimental results this implied the presence of the reaction OE ⇄ PE + DI. Note that Boyd & Schairer also choose to interpret their runs in this manner.

The experimental evidence for the existence of the reaction OE ⇄ PE + DI is certainly equivocal and the phase relations on the Mg-rich side of the OE-DI join are subject to interpretation. It is interesting to note that if the above reaction is accepted then the PE and/or CE phase would need to contain 5-12% Di (~1.2-3% CaO). This is difficult to reconcile with the chemistry of naturally occurring clinoenstatite in HMA and the demonstration that the occurrence of clinoenstatite is sensitive to the Ca-content (normative Di/Di+Hy) of

the magma (see Chapter 2). Based on the experimental results from this study it would suggest that the lack of evidence for OE in the temperature range 1000-1235°C is probably due to the persistence of metastable CE, in a manner similar to that observed in the 1400°C experiments noted earlier.

4.4 CONCLUSIONS

Experimental studies in the systems CMS and CFMS have indicated that orthopyroxene is a stable phase at least up to 1400°C. These results are consistent with the results from liquidus experiments in the forsterite-diopside-silica and anorthite-diopside-enstatite silica at 1 atm. (Yang, 1973; Kushiro, 1972b; Longhi & Boudreau, 1980; Huebner, 1980). The results can be interpreted to imply that ortho-enstatite is a stable phase from <1000°C to >1400°C in the system CMS. This is consistent with the suggestion of Huebner (1980) and suggests that the explanation offered by Longhi & Boudreau (1980) for the existence of two separate temperature stability fields of orthopyroxene is unnecessary.

The experimental results have unfortunately not been of great value in ascertaining the temperature of eruption of HMA. The assemblage present in HMA is not sufficient to pinpoint a point at which the liquidus of HMA intersects the pyroxene solidus. Compositional rather than temperature control determines the appearance of clinoenstatite in HMA. However, the phase relations as depicted in Figure 4.3 and their extensions to CFMS (Figure 4.4) may be of use in interpreting the origin of volcanic rocks which are richer in CaO, and either lack or contain magnesian pigeonite. These relations would then help in deciding on the water content/liquidus temperature for second-

stage lavas found in some ophiolite complexes (cf. Duncan & Green, 1980, 1980b; Cameron, 1980).

Chapter 5

LIQUIDUS STUDIES ON HIGH-Mg ANDESITES

5.1 INTRODUCTION

Experimental studies were undertaken on selected high-Mg andesite compositions from Cape Vogel and on a sample from the Mariana Trench. These studies may constrain the conditions of origin and of extrusion of these rocks in two ways:

(a) by reproducing the observed mineral phases, mineral compositions, and sequence of appearance of phases as displayed in the natural rocks, and

(b) by defining conditions of P, T, and $\%H_2O$ at which the liquids are saturated with both olivine and orthopyroxene, of compositions appropriate to upper mantle lherzolite or harzburgite, i.e. Mg_{90}.

In evaluating this question experimentally it must be recognized that a reaction relation (ol + $SiO_{2\,liquid}$ ⇄ opx) may exist, thus a *liquid* saturated at P1T1 with olivine + orthopyroxene and lying on the reaction boundary will crystallize only orthopyroxene at P1T1. Addition of even 1% of olivine at P1T1 leads to persistence of olivine demonstrating both saturation in olivine and the existence of the reaction relationship.

Compositions of the samples selected for experimental study are given in Table 5.1. Specimen V1 was originally selected because the phenocryst-rich character of the Cape Vogel rocks suggested that many of the more magnesian compositions could be partially accumulative and because a Mg-number of ~71 is appropriate for a liquid in equilibrium with olivine in a possible mantle source peridotite. Specimens V4 and V5 were selected after the study on V1 failed to reproduce the mineral assemblage observed in the HMA. M1 was selected for experimental study to compare

TABLE 5.1

Starting Compositions

	M1 2980	V1 2984	V4 2987	V5 47790
SiO_2	58.14	57.42	57.60	56.84
TiO_2	0.23	0.31	0.27	0.20
Al_2O_3	10.54	11.38	8.50	7.89
FeO*	8.38†	9.11†	9.83	9.46
MgO	14.62	12.37	17.10	19.99
CaO	5.59	8.44	5.10	4.51
Na_2O	1.68	1.08	0.60	0.70
K_2O	0.99	0.51	0.40	0.20
Mg no.	75.7	70.8	75.6	79.0

* total Fe as FeO

† Fe determined by wet chemical analysis (100 mg samples).

with results on the Cape Vogel samples and also those on other magnesian andesites.

5.2 EXPERIMENTAL TECHNIQUE

5.2.1 Starting Mixes

Glass starting mixes for M1, V1 and V5 were prepared by fusion of natural rock powders in Pt buckets, under an inert atmosphere, in an RF heater. M1 and V1 were free from crystals, while V5 had ~5-10% pyroxene crystals. Large area scan microprobe analyses of pieces of the glasses (+ crystals) are given in Table 5.1. In olivine addition runs on V1 the olivine was added as finely ground natural olivine (Fo_{92}) and mixed in by grinding under acetone in an agate mortar.

The starting mix for runs on V4 was prepared by sintering a 1 gram compressed pellet of the natural rock powder under low fO_2 (IW buffer?) conditions for 4 hours. V4 + olivine runs were made on sintered oxide mixes prepared from AR grade chemicals, carefully ground under acetone and sintered at 1000°C for 24 hours. Fe was added as Fe_2O_3 and Fe metal in proportions to ensure only Fe^{2+} was present in the mix.

5.2.2 Apparatus and Methods

One atmosphere liquidus experiments were performed in a vertical quenching furnace using 20-40 mg of sample in either spec-pure Fe or Pt capsules, sealed in evacuated SiO_2 tubes. Oxygen fugacity conditions reflect the initial reduced composition of the mix and probably lie between WM and IW. This low fO_2 is reflected in the absence of spinel in spite of the Cr_2O_3 content of the rocks (Hill & Roedder, 1974). Temperatures are accurate to ±3°C.

High pressure experiments were carried out in a solid media piston-cylinder apparatus using a piston-in technique and a pressure correction of -10% nominal piston pressure. Temperatures (±5°C) were measured by a

$Pt\text{-}Pt_{90}Rh_{10}$ thermocouple. No correction was made for the effects of pressure on the thermocouple emf. Pressures in these runs are considered to be ±3% at ~15 kb (Jaques & Green, 1980). At pressures less than 5 kb errors in the pressure determination are uncertain but may increase to ±25%.

Anhydrous runs at high pressure were made in spec-pure Fe capsules at pressures <10 kb and in graphite capsules at >10 kb. Pyrex glass sleeves with graphite inserts were used in the 0.5 inch diameter furnace assemblies. Runs contain ~5-10 mg of sample.

Hydrous runs were made in either $Ag_{50}Pd_{50}$ or Pt capsules in a boron nitride assembly within a graphite heater. Water was added to the runs by use of a micro-syringe. Capsules were sealed by arc welding and checks on weight were made during preparation of the run, and after, to determine if the runs had remained sealed. Water plus mix totalled 15 mg for hydrous runs.

The oxygen fugacity in high pressure runs is below that of the buffer NNO (Jaques & Green, 1980).

5.2.3 Phase Identification

Portions of the charge were randomly selected for examination and analysis using the microprobe, and for crushing and optical examination in refractive index oils.

The microprobe used is a JEOL JX50A equipped with scanning electron microscope (SEM) capabilities and an energy dispersive (EDAX) analytical system. Simultaneous quantitative analysis of ten elements is possible using this system and the data reduction techniques described by Griffin (1979). Operating conditions employed are: accelerating voltage - 15 kv; beam current - 3 nA; beam diameter - <0.5-1 μm; and 80 or 100 second live counting time. Glass analyses and analyses of bulk charges are made using (rapid) reduced area scans.

Whenever possible identification of phases has been accomplished by combining the results of both optical and microprobe/SEM examinations. However, crystal settling and/or scarcity of crystals has given rise to occasions when no crystals were observed in the portion of the experiment selected for the probe mount.

In general we were not able to determine on optical grounds which polymorph of enstatite, i.e. clino-, proto-, or ortho-enstatite, was present. The non-specific term *enstatite* includes all three polymorphs and is used where we cannot specify the polymorph present. Minor amounts of multiply twinned clinoenstatite are present in some runs on V4 at 1 atmosphere. CE in these runs was chemically indistinguishable from some untwinned crystals in these and other runs.

5.2.4 Fe gain/loss

Liquidus studies are hampered by our inability to maintain constant composition due to Fe exchange with the sample container. This problem has been discussed by a number of authors, e.g. Ford (1978), Biggar (1977), Stern & Wyllie (1975) and Jaques & Green (1979). It is theoretically possible to stop Fe gain or loss by matching the activity of Fe in the capsule with that of the silicate charges but this is virtually impossible because of the number of variables involved (e.g. P, T, H_2O, bulk composition, fO_2, etc.) (Jaques & Green, 1979; Stern & Wyllie, 1975).

The most serious problem encountered in the present study has been the extensive Fe loss (up to ~40%) suffered during high pressure hydrous runs in either AgPd or Pt capsules. The loss of Fe depresses the role of olivine relative to orthopyroxene, i.e. normative quartz content of the liquid increases. We have limited the run times of experiments, particularly for near liquidus runs, in an attempt to circumvent this problem. This may introduce some uncertainty in attaining equilibrium calcium and alumina distribution in pyroxenes, however this is unavoidable.

While recognizing that Fe loss is significant the problem is not as severe or debilitating as might first appear since Fe loss is not uniformly distributed amongst all the phases in crystal-liquid assemblages (Jaques & Green, 1979; Stern & Wyllie, 1975). For example, Jaques & Green (1979) have shown that Fe is preferentially lost from the charge in the order liquid > olivine > pyroxene. This feature is a disturbing one in partial melting experiments (Jaques & Green, 1979, 1980), but in liquidus experiments means that the crystal phases are likely to preserve compositions which reflect equilibrium with the original bulk composition, or at least not be as far removed from equilibrium compositions as the glasses in which they occur. In the present set of experiments this feature has been observed; however to make use of this observation it must be assumed that olivine/liquid and orthopyroxene/liquid Fe/Mg partition coefficients determined in 1 atm. anhydrous runs (where Fe gain/loss is much less or better controlled) are applicable. The recent findings of Takahashi *et al.* (1981) substantiate this assumption and an olivine and orthopyroxene Fe/Mg distribution coefficient of 0.30 ± 0.02 (Roedder & Emslie, 1970; this study) has been used. For example, in the near liquidus runs on V5 + H_2O at 10 kb the crystals should be in equilibrium with glasses of Mg-numbers 77-80, whereas the glasses in the runs have Mg-numbers of 84-86. Crystals with Mg-numbers higher than those which would have been expected for a given bulk composition do occur. For example, rims of olivines in 2 kb runs on V5 + H_2O gave $Mg_{94.5}$. This problem has been circumvented to a certain extent by analyzing the cores of crystals (cf. Jaques & Green, 1980; Green & Ringwood, 1967).

Fe gain in 1 atm. and higher pressure anhydrous runs enhances the appearance of olivine relative to orthopyroxene, i.e. normative quartz content of the liquid decreases. This effect can be particularly important in near liquidus compositions which are near olivine saturation.

For example Fe gain (~24%) in V5 led to stabilization of olivine at 1380°C, however comparison with V4 + 10% olivine (negligible Fe gain) and 1 atm. runs in Pt on V5 show that orthopyroxene is the 1 atm. near liquidus phase. Note that Fe gain in near liquidus runs was found to be quite variable, ranging from 24% in V5, to 9% in M1 and V1, to negligible in V4 + olivine. Fe gain in runs removed from near liquidus composition has occurred but is not a particularly important problem in the context of this study.

5.3 RESULTS

Details of run conditions are given in Table 5.2, and selected analyses of run products are given in Tables 5.3- 5.6. Liquidus diagrams for V1, V4, V5 and M1 are shown in Figures 5.1-5.4 respectively.

5.3.1 V1

Orthopyroxene is the anhydrous liquidus phase from 0-10 kb. Olivine occurs on the water-saturated liquidus at 2, 5 and 10 kb and its liquidus stability field extends from ~1 to ~11 kb. Orthopyroxene replaces olivine as the liquidus phase under water-saturated conditions at pressures <1 kb and >11 kb. Olivine and orthopyroxene were found to occur together near or on the liquidus at 10 kb/1100°C (~270°C below the anhydrous liquidus) and are interpreted to occur on the water-saturated liquidus at ~1 kb/1200°C. Olivine and orthopyroxene occur together in subsolidus runs at 5 kb (1060, 1100°C) and 2 kb (1100°C). Clinopyroxene occurs 100°C and 50°C below the liquidus at 10 and 15 kb, respectively.

A number of experiments were made to determine the position of an olivine-saturated water-undersaturated liquidus, however these runs were unsuccessful. This was due in part to the very narrow field over which olivine can occur under water-undersaturated conditions, because of the lack of olivine on the anhydrous liquidus.

TABLE 5.2

Run Conditions.

Run	Probe Mt	Composition	Capsule	Pressure (kb)	Temp. (°C)	Time (min)	Products
At23	H76	2984	Fe	0*	1170	240	opx(81),gl
At20	H76	2984	Fe	0	1210	60	opx(83),gl
At22	H76	2984	Fe	0	1240	120	opx(85),gl
At18	H76	2984	Fe	0	1270	25	opx(86),gl
At19	H76	2984	Fe	0	1290	20	opx(87.5),gl
At21	H76	2984	Fe	0	1300	45	gl(above liquidus)
At34	H87	2984+10%Fo_{92}	Fe	0	1300	60	ol(88.5),opx(89.5),gl
At35	H87	2984+10%Fo_{92}	Fe	0	1320	45	ol(89),gl
At37	H87	2984+10%Fo_{92}	Fe	0	1340	60	gl(above liquidus)
T269	H56	2984	Fe	2	1260	25	opx(87.6),gl
T272		2984	Fe	2	1280	30	v.minor opx,gl
T264	H56	2984	Fe	5	1270	30	opx(87.4),gl
T267	H56	2984	Fe	5	1310	30	opx,gl
T268		2984	Fe	5	1320	30	gl (above liquidus)
T325		2984	graphite	10	1360	30	opx,gl
T326		2984	graphite	10	1380	30	gl (above liquidus)
T258	H55	2984+5%H_2O	$Ag_{50}Pd_{50}$	2	1100	30	ol(86.5),opx(88),gl
T262	H55	2984+5%H_2O	$Pt_{50\ 50}$	2	1140	20	ol(90),gl
T271	H55	2984+5%H_2O	Pt	2	1180	30	gl(above liquidus)
T254	H56	2984+5%H_2O	$Ag_{50}Pd_{50}$	5	1100	30	opx(86.6),gl
T251	H56	2984+5%H_2O	$Ag_{50}Pd_{50}$	5	1120	30	opx(88.7),gl
T253	H56	2984+5%H_2O	$Ag_{50}Pd_{50}$	5	1140	30	opx(89),gl
T261	H56	2984+5%H_2O	Pt	5	1160	15	opx(92.4),gl
T256		2984+5%H_2O	Pt	5	1170	15	gl(above liquidus)
T56	H16	2984+8%H_2O	$Ag_{50}Pd_{50}$	5	1060	20	ol(85),opx(86),gl
T61	H16	2984+8%H_2O	$Ag_{50}Pd_{50}$	5	1100	20	ol(87),opx(89),gl
T63	H16	2984+8%H_2O	$Ag_{50}Pd_{50}$	5	1120	30	ol(88),gl
T57	H16	2984+13%H_2O	$Ag_{50}Pd_{50}$	10	1000	120	opx(84),cpx(85),gl
T51	H16	2984+13%H_2O	$Ag_{50}Pd_{50}$	10	1060	15	opx(86.5),gl
T50	H16	2984+13%H_2O	$Ag_{50}Pd_{50}$	10	1100	30	ol(88),opx(89),gl
T98	H55	2984+13%H_2O	$Ag_{50}Pd_{50}$	10	1120	30	gl(above liquidus)
T64	H16	2984+18%H_2O	$Ag_{50}Pd_{50}$	15	1060	30	opx(86),gl
T67	H16	2984+18%H_2O	$Ag_{50}Pd_{50}$	15	1100	50	opx(88.5),gl
At46	H122	2987	Fe	0	1290	60	opx(86.3,80),gl
At48	H122	2987	Fe	0	1320	60	opx(88),gl
At45	H122	2987	Fe	0	1360	60	opx(89),gl
At44	H122	2987	Fe	0	1380	45	opx(91),gl
At63	H200	2987+5%Fo_{92}	Fe	0	1360	30	opx(90.7),gl
At64	H200	2987+5%Fo_{92}	Fe	0	1370	30	opx(91),gl
At65	H200	2987+5%Fo_{92}	Fe	0	1380	30	opx(92),gl
At62	H200	2987+5%Fo_{92}	Fe	0	1400	30	gl(above liquidus)
At61	H200	2987+5%Fo_{92}	Fe	0	1420	30	gl(above liquidus)
At71	H219	2987+6%Fo_{92}	Fe	0	1380	30	opx(92),gl
At73	H219	2987+6%Fo_{92}	Fe	0	1390	30	opx(93),gl
At72	H219	2987+6%Fo_{92}	Fe	0	1400	30	gl(above liquidus)
At79	H219	2987+10%Fo_{92}	Fe	0	1360	30	opx(91.6),gl
At78	H219	2987+10%Fo_{92}	Fe	0	1380	30	opx(92.4),gl
At77	H219	2987+10%Fo_{92}	Fe	0	1400	30	opx(93),gl
T571	H123	2987	Fe	2	1360	20	opx,gl
T570	H123	2987	Fe	2	1380	20	opx,gl
T563	H123	2987	Fe	5	1360	30	opx,gl
T564	H123	2987	Fe	5	1400	20	opx,gl
T568	H123	2987	Fe	5	1420	20	opx,gl
T567	H123	2987	Fe	5	1440	20	gl(above liquidus)
T649	H154	2987+5%H_2O	Pt	2	1250	15	opx(89),gl
T647	H154	2987+5%H_2O	Pt	2	1270	15	opx(94),gl
T642	H154	2987+5%H_2O	Pt	2	1290	15	opx(94),gl
T600	H154	2987+8%H_2O	Pt	5	1220	15	opx(85),gl
T605	H154	2987+8%H_2O	Pt	5	1240	15	opx(87),gl
T641	H154	2987+8%H_2O	Pt	5	1260	15	gl(above liquidus)
T684	H176	2987+2%Fo_{92}+5%H_2O	Pt	2	1290	10	opx,gl
T692	H176	2987+5%Fo_{92}+5%H_2O	Pt	2	1280	15	ol,?opx,gl
T697	H176	2987+5%Fo_{92}+8%H_2O	Pt	5	1245	10	ol,opx,gl
T698	H176	2987+5%Fo_{92}+13%H_2O	Pt	10	1235	15	opx(91),gl
At100	H247	47790	Fe	0	1280	60	opx(87.7),gl
At99	H247	47790	Fe	0	1320	45	opx(88.9),gl
At96	H247	47790	Fe	0	1360	30	opx(90.6),gl
At98	H247	47790	Fe	0	1380	30	opx(90),ol(88.7),gl
At97	H247	47790	Fe	0	1400	30	gl(above liquidus)
At101	H253	47790	Pt	0	1360	30	opx(92),gl
At102	H253	47790	Pt	0	1380	20	opx(93),gl
T908	H256	47790+5%H_2O	Pt	2	1280	20	ol(93),gl
T897	H253	47790+8%H_2O	Pt	5	1180	20	ol(91.6),opx(92.6),gl
T896	H253	47790+8%H_2O	Pt	5	1220	20	ol(92),gl
T893	H253	47790+8%H_2O	Pt	5	1240	20	ol(93.6),gl
T900	H254	47790+13%H_2O	Pt	10	1180	20	ol,opx(92),gl
T901	H254	47790+13%H_2O	Pt	10	1200	20	ol(91.5),gl
T898	H254	47790+13%H_2O	Pt	10	1220	20	gl(above liquidus)
T902	H254	47790+18%H_2O	Pt	15	1180	20	ol(91),opx(92.5),gl
T904	H254	47790+18%H_2O	Pt	15	1200	20	ol(90.6),gl
T907	H256	47790+25%H_2O	Pt	20	1180	20	opx(93.6),gl
T906	H256	47790+25%H_2O	Pt	20	1200	20	gl(above liquidus)
At38	H88	2980	Fe	0	1250	180	ol(84.5),opx(86),gl
At29	H88	2980	Fe	0	1290	120	ol,opx,gl
At31	H88	2980	Fe	0	1330	60	ol(88),gl
At33	H88	2980	Fe	0	1350	45	gl(above liquidus)
At32	H88	2980	Fe	0	1370	30	gl(above liquidus)
T423	H87	2980	Fe	2	1340	30	opx,gl
T422	H87	2980	Fe	2	1360	30	gl(above liquidus)
T416	H86	2980	Fe	5	1340	30	opx(90),gl
T417	H86	2980	Fe	5	1360	30	opx(91),gl
T418	H86	2980	Fe	5	1370	30	gl(above liquidus)
T689	H175	2980+5%H_2O	Pt	2	1220	15	ol(89),opx,gl
T687	H175	2980+8%H_2O	Pt	5	1180	15	opx,gl
T686		2980+6%H_2O	Pt	5	1200	15	opx,gl
T961		2980+13%H_2O	$Ag_{50}Pd_{50}$	10	1160	20	ol,opx,gl
T962		2980+18%H_2O	$Ag_{50}Pd_{50}$	15	1180	20	v.minor opx,gl

Abbreviations: ol - olivine; opx - orthopyroxene; cpx - calcic clinopyroxene;
gl - glass, including quench products; v. - very
* 1 atmosphere runs in Fe capsules sealed in evacuated silica tubes.

Table 5.5

SUMMARY OF PHASE COMPOSITIONS OCCURRING IN EXPERIMENTS ON V1 (2984)

Run	At23	At23	At19	At19	T264	T264	T57	T57
P/T/H_2O	0/1170	0/1170	0/1290	0/1290	5/1270	5/1270	10/1000/13	10/1000/13
Phase	gl	opx	gl	opx	gl	opx	opx	cpx
No.	4	1	4	1	1	12	7	4
SiO_2	57.99	55.64	56.82	57.27	56.86	56.49	55.95	54.07
TiO_2	0.38	-	0.32	-	0.27	-	-	-
Al_2O_3	14.71	1.38	11.55	1.30	11.22	1.19	1.32	1.39
FeO	8.81	11.31	9.18	7.76	9.69	8.36	10.36	5.77
MnO	0.28	0.31	0.31	-	-	-	-	-
MgO	5.72	28.16	12.09	32.37	11.86	32.55	30.06	18.80
CaO	10.39	2.94	8.39	1.32	8.52	1.38	2.01	19.45
Na_2O	1.37	-	0.99	-	1.09	-	-	-
K_2O	0.57	-	0.40	-	0.48	-	-	-
Mg no.	53.64	81.61	70.12	86.0	68.57	87.4	83.8	85.3

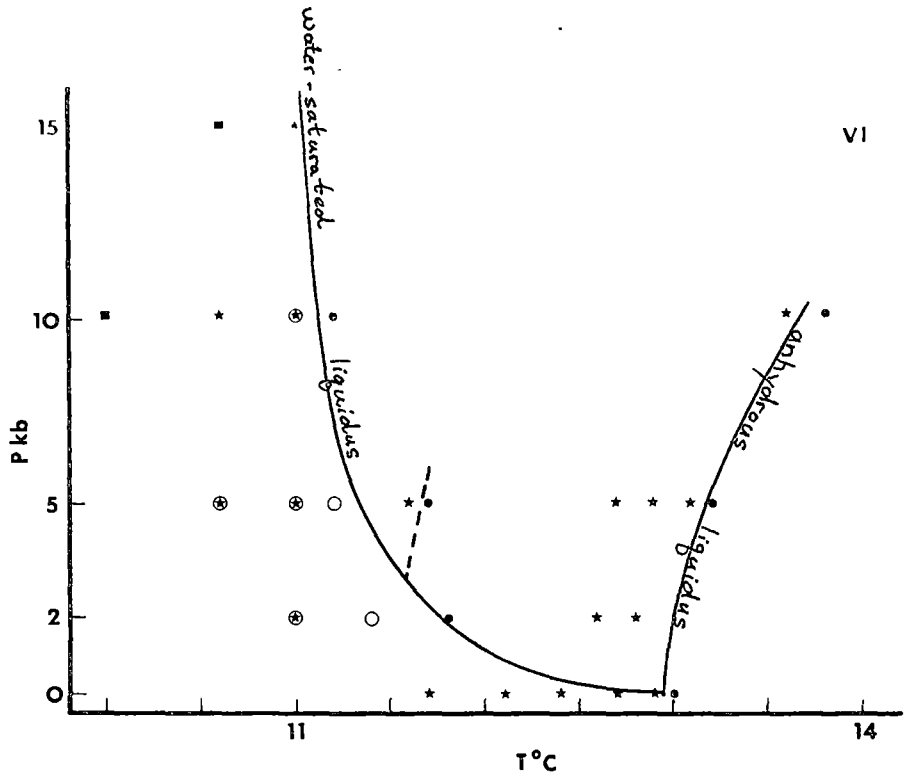

Figure 5.1(a) Liquidus phase relations in V1 (Cape Vogel). Dashed line is for the water-undersaturated liquidus at 5% H_2O. Above liquidus (solid dots), orthopyroxene (asterisks), olivine (circles), orthopyroxene + clinopyroxene (squares). (T, °C x 100).

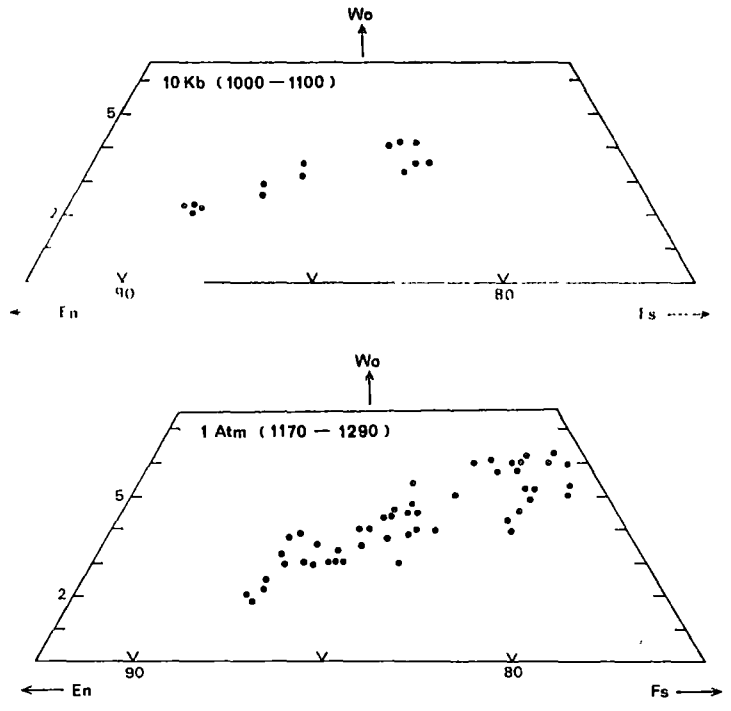

Figure 5.1(b) Composition of orthopyroxene produced experimentally in V1 at 1 atmos. and 10 kb (water-saturated).

Compositions of orthopyroxene produced at 1 atm. and 10 kb are shown in Figure 5.1b. The compositions produced experimentally overlap the natural pyroxenes to a large extent, however no low Ca-Al compositions resembling those of clinoenstatite from the natural rocks were formed. It is also noteworthy that it is not possible to identify any pressure effect on partitioning of Ca, Mg, Fe, Al or Cr between liquid and orthopyroxene in the 0-10 kb interval.

One atmosphere experiments on 2984 + 10% Fo_{92} were made to determine whether clinoenstatite would appear in a more magnesian mix and also to check when olivine would appear on the 1 atm. liquidus. Olivine appeared alone between 1320 and 1340°C and was joined by orthopyroxene at 1300°C. The orthopyroxene produced had an Mg-number of 89-90 but was characterized by CaO and Al_2O_3 contents of the order of 1%.

5.3.2 V4

Enstatite is the liquidus phase under both hydrous (water-saturated) and anhydrous conditions for this composition. Addition of 5, 6 or 10% olivine (~Fo_{92}) produced only more magnesian enstatites on the 1 atm. liquidus. Under water-saturated conditions V4 + 5% olivine produced olivine at 2 and 5 kb at near liquidus conditions, however enstatite was the liquidus phase at 10 kb. These results indicate that the olivine-orthopyroxene multiple saturation point for V4 + 5% olivine lies somewhere between 5 and 10 kb.

One atmosphere experiments of V4 produced multiply twinned crystals of pyroxene which have the low Ca-Al contents typical of clinoenstatites from the natural rock. These crystals were probably clinoenstatite, however compositionally identical or similar crystals without twinning, were produced in the experiments on V4 and V4 + olivine at various P, T and P_{H_2O} conditions.

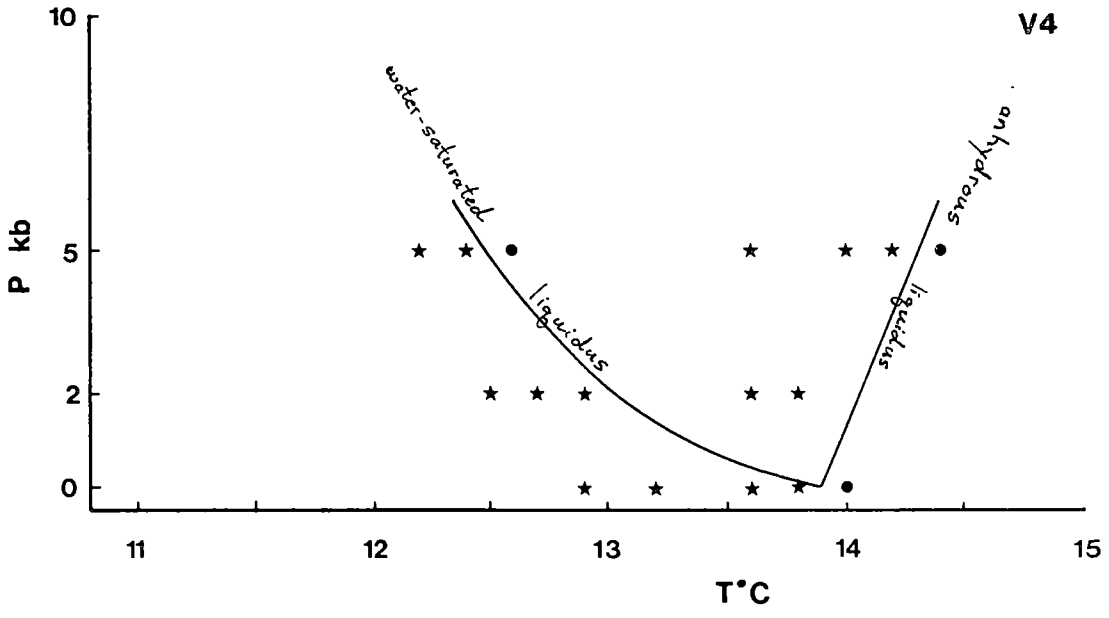

Figure 5.2 Liquidus phase relations in V4 (Cape Vogel). Symbols: ● - above liquidus; ★ - enstatite. (T, °C x 100)

Table 5.4

SUMMARY OF PHASE COMPOSITIONS OCCURRING IN EXPERIMENTS ON V4 (2987)

Run	At46	At46	At46	At48	At48	At45	At45	At44
P/T/H_2O	0/1290	0/1290	0/1290	0/1320	0/1320	0/1360	0/1360	0.1380
Phase	opx	opx	gl	opx	gl	opx	gl	opx
No.	4	1	2	1	2	1	3	5
SiO_2	56.92	54.53	57.13	57.22	56.30	57.82	56.60	58.01
TiO_2	-	-	0.39	-	0.33	-	0.28	-
Al_2O_3	0.52	1.55	11.98	0.40	10.60	-	9.04	-
FeO	9.30	12.99	10.14	8.14	11.34	7.14	10.74	6.30
MnO	-	-	-	-	-	-	0.26	-
MgO	32.80	29.43	10.82	33.81	13.67	34.74	16.58	35.63
CaO	0.59	1.23	7.02	0.41	6.02	0.29	5.14	-
Na_2O	-	-	1.34	-	1.12	-	1.00	-
K_2O	-	-	0.62	-	0.49	-	0.44	-
Mg no.	86.3	80.13	65.53	88.12	68.24	89.67	73.34	90.98

Run	At44	At77	At78	At78	T642	T642
P/T/H_2O	0/1380	0/1400	0/1380	0/1380	2/1290/5	2/1290/5
Phase	gl	gl+10%ol	gl+10%ol	opx	opx	gl
No.	2	5	2	1	1	2
SiO_2	56.54	56.43	56.60	57.89	58.55	59.89
TiO_2	0.27	-	0.30	-	-	0.27
Al_2O_3	8.14	8.01	9.00	0.77	-	8.86
FeO	10.93	9.74	9.00	5.52	3.99	6.46
MnO	-	-	-	-	-	-
MgO	18.30	20.18	18.66	35.56	37.47	18.07
CaO	4.64	4.56	5.22	0.26	-	5.12
Na_2O	0.84	0.84	0.89	-	-	0.74
K_2O	0.38	0.24	0.33	-	-	0.48
Mg no.	74.92	78.70	78.69	92.0	94.34	83.29

The pyroxene compositional trend observed in the natural rock (V4) (and other HMA - see Chapter 2), i.e. clinoenstatite crystallization up to ~Mg_{88} followed by the crystallization of bronzite, was not duplicated in the experiments. In the lowest temperature 1 atm. experiments on V4 (1290°C) two populations of pyroxene compositions were present, one at ~Mg_{86} with 0.5% CaO and another at ~Mg_{80} with 1.2% CaO. There were no obvious differences in texture or appearance amongst the pyroxene crystals in the run which could be correlated with the chemical groupings. The origin of the two groupings is not understood, however it is possible that they represent disequilibrium crystallization.

5.3.4 V5

Liquidus relations for this composition are shown in Figure 5.3. No anhydrous high pressure runs were made since olivine was not a liquidus phase at 1 atm. and results from V1 and V4 could be used to delineate approximately the anhydrous liquidus.

Olivine is on the water-saturated liquidus from pressures of ~1 kb to ~17 kb, with orthopyroxene replacing it as the liquidus phase at both higher and lower pressures. The most magnesian olivine and orthopyroxene compositions are similar to those in the natural rocks, i.e. Mg_{92-93}. Low Ca and Al characterize the enstatites which are chemically indistinguishable from those found to occur in the HMA. Two groups, bronzites (Mg_{89}, 1-1.25% CaO) and enstatite (Mg_{93}, 0.28-0.74% CaO) are found at 5 kb/1180°C, however occasional crystals with high Ca (>1%) and high Mg-numbers (>90) are also found.

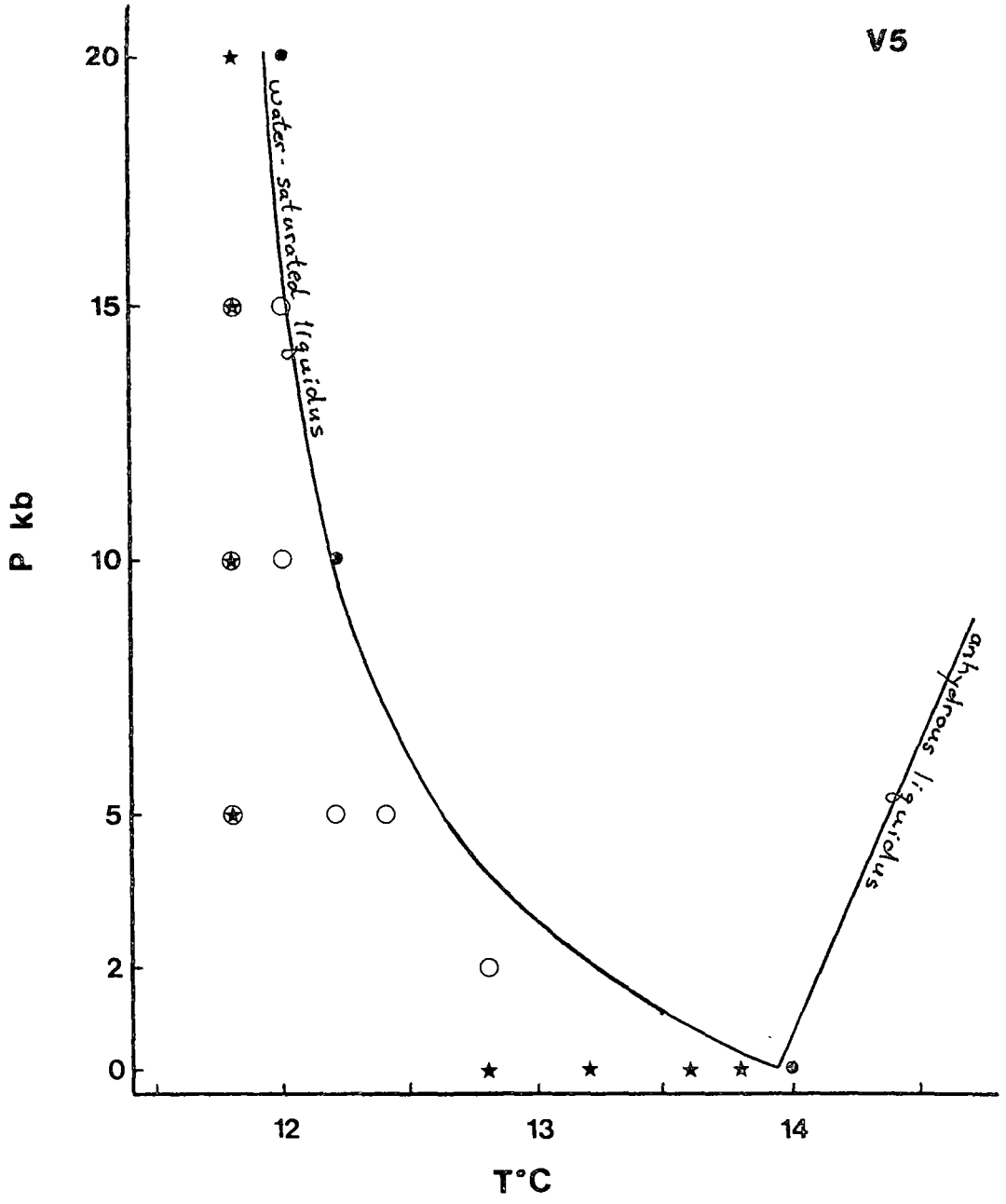

Figure 5.3 Liquidus phase relations in V5 (Cape Vogel).
Symbols: ● - above liquidus, ○ - olivine, ★ - enstatite. (T, °C × 100).
Anhydrous liquidus based on comparison with V1 and V4.

Table 5.5

SUMMARY OF PHASE COMPOSITIONS OCCURRING IN EXPERIMENTS ON V5 (47790)

Run	At96	At98	T908	T908	T900	T900
P/T/H_2O	0/1360	0/1380	2/1280/5	2/1280/5	10/1180/13	10/1180/13
Phase	gl	gl	gl	ol	opx	bulk
No.	4		1	1	1	1
SiO_2	56.46	55.34	58.92	41.1	57.7	59.34
TiO_2	-	0.20	0.22	-	-	0.29
Al_2O_3	9.53	8.35	8.32	-	0.52	9.85
FeO	10.62	11.73	5.33	7.01	4.74	5.62
MnO	-	0.20	0.23	-	-	0.20
MgO	16.58	18.37	21.63	51.66	36.08	17.9
CaO	5.26	4.49	4.38	-	0.42	5.24
Na_2O	1.33	1.35	0.72	-	-	0.97
K_2O	0.22	0.22	0.26	-	-	0.39
Mg no.	73.57	73.6	87.85	92.92	93.12	85.1

Run	T900	T907	T907
P/T/H_2O	10/1180/13	20/1180/25	20/1180/25
Phase	opx	opx	gl
No.	1	1	3
SiO_2	55.44	58.00	59.01
TiO_2	-	-	0.43
Al_2O_3	3.60	0.66	9.74
FeO	6.65	4.60	5.23
MnO	-	-	0.31
MgO	32.35	35.82	18.24
CaO	1.58	0.35	4.93
Na_2O	-	-	0.89
K_2O	-	-	0.61
Mg no.	89.65	93.26	86.16

5.3.5 M1

Olivine is the liquidus phase at 1 atm. and crystallizes over at least a 100°C interval. Orthopyroxenes coexisting with olivine have greater than 1-1.5% CaO and Al_2O_3 greater than 0.6%. Enstatites are present on the anhydrous liquidus at 2 and 5 kb and are similar in composition to clinoenstatites found on the natural rocks. Under water-saturated conditions olivine is the liquidus or is a near liquidus phase up to approximately 12 kb. Orthopyroxene (?enstatite) is the liquidus phase at higher pressures.

5.4 DISCUSSION

5.4.1 Multiple Saturation and Parental Magmas among HMA

M1, V1 and V5 can each be assigned conditions of origin appropriate to a primary melt, segregating from residual olivine and enstatite (± chrome spinel); however, this does not ensure that these compositions are parental to the HMA suite in which they occur. In the experimental liquidus studies on these compositions each has in some way or another failed to satisfy the requirement of reproducing the observed mineral phases, mineral compositions and sequence of appearance of phases as displayed in the natural rocks. V1, of the three, is the most inappropriate composition for a parental magma since it did not crystallize low Ca-Al enstatites, nor is it capable of producing as primitive (magnesian-rich) enstatite or olivine compositions as those observed to occur naturally in the HMA (i.e. $>Mg_{92}$). The more magnesian-rich compositions, M1 and V5, will crystallize low Ca-Al enstatites chemically identical to the naturally occurring clinoenstatites, and also satisfy the requirement of crystallizing enstatite and olivine as magnesian as those observed in the natural rocks. The sequence of pyroxene crystallization, i.e. clino-enstatite (Mg_{88-93}) followed by bronzite (starting at $\sim Mg_{88}$) was not duplicated in the present set of experiments. Pyroxenes produced in the

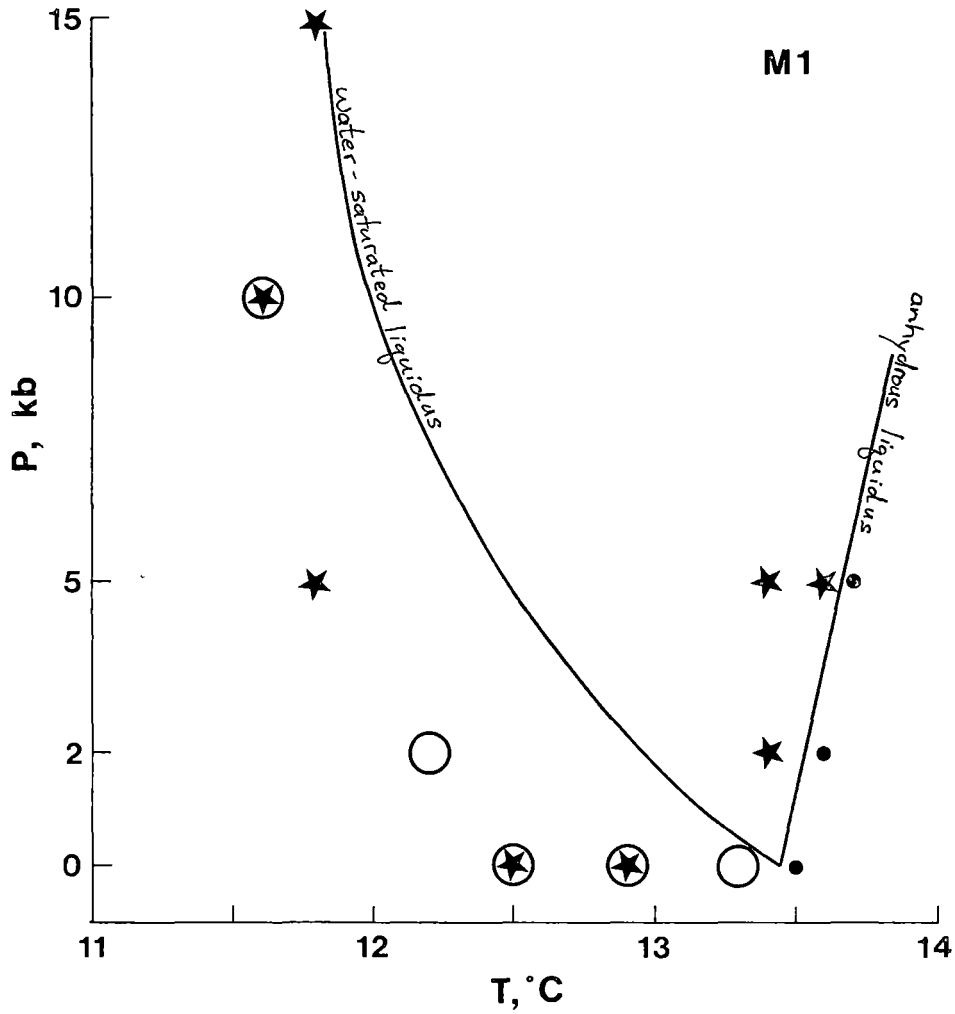

Figure 5.4 Liquidus phase relations in M1 (Mariana Trench). Symbols as for Figure 5.3. (T, °C x 100)

Table 5.6

SUMMARY OF PHASE COMPOSITIONS OCCURRING IN EXPERIMENTS ON M1 (2980)

Run	T416	T416	T417	T417	T417	T689	T689
P/T/H_2O	5/1340	5/1340	5/1360	5/1360	5/1360	2/1220/5	2/1220/5
Phase	opx	gl	opx	glass	bulk	ol	gl
No.	6	2	6	3	1	4	5
SiO_2	57.84	57.99	58.18	58.51	58.01	40.33	59.72
TiO_2	-	0.26	-	0.35	-	0	0.26
Al_2O_3	0.73	11.94	0.62	10.98	10.66	-	11.38
FeO	6.51	8.61	5.98	8.34	9.06	11.06	6.73
MnO	-	-	-	-	-	-	-
MgO	34.53	11.78	34.77	13.37	14.26	48.36	12.97
CaO	0.44	5.92	0.45	5.65	5.30	-	6.12
Na_2O	-	2.18	-	1.77	1.70	-	1.19
K_2O	-	1.23	-	1.07	1.00	-	1.18
Mg no.	90.43	70.91	91.20	74.07	73.73	88.65	77.47

Run	At38	At38	At38
P/T/H_2O	0/1250	0/1250	0/1250
Phase	ol	opx	gl
No.	5	3	2
SiO_2	40.24	56.78	58.94
TiO_2	-	-	0.27
Al_2O_3	-	0.57	13.29
FeO	14.74	9.22	8.66
MnO	-	-	-
MgO	44.98	32.25	8.61
CaO	-	0.97	6.50
Na_2O	-	-	2.50
K_2O	-	-	1.30
Mg no.	84.47	86.17	63.92

5 kb/1180°C experiment under water-saturated conditions in V5 came closest to reproducing the pyroxene trend found in the HMA. However the enstatites showed only restricted Mg-number variation (Mg_{92-94}) followed by bronzite. Complicating this trend were occasional pyroxene crystals with high Ca and high Mg-numbers. The failure to reproduce the naturally occurring pyroxene trend is due to at least the following reasons: (i) extensive Fe gain/loss limits run times and in near-liquidus experiments this may have hampered the attainment of equilibrium Ca distribution. Disequilibrium (?) pyroxenes were also found to occur in 1 atm. experiments run for longer times at temperatures well below the liquidus (see V4); and (ii) difficulties in establishing a possible parental composition in the Cape Vogel HMA, along with the observations that pyroxene equilibrium was difficult to check, given the limitations of the experimental technique, led us to treat the appearance of bronzite as a secondary problem.

While the liquidus phase relationships of V1, V4, V5 and M1 (+ olivine addition related compositions) show that conditions (P, T, P_{H_2O}) exist where crystal fractionation by olivine removal, enstatite removal or the reaction relation olivine + $SiO_{2_{liquid}}$ → enstatite (olivine addition accompanied by enstatite removal) can be invoked to construct models of parent/daughter relations, it is clear that small but significant compositional differences can prevent simple parent/daughter relationships. For example, the phase relations in V1 are inconsistent with its derivation from V4 and V5 by olivine and/or orthopyroxene fractionation. V4 may be related to V5 by ~10% olivine fractionation although Na_2O and K_2O abundances cannot be accounted for satisfactorily. M1 and V4 have markedly different liquidus phase relationships although they have similar Mg-number and CaO/Al_2O_3 ratios. The major difference between M1 and V4 would appear to be Na_2O and K_2O. According to Kushiro (1973), Na_2O and K_2O prevent polymerization of

SiO_4^{4-} tetrahedra, so that olivine would be favoured over enstatite. This is in agreement with the different phase relations observed between M1 and V4, and this effect may also account for some of the different phase relations found in V1 versus V4 and/or V5. Unfortunately, as noted in Chapter 3, Na_2O and K_2O are mobile elements during weathering and metamorphism and it is difficult to establish primary igneous contents of these elements in the HMA. The inability to specify Na_2O and K_2O abundances makes it difficult to ascertain what effect original differences might have had in HMA petrogenesis.

The general pattern of liquidus phase relationships in Cape Vogel HMA is shown in Figure 5.5. The figure as drawn is not directly applicable to M1, however similar arguments to those made below can be made for M1 if it is remembered that the dashed line limiting the field of olivine + liquid or olivine + orthopyroxene + liquid would extend to a point somewhere on the dry liquidus between 1 atm. and 2 kb for the M1 composition. The form of the liquidus diagram (Figure 5.5) is based on the present studies (especially on V5) and on past studies (i.e. Morse, 1980; Burnham, 1967).

Referring to the liquidus relations shown in Figure 5.5, it can be seen that the present results reinforce conclusions, based on studies in both simple and complex systems, that the role of high water pressure is to expand the field of olivine crystallization in quartz normative liquids (Kushiro, 1972; Green, 1973, 1976; Nicholls, 1974; Mysen & Boettcher, 1975). For possible parental magma compositions such as M1 and V5 the maximum depth of segregation from the residual peridotite is at ~17 kb. Even under water-saturated conditions note that the temperature at segregation is of the order of 1200°C (V1 with liquidus at ~1100°C is not suitable as a parental magma as previously noted). The range of possible depths of segregation for clinoenstatite-bearing lavas is further constrained by two factors. First, that in order to crystallize protoenstatite we infer that

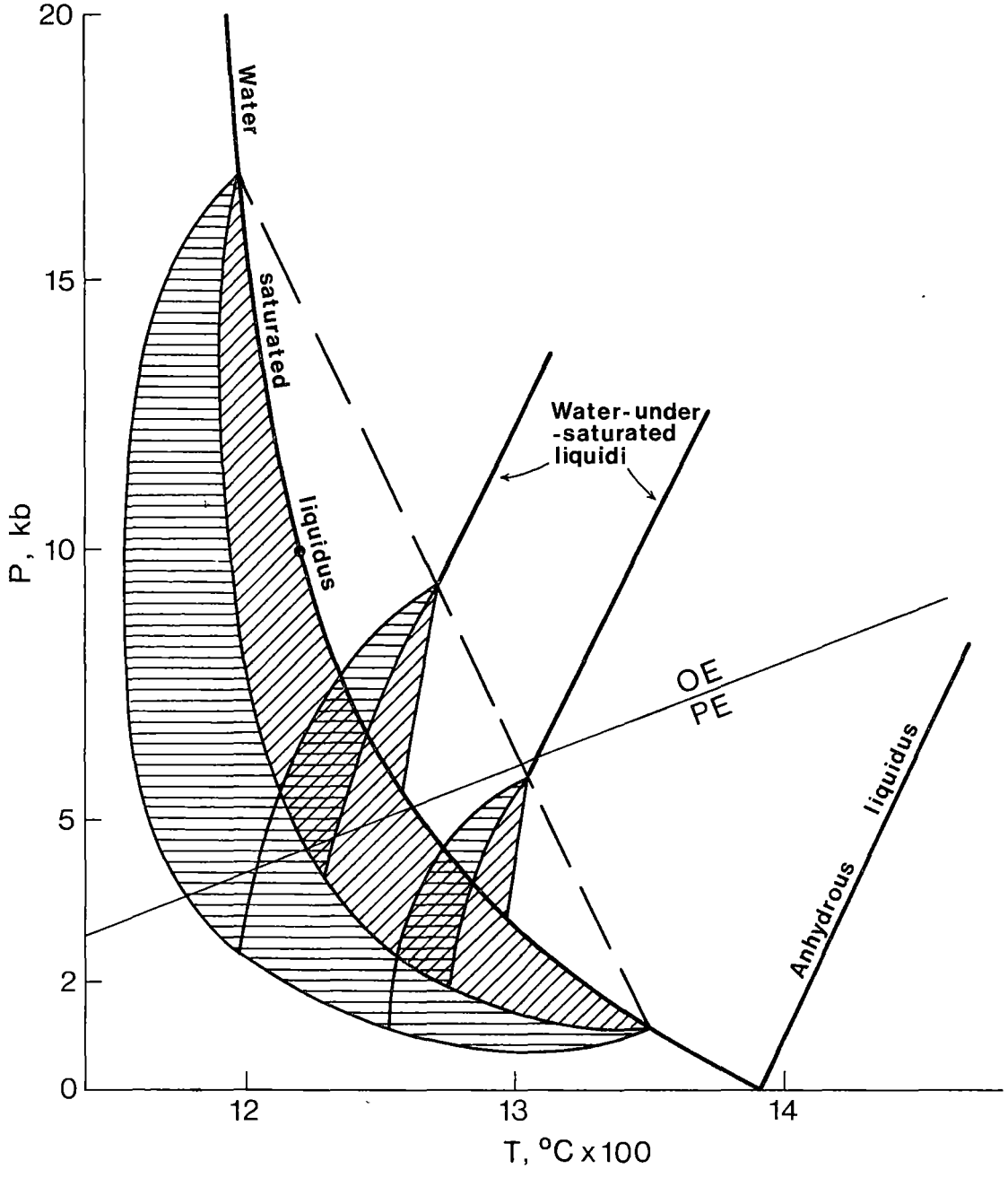

Figure 5.5 Schematic illustration of olivine and pyroxene relationships for varying water contents in a high-Mg andesite (after V5, this study; and Warner, 1975). Horizontal lines = ol+opx+liq. Inclined lines = ol+liq. Dashed line limits the fields of ol+liq, ol+opx+liq. Segregation of a HMA melt from a peridotite source must take place in the area bounded by the limits of the field ol+opx+liq and the dashed line. OE = orthoenstatite, PE = protoenstatite.

the Di/Di+Hy ratio must be <0.2 (Chapter 2), and secondly, that the most common magnesian phase present in many HMA is clinoenstatite (after protoenstatite). The first criterion limits the amount of olivine fractionation which can take place since this will have the effect of increasing the ratio Di/Di+Hy. It is not possible to quantify this rigorously, however it is obviously a more important factor in compositions with Di/Di+Hy ~0.2 (i.e. Bonin Islands HMA). To illustrate this point, consider the following. In V1 the Di/Di+Hy ratio is 0.266 which with 10% olivine addition reduces to 0.205, while in V4 Di/Di+Hy is 0.079 and is reduced to 0.063 with 10% olivine addition. Olivine fractionation from V1 + 10% olivine could cause the Di/Di+Hy ratio to exceed the value which appears to limit clinoenstatite crystallization. In V4 + 10% olivine extensive fractionation (~30%) could occur without raising the Di/Di+Hy ratio to near the limiting Di/Di+Hy value for clinoenstatite crystallization. Note however that such large amounts of olivine fractionation would preclude crystallization of orthopyroxene as magnesian as that observed in the natural rocks.

The second criterion precludes paths of crystallization which begin pyroxene fractionation in the orthoenstatite stability field. The orthoenstatite (OE) to protoenstatite (PE) inversion line illustrated in Figure 5.5 is based on experiments in the pure $MgSiO_3$ system. With addition of Fe (Huebner, 1980; Dallwitz *et al.*, 1966) and Ca (this study) the PE → OE inversion will increase in temperature. Thus the OE/PE inversion reaction is probably at a maximum, which in natural systems, and with fractionation, will migrate to higher temperatures than that indicated.

The combination of the two criteria discussed above and the liquidus phase relations in Figure 5.5 suggest that the conditions most suitable to give rise to HMA are low pressure (<5-10 kb), high temperature (>1200°C), under hydrous but not necessarily water-saturated conditions. Water-undersaturated conditions are more favoured than those of water saturation since they require less water in the source and perhaps more importantly

facilitate the uprise and eruption of the magma (see Burnham, 1967). For example, assume the melt segregates at ~15 kb and ~1200°C under water-saturated conditions [Note: for a 10% partial melt whis would require ~2% H_2O in the source.]. Immediately upon uprise the magma will begin to crystallize olivine and/or olivine + orthopyroxene and the parental composition will be modified, in particular the Mg-number will decrease and the Di/Di+Hy will increase. In this situation it is difficult to visualize the magma arriving in the protoenstatite stability field with a sufficiently Mg-rich composition or low enough Di/Di+Hy ratio to crystallize protoenstatite (~Mg_{92}), or in fact reach the surface at all. Secondly, assume that the melt segregates at ~5 kb and ~1300°C under water-undersaturated conditions leaving residual olivine and enstatite. As the magma rises it initially remains above the liquidus until intersecting the water-saturated liquidus in the olivine field. With only limited olivine crystallization the liquid passes back into the protoenstatite field. Only if the liquid has crystallized very little olivine will it enter the protoenstatite + liquid field at sufficiently high temperature to crystallize the observed highly magnesian protoenstatite (Mg_{92}).

In the above discussion it has been assumed that the ascent path followed by the magma body is one involving adiabatic decompression (Spera, 1980). It is possible that the HMA follow a more complex ascent path involving heating (e.g. Marsh & Kantha, 1978). Such paths may provide opportunity for olivine to react out of the system. However, the uncertainties in modelling ascent paths do not allow any model to be rigorously defined (Spera, 1980).

5.4.2 Comparison with other Experimental Studies and Nature of Source Compositions

It is possible to examine the experimental results from this and other studies within a conceptual framework which will allow estimation of the positions of olivine-orthopyroxene cotectics and at the same time

place limits on the source compositions. To do so one must first ascertain the effects of variable percentage melting of a common source, variable source compositions and variable P, T, P_{H_2O} conditions of melting. Needless to say it is unlikely that all variables can be understood or ambiguities eliminated, however some attempt at a synthesis of the available data is warranted.

Based on previous studies (Green, 1970; Jaques & Green, 1980), the diagram [jadeite (Jd) + Ca - Tshermak's silicate (Ts)] - quartz (Qz) - olivine (Ol) has been chosen as the best available method of visualizing the data. This diagram approximates a plane, at some defined Di content, through the "Basalt Tetrahedron" (Qz-Ol-Ne-Di). Coordinates for plotting compositions are calculated from the Ne, Ab, An, Hy, Ol, Qz components of the molecular norm (based on analyses recalculated anhydrous with $Fe_2O_3/FeO = 1/9$) as follows: Jd+Ts = Ab+An+Ne; Qz = Qz+Ab+An-Ne+Hy/2; Ol = Ol+Hy/2.

Previous work by Green (1973, 1976) and Jaques & Green (1980) has shown that it is possible to generate a series of liquids with ol±opx±cpx± sp±amph saturation from a given source at given P, T, P_{H_2O} conditions. These liquids can be used to define cotectics, which are then visualized by projection onto a (Jd+Ts)-Qz-Ol diagram. Figure 5.6 illustrates an example of this for anhydrous and water-saturated melting of pyrolite at 10 kb. The effect of water on producing more Qz-normative liquids, as discussed in the previous section is clearly illustrated. The effects of changing bulk compositions of peridotite sources and changes in pressure of segregation are illustrated in Figure 5.7. First note that for a given peridotite composition the liquids produced by partial melting are more Qz-normative at low pressure. The compositional effect if illustrated by the shift in position of the cotectics for Pyrolite and Tinaquillo. Tinaquillo is a more refractory peridotite composition being depleted in, particularly, Na_2O, K_2O, TiO_2 and P_2O_5 relative to Pyrolite (Jaques & Green,

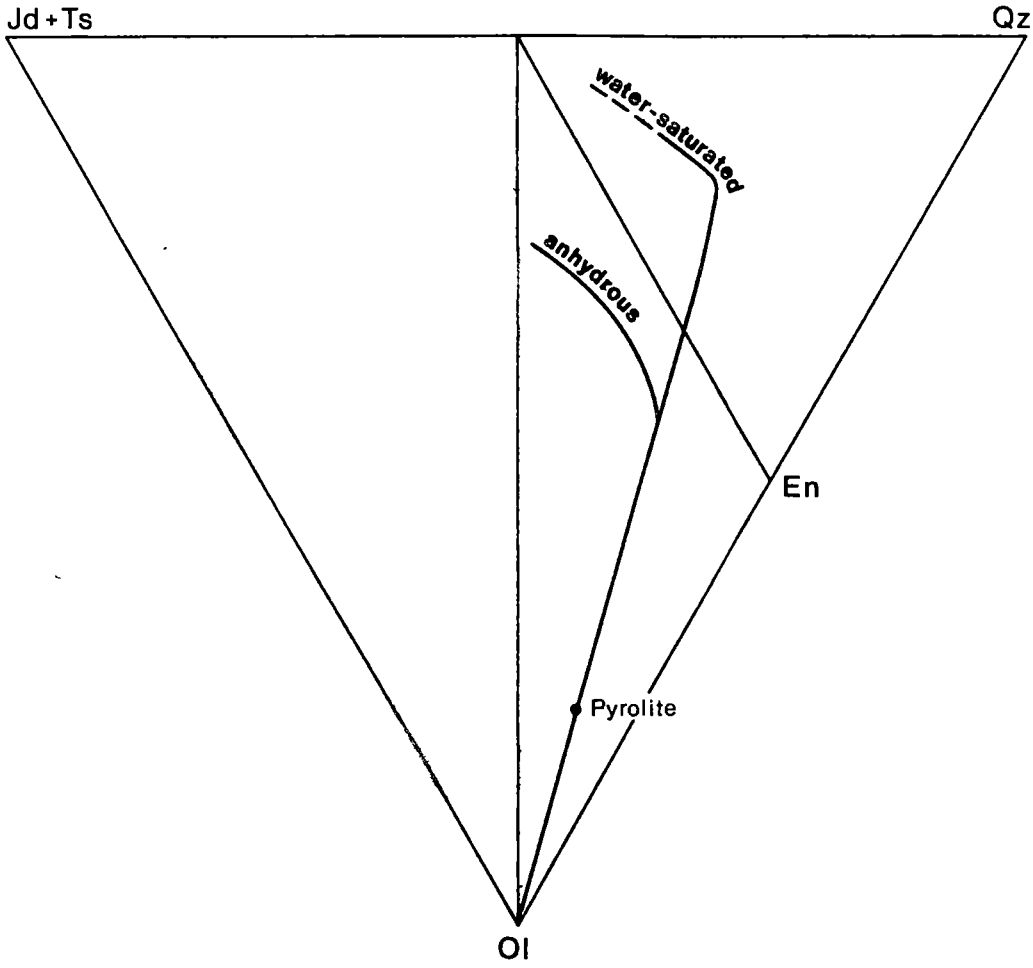

Figure 5 6 Water-saturated and anhydrous cotectics for pyrolite at 10 kb (after Green, 1976, Jaques & Green, 1980). Dashed line indicates approximate position.

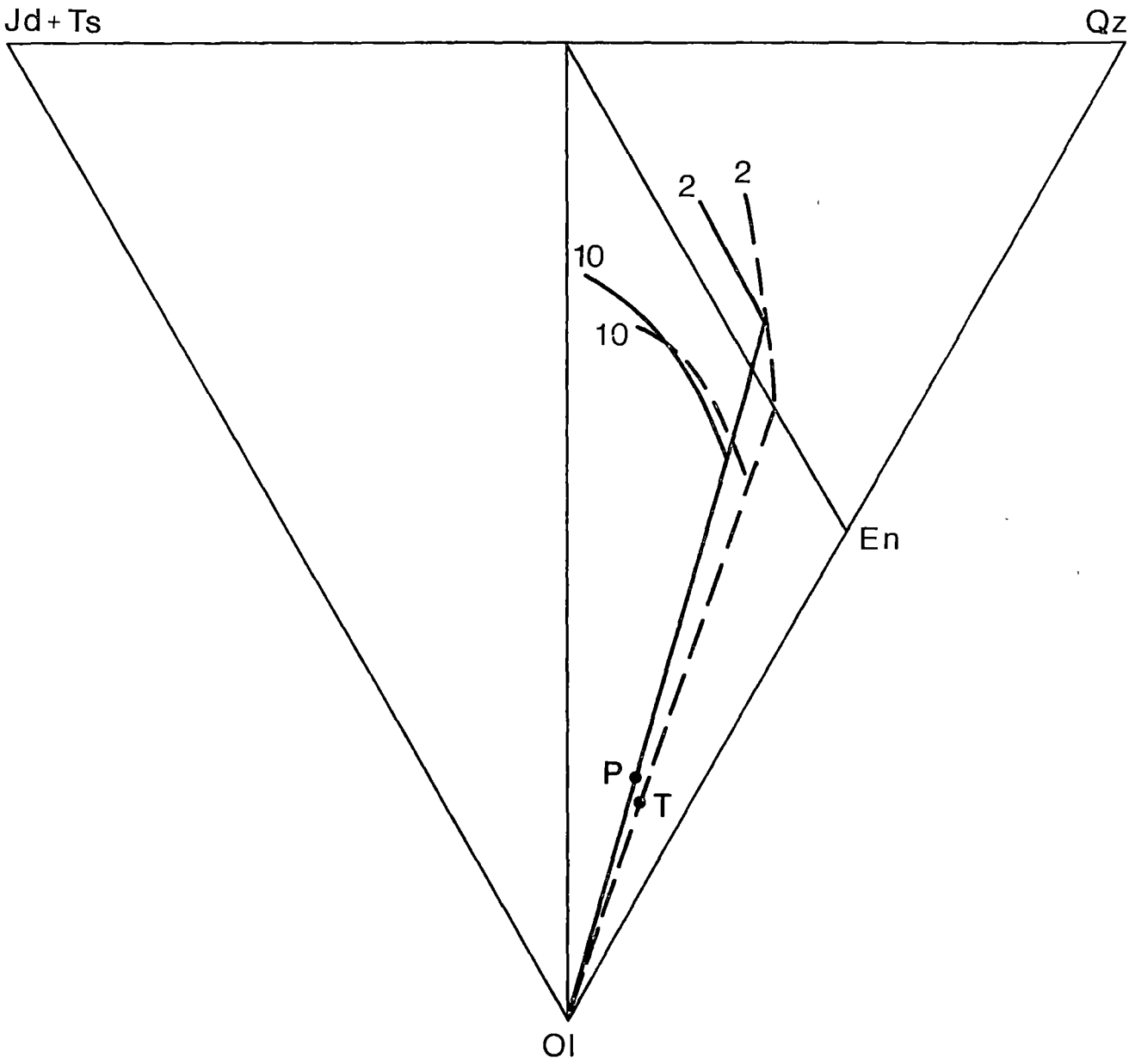

Figure 5.7 Anhydrous cotectics for Pyrolite (P, solid lines) and Tinaquillo (T, dashed lines) at 2 and 10 kb (after Jaques & Green, 1980).

1980). Tinaquillo can produce more Qz-normative melts (at a given pressure) than Pyrolite (Jaques & Green, 1980) and although there are probably several factors contributing to this difference it is interesting to note that Tinaquillo has a normative An/Ab ratio of 5.27 versus 1.32 in Pyrolite.

To determine some of the effects compositional changes can have on the positions of cotectics in the (Jd+Ts)-Qz-Ol diagram the simple systems Fo-Di-SiO_2, Fo-Ts-SiO_2 and Fo-Jd-SiO_2 were considered. Data for these systems are from Kushiro (1972), however the plots presented (Figure 5.8) have been recalculated from wt.% to mole % basis. The effect of varing Di content is illustrated in Figure 5.8a. The position of the ol-opx cotectic on the join Ol-SiO_2, as projected from Di through Di contents of ~5 and 22% are very similar. Effectively this means that variation in Di content of 0-25% has little effect on the projected position of the ol-opx cotectic on the plane (Jd+Ts)-Qz-Ol. Figure 5.8b and 5.8c illustrate the effect of Ca and Na on the slope and position of the ol-opx cotectics. Consideration of these diagrams and the position of the cotectics in the simple systems Ab-SiO_2 and An-SiO_2 leads to the suggestion that Ca-rich, Na-poor compositions will tend to plot more towards the Qz-apex in the (Jd+Ts)-Qz-Ol projection. Changes in the Ca/Na ratio, or perhaps more accurately normative An/Ab will cause shifts in the positioning of the cotectics in the (Jd+Ts)-Qz-Ol projections. There are two ways in which this will be manifested: (i) in an overall manner which reflects compositional differences in the sources, for example, as illustrated by differences between Tinaquillo and Pyrolite cotectics; and (ii) varying An/Ab ratio with degree of partial melting in liquids derived from a given composition will cause a change in direction of the cotectic.

The paths that liquids in equilibrium with a peridotite source, at some P, P_{H_2O} conditions, might take as they change residual phases can be illustrated on the (Jd+Ts)-Qz-Ol diagram. Specific examples from Pyrolite

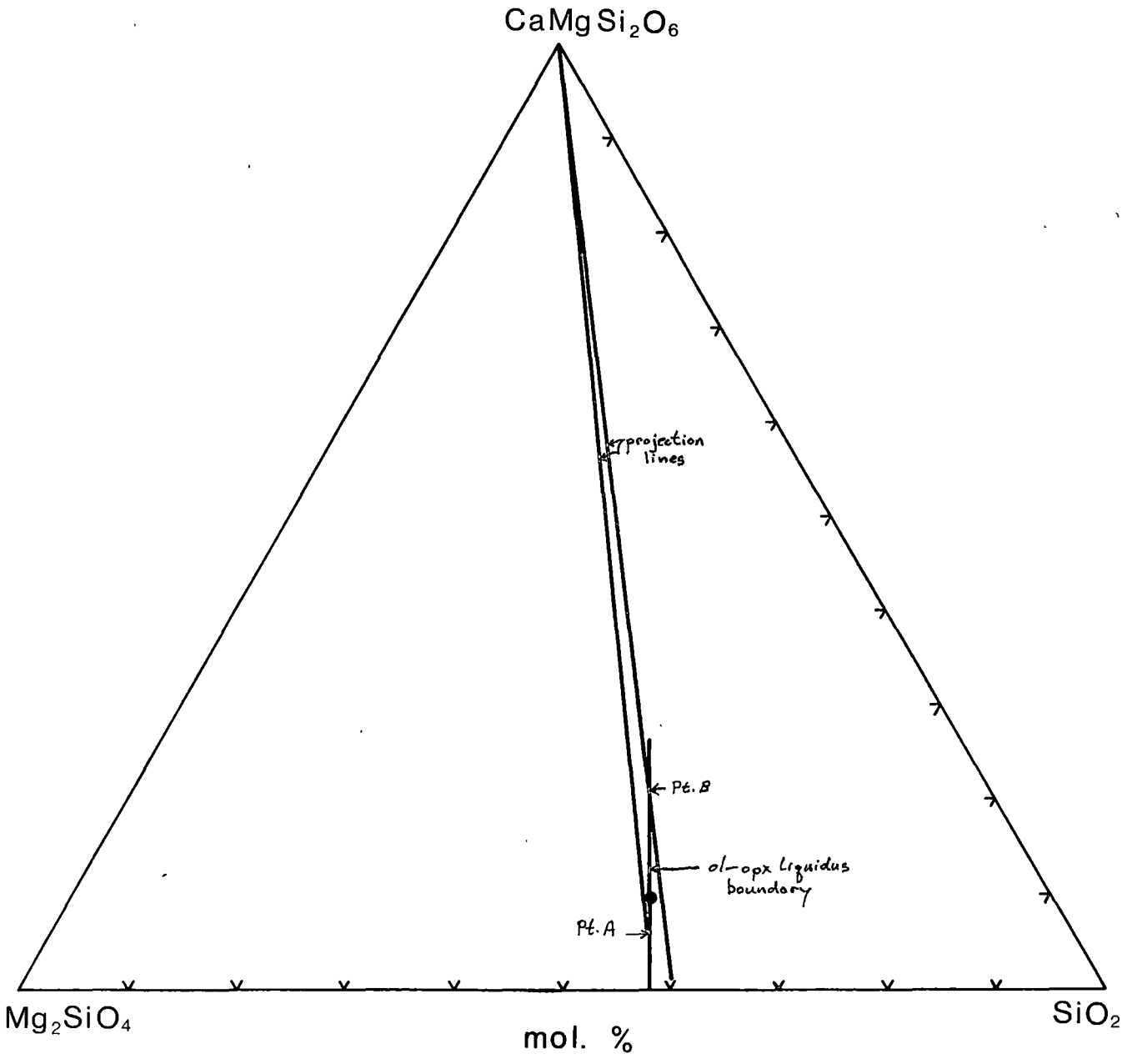

Figure 5.8a Ol-opx liquidus boundaries (in mole percent) for $CaMgSi_2O_6$-Mg_2SiO_4-SiO_2 (water-saturated, 20 kb). After Kushiro (1972).

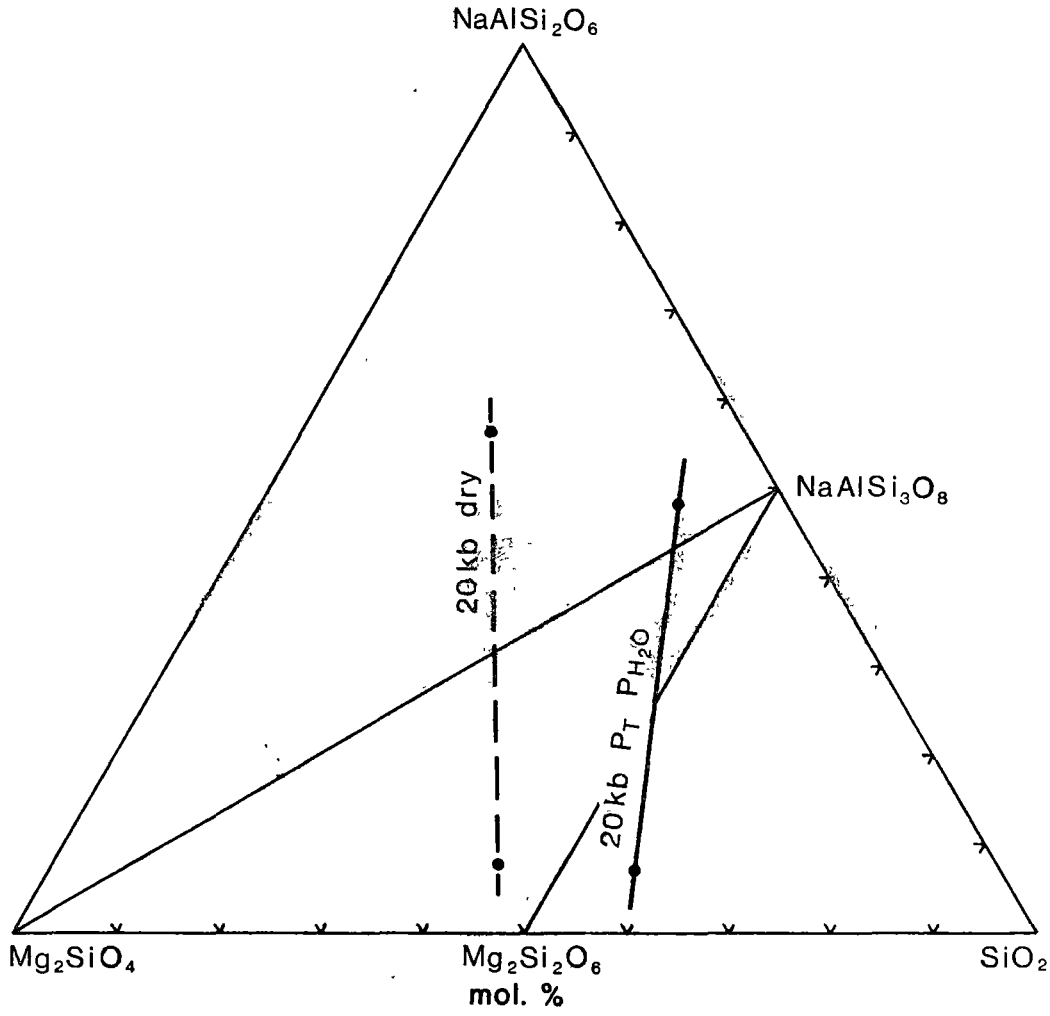

Figure 5.8b Ol-opx liquidus boundaries (in mole percent) for $NaAlSi_2O_6$-Mg_2SiO_4-SiO_2. After Kushiro (1972).

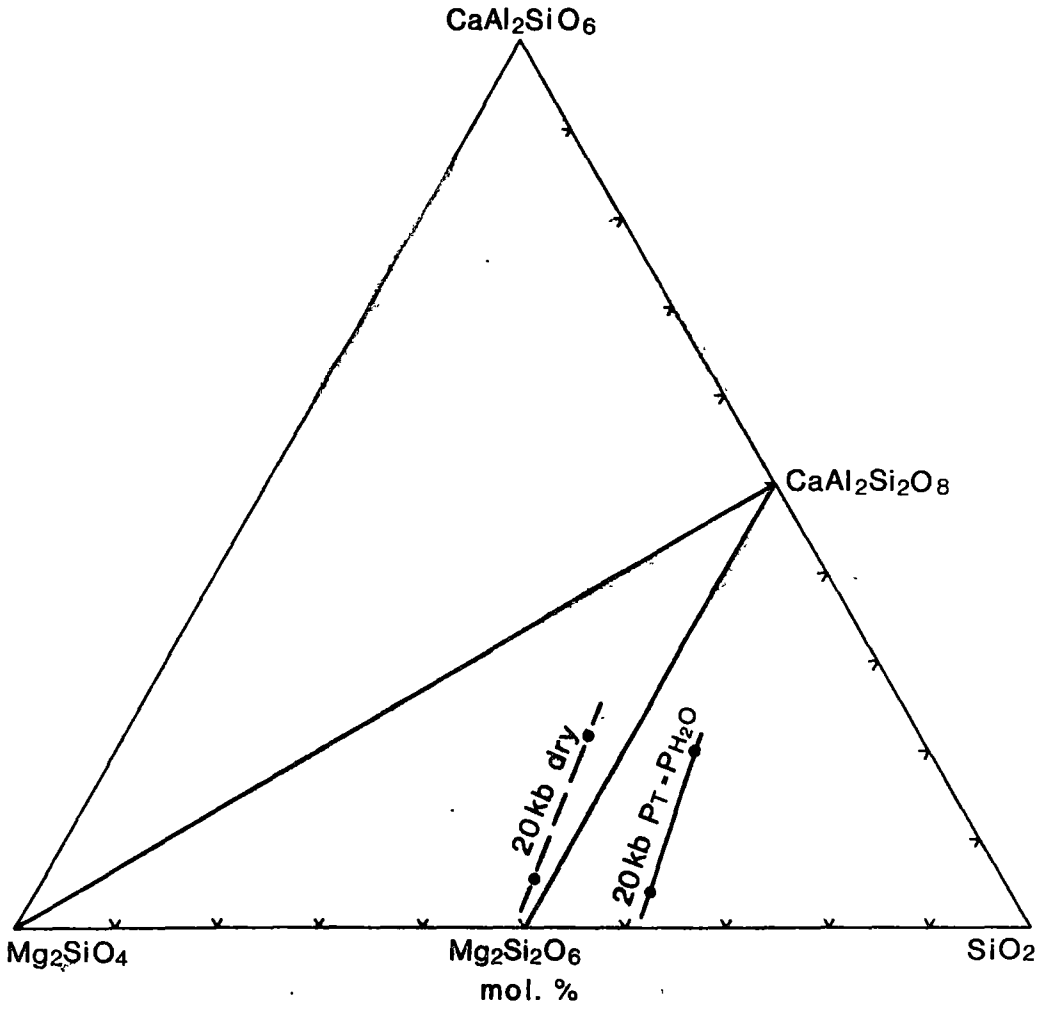

Figure 5.8c Ol-opx liquidus boundaries (in mole percent) for $CaAl_2Si_2O_8$-Mg_2SiO_4-SiO_2. After Kushiro (1972).

and Tinaquillo compositions are illustrated in Figure 5.9a and a generalized case is given in Figure 5.9b. The source composition will control the melting range (percent melting limits and temperature range) over which a specific set of minerals will coexist with the melt. For example, clinopyroxene remains in the residuum over a longer T or percentage partial melting interval in a Pyrolite versus Tinaquillo type composition (Jaques & Green, 1980). For water-saturated melting of Pyrolite the assemblage ol+opx+cpx+amph+liquid exists only for a short interval (<40°C) before the amphibole is consumed (Green, 1973, 1976). Amphibole may well exist for even smaller temperature intervals in less alkali and/or water-rich peridotite compositions. Another feature of peridotite melting illustrated in the paths shown is that after all phases excluding olivine are eliminated by increasing T or degree of partial melting, the liquids in equilibrium with olivine alone must fall on an olivine control line that passes through the bulk composition of the source. This feature provides some constraint on the nature of the source composition. For example, the HMA of this study all plot to the right of either the Pyrolite or Tinaquillo olivine control line and cannot have been derived from sources similar to these.

Compositions used in the present experimental study are shown on Figure 5.10 on the (Jd+Ts)-Qz-Ol diagram. Liquidus studies on the compositions defined the conditions (under water saturation) at which olivine, orthopyroxene or olivine + orthopyroxene appear on the liquidus. Because of the tight clustering of compositions, and based on comparisons with other studies and the conceptual framework outlined above, it has been possible to interpret the data in terms of the positions of cotectics at 2, 5, 10 and 15 kb. The configuration is not unique and in fact the range of compositions used cannot have been derived from a given source composition, however we were able to use the data from Cape Vogel HMA to predict liquidus relations in the Mariana Trench composition (M1).

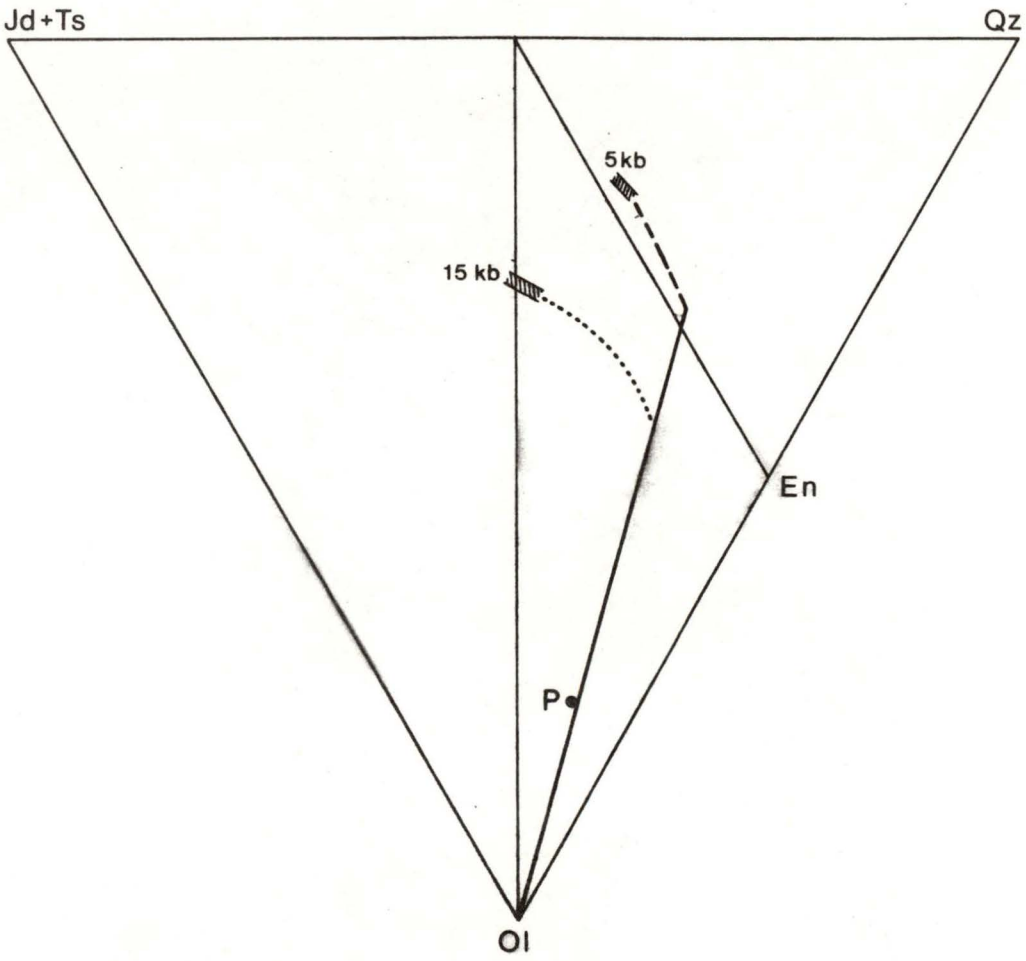

Figure 5.9a Equilibrium melt compositions for Pyrolite (P) at 5 and 15 kb anhydrous. Hatched areas: ol+opx+cpx residue; dashed lines: ol+opx residue; solid lines: ol residue. After Jaques & Green (1980).

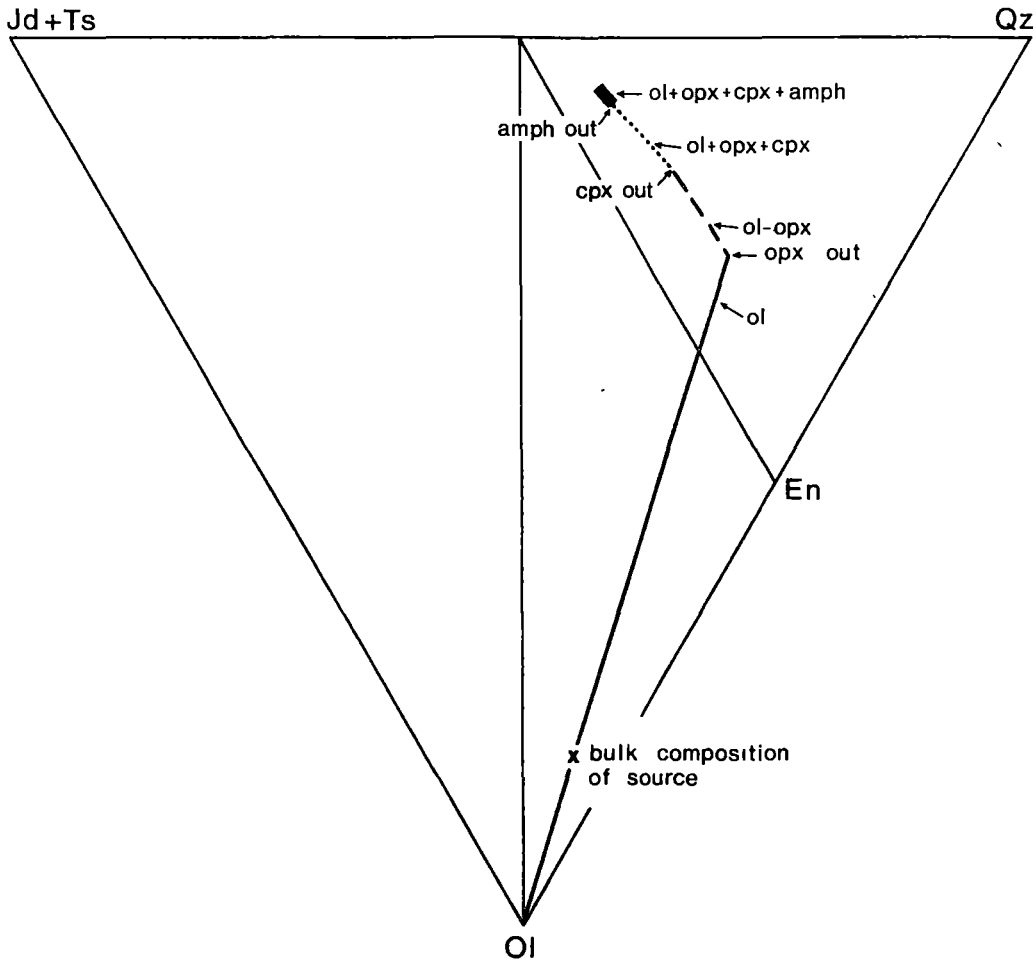

Figure 5 9b Schematic diagram indicating possible residual assemblages for liquids formed by partial melting of peridotite of composition X.+H_2O. Liquids in equilibrium with X are constrained to lie to the left of the line through Ol and X (or its extension)

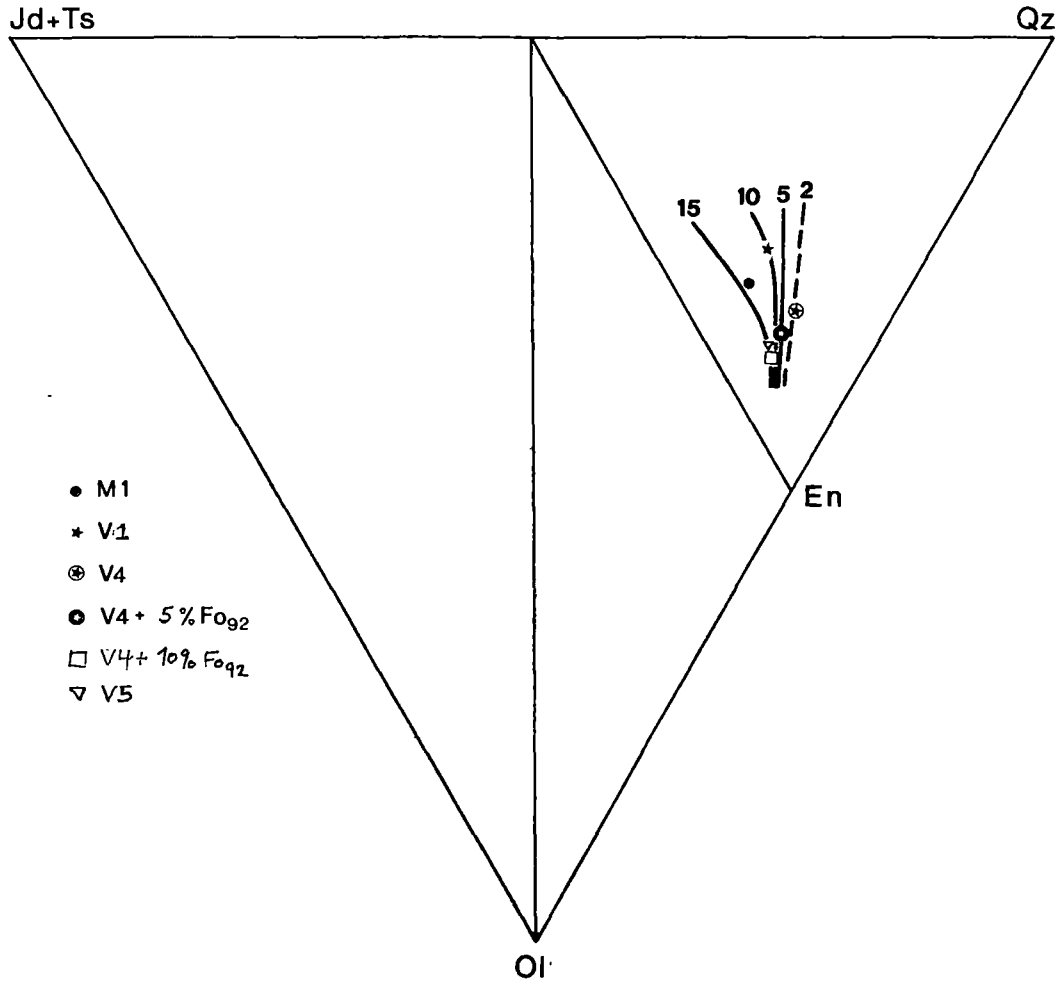

Figure 5 10 Possible configuration of ol-opx cotectics in HMA
Numbers refer to pressure in kbar.

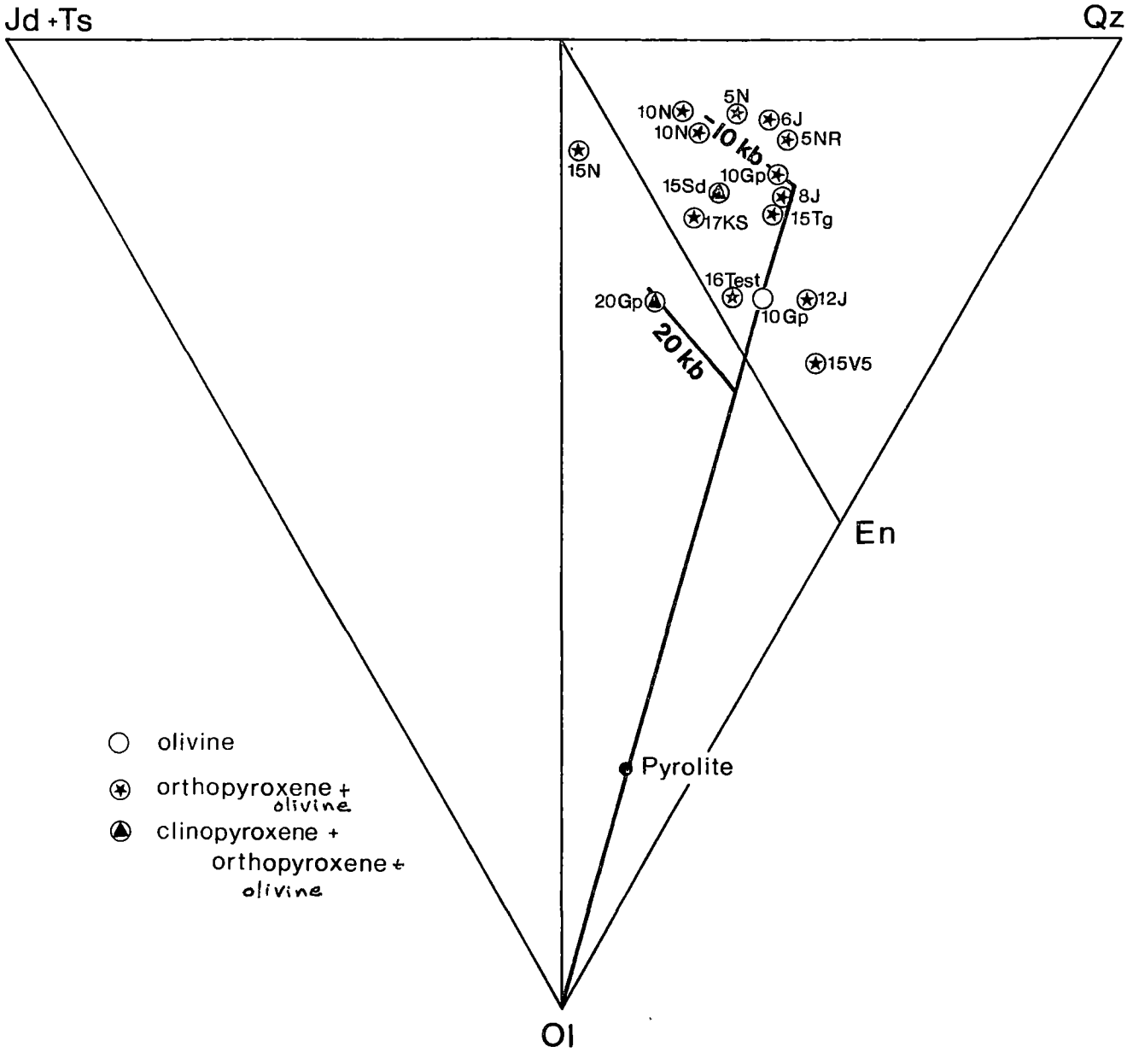

Figure 5.11 Composition of liquids, and their liquidus phase relations, formed in equilibrium with peridotite compositions with $P_T = P_{H_2O}$.

N	Nicholls (1974), liquidus studies andesites, T = 1000°C (at 5,10,15 kb) and 1020°C (at 10 kb).
NR	Nicholls & Ringwood (1974), composition of partial melt formed at 1050°C from Pyrolite (data in Nicholls, 1974).
J	Johnstone (1979), partial melting experiments simple system (Fe-free) 6 kb - 1000°C, 8 kb - 1050°C, 12 kb - 1100°C.
Gp	Green (1976), partial melting of Pyrolite. 10,20 kb - 1100°C and 10 kb - 1200°C.
KS	Kamiya magnesian andesite. Kushiro & Sato (1978), T = 1050°C.
Sd	andesite liquidus study on SD-261. Tatsumi & Kushiro (1981). T = 1030°C.
Tg	andesite liquidus study on TG-1. Tatsumi (1981). T = 1080°C.
Test	andesite liquidus study on estimated primary composition of Hatari andesite. Tohara (1981). T = 1120°C.
V5	HMA composition V5, this study. T = 1200°C.

Labelled lines indicate approximate position of 10 and 20 kb $P_T = P_{H_2O}$ cotectics for Pyrolite (Green, 1976).

For example, when M1 was plotted on Figure 5.10 it was apparent that olivine + orthopyroxene cosaturation should occur at a maximum pressure of 10-15 kb. Preliminary experiments confirmed this with olivine + orthopyroxene near the liquidus at 10 kb and orthopyroxene alone on the liquidus at 15 kb (water-saturated conditions).

Data from experimental melting studies by Green (1973, 1976) and Nicholls (1974) are shown along with the results from liquidus studies on magnesian andesite compositions from Japan in Figure 5.11. The characteristics of the Japanese compositions are discussed in some detail in Chapter 6, however these rocks have features which indicate they formed as partial melts in equilibrium with peridotite compositions. In general they show olivine + orthopyroxene saturation at 15-17 kb and 1100 ± 20°C, under water-saturated conditions. The complex effects of compositional parameters on the positioning of cotectics in the (Jd+Ts)-Qz-Ol diagram is well illustrated by these data and that of the HMA of this study. Like the HMA of this study, the Japanese andesites have a low CaO/Al_2O_3 ratio (~0.4-0.6) which is interpreted as reflecting their source peridotite composition (Sato, 1981), however they are enriched in Na_2O, K_2O, TiO_2, REE, etc. (see Chapter 6). The apparent movement of their cotectic(s) towards the Jd+Ts corner on the (Jd+Ts)-Qz-Ol diagram is consistent with the interpretation one could make of their compositional differences, based on the conceptual model and results reported above. The Japanese andesites plot in the compositional field covered by the Pyrolite and Tinaquillo compositions, i.e. to the left of their olivine control lines, and in a general way the results are consistent with the positions of the 10 and 20 kb cotectics produced by water-saturated Pyrolite.

As noted previously the projection does not account for different normative diopside contents (which are related to differing $CaO+Na_2O/Al_2O_3$ ratios). This leads to the situation in which the phase relations of

liquids derived from a Pyrolitic source with a CaO/Al_2O_3 ratio of 0.8-1.0 are equated with those of the Japanese andesites which must have been derived from a source with a CaO/Al_2O_3 ratio of 0.4-0.6.

Unlike petrogenetic models for MORB (Nisbet & Fowler, 1978; Green *et al.*, 1979) in which a constant source composition is a reasonable assumption, currently popular models for magma genesis in island-arc settings envisage variable source compositions and variable metasomatic/magmatic alteration to such source compositions (Green, 1973, 1976; T.H. Green, 1980; Perfit *et al.*, 1980; Saunders *et al.*, 1980b). This feature of island-arc petrogenesis makes it difficult to erect generalized petrogenetic models for island-arc volcanics, since a number of possible combinations of factors can be instrumental in determining the P, T conditions of origin of a given magma.

The HMA from Cape Vogel, the Mariana Trench and Bonin Islands are derived from a refractory mantle source, characterized by a low CaO/Al_2O_3 ratio. Differences in phase relations and chemistry within the HMA indicate that the source for the Bonin Islands and Mariana Trench HMA may have been less refractory than that of the Cape Vogel HMA, in that higher amounts of $Na_2O + K_2O$ may have been present. This comparison may perhaps be extended to include the SMA of Japan whose source is characterized by a refractory or low CaO/Al_2O_3 ratio but must have had higher abundances of Na_2O, K_2O, TiO_2, etc. Differences in the chemistry of the sources for these rocks are not directly equatable with any specific mantle compositions but may reflect differences such as those observed between Pyrolite, Tinaquillo and harzburgite compositions (Jaques & Green, 1980; Berry, 1981).

Chapter 6

HIGH-Mg, HIGH-SiO_2 LIQUIDS: COMPARISONS AND CONTRASTS

6.1 INTRODUCTION

In the previous chapters, the mineralogy, geochemistry and petrology of the HMA have been described in some detail. The purpose of this chapter is to briefly review the important characteristics of the HMA and compare them with suggested equivalents or possibly related rocks. The similarities and differences between HMA and some other primary mantle derived liquids is analysed to establish their petrogenetic significance. Finally the tectonic implications of HMA will be analysed.

To clarify the following discussion, two points must be made: firstly, geochemical comparisons with other rock types are based on analyses which have been recalculated anhydrous and whose Fe content is reported either as total Fe as FeO or with Fe_2O_3/FeO fixed at a specific value; secondly, to avoid the possibility of the discussion becoming too long only the major points of arguments are summarized. More complete arguments on nomenclature and tectonic environment of formation have been presented in the referenced literature.

6.2 CHARACTERISTICS OF HMA

The term *high-Mg andesites* (HMA), adopted for use in this thesis (after Green, in Sun & Nesbitt, 1978), describes rocks characterized by the following features:

(i) SiO_2 content of ~56-59% accompanied by high MgO (> 9 wt.%), high Cr (664-2976 ppm), Ni (194-657 ppm), Cr/Ni (>3), and Mg-numbers >66;

(ii) low CaO/Al_2O_3 ratios (<0.6), which based on liquidus phase relations and compositions are also necessarily those of the peridotitic source;

(iii) low incompatible element abundances (~<10x chondritic or primitive mantle); TiO_2 <0.46%; low Ti/Zr (<60); high Zr/Y (>4); and variable LREE enrichment and Zr/Nb ratios (see below);

(iv) orthopyroxene and/or clinoenstatite is the major phenocryst phase, and was dominant in the fractionation process relating more fractionated members of a suite;

(v) olivine is a minor phase (<5-10%) which often exhibits a reaction relationship with orthopyroxene and/or clinoenstatite;

(vi) equilibrium (in contrast to metastable or quench) clinopyroxene phenocrysts appear with Mg-numbers <80, indicating they are not a near-liquidus phase (in agreement with experimental studies). These clinopyroxene phenocrysts have 17-20% CaO. The existence of equilibrium (stable) pigeonite compositions cannot be unequivocally established;

(vii) plagioclase is not a near-liquidus phase and is absent in quenched examples of HMA. Plagioclase appears in fractionated members of the HMA suite (i.e. bronzite andesites and dacites);

(viii) the rocks are generally phenocryst-rich, vesicular, with glassy groundmass and have textures indicating rapid cooling.

Bronzite andesites and (perlitic) dacites found in association with HMA have generally less than 5-10% phenocrysts of orthopyroxene, clinopyroxene and plagioclase which occur in a glass-rich groundmass (>35 to ~70%) which may have microlites of orthopyroxene, clinopyroxene and plagioclase. These fractionated representatives of HMA have low CaO/Al_2O_3 ratios, low incompatible element abundances, low Ti/Zr, and high Zr/Y ratios,

inherited from their parental magmas and remain chemically distinctive from most island-arc andesites and dacites.

The geochemistry of the HMA results from a combination of depletion and enrichment events superimposed on their source peridotite compositions. The depletion events led to the low CaO/Al_2O_3 ratios and low incompatible element abundances observed in HMA. Perhaps more significantly the depletion events have given rise to a source, which although later having probably been enriched in Na_2O, K_2O, and ?SiO_2, maintains a distinctive major element composition. This point is clearly illustrated in Chapter 5 where it was demonstrated that the source peridotite composition for HMA must lie to the right of the olivine control line through Pyrolite and Tinaquillo peridotite compositions. This is indicative of a refractory source probably with a significant orthopyroxene component. The enrichment events superimposed on the depleted and/or refractory peridotite compositions in the source regions for HMA have left a unique combination of geochemical characteristics (see Chapter 3). The nature of the enrichment process is difficult to establish,but two different groups of HMA enrichment patterns were observed, giving rise to type-C and type-E HMA. In type-C HMA the enrichment in LREE is not not correlated with Ti/Zr or Zr/Nb, however in type-E HMA increasing LREE enrichment is correlated with a decrease in Ti/Zr and Zr/Nb ratios. Type-C HMA are furthermore characterized by a positive Sr anomaly on incompatible element plots normalized relative to chondrites and primitive mantle abundances. Differences in the enrichment trends and patterns imply that there is at least a two-stage enrichment process, or an enrichment process in which the nature of the process changes so significantly that it is valid to discuss this in terms of different stages.

A possible hypothesis for the prehistory of the mantle source(s) for HMA is as follows:

(i) primitive mantle abundances of trace elements (Sun *et al.*, 1979; Wood, 1979; Gast, 1968);

(ii) small degree of partial melting of the primitive mantle giving rise to alkali volcanism and a residual peridotite characterized by N-MORB characteristics (Green, 1971; De Paolo, 1981; Gast, 1968). A possible residual mantle composition is given by Green *et al.* (1979); [Note CaO/Al_2O_3 ratio in source and residue = 0.8-1.0.]

(iii) partial melting giving rise to MORB basaltic volcanics (Green *et al.*, 1979);

(iv) partial melting of the residual mantle left after MORB volcanism gives rise to low-Ti ophiolitic basalts (Sun & Nesbitt, 1978; Duncan & Green, 1980). Residual mantle composition now is lacking or very low in clinopyroxene component, very low trace element abundances, CaO/Al_2O_3 ratio ?<0.6. This source composition is refractory (cf. Jaques & Green, 1980) and high temperatures would be needed to generate a partial melt (cf. Sun & Nesbitt, 1978);

(v) refractory peritotite source undergoes an enrichment event or events giving rise to the trace element characteristics of HMA (Jenner, 1981; Nesbitt & Sun, 1980). Alteration of the trace element geochemistry of the refractory source is probably accompanied by an influx of water, alkali elements and perhaps silica (cf. Saunders *et al.*, 1980b).

Petrologic and geochemical studies provide evidence for the individual events given in the outline of the prehistory of the source for HMA. However it is quite likely that the sequence of events given may be too specific. For instance, events (ii) and (iii), or (iii) and (iv) could be one event. The main point is that there is a spectrum of residual refractory compositions produced by mid-ocean ridge and intraplate

volcanism but the most refractory of such residues is required to act as the parent to HMA.

Experimental petrology on the HMA, in conjunction with their petrography and mineralogy, helps to further characterize the nature of the HMA and their origin. Arguments were presented in Chapter 5 which considered together effectively limit the conditions of origin of the HMA to that of: $T > 1200°C$; $P < 10$ kb, and probably nearer 2-5 kb; P_{H_2O} ranging from water-saturated with temperatures of ~1200°C to near undersaturated with temperatures in the order of 1300-1400°C.

The characteristics of the HMA, both geochemically and petrogenetically, limit detailed comparisons with other rock types as has been shown in the relevant chapters in this thesis. However there have been attempts made to utilize the HMA and some possibly similar rocks to attempt a general understanding of what these rocks may imply. Before embarking on a more general discussion of the petrogenetic and tectonic significance of HMA it is necessary first to review the characteristics of their possible correlatives.

6.3 COMPARISONS

6.3.1 Comparisons with "Boninites"

Cameron *et al.* (1979, 1980) proposed that the usage of the term "boninites", originally used to describe the Mg-rich rocks of the Bonin Islands, be expanded to include within its coverage certain other low-Ti high-Mg volcanics. As defined by these authors boninites are a highly magnesian but relatively siliceous, glassy rock containing one or more varieties of pyroxene, some or all of which have a morphology characteristic of rapid growth, accessory magnesiochromite, and commonly minor amounts of olivine. Laths of amphibole or plagioclase microlites are rare. In addition to the HMA of this thesis, the following are also included by Cameron *et al.* (1979. 1980) within this definition: the uppermost Upper

Pillow Lavas (UPL) of the Troodos Massif and Arakapas Fault Belt lavas in Cyprus, and rocks of the Agrilia Formation, Othris Mountains, Greece.

Meijer (1980) proposed that the definition given by Cameron *et al.* (1979, 1980) was *too specific*, particularly in its petrographic requirements, and that a wider definition based on selected chemical characteristics was preferable. Based on a ternary plot of the normative mineral components, En, Qz, and Ilm, Meijer defined a boninite series which included, in addition to those rocks mentioned above, rocks from Tafahi Island (Tongan Arc); Blup Blup, Kadovar and Manam Islands, PNG; and rocks of the Lower Facpi Member, Guam.

Descriptions of rocks included in the definition of boninite or boninite series are given below.

6.3.1.1 Uppermost Upper Pillow Lavas (UPL) and Arakapas Fault Belt Lavas

According to Cameron *et al.* (1980) lavas from the two areas are almost identical petrographically, so they are considered together here. Petrographically these rocks show the following features (after Cameron *et al.*, 1979, 1980; Simonian & Gass, 1978):

(i) crystallization sequences - chrome-rich spinel → olivine → orthopyroxene and/or clinopyroxene → plagioclase;

(ii) olivine (Fo_{80-90}) shows no reaction relationship; and

(iii) orthopyroxene up to Mg_{89} and clinopyroxene to Mg_{86} occur. Green (pers. comm., 1981) has also studied rocks from these areas and found coexisting orthopyroxene and clinopyroxene of Mg_{89}.

Chemically (see Table 6.1) the rocks are lower in SiO_2, and have much higher CaO/Al_2O_3 ratios than HMA (~0.8-1.0 versus <0.6). The trace element geochemistry is also different in that they have (i) higher Ti/Zr and lower Zr/Y ratios; (ii) lower Cr/Ni ratios (~1-3); and (iii) are depleted in LREE.

Table 6.1

Analyses of "boninites".*

	Arakapas	UPL	Tafahi Island	Manam Island	Blup Blup	Kadovar	Low-Ti Facpi, Guam, upper	Low-Ti Facpi, Guam, lower	Umatac Fm - Facpi, Guam	1438/ C	1438/ B+E	Kopi, New Zea-land	Bush-veld
Number	13	1	3	1	1	1	2	2	1	1	2	6	1
SiO_2	54.16	55.30	52.85	51.74	59.40	57.60	56.18	53.78	53.17	50.30	61.09	53.62	55.70
TiO_2	0.24	0.32	0.39	0.32	0.32	0.31	0.36	0.40	0.57	0.46	0.71	0.18	0.36
Al_2O_3	12.75	11.86	17.09	16.68	15.43	13.50	14.66	14.44	16.68	15.53	14.77	13.17	12.74
FeO	8.40	8.32	10.01	8.33	7.47	8.87	7.93	8.09	7.77	6.88	8.23	9.01	8.78
MnO	0.17	0.16	0.19	0.18	0.15	0.16	0.12	0.16	0.21	0.12	0.14	0.17	0.09
MgO	11.90	13.27	6.37	8.71	4.67	5.95	8.95	10.47	9.86	12.74	3.23	11.25	12.44
CaO	10.90	9.25	11.73	11.10	7.82	9.00	8.13	9.98	8.91	10.66	8.68	10.70	6.96
Na_2O	0.81	1.32	1.09	1.80	2.44	2.00	2.42	1.99	2.04	1.86	2.48	1.47	2.02
K_2O	0.31	0.16	0.14	0.72	1.72	1.45	1.17	0.36	0.50	0.88	0.59	0.12	1.03
P_2O_5	0.03	0.03	0.10	0.18	0.23	0.24	0.08	0.04	0.14	0.01	0.07	0.21	
CaO/Al_2O_3	0.85	0.78	0.69	0.67	0.51	0.67	0.55	0.69	0.53	0.69	0.59	0.81	0.55
Mg/Mg+Fe	71.63	74.0	53.0	65.1	53.0	54.4	66.8	69.8	69.3	76.7	41.2	69.0	71.6
Cr	833	976	64							879	44	1133	970
Ni	376		23							204	25	224	292
Y	4.8	10	8							8	24	7.7	
Zr	12.5	23	8							16	29	9	70
$(La/Sm)_N$	0.48	0.50	1.07	1.66-2.18									
$(La/Yb)_N$	0.23	0.38	0.79	1.83-2.74									
Ti/Zr	115	83	292							172	147	120	31
Ti/Y	300	192	292							345	177	146	
Zr/Y	2.6	2.3	1							2	1.2	1.2	
Cr/Ni	2.22	-	2.78							4.31		5.06	3.32

Data sources: Arakapas - Simonian & Gass (1978), note La by extrapolation; UPL - Kay & Senechal (1976)(6aXT); Manam,Blup Blup,Kadovar - Morgan (1966), Johnson *et al.* (1981); Guam - Stark (1963), Shiraki *et al.* (1978); 1438 - Beccaluva *et al.* (1980). Kopi, New Zealand - Wood (1980); Bushveld - Davies *et al.* (1980).

* analyses recalculated anhydrous with total Fe as FeO.

6.3.1.2 Agrilia Formation, Othris Mountains

Cameron *et al.* (1980) described these "boninites" as olivine, olivine + clinopyroxene, and clinopyroxene + plagioclase phyric, Orthopyroxene is conspicuously absent. The geochemical data given by Cameron *et al.* (1979, 1980) shows these rocks to have moderate TiO_2 contents of 0.7%, a Ti/Zr ratio of 94, and CaO/Al_2O_3 ratio >0.9.

6.3.1.3 Tafahi Island

Descriptions of these rocks and their geochemistry are given in Ewart *et al.* (1977) and Ewart (1976). They do not appear to be petrographically different from other Tongan basaltic andesites and are plagioclase phyric with minor orthopyroxene and augite.

Chemically the Tafahi rocks (Table 6.1) are low in SiO_2, K_2O and Na_2O, and higher in Al_2O_3, CaO and CaO/Al_2O_3 compared to the Bonin Islands (B1) bronzite andesite (of similar Mg-number). The Ti/Zr ratio of 292 in these rocks is very high and they have a low Zr/Y ratio. The REE are similar in abundance to the Bonin Islands bronzite andesite but the pattern is more typical of that of IAT and lacks any concave nature.

6.3.1.4 Blup Blup, Kadovar and Manam Islands

Descriptions of the petrography and geochemistry of these rocks is given in Morgan (1966), and some detailed geochemical and mineralogic information on Manam Island is reported in Johnson *et al.* (1981).

The Manam Island samples are tholeiitic basalts - basaltic andesites with SiO_2 contents of 50-54 wt.% and Mg-numbers of 60-66 (Johnson *et al.*, 1981). Al_2O_3 contents are reasonably high (~16%) and TiO_2 contents are low (0.3-0.4%). REE patterns are marked by LREE enrichment, with abundance levels similar to those found in the THS and CAS series volcanics of Whitford *et al.* (1979) (Jaques, pers. comm., 1981). εNd ranges from +6.2-7.6. Phenocrysts and xenocrysts are common with plagioclase (An_{86-82} cores) most abundant. Olivine (Fo_{92-77}) occurs and Mg_{89} diopside is found as cores in some clinopyroxene grains.

Blup Blup rocks are olivine, clinopyroxene and plagioclase phyric, while olivine is absent in Kadovar Island samples. These rocks are therefore petrographically unlike the bronzite andesites (see Chapters 2 and 3) with which they have some geochemical affinities (see Table 6.1).

Johnson *et al.* (1981) have noted the low volatile contents in the Manam Island rocks, and have argued on this basis and their petrography that these rocks were derived from a mantle source under strongly water-under-saturated conditions.

6.3.1.5 Lower Facpi Member, Guam

The stratigraphic sequence of volcanic rocks on Guam is as follows (after Stark, 1963):

Late Tertiary
  Umatac Formation
    Dandan Flow Member (see Table 6.1, column 9)
    Bolanos Pyroclastic Member
    Macmong Limestone Member
    Upper Facpi Volcanic Member (see Table 6.1, column 7)
    Lower Facpi Volcanic Member (see Table 6.1, column 8)
  -- unconformity --
Early Tertiary
  Alutom Formation

The Facpi Volcanics are olivine, plagioclase and augite phyric basalts and andesites. Bronzite or hypersthene form rare phenocrysts in some basalts and andesites. The Lower Facpi Volcanic Member is divisible into two groups based on geochemistry (Table 6.1): an upper group with ~56% SiO_2, and a lower group with ~53-54% SiO_2. These is close similarity between the lower group and the uppermost UPL lavas of Troodos. The upper groups have a low CaO/Al_2O_3 ratio, but lower SiO_2 and higher alkalis and alumina compared to HMA of similar Mg-numbers.

The Upper Facpi Volcanic Member flows (not tabulated in Table 6.1) are basalt to basaltic andesite and have significantly higher TiO_2 contents (0.92-1.08) than those of the Lower Facpi (Stark, 1963; Shiraki *et al.*, 1978).

The Dandan Flow Member overlying the Facpi Members has basalts and andesites with 0.56-0.73% TiO_2 and 0.19-0.33% P_2O_5 (Table 6.1, column 9). These rocks appear to have the chemical characteristics of many island-arc volcanics (cf. Shiraki *et al.*, 1978; Stark, 1963).

6.3.1.6 Leg 60 IPOD - Site 458

Meijer *et al.* (1980), Meijer (1980), and Hickey & Frey (1981) have drawn attention to similarities between some of the lavas from this site and bronzite andesites from the Bonin Islands. The rocks they considered "boninites" occur as (i) glassy vesicular volcanics with rare (~5%) phenocrysts of clinopyroxene and orthopyroxene and lacking feldspar phenocrysts; (ii) medium grained plagioclase + clinopyroxene rocks with essentially the same chemistry as that observed in the glassy rocks. Phenocryst compositions in the glassy rocks are similar to those reported in Chapter 2 for the bronzite andesite.

The rocks have Mg-numbers of 50-61, TiO_2 contents <0.5% and 57-60% SiO_2. Volatile contents are in the order of 3-4%. CaO/Al_2O_3 ratios range from 0.57-0.81 and average 0.68, however values for the most magnesian samples (Mg-number 58) are 0.74. Trace elements show (i) low Ti/Zr (<60), Zr/Y >3, and Ti/Y of 200-360; (ii) Rb (8 ppm) and Sr (90 ppm) are similar in abundance to Bonin Islands bronzite andesites; (iii) REE patterns show LREE depletion and have HREE at ~3x chondrites; and (iv) ΣNd of +5.9-6.2.

6.3.1.7 Yap Trench

Beccaluva *et al.* (1980) and Crawford *et al.* (1981) described boninites occurring at the northern end of the Yap Trench. These rocks are ~8 m.y. old. Phenocryst phases are olivine, orthopyroxene, clinopyroxene and plagioclase. The andesites are fresh, have hyalopilitic texture and are highly vesicular. Analyses are given in Table 6.1 for a magnesian basalt and an average of two andesites. The basalt has low TiO_2 but a high Ti/Zr

and low Zr/Y ratio. The andesites are similar to the Bonin Islands bronzite andesite in most major elements but have much higher TiO_2 and Ti/Zr and lower Zr/Y.

6.3.1.8 Bushveld Parental Magma

High SiO_2, high MgO, low TiO_2 sills associated with the Bushveld Complex have been described by Davies *et al.* (1980) and Cawthorn *et al.* (1981) (see also Table 6.1). These rocks are characterized by hopper and branching olivine and abundant bladed to feathery orthopyroxenes. Microlites of clinopyroxene and plagioclase occur in the matrix of devitrified glass.

Experimental studies on selected compositions (Cawthorn *et al.*, 1981) indicated that olivine + orthopyroxene cosaturation occurs at 3-4 kb and 1275-1300°C. The high Mg-numbers in the rocks indicate that they may be mantle derived and their crystallization sequence of olivine, orthopyroxene, orthopyroxene + plagioclase, orthopyroxene + plagioclase + clinopyroxene is similar to that observed in the Bushveld Complex (Davies *et al.*, 1980; Cawthorn *et al.*, 1981).

Compositionally the rocks are characterized by a low CaO/Al_2O_3 ratio of 0.55, Cr/Ni of 3.32, Ti/Zr of 31 and SiO_2 contents of 53-56%. The rocks have high Na_2O and K_2O and it is likely that there has been some crustal contamination (Davies *et al.*, 1980; Cawthorn, pers. comm., 1980).

6.3.1.9 Kopi, New Zealand

A boninite-like lava containing olivine, orthopyroxene and clinopyroxene was found interbedded with Cretaceous sedimentary rocks in New Zealand (Wood, 1980). The lavas appear to form pillows which are characterized by quench pyroxenes. The groundmass is variable in texture but may contain plagioclase (An_{67-79}).

An average analysis of these rocks, known as Kopi boninite, is given in Table 6.1. The Kopi rocks have ~53.5% SiO_2, CaO/Al_2O_3 ratio of 0.81, Ti/Zr of 120, and Cr/Ni of 5.06. The rocks are quite similar to the Arakapas and uppermost UPL of Troodos (see also Table 6.1).

6.3.2 Comparison with Komatiites

Cameron *et al.* (1979) suggested there was a remarkable resemblance between basaltic komatiites and boninites (including the HMA of this study).

There are a number of uncertainties involved in defining the term *komatiite* or basaltic komatiite (see for example Nisbett *et al.*, 1979; Arndt *et al.*, 1977); however,there is some agreement that spinifex-textured extrusive volcanics with MgO contents between 12-20% can be termed basaltic komatiites. These volcanics although generally altered show textural evidence for olivine and clinopyroxene phenocrysts and/or microlites (Nesbitt *et al.*, 1979; Cameron *et al.*, 1979; Binns *et al.*, 1981; Williams, 1971; Sun & Nesbitt, 1978). Plagioclase may be present, however orthopyroxene, as is generally the case in extrusive komatiites, is conspicuous by its absence (Williams, 1971; Cameron *et al.*, 1979; Hallberg, pers. comm., 1980).

Amongst this broad subdivision of the komatiites, i.e. basaltic komatiites, Nesbit & Sun (1980) noted some rocks with geochemical similarities to HMA. In particular they drew attention to high SiO_2 content, low Ti/Zr ratio, and REE patterns which are similar to HMA in that they show the same mixing characteristics. No complete chemical analyses of these rocks have been published, however data from Sun & Nesbitt (1978b) show these rocks to have 52-56% SiO_2, CaO/Al_2O_3 ratios of 0.55 to 0.85, TiO_2 contents of 0.39-0.54%, and Mg-numbers of 66-75. Green (1981) has done some liquidus experiments on one of these rocks (331.338) which had an Mg-number of 70, and 56% SiO_2. The results indicated olivine and orthopyroxene cosaturation at 7-8 kb and 1280-1300°C under *anhydrous* conditions.

6.3.3 Mg-rich Andesites (Sanukitoids), Japan

Amongst Tertiary volcanic rocks from the Setouchi volcanic province of southwest Japan, are occurrences of magnesian andesites with characteristics indicative of their being primary magmas (Tatsumi, 1981; Tohara, 1981; Kushiro & Sato, 1978; Sato, 1981; Ujike, 1972). These magnesian andesites form part of a suite of volcanics termed *sanukitoid* (Sato, 1981; Tatsumi & Ishizaka, 1981), which has SiO_2 contents ranging from 50-66%, but which is clearly not related by fractionation to more basic rocks (Tatsumi & Ishizaka, 1981b). The sanukitoid magnesian andesites (SMA) are relatively aphyric volcanics (<20% phenocrysts, Tatsumi & Ishizaka, 1981) with phenocrysts of olivine and pyroxene but plagioclase phenocrysts are rare or absent. Orthopyroxene is an important phenocryst phase in these rocks and ranges up to ~Mg_{92} with high Cr_2O_3 contents (up to 1%), Al_2O_3 of 1-3%, and CaO of 0.8-1.6% (Sato, 1981; Tatsumi & Ishizaka, 1981; Appendix 2). No low Ca-Al pyroxenes resembling clinoenstatites (i.e. <0.6% CaO), either chemically or optically have been found. Furthermore liquidus studies on these volcanics (Tatsumi, 1981; Kushiro & Sato, 1981) have produced only relatively Ca- and Al-rich orthopyroxenes. Clinopyroxenes of Mg_{80-90} have been reported, however these are relatively rare (Tohara, 1981; Tatsumi, 1981; Tatsumi & Kushiro, 1981; this study, Appendix 2). Plagioclase compositions range from An_{32-66} (Appendix 2) in the sanukitoids and associated felsic volcanics. Cr-rich spinels have been reported (up to ~60% Cr_2O_3) (Tohara, 1981; Tatsumi & Ishizaka, 1981).

Compositions of some of the sanukitoids are given in Table 6.2 and further analyses of these and related rocks can be found in Ujike (1972), Tatsumi & Ishizaka (1981b), and Appendix 2. Compared to HMA, the SMA have greater concentrations of Na_2O, K_2O, TiO_2, Al_2O_3, and P_2O_5, and lower MgO. Some of these differences are clearly reflected in the norms where the HMA generally have higher Qz and Hy, and lower Or, Ab, An, and Ilm. CaO/Al_2O_3

Table 6.2

Mg-andesites (sanukitoids), Japan.*

	705B	TG1	SD261	WS17	T1	T2	T3	T4	Test	BI	MT	V5
SiO_2	56.76	59.55	57.09	57.78	58.12	57.24	57.03	59.19	55.81	58.10	57.97	56.67
TiO_2	0.69	0.44	0.73	0.64	0.57	0.76	0.74	0.54	0.70	0.16	0.23	0.20
Al_2O_3	15.25	13.54	15.82	14.45	13.54	14.56	13.48	13.46	12.60	11.08	10.51	7.87
Fe_2O_3	0.68	0.70	0.70	0.66	0.68	0.76	0.81	0.68	0.80	0.97	0.92	1.05
FeO	5.49	5.68	5.69	0.34	5.50	6.17	6.53	5.52	6.48	7.68	7.43	8.49
MnO	0.12	0.12	0.13	0.12	0.19	0.07	0.07	0.14	0.10	0.20	0.13	0.21
MgO	9.16	9.64	7.39	10.62	11.17	9.95	11.26	10.39	14.20	12.49	14.58	19.93
CaO	7.00	6.24	7.16	6.13	6.39	6.60	6.61	5.69	6.00	7.32	5.57	4.50
Na_2O	3.16	2.66	2.89	2.44	2.59	2.84	2.24	2.74	2.40	1.51	1.68	0.90
K_2O	1.69	1.30	2.26	1.69	1.25	1.05	1.24	1.65	0.90	0.52	0.99	0.20
P_2O_5	0.00	0.13	0.14	0.13								
CaO/Al_2O_3	0.46	0.46	0.45	0.42	0.47	0.45	0.49	0.42	0.48	0.66	0.53	0.57
Mg no.	74.8	75.2	69.8	77.3	78.4	74.2	75.4	77.0	79.6	74.3	77.8	80.7
Qz	1.98	9.41	4.00	6.00	6.03	5.27	5.76	7.06	1.60	10.01	7.00	5.79
Or	9.99	7.70	13.38	9.97	7.38	6.19	7.32	9.75	5.32	3.09	5.83	1.18
Ab	26.74	22.48	24.44	20.68	21.90	24.04	18.94	23.17	20.31	12.78	14.14	7.59
An	22.44	21.17	23.51		23.48	21.64	23.88	23.08	20.96	21.90	18.24	16.85
Di	9.88	7.18	8.96	4.84	8.04	7.13	7.78	6.93	7.04	11.63	7.55	4.36
Hy	26.67	29.91	22.97	32.54	32.94	30.94	34.54	31.51	42.28	38.91	45.43	62.33
Ol												
Mt	0.98	1.02	1.02	0.96	0.99	1.11	1.17	0.99	1.16	1.37	1.33	1.52
Ilm	1.31	0.83	1.38	1.22	1.08	1.44	1.40	1.02	1.33	0.31	0.44	1.38
Hap		0.31	0.34	0.31								
Jd+Ts	28.3	21.4	28.1	22.3	22.0	24.4	21.3	21.8	20.9	16.3	15.4	10.4
Qz	52.6	60.2	55.3	56.8	56.8	56.0	56.6	58.0	51.9	60.7	57.4	55.6
Ol	19.2	18.3	16.6	20.9	21.0	19.6	22.1	20.2	27.2	23.0	27.2	34.0

Sources of data: 705B - Kushiro & Sato (1978); TG1,SD261 - Tatsumi (1981); WS17 - Tatsumi & Ishizaka (1981); T1-T4,Test - Tohara (1981); BI (Bonin Islands HMA), MT (Mariana Trench HMA), V5(Cape Vogel) - this study.

* analyses recalculated anhydrous, $Fe_2O_3/FeO = 1/9$.

ratios in SMA are low, ranging from 0.4 to 0.6 (Sato, 1981), and on the basis of their mineralogy and experimental liquidus studies can be said to reflect the CaO/Al_2O_3 ratio of their peridotitic source region (cf. Tatsumi, 1981; Tohara, 1981; Kushiro & Sato, 1978; Sato, 1981). Cr/Ni fall in the range 1-3 (Tatsumi & Ishizaka, 1981b). REE patterns in SMA and related volcanics from the Shikoku district (Appendix 2) show LREE of 20-50x chondritic and HREE of 3-7x chondritic, giving rise to a REE pattern substantially steeper and less notably concave than that observed in HMA and related volcanics.

6.3.4 Discussion

In this section, and that immediately preceding it, some of the petrographic and geochemical features of high-Mg andesites, boninites, komatiites and sanukitoids have been presented. There are two important questions which may be asked: firstly, what similarities and differences are there between these rocks, and has there been too much emphasis placed on drawing some of these rocks together under one name (i.e. boninites); and secondly, what are the petrogenetic implications of high-SiO_2, high-MgO volcanics.

The petrographic and geochemical characteristics of the rocks included within the definition of "boninites" and "boninite series" are wide ranging. For example, these terms include the HMA of this study and the basaltic volcanics of the Agrilia Formation, Othris Mountains, which show little or no similarity. In general, the comparisons are not as misleading as that noted above but significant differences nonetheless exist. The low-Ti uppermost UPL and Arakapas Fault Belt lavas differ from HMA as illustrated by the presence of magnesian calcic clinopyroxene of Mg_{80-85}, a CaO/Al_2O_3 ratio of 0.8-1.0 and a strongly LREE depleted pattern. Many of the rocks described as boninites have plagioclase as a major or

notable phenocryst phase, have SiO_2 contents <56% and Ti/Zr >60. The Bushveld "boninites" display some features of HMA in that they have low Ti/Zr and CaO/Al_2O_3 ratios; however, their crystallization sequences differ from that observed in HMA or their fractionated equivalents and they have lower SiO_2 contents (52-56%).

The Blup Blup, Kadovar and Yap Trench andesites are somewhat similar to the Bonin Islands bronzite andesite and give rise to the difficult question of recognition of the fractionated end-members of a HMA association when the parental lavas are missing. The difficulties in answering this question are nowhere more apparent then then one considers the bronzite andesite from site 458. These andesites have some mineralogical features displayed in the Bonin Islands bronzite andesites, along with the chemical criteria of low Ti/Zr, high Zr/Y and low ΣNd. They however do not show LREE enrichment or a particularly low CaO/Al_2O_3 ratio. The low Ti/Zr ratio of these rocks without LREE enrichment may indicate that the HFS and REE elements behave independently, as is observed to a certain extent in type-C HMA (i.e. Ti/Zr of ~50-20, with no differences in La/Yb). In the site 458 andesites it is possible to find significant petrologic and geochemical affinities with HMA, which is more than can be said for a number of examples, and it is not untoward to suggest HMA may have been present. In general, however, inferring the presence of HMA on the basis of fractionated andesites is fraught with problems.

The terms "boninite" and "boninite series" are based to a large extent on comparisons with HMA, and in particular the occurrence of these rocks in the Bonin Islands. There are significant geochemical and petrologic differences between the HMA and many "boninites" or members of the "boninite series". Usage of the later two terms should be avoided. As will be shown in the discussion of tectonic environment of formation there has already been considerable misuse of the terms "boninite" and "boninite series".

The comparison of HMA with basaltic komatiites is in most instances misleading, however there are some similarities with the high-SiO_2 varieties as noted by Nesbitt & Sun (1980). The limited data available make it difficult to ascertain many of the geochemical features of the high-SiO_2 basaltic komatiites; however, the experimental petrology on these rocks does show a marked dissimilarity with that observed for the HMA.

The sanukitoid andesites from Japan share with the HMA characteristics of primary mantle derived andesites; however, there are marked differences in their petrology and geochemistry (Chapter 5, and above).

The role of water in the origin of the HMA appears to be crucial. Only when water was present in the experimental studies on the HMA, described in Chapter 5, was it possible to get olivine and orthopyroxene cosaturation, with the requisite mineral compositions. Derivation of the HMA by partial melting of a peridotite source under water-saturated conditions is a possibility for explaining the origin of these rocks; however, for the reasons outlined in Chapter 5, water-undersaturated conditions at low pressures (<5-10 kb) and high temperatures (>1200°C) are required.

In contrast to the HMA, experimental studies on a possible parental magma composition for the uppermost UPL of Troodos (Duncan & Green, 1980, pers. comm., 1980, 1981) indicate that lavas of this type may form by partial melting of a peridotite source under anhydrous conditions. The conditions of segregation from an anhydrous peridotite source for this composition are: P ~7-8 kb, T ~1320-1350°C (Duncan & Green, pers. comm., 1980).

Experimental studies on the high-SiO_2 basaltic komatiite indicate anhydrous conditions, as did results of studies on the Bushveld "boninite". The Manam Island basaltic andesites are also thought to originate under strongly water-undersaturated conditions (Johnson *et al.*, 1981).

Extensive liquidus studies on the sanukitoid andesites have not yet been completed, however these rocks may originate at pressures of less than 15 kb under water-undersaturated conditions. The temperatures at magma segregation for the sanukitoid water-undersaturated magmas could well be in the range of 1200-1300°C.

Taken as a whole the HMA, sanukitoid and "boninite" lavas represent a group of lavas which may form at low pressures (<15 kb). The temperature of formation of these lavas will vary with composition and water content, but lies for the most part in the range >1100°C to <1400°C. As possible primary derivatives from the mantle these lavas occupy petrogenetic niches which are fundamentally different from that shown by parental magmas to mid-ocean ridge volcanism (Green *et al.*, 1979) or ocean-island volcanism (Green & Ringwood, 1967; Green, 1971). The petrogenetic characteristics of these rocks will form an integral part of the attempt to derive an overall model for understanding of the characteristic magmatism of various regions (cf. Green, 1973b); however, they can not in themselves be used to delineate tectonic environments of formation (contrast the Bushveld, Kopi, Mariana Trench and komatiite occurrences).

6.4 TECTONIC SETTING OF HMA

The tectonic settings of the HMA localities at Cape Vogel, the Bonin Islands and the Mariana Trench, at the time of eruption of these rocks are not well constrained. The Cape Vogel HMA are associated with tholeiitic volcanics similar to IAT and this feature combined with the geochemical comparison of HMA with some PNG Eocene tonalite has led to the suggestion that the Cape Vogel HMA formed during the early stages of island-arc magmatism associated with a northeast-dipping subduction zone (Eocene) (Jaques & Chappell, 1980). The tectonic events which led to the present position of the Bonin Islands are complex and the age of volcanism and evolution of the back-arc basins in this portion of the Mariana

island-arc system are not well known (Karig & Moore, 1975). Similar comments also apply to the Mariana Trench HMA and associated bronzite andesites, also there are large uncertainties in the age of the HMA and the bronzite andesites of site 458.

Despite the uncertainties in the spatial and temporal relations between the HMA and other volcanics in the Mariana island-arc/back-arc basin system a number of tectonic models for the origin of the HMA have emerged, i.e. Crawford *et al.* (1981), Meijer (1980), Shiraki *et al.* (1978), and Mrozowski & Hayes (1980). Excluding Shiraki *et al.* (1978) the models for the tectonic setting of the HMA have attempted to provide an adequate heat source(s) to allow for the partial melting of a refractory peridotite source. Since the basis on which these models were constructed used the following conditions of origin for HMA: P = 10 kb; T = 1100°C; water-saturated melting (after Green, 1973, 1976), they have underestimated by as much as 100-300°C the temperatures which are likely to be required.

Crawford *et al.* (1981) (see also Beccaluva *et al.*, 1980) have presented a model for formation of the HMA which draws heavily on comparisons with "boninites" and regions outside the Mariana island-arc system. Implicit in the model presented by Crawford *et al.* (1981) is a petrogenetic and geochemical equivalence between HMA and other "boninites". As has been argued earlier there is very little firm evidence for this. The misuse of the term "boninite" in their paper is illustrated by the following.

According to Crawford *et al.* (1981) there is a "general association of boninites with MORB-like tholeiites". More specifically they suggest MORB-like tholeiites should overlie the boninites and that associated island-arc volcanics (CAS and/or IAT) may be older. Evidence supporting the association with MORB tholeiites is (i) occurrence of MORB-like tholeiites in dredge sites 1403 and 1404 from the Mariana Trench;

(ii) occurrence of MORB-like basalts with "boninites" at Rambler and Betts Cove, Newfoundland, and Cambrian greenstone belts in Victoria; and (iii) possible MORB with boninites in Pindos and at Cape Vogel. The first occurrence is of dredged samples in which the age relationships are unknown (cf. Meijer, 1980). In the third case there is no published data from Pindos and as was shown in Chapter 2 (and Appendix 1) the tholeiites associated with the HMA at Cape Vogel form part of a suite including andesites and dacites which are not unlike those found in the island-arc tholeiite association. Age relations between the volcanics have not been established. The boninites from Victoria are characterized by 10.4% CaO, 2.73% Al_2O_3, <0.05% TiO_2 and K_2O, and <0.5% Na_2O. These rocks have been highly altered and their original characteristics are unknown. The "boninites" from Betts Cove are overlain by a succession of basaltic lavas ranging from depleted MORB to those with characteristics of aseismic ridges or oceanic islands (Coish & Church, 1979; Jenner & Fryer, 1980) and no island-arc volcanics have been found in association with them in contrast to the general case for HMA. The Betts Cove, Rambler and Victorian "boninites" furthermore do not have characteristics similar in detail to those of HMA. MORB-like tholeiites are not found in association with HMA in the Bonin Islands (Chapter 2) and if there is an association on "boninites" with MORB then it is in the case of Troodos, one in which the "boninites" overlie the MORB-tholeiites.

While the model of Crawford *et al.* (1981) to explain the Mariana HMA is in part erroneously based on comparisons with "boninites", it nonetheless has some plausibility. The model presents the hypothesis that the HMA form as a result of an island-arc rifting event associated with back-arc basin formation. Diapiric uprise of mantle into the rift creates an abnormal geothermal gradient which is capable of melting a refractory mantle source.

Mrozowski & Hayes (1980) and Meijer (1980) have suggested that westward subduction of the Pacific Plate under a young (<10 m.y.) Philippine Sea Plate could create an anomalously hot subduction region because of the slow thermal decay time for new lithosphere (i.e. Philippine Sea Plate). Mrozowski & Hayes (1980) suggested that the HMA form near the trench *soon* after subduction. Meijer (1980) dated the "boninitic" volcanism at 34-36 m.y., which is approximately 6 m.y. after the initiation of subduction. The timing of the origin of the HMA in Meijer's model is dependent to a certain extent on the assumption that the low-Ti Facpi volcanics on Guam are equivalent to HMA and bronzite andesites. The presently available petrographic and geochemical evidence do not substantiate this view.

6.5 SUMMARY

Comparison of the high-Mg andesites studied in this thesis with "boninites"*, basaltic komatiites and sanukitoids details a number of petrographic, petrologic and geochemical dissimilarities. These differences preclude a common peridotite source, and more significantly suggest a different history for the source regions of these rocks. Earlier in this chapter a possible scenario for the evolution of the mantle source for HMA was presented and it is possible to suggest where differences between HMA and "boninites" and sanukitoids may have arisen using this outline. Some "boninitic" lavas are characterized by low-TiO_2 LREE depletion, CaO/Al_2O_3 ratios of 0.8-1.0 and SiO_2 of 52-56%, i.e. the Arakapas and uppermost UPL of Troodos. Duncan & Green (1980) have proposed that these rocks form by second-stage melting, i.e. partial melting of the

---

* excluding HMA

residual peridotite left after removal of MORB. Many "boninites" may thus represent a stage in the evolution of a mantle source before HMA are formed. The tectonic setting for "boninite" formation is not clearly defined. "Boninites" may form in an island-arc environment (Meijer, 1980; Cameron *et al.*, 1980), in a continuously melting uprising diapir irrespective of tectonic setting (Brown *et al.*, 1980), in a continental rift setting (Wood, 1980), in a stable cratonic environment (Davies *et al.*, 1980; Cawthorn *et al.*, 1981), or perhaps at a mid-ocean ridge (Duncan & Green, 1980). In "boninites", unlike HMA, water may not play a significant role and there is no reason to attempt to associate them with a tectonic setting which provides a source for water, i.e. island-arcs.

The sanukitoids are primary mantle derived andesites which formed in an island-arc environment (Tatsumi & Ishizaka, 1981). These rocks may represent a source peridotite which has undergone a depletion history similar to HMA but which has been more comprehensively metasomatized or altered before partial melting took place.

It is possible then the view the "boninites", HMA and sanukitoids as representing a continuum in the evolution of a mantle source(s). These rocks share a common petrogenetic implication, i.e. they represent partial melting of a peridotitic source at low pressures (<15 kb) and moderate to high temperatures (1100-1400°C). However it is clear that it is erroneous to determine a tectonic environment of formation, or erect models for their petrogenesis, by assuming these rocks can be discussed as equivalents. The major point of disagreement I have with the usage of the term "boninite" or "boninite series" arises from this last point. While the terms may be valid for describing a broad spectrum of volcanics characterized by high SiO_2 (>52%), high MgO (>5%), and low TiO_2 (<0.7%), its use has not been restricted to this purpose. Both Crawford *et al.* (1981) and Meijer (1980) have implied a degree of equivalence between these rocks and HMA which does not exist in attempting to support their tectonic models.

In particular their usage of the terms implies a common or similar geochemical "history" and similar conditions for petrogenesis. Neither of these are necessarily true.

At present there is no unequivocal tectonic model for the origin of HMA. The association of these rocks with an island-arc environment seems likely. This is substantiated by their rock associations and by the likelihood that the conditions necessary for their origin can be met in this environment. For instance an island-arc environment provides (i) an area in which depleted or refractory mentle is accessible (Green, 1973b); (ii) a variety of processes can occur which may provide the enriching fluids necessary to explain HMA geochemistry (Saunders *et al.*, 1980b); (iii) the tectonic environment capable of producing the required high temperature at shallow depths. Either of the two proposed alternatives, i.e. subduction under a "hot" plate, or additional heat being added from diapirs of basalts formed during back-arc basin rifting seem viable; and (iv) water, crucial to the petrogenesis of HMA, is likely to be present in sufficient quantity (Anderson *et al.*, 1978). It is important to note that these conditions may be met in another tectonic environment and the dogma that HMA imply the presence of an island arc should not be propagated.

Brown *et al.* (1980), Varne & Brown (1978), Duncan & Green (1980), and Green *et al.* (1979) have noted that the mineralogical characteristics of cumulate sequences in some ophiolites are not explicable as crystallization products from a MORB-type magma. These authors have suggested that crystallization from a more siliceous and magnesian melt than MORB may explain the discrepancies. The establishment of the nature of the fractional crystallization sequence in HMA (this study) will form part of the body of information needed to evaluate the nature of the parental magmas to individual ophiolite complexes.

Chapter 7

SUMMARY

The origin of the HMA has been studied by a variety of techniques and approaches. Not all the questions concerning the origin of these rocks have been answered. Nonetheless significant progress has been made in understanding their genesis and in unravelling the related problems of pyroxene equilibria.

The occurrence of protoenstatite (precursor of clinoenstatite) in the HMA is dependent on the P, T and composition. In this study it has been demonstrated that the pyroxenes sensitively reflect the chemistry of the magmas and that the appearance of protoenstatite, within its predicted P, T field is controlled by magma composition, and is restricted to strongly quartz normative liquids with Mg-numbers >70 and Di/Di+Hy ratio <0.2.

Experimental studies in the Mg-rich part of the pyroxene quadrilateral did not closely constrain the conditions of origin of the HMA. It had been hoped to limit the extrusion temperatures of the HMA using the protoenstatite-to-orthoenstatite inversion, however compositional rather than temperature control determines the appearance of protoenstatite in HMA. However the findings are a fundamental contribution to our understanding of the pyroxenes. In particular, the demonstration that there is a high T stability field of orthopyroxene, challenges the existence of the invariant point defined by the reactions OE $\rightleftarrows$ PE+DI, PE+DI $\rightleftarrows$ PI and OE+DI $\rightleftarrows$ PI, in the system $CaMgSi_2O_6$-$Mg_2Si_2O_6$. The findings suggest a continuous field of orthopyroxene stability from low to high temperatures and corroborate the hypothesis of Huebner (1980) concerning phase relations on the join $Mg_2Si_2O_6$-$CaMgSi_2O_6$ and in the system CaO-FeO-MgO-SiO_2.

Liquidus studies on HMA indicate that the parental magmas for these rocks form at temperatures > 1200°C and pressures < 15 kb, under hydrous

conditions. Water plays an important role in the petrogenesis of the HMA although it is unclear what amounts are necessary in the source. High temperature (>1200°C), low pressure conditions (<5 kb) with low water contents, are favoured since these provide better opportunity for the development of protoenstatite and allow ascent/extrusion of the HMA without extensive olivine fractionation.

The geochemistry of the HMA reveals a complex history for the source region. The overall low abundance of incompatible trace elements and the fractionated CaO/Al_2O_3 ratio are consistent with a mantle source which had previously undergone partial melting events. Enrichment processes superimposed on this highly refractory source have played a major role in determining the incompatible trace element ratios. Two types of HMA are recognized based on REE patterns and incompatible trace element ratios: these are type-C and type-E. Type-C are common to all HMA localities, whereas type-E are as yet only found at Cape Vogel, PNG. The enrichment processes responsible for the two types differ. It is possible that the enrichment pattern observed in type-E HMA was superimposed on a source characterized by type-C incompatible element ratios. It is not possible to determine the nature of these processes to any significant extent; however, a role for sediment subduction cannot be excluded. The imposition of enrichment events on a refractory source has given the HMA distinctive combinations of geochemical features and detailed comparisons with other rocks have failed to uncover any with identical features.

Careful analysis of the similarities and differences between the HMA and other high-SiO_2, high MgO liquids demonstrated that while these rocks can be used to define an environment of formation characterized by low pressure (<15 kb) and moderate to high temperatures (1100-1400°C) their origin is not restricted to a particular tectonic setting.

The origin of the HMA may be favoured by an island-arc environment and more accurate dating of events in the Mariana island-arc/back-arc system could be instrumental in determining how the unusual thermal conditions required for their petrogenesis originate. However, it must be stressed that there is no *a priori* reason to equate HMA with an island-arc setting.

Whether or not HMA form in an island-arc, comparison of the results of the liquidus studies on HMA and the SMA of Japan with partial melting studies illustrates that there are a number of difficulties to be overcome before an integrated petrogenetic scheme for island-arc lavas is established. Since compositional characteristics of the sub-arc mantle are influenced by a plethora of processes, including mantle metasomatism, a wide range of possibilities exists for determining the P, T, $P_{volatile}$ conditions for olivine ± orthopyroxene ± clinopyroxene saturation in magmas derived from sub-arc mantle.

The results of this study will also be of use in determining the nature of the parental magmas to some ophiolite complexes.

Appendix 1

NEW DATA ON DABI VOLCANICS, PNG.

	LB86	LB51	47800	47802	47798	47813
SiO_2	49.77	56.73	56.35	58.38	65.07	68.93
TiO_2	1.31	1.06	0.83	0.86	0.96	0.34
Al_2O_3	14.42	14.51	14.81	15.89	13.12	9.73
FeO^t*	11.30	11.96	11.38	9.85	8.18	7.28
MnO	0.19	0.23	0.21	0.12	0.11	0.10
MgO	8.15	5.84	5.89	3.38	2.73	4.80
CaO	12.04	4.98	5.55	8.71	6.98	4.94
Na_2O	2.55	2.42	2.91	2.60	2.57	1.47
K_2O	0.15	2.18	1.93	0.14	0.21	2.25
P_2O_5	0.10	0.08	0.13	0.08	0.08	0.16
Ba	100	28	81	34	43	47
Sr	149	94	88	13	97	81
Rb	1	9	11	2	3	4
Zr	61	53	39	37	43	60
Nb	4	3.4	2	1.5	-	1
Y	27	20	21	37	25	10
Cr	262	13	25	31	47	
V	332	4	431	458	419	135
Sc	39	44	45	47	36	29
Ni	98	23	24	23	23	

* total Fe as FeO - recalculated volatile free.

Appendix 2

DATA ON TERTIARY SHIKOKU VOLCANICS, JAPAN.

Rocks described in this section are from the Tertiary Shikoku volcanics of southwest Japan. Descriptions of these volcanics can be found in Ujike (1972). Dr H. Sato kindly supplied the samples of these volcanics.

REE analyses (Table A2.1) were done using the XRF ion-exchange procedure described in Appendix 3. Microprobe analyses were performed using the operating conditions and equipment described in Chapters 2 and 5.

The pyroxene analyses from these volcanics provide an interesting comparison with those of the HMA. Both groups of rocks are characterized by low CaO/Al_2O_3 ratios and high Mg-numbers, however as noted in Chapter 6 the Shikoku rocks are much richer in Na_2O, K_2O, TiO_2, etc.

Ca enrichment patterns in the orthopyroxenes are variable from rock to rock (see Figures A2.1-4). The pattern observed in 705B (Fig. A2.1) appears similar in nature to that seen in the HMA, however in detail there are major differences. For example, the Ca enrichment continues to occur past the incoming of clinopyroxene (~Mg_{86} in this sample). There is some Ca enrichment in the orthopyroxenes from 1309 and 609 (Figures A2.3 and A2.4 respectively), this trend levels off at ~Mg_{84} in 1309 but is not correlatable with the incoming of clinopyroxene.

Unlike the HMA there are some examples of marked zoning in the orthopyroxenes. It is not unusual to find Mg_{83} cores rimmed by Mg_{89-91} rims (see Table A2.2). Sato (1981) has postulated that this reflects magma mixing between high-Mg liquids and a more siliceous less-magnesian melt (?dacite).

Sample 609 (Figure A2.3) is characterized by orthopyroxenes of Mg-numbers up to ~Mg_{92}. These have CaO ~0.89% and Al_2O_3 of ~1-2%.

Olivine coexists with orthopyroxene over a wide compositional range in 705B, with Mg-numbers of 75 found in the olivines. Plagioclase

in these rocks is, as expected, less An-rich than that of the HMA.

The absence of clinoenstatite in these rocks may be attributed to a number of factors. Possibilities include: (i) crystallization within the orthoenstatite field; (ii) increased Na_2O and K_2O in the melts is linked to Al_2O_3 and effectively causes a much higher CaO/Al_2O_3 ratio, prohibiting clinoenstatite crystallization; and (iii) the compositions may reflect the PE/OE miscibility gap.

Table A2.1

PRELIMINARY DATA ON TERTIARY VOLCANICS FROM SHIKOKU, JAPAN.

	1	2	3	4	5	6	7
	7201705B	72010609	69032915	74122702	72010613	72010707	69072533
SiO_2	56.75	62.62	64.07	65.64	67.33	72.68	59.57
TiO_2	0.69	0.42	0.56	0.47	0.40	0.12	0.66
Al_2O_3	15.25	17.37	17.89	17.82	17.60	16.01	17.08
FeO*	6.10	4.14	3.85	3.50	2.10	1.61	5.43
MnO	0.12	0.10	0.12	0.09	0.08	0.03	0.11
MgO	9.16	4.01	2.35	1.61	0.08	0.25	4.85
CaO	7.00	4.92	4.43	3.83	4.04	2.16	6.31
Na_2O	3.16	3.94	4.01	4.18	4.26	4.24	3.63
K_2O	1.69	1.59	2.74	2.90	2.23	2.73	1.23
P_2O_5		0.08	0.03	0.16			0.10
Mg no.	72.8	63.3	52.1	45.0		21.7	61.4
La**	9.57	9.24	14.69	14.7	12.05		
Ce	21.5	20.7	33.0	34.3	27.7		
Nd	10.32	9.78	12.9	13.5	12.5		
Sm	2.03	2.03	2.84	2.23	2.33		
Eu	0.66	0.78	0.31	0.31	0.78		
Gd	2.24	1.52	2.61	1.82	1.82		
Dy	1.50	1.74	1.95	1.80	1.27		
Er	0.96	0.90	-	0.86	0.67		
$(La/Sm)_N$	2.6	2.4	2.8	3.6	2.8		
$(La/Er)_N$	6.0	6.0	-	10.5	10.9		

	8	9
	70041309	76011601
La	9.9	7.92
Ce	22.7	18.0
Nd	10.2	9.3
Sm	1.9	2.0
Eu	0.50	2.45
Gd	1.89	2.27
Dy	1.86	2.36
Er	0.72	1.16
$(La/Sm)_N$	2.8	2.2
$(La/Er)_N$	8.3	4.3

1. augite-bronzite-olivine andesite (Goshikidai-Kamiya)
2. olivine-enstatite-andesite (Goshikidai-Negoro-ji)
3. bronzite-olivine sanukite (Goshikidai-quarry)
4. bronzite-olivine-hornblende sanukite (Goshikidai - Shiramine)
5. hornblende dacite (Goshikidae-Shirgen-ike)
6. garnet-biotite rhyolite (Goshikidai-Kamiya)
7. augite bronzite andesite (Yashima)
8. olivine-augite-bronzite andesite (Goshikidai-Eboshi-ima)
9. augite-olivine basalt (high alumina basalt) (Marugame Castle).

* total Fe as FeO, analyses recalculated anhydrous.

** REE - by XRF ion exchange prodecure described in Appendix 3.

Major element analyses from Ujike (1972) and Sato pers. comm., 1978).

Table A2.2

SELECTED MINERAL ANALYSES

70210705B*

	opx	opx	oliv	oliv	cpx	plag.(5)
SiO_2	55.68	54.70	40.73	37.84	52.30	An_{34}-An_{66}
Al_2O_3	2.61	1.10		0.38	4.53	
FeO	6.54	12.04	10.30	22.94	5.09	
MgO	33.03	29.33	48.95	38.39	17.13	
CaO	1.19	2.01			20.39	
Cr_2O_3	0.96				0.56	
Si	1.93	1.949	0.999	0.988	1.902	
Al	0.106	0.045		0.011	0.194	
Fe	0.189	0.358	0.211	0.506	0.154	
Mg	1.706	1.558	1.789	1.494	1.928	
Ca	0.044	0.076			0.794	
Cr	0.026				0.015	
Total	4.004	3.991	3.000	3.005	3.992	
Mg no.	90.0	81.3	89.4	74.9	85.7	

72010609 (orthopyroxenes)

	A8rim	A8core	A5core	A5rim	AS2core	plag.(17)
SiO	56.62	56.35	54.49	55.65	51.88	An_{32}-An_{63}
Al O	1.93	1.64	3.29	1.63	2.00	
FeO	5.66	7.13	9.02	5.92	20.92	
MgO	34.26	33.54	31.17	34.29	22.77	
CaO	0.83	0.99	1.27	0.90	1.33	
Cr O	0.77	0.34	0.76	0.63	(1.10)	
Si	1.95	1.953	1.91	1.953	1.927	
Al	0.078	0.067	0.135	0.066	0.087	
Fe	0.161	0.206	0.264	0.170	0.650	
Mg	1.758	1.733	1.629	1.763	0.261	
Ca	0.030	0.036	0.047	0.066	0.052	
Cr	0.021	0.009	0.021	0.017	(0.032)	
Total	4.000	4.008	4.010	4.004	4.013	
Mg no.	91.6	89.4	86.0	91.2	66.0	

( ) - other components (MnO and/or TiO_2) excludes Cr_2O_3
* - core analyses

Table A2.2 cont.

70041309 (orthopyroxenes)

	B1core	B2core	D1core	C1core	C1rim	plag.(1)
SiO_2	53.86	57.33	55.38	54.57	56.47	An_{53}
Al_2O_3	3.14	0.87	2.02	3.48	1.68	
FeO	13.34	6.16	8.79	10.59	6.96	
MgO	28.50	34.36	31.47	30.33	33.30	
CaO	0.84	0.97	1.67	0.63	0.94	
Cr_2O_3	(0.32)	0.32	(0.67)	0.42	0.64	
Si	1.922	1.977	1.942	1.920	1.956	
Al	0.131	0.035	0.083	0.144	0.068	
Fe	0.398	0.177	0.257	0.311	0.201	
Mg	1.516	1.766	1.645	1.590	1.719	
Ca	0.032	0.035	0.062	0.023	0.034	
Cr	(0.009)	0.008	(0.018)	0.011	0.017	
Total	4.012	4.001	4.011	4.002	4.000	
Mg no.	79.2	90.9	86.5	83.6	89.5	

69032915

	oliv B5core	oliv B5rim	opx A2core	opx D core	opx E2core	opx E2rim	plag.(6)
SiO_2	40.97	40.43	56.20	55.17	54.57	54.91	An_{36}-An_{56}
Al_2O_3			1.93	2.59	2.51	1.74	
FeO	11.06	11.31	6.82	8.09	12.43	11.91	
MgO	47.71	48.25	33.03	31.80	29.22	29.86	
CaO			1.26	1.41	0.94	0.99	
Cr_2O_3			0.77	0.96	(0.31)	(0.63)	
Si	1.008	0.996	1.948	1.927	1.939	1.949	
Al			0.078	0.106	0.105	0.072	
Fe	0.227	0.233	0.197	0.236	0.369	0.353	
Ca			0.046	0.052	0.035	0.037	
Cr			0.021	0.026	(0.009)	(0.018)	
Total	2.986	3.003	4.001	4.001	4.007	4.009	
Mg no.	88.5	88.4	89.6	87.5	80.7	81.7	

( ) - other components (MnO and/or TiO_2) excludes Cr_2O_3.

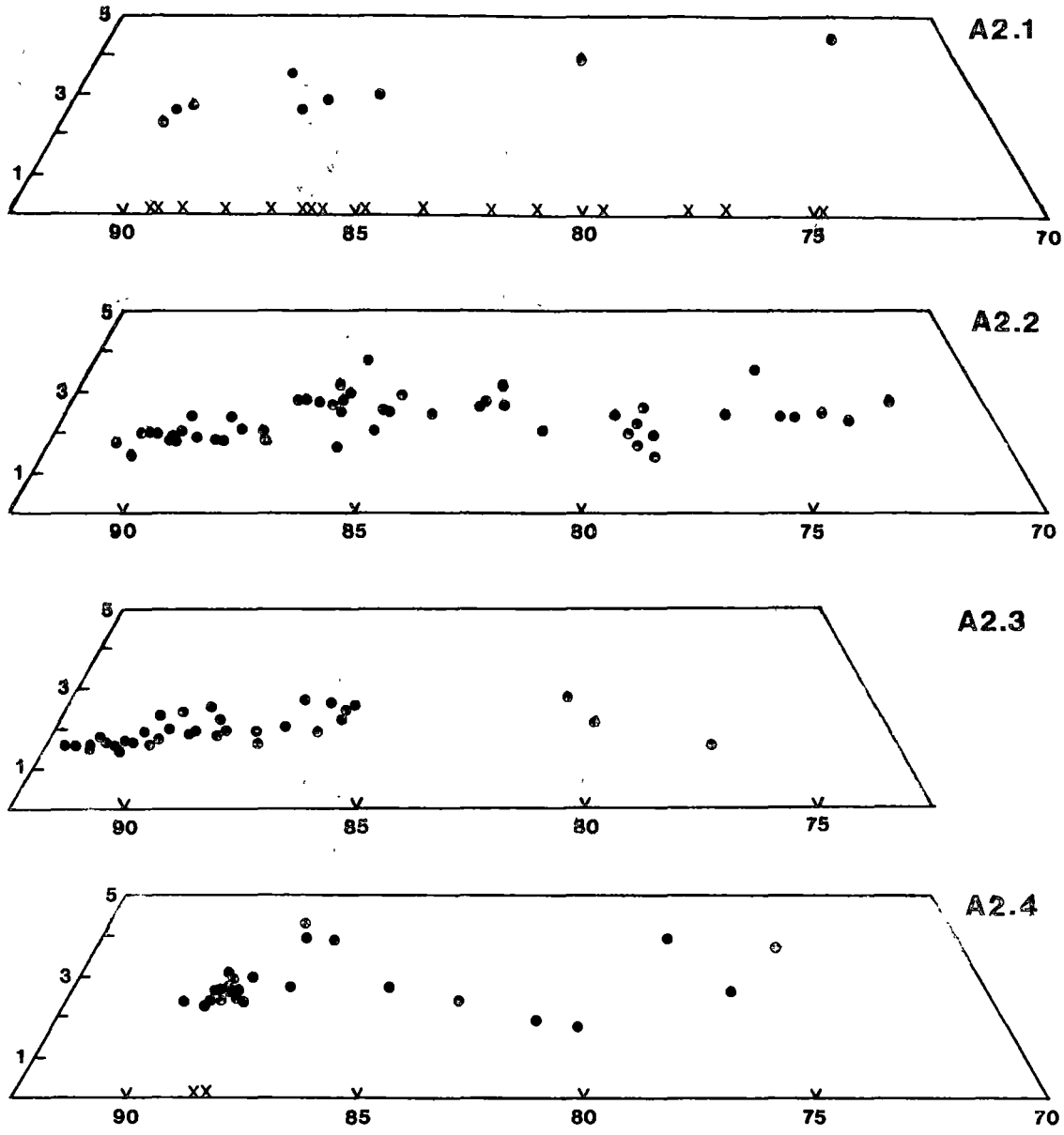

Figures A2.1-4 Compositional variation in orthopyroxenes (dots) and olivines (crosses) in SMA from the Shikoku area. 1 = 72010705B, 2 = 70041309 3 = 72010609, 4 = 69032915 (see Table A2.1).

Appendix 3

DESCRIPTION OF ION EXCHANGE (IE-XRF) THIN FILM - X-RAY FLUORESCENCE REE TECHNIQUE.

N. Higgins, G.A. Jenner and P. Robinson, Geology Department, University of Tasmania.

1. INTRODUCTION

Geochemical studies on the origins of sedimentary rocks (Jenner *et al.*, 1981; Fryer, 1977; Nance & Taylor, 1976), volcanics (Fryer & Jenner, 1978), and economic deposits (Graf, 1977; Higgins, 1980; Kerrich & Fryer, 1979; McLennan & Taylor, 1979; Taylor & Fryer, 1980, 1980b) have become popular and more sophisticated over the last decade. In particular the use of the rare earth elements (REE) in delineating the geologic processes occurring has been notable.

At present the most commonly used techniques for determining REE are neutron activation (radiochemical and instrumental), isotope dilution and spark source mass spectrography. RNAA and isotope dilution require extensive chemical separation procedures, INAA and SMSS are predominantly instrumental techniques. All of these techniques are time consuming, require expensive and sophisticated equipment and use small sample sizes (100-200 mg).

Eby (1972) and Fryer (1977) have advocated the use of ion exchange X-ray fluorescence for determination of REE, which while sacrificing some sensitivity and precision has the advantages of being rapid, relatively cheap, and requires much less sophisticated or expensive equipment. The ease of duplicating analyses, in combination with use of 1-3 gram samples, in the XRF technique considerably lessens the probability of obtaining an unrepresentative analysis compared to other techniques where small sample size and restrictions on the number of samples which can be processed are limitations.

In this paper we outline the ion-exchange X-ray fluorescence procedure for determining REE that we have developed at the Geology Department of the University of Tasmania. Comparison of results on standard rocks analysed by our IE-XRF technique, SMSS and INAA indicate that given sufficient care the IE-XRF technique is a valuable geochemical tool.

2. EXPERIMENTAL

2.1 Apparatus

The X-ray fluorescence spectrometer used in this study was a Phillips PW1410 manual X-ray spectrometer, which has been automated using a TRS-80 microcomputer system. A four sample chamber is used. The sample holders have a 28 mm opening and Al masks are used on both sides of the ion-exchange paper. A Mylar insert is also used to back the ion- exchange paper. Operating conditions used are (1) 50 kV/50 mA; (2) LiF_{200} crystal; (3) fine collimator; (4) gas flow scintillation counter; (5) PHD window voltage - 2 v; (6) Au tube; (7) vacuum; and (8) 40 seconds/element/side counting time (see also Table A3.1).

Pyrex ion-exchange columns were used. The columns are 14 mm wide (O.D.), 30 cm high and stopped by a teflon tap assembly and 2-3 cm of glass wool. Resin height in the columns is 18 cm. Pyrex glassware and teflon beakers were used throughout the procedure.

Parr teflon-lined acid digestion bombs have been used in instances where a significant heavy (or resistant) mineral portion was present. The bomb size is 23 ml.

2.2 Reagents and Standards

Commercial ACS reagent grade hydrofluoric, sulphuric and nitric acids were used. A sub-boiling still constructed from Pyrex glass and heated externally (2 x 750 W heat lamps) was used to distill the hydrochloric acid. Water is distilled only.

Table A3.1

STANDARD INTENSITIES FOR THE ANALYTICAL LINES

Line	2θ, °	Background (c/s)	Counts/sec/μg above background	Detection limit (3σ, μg)
$BaL\alpha_1$	87.15	32.84	9.98	0.4
$LaL\alpha_1$	82.90	42.50	9.39	0.5
B1	81.00	58.99	-	-
$CeL\alpha_1$	78.99	64.43	11.05	0.5
$PrL\alpha_1$	75.40	62.53	13.99	0.4
$NdL\alpha_1$	72.11	78.77	18.56	0.3
$CrL\alpha_1$	69.34	268.61	69.90	0.2
$SmL\alpha_1$	66.22	123.98	27.46	0.3
$EuL\alpha_1$	63.57	143.57	37.11	0.2
$MnL\alpha_1$	62.95	220.31	97.84	0.1
B2	62.20	171.36	-	-
$GdL\alpha_1$	61.09	165.67	39.54	0.2
$TbL\alpha_1$	58.77	229.05	45.20	0.2
$FeL\alpha_1$	57.52	2774.57	127.83	0.3
$DyL\alpha_1$	56.59	253.35	47.91	0.2
B3	55.30	261.38	-	-
$HoL\alpha_1$	54.54	280.93	59.09	0.2
$ErL\alpha_1$	52.61	322.00	65.19	0.2
$TmL\alpha_1$	50.79	344.05	71.61	-
$YbL\alpha_1$	44.05	449.06	78.37	0.2
B4	48.00	412.86	-	-
$LuL\alpha_1$	47.41	429.82	92.97	0.2
$NiK\beta_1$	43.73	907.10	35.03	0.6
$YL\alpha_1$	23.78	1511.33	49.27	0.5

Bio-Rad AG50W-X8, 100-200 mesh hydrogen form cation exchange resin was used in the ion-exchange columns. Reeve Angel SA-2 ion ion-exchange paper was used as the ion collector and support for the X-ray portion of the procedure. The ion-exchange resin used in this paper in Amberlite IR-120 (Eby, 1972).

REE standards were prepared from high purity (4.9s or 5.9s) oxides of the rare earths supplied by Spec-Pure Chemicals. Other standards were prepared from (>99.99%) oxides or metals.

The yield correction procedure used is that of Fryer (1977). 50 µg of Tm (in 2N HCl) are pipetted onto each sample and onto standard papers. Count rates on Tm papers (with 50 µg of Tm) are compared to those found for Tm in the samples and allowing for sample weight and interference corrections the yield is calculated. Tm was chosen for the yield correction because of its low abundance and while it is a satisfactory element for this purpose, care must be taken to ensure that LREE fractionation does not occur during the ion-exchange procedure.

2.3 Procedure

1. ~1.0 g aliquots of finely powdered sample is weighed accurately into 100 ml teflon beakers.
2. 50 µg of Tm solution is pipetted accurately into each beaker. We use an Oxford antomatic pipetter taking care to discard the drop left on the pipette during the uplift motion of the dispenser.
3. Add 25 ml of conc HF and 3 ml of conc $HClO_4$ and evaporate to dampness (just fuming). Do not let sample dry out at this stage.
4. Add 15 ml conc HF and 5 ml of conc $HClO_4$ and evaporate to near dryness (strong, dense $HClO_4$ fumes).
5. Add 5 ml of $HClO_4$ and evaporate to dryness (heat fairly strong).
6. Add 5 ml of 2N HCl and 5 ml of conc $HClO_4$ and evaporate to dryness.
7. Add 10 ml of 6N HCl rinsing sides of beaker with it. Warm to dissolve the residue (solution should consist of soluble chlorides).

8. Slowly evaporate to dryness.
9. After evaporation the sample is redissolved in <1N HCl. Rinse sides of beaker. Cool before proceding to step 10.
10. Filter sample into ion-exchange column using #1 Whatman filter paper (11 cm size) in a glass funnel. Let sample go into the ion-exchange resin, i.e. no solution on top of resin.
11. Wash beaker with 5 ml H_2O and rinse filter with same solution. Let it go into ion-exchange resin.
12. Wash filter with 5 ml H_2O. Let it go into resin.
13. Wash beaker with 5 ml 2N HCl and rinse filter with same solution. Let it go into resin.
14. Rinse filter with 2 ml 2N HCl. Let it go into resin.
15. Remove filter being careful not to touch tip of funnel to the side. Wash column with 5 ml of 2N HCl and let it go into the resin.
16. Repeat wash with 5 ml 2N HCl (a yellow coloured solution of Fe-chloride will probably be coming off the column by this stage).
17. Add 5 ml + 100 ml of 2N HCl. The 5 ml is added using a squeeze bottle taking care not to disturb the resin. The remaining 100 ml is poured on carefully. (Total 2N HCl added to the column = 122 ml.)
18. After the 2N HCl has passed through the column clean column tip and stop cock. Eluted solution can be discarded or saved for AA analysis.
19. Place clean 250 ml pyrex beaker under column and add 5 ml of 6N HCl to equilibrate column (use squeeze bottle). Let it go into resin.
20. Add 5 ml of 6N HCl then an additional 160 ml of 6N HCl (see step 13 for methodology). Eluted solution now contains the REE.
21. Evaporate eluted solution to dryness.
22. Moisten residue with a few drops of 2N HCl and then dilute to 20 ml with distilled H_2O.

23. Add 2 drops of conc H_2SO_4 and warm on hot plate for 10-20 minutes. Do not evaporate to dryness. This step is to remove Ba as $BaSO_4$. If HCl strength increases too much, the Ba will not precipitate.
24. After cooling filter solution into a 50 ml Pyrex beaker using #2 Whatman paper. Rinse beaker and filter with H_2O.
25. Evaporate solution to dryness on hot plate. H_2SO_4 must be completely removed. To ensure this put in oven for 1 hour after bottom of beaker is dry to rid sides of any condensate.
26. Wash sides of beaker with 5-10 ml of 6N HCl and evaporate (converts sulphates to chlorides).
27. Add 15 ml of very dilute HCl (<0.1N). Warm to dissolve the REE chlorides and then cool.
28. Add ion-exchange paper and allow to equilibrate for 24 hours.
29. Evaporate solution slowly under a heat lamp (should take 12-24 hours minimum).
30. Store ion-exchange paper in labelled envelope.
31. Clean resin and columns before re-use by washing with 50 ml of 6N HCl. Then add 5-10 ml of H_2O. Resin should be removed from columns and washed in distilled water after every other run.

2.4 Bomb Dissolution Method

If the sample has a heavy mineral content then it may be necessary to use the bomb. A slightly different dissolution procedure must be used in this method.

1.. Accurately weigh ~1.0 g of finely powdered rock sample into the teflon insert of the bomb.
2. Add spike solution.
3. Add 15 ml conc HF and evaporate to dampness at low temperature (150°C) on a sandbath.
4. Add 15 ml conc HF and 3 ml conc HNO_3 and evaporate to dryness.

5..Add 10 ml HF and 1 ml HNO_3 and seal teflon cup with teflon cap. Pur teflon insert into PTFE bomb abd seal. Place in oven at 140°C for 12 hours.

6. Remove bomb from oven. LET IT COOL.

7. OPEN bomb - COLD! Remove teflon cup and add 5 ml of $HClO_4$ and evaporate to dryness on sandbath.

8. Add 5 ml $HClO_4$ and 5 ml 6N HCl and evaporate to dryness.

9. Add 10 ml 6N HCl and warm to dissolve residue then evaporate slowly to dryness.

10. Take up residue in <15 ml of <1N HCl. Warm to dissolve residue then cool and filter into ion-exchange columns.

2.5 XRF Control

An XRF control program, CONTROL/REE, gives each of four samples a count of 40 seconds over 24 analytical lines. Raw data in stored on a minidisk, the papers turned over and the analysis repeated. The two data files are then used in conjunction with the data reduction program, REE. This program combines the two sides, subtracts background, corrects for interferences and finally makes the yield corrections. The concentration of REE (ppm) and chondrite normalized values are printed out along with Australian shale normalized values, if required. Also on the print-out is the yield (%), weight of sample (g), sum of 10 REE, Eu/Eu* and the residual Ni, Fe, Mn, Cr and Ba left on the paper.

3. RESULTS AND DISCUSSION

3.1 Ion Exchange Procedure

Eluction with 2N HCl on a strong acid cation exchange resin removes all cations except the REE, Y, Ba, Sc, Th and Zr. The major elements Fe, Ti, Mg, Mn, Na and K, and trace elements are removed with or ahead of Al and Ca. The REE Y, Ba and Sc, are readily removed with 6N HCl. Sc comes off first followed by Y, Ba, and the REE starting with Lu and ending with La (Eby, 1972; Strelow & Jackson, 1974).

The columns were calibrated with a mixture of Al, Y, Lu and La. Figure A3.1 shows the elution curve for the solution of 800 µg Al and 70 µg Lu. 20 ml portions were taken and, after evaporation, the residue dissolved in 15 ml of <0.1N HCl. An ion-exchange paper was added to each solution and after the paper was ready Al, Lu, Y and La were analyzed by XRF. The figure shows considerable tailing-off of the Al. 120 ml of 2N HCl was selected as the optimum volume to remove the major and minor rock elements without affecting the REE. The residual Al is less than 50 µg and should not alter the thin film characteristics of the ion-exchange paper, where a maximum of 500 µg elements is allowed. Y closely followed Lu, while La was not eluted in the first 200 ml of 2N HCl. Strelow & Jackson (1974) found that 200-400 mesh resin gave a better separation of Al and Lu then 100-200 mesh resin and we will evaluate the benefits of this resin in the future.

Figure A3.2 shows the elution curve for 100 µg La with 4N and 6N HCl. Strelow & Jackson (1974) used 4N HCl because the distribution coefficient of La, the most strongly adsorbed of the lathanides, does not decrease appreciably in 5N HCl and even increases above 6N HCl. There is an extensive tail on the La elution and 180 ml of 6N HCl or 240 ml of 4N HCl are needed to ensure total recovery of La. As the element must be evaporated to dryness for subsequent transfer to ion-exchange papers, the use of 6N HCl results in a significant time saving.

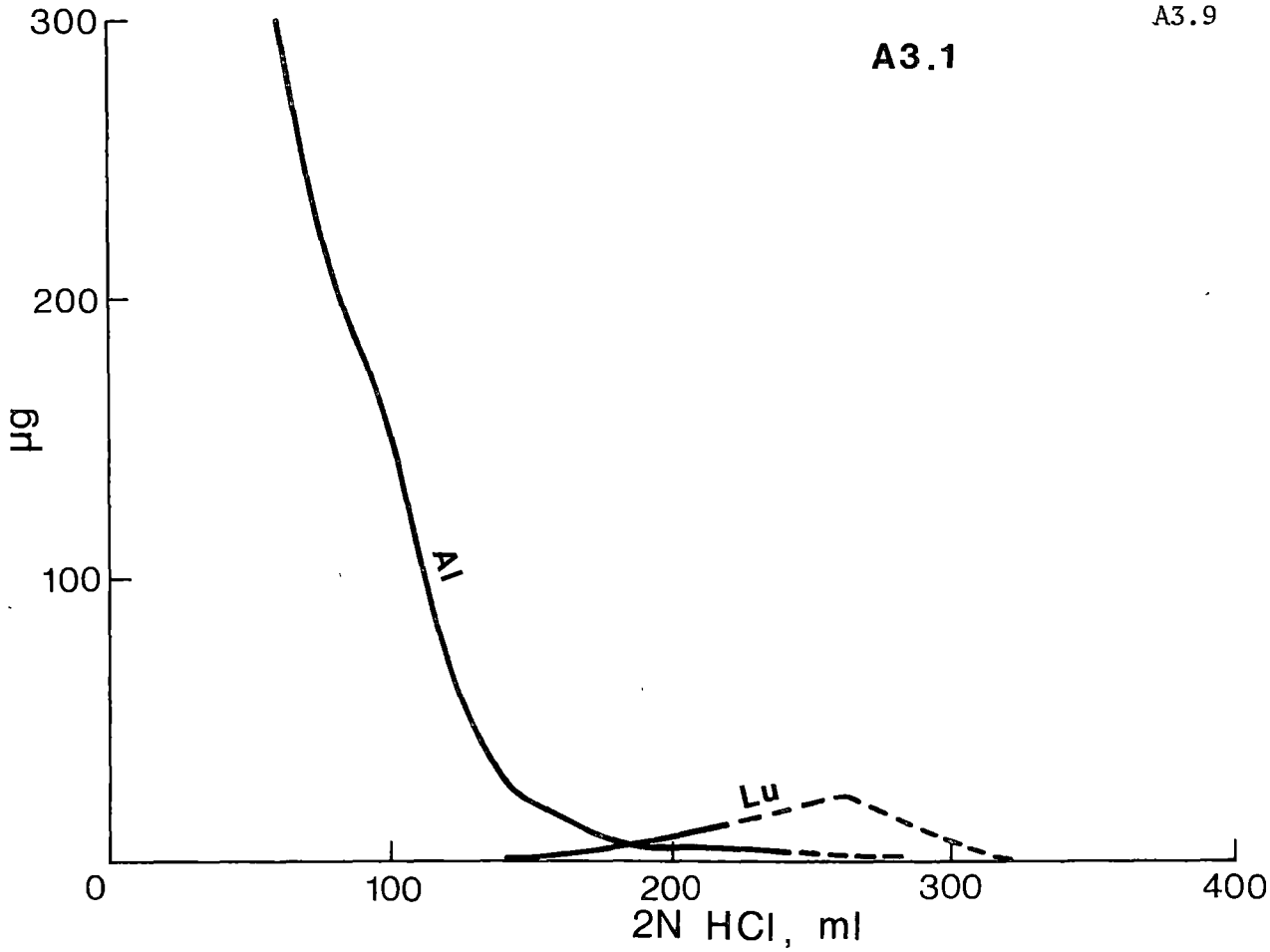

Figure A3.1 Separation of aluminium and lutetium. AG50W-X8 ion exchange resin (100-200 mesh). Column size. 18 x 1 cm. Flow rate 2 ml/min. Eluent: 2N HCl.

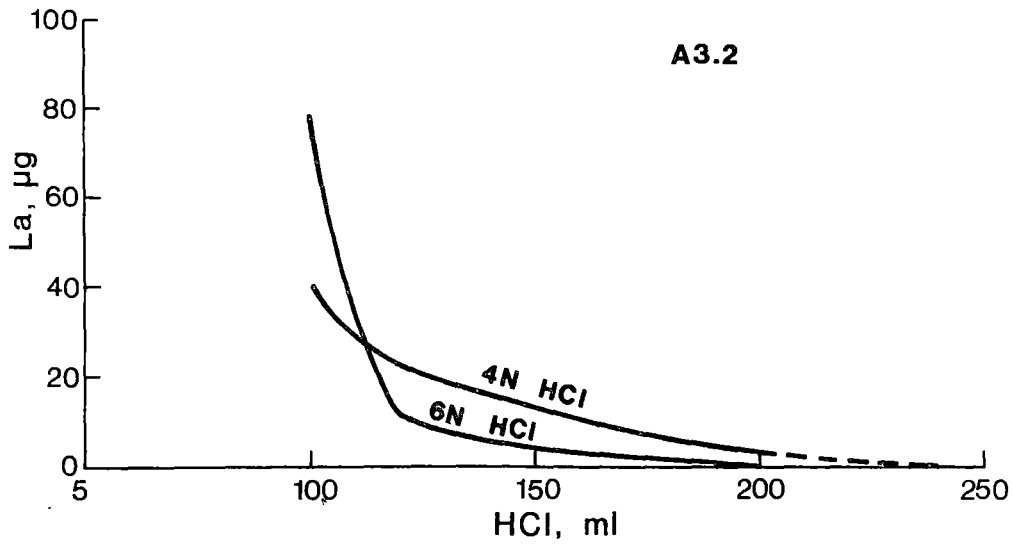

Figure A3 2 Elution of lanthanum. AG50W-X8 ion exchange resin (100-200 mesh). Column size 18 x 1 cm. Flow rate 2 ml/min. Eluents 4N HCl and 6N HCl.

The flow rate through the columns was 2 ml per minute with the tap fully open. Slower flow rates did not improve the separation.

The ion-exchange papers were left to equilibrate for 24 hours before being placed under the heat lamp. The acidity in the REE solution had to be kept below 0.1N HCl otherwise crystals developed on the papers during drying. The combination of 24 hours equilibration and 24 hours drying appears to lead to absorption of all the REE. Tests made using longer equilibration and drying times (up to 5 days) showed no differences from those left for 2 days.

Eby (1972) calculated the X-ray absorption effects for various quantities of REE on the ion-exchange papers and concluded that if the total concentration was less than 500 µg, the absorption effects did not exceed 10%. This theory was tested by comparing the Tm X-ray intensity on 50 µg Tm papers with those containing 50 µg Tm, 600 µg Al, 200 µg Na, 100 µg La, 50 µg Y, and 50 µg Fe (i.e. 1050 µg total elements). The difference in intensity was <5%.

3.2 Calibration

Standard ion-exchange papers were prepared from spec. pure solutions of the rare earth elements, Y, Ba, Cr, Mn, Fe and Ni. For each element the average of 6, 200 µg, papers was used to determine the net count rate (counts/sec/µg) and inter-element correction factors.

The standard papers were counted for 100 seconds/side. Average counts per second were calculated and the background, measured on blank papers, was subtracted.

Although there are many inter-element corrections (Table A3.2) most are small. The correction factors were obtained from the single element papers by measuring the count rates at the analytical lines interfered with. For example: La lines interfere with Bl, Pr, Nd, Sm, Eu, Gd and Tb. The 200 µg La papers were measured at all these lines. The correction factors are worked out as follows -

Table A3.2

INTER-ELEMENT CORRECTION FACTORS: INTERFERING ELEMENTS

	Ba	La	Ce	Pr	Nd	Cr	Sm	Eu	Mn	Gd
Ba										
La					.0071					
Bl		.0034	.0072							
Ce	.2752									
Pr		.4723								
Nd		.0072	.0227							
Cr										
Sm		.0046	.0563	.0073						
Eu		.0054		.227	.0662	.0086			.0125	
Mn										
B2	.0002				.0034	.0864		.0016		.0038
Gd		.0571	.1683		.0218	.0066				
Tb		.0054	.0024				.0163			
Fe										
Dy							.0005	.0653	.1544	
B3				.0239	.0209		.0146	.0104	.0046	.0067
Ho										.7288
Er							.0053	.0034		
Tm							.1575			.0109
Yb							.008	.0117		
B4										.0029
Lu										
Ni										
Y										

	Tb	Fe	Dy	Ho	Er	Tm	Yb	Lu	Ni
Ba									
La									
Bl									
Ce									
Pr									
Nd									
Cr									
Sm									
Eu									
Mn									
B2				.0127					
Gd									
Tb		.0015							
Fe									
Dy		.0016							
B3		.0001	.0018	.008					
Ho								.0057	
Er	.1808	.0018							
Tm	.0079		.0285						
Yb	.0148		.0199	.0057					.1385
B4			.0073	.1000			.0089	.0211	.0267
Lu			.1099	.1280					.0034
Ni									
Y									

e.g. La correction factor on Pr =

$$\frac{\text{background corrected counts on Pr line}}{\text{background corrected counts on La line}}$$

and applied: La correction on Pr = La net counts x correction factor. A computer program, REE/INT, was written to calculate count rates and correction factors.

Ba, Fe, Ni, Cr and Mn are almost entirely removed during the separation procedure, however even small amounts of these elements can interfere with the REE. Accordingly these lines are measured during the analytical procedure and the residual concentration determined and corrections made.

Standard (counts/sec/µg) and background (counts/sec) count rates are stored in the computer program and checks on this count rate indicate very little change over a period of several months. As a regular background check, four positions: B1 (81.00°), B2 (62.20°), B3 (55.30°) and B4 (48.00°) spread through the REE lines, are measured in each sample run. The net count rate at these positions after blank paper, background and interference corrections should be equivalent to <0.2 µg of the REE.

REE contamination in the procedure was checked by processing five 1 gram samples of spec. pure silica. Analysis of the five resulting papers showed there was no detectable contamination.

A number of rocks were analyzed using the pure element calibration described above. Tesults on TASDOL1*, repeated many times, along with BCR1 and SCo-1 were within 20% of SMSS values (Taylor & Gorton, 1977; Taylor & McLennan, 1980; McLennan, pers. comm., 1980). A decision was then made to set up the calibration using standard rocks. The pure element count rates were adjusted to fit the SMSS results on BCR1, SCo-1, along with SMSS results on TASBAS1 and TASGRAN1 (S.R. Taylor, pers. comm., 1981).

---

* TASDOL1, TASBAS1 and TASGRAN1 are University of Tasmania, Geology Department internal standards. Complete analyses are available upon request.

The standard count rates (counts/sec/μg), background count rates (counts/sec) and detection limits (3) are listed in Table A3.1.

Results on two samples, TASDOL1 (analysed five times) and CGD1* (only one analysis) are given in Table A3.3, along with values determined for these rocks by either SMSS or INAA. Results for La, Ce, Nd and Y on XRF pressed powder pill values are also given. Precision and accuracy for the results are generally within ±10%. Chondrite normalized plots for TASDOL1 and CGD1, our results plus expected results, are shown in Figure A3.3, and demonstrate that there is more than adequate agreement between the techniques.

3.3 Maximizing Chemical Yield

Our experience with this technique has shown that it is important to take great care to ensure the maximum yield possible. In particular the three most critical areas in the procedure where yield loss can occur are in the sample dissolution, loading of the sample onto ion-exchange columns, and the barium precipitation.

Sample dissolution Experimentation established that for a 1 gram sample of most rocks approximately 45 ml of concentrated HF and 5-10 ml of concentrated $HClO_4$ were needed to ensure complete digestion. The HF and $HClO_4$ are added in two steps ensuring that fresh strong HF is available for attacking the more resistant minerals, i.e. zircon, apatite, monazite, etc.

An important consideration in the digestion of any granitoid rock (or derived sedimentary rock) is that the majority of REE may reside in accessory phases, which are resistant to acid dissolution. Errors in the REE analysis may occur through inhomogenous distribution of phases

---

* CGD1 is a University of Melbourne, Geology Department, internal standard (granite). REE results were made available by Helen Waldron (pers. comm., 1980).

Table A3.3

PRECISION AND COMPARISON OF RESULTS (ppm) WITH OTHER ANALYTICAL TECHNIQUES

	TASDOL1				CGD1		
	XRF/IE(5x)		SSMS	XRF/pill	XRF/IE(1x)	INAA	XRF/pill
	ppm	sd(%)					
La	35.5	8.5	32.9	31	29.2	35.06	32
Ce	79.5	3.8	79.8	78	73.8	78.78	71
Pr	10.4	5.8	10.3		8.9		
Nd	43.4	4.1	46.4	44	34.1	35.67	30
Sm	9.9	4.0	10.3		7.5	7.32	
Eu	2.6	7.7	2.87		1.2	1.29	
Gd	9.8	4.1	8.37		6.8	6.69	
Tb	1.4	7.1	1.39		1.2	1.18	
Dy	9.5	3.2	8.80		7.4		
Ho	1.9	5.3	1.80		1.3		
Er	5.0	4.0	4.74		4.0		
Yb	4.0	3.8	4.28		3.3	3.91	
Lu	0.6	33.3	0.65		0.5	0.56	
Y	51.0	7.6	60.3	50	39.5		40

XRF/IE	X-ray fluorescence/ion-exchange paper method. TASDOL1 analyzed five times, CGD1 analyzed once.
sd(5)	Standard deviation in percent.
SSMS	Spark source mass spectrometry (S.McLennan, pers. comm., 1980).
XRF/pill	University of Tasmania XRF pressed powder pill method.
INAA	Instrumental neutron activation analysis method, Melbourne University, (H. Waldron, pers. comm., 1980).

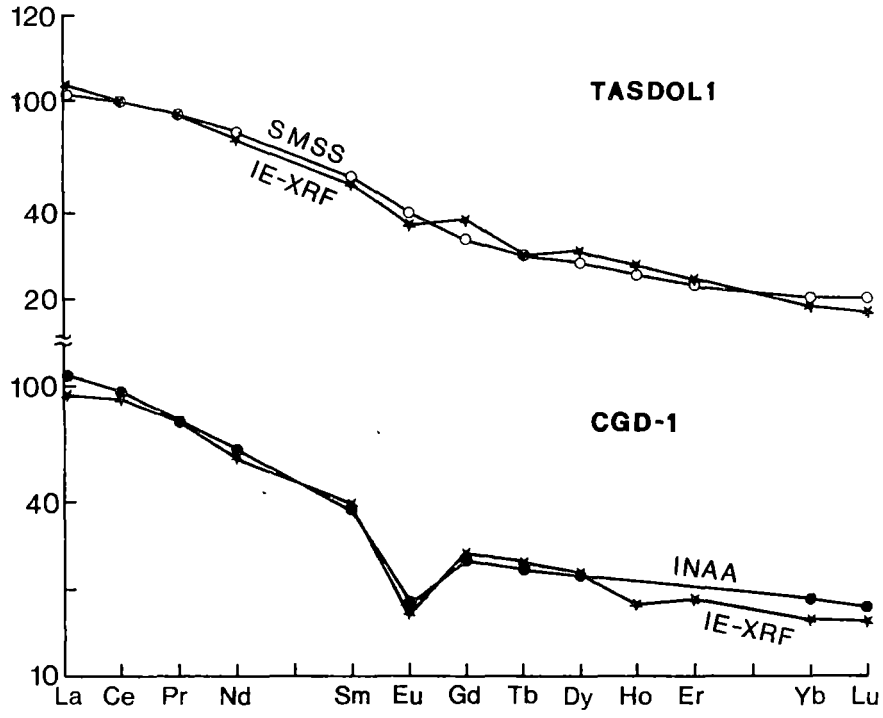

Figure A3 3 Chondrite normalized REE patterns for TASDOL1 and CGD-1. Chondrite values from Taylor & Gorton (1977). IE-XRF = ion exchange-XRF technique. SMSS = spark source mass spectrography (values from Taylor, pers comm., 1981). INAA = instrumental neutron activation (values from Waldron, pers. comm., 1980).

and/or incomplete dissolution. The large sample size (1 gram) of the IE-XRF method reduces the possible error caused by inhomogeneity and is superior in this respect to other techniques. The open beaker dissolution technique is apparently successful in dissolving rocks containing small amounts of resistant minerals, as is indicated by the agreement between the three analytical techniques used in the course of this study (SMSS, INAA, IE-XRF). We have made a preliminary investigation of the use of a bomb dissolution technique (Figure A3.4) which substantiates this view. In the case of samples where high concentrations of resistant minerals are present (e.g. biotite separates containing apatite and zircon inclusions) the bomb technique appears to be more successful in attaining complete dissolution.

Apart from considerations of ensuring digestion of resistant minerals at is also important to obtain a complete dissolution of the sample. If the sample dries out during the sample dissolution before step 5, insoluble fluorides may precipitate (cf. Croudace, 1981). This may cause not only a loss in yield but fractionation of the REE may occur. White precipitates occasionally appear on cooling during step 9, but apparently do not affect the yield or contain any REE (confirmed by XRF analysis).

Ion-exchange columns At the ion-exchange separation stage the final solution must be less than 15 ml of less than 2N HCl. This point is critical and errors will result in REE fractionation, with incomplete recovery of the heavy REE. Loss of yield due to absorption on filter papers, funnels, etc. are minimized by thorough washing with H_2O. While adding H_2O or acid to the ion-exchange columns, it is important to disturb the resin bed as little as possible.

Ba precipitation The greatest potential for yield loss occurs during the Ba precipitation step. Tests indicate that 3-4% loss of all REE occurs at this step. Preferential loss of LREE was recorded from

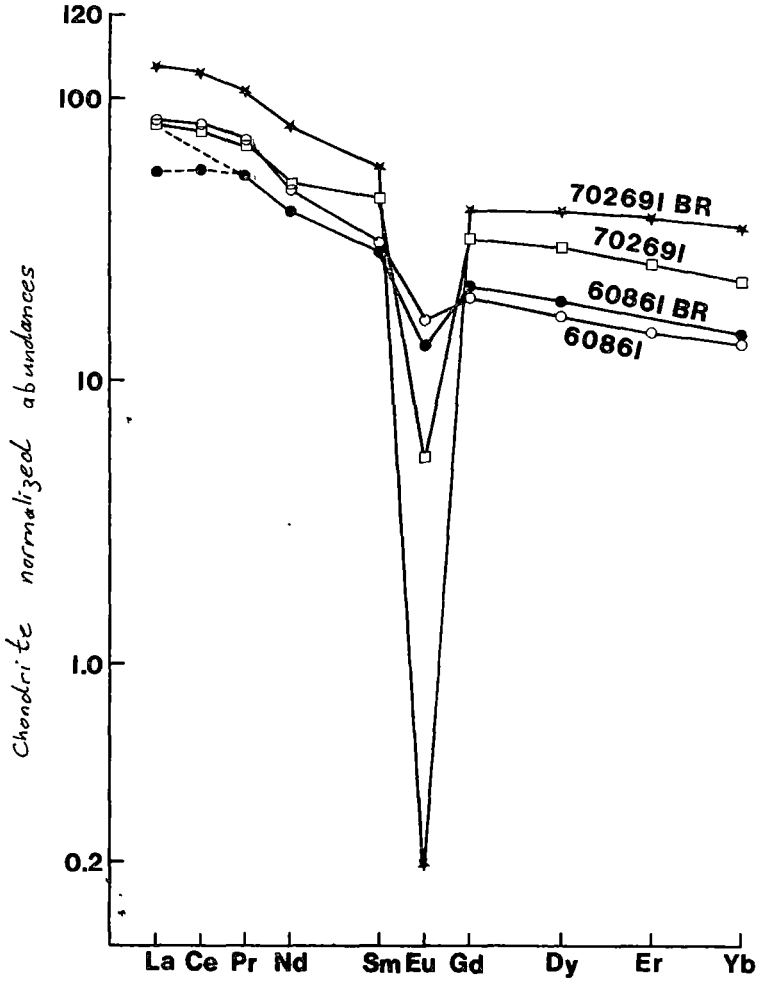

Figure A3.4 Comparison of results for open beaker and bomb digestions on a whole rock and mineral separate.
60861 - whole rock, amph-biotite granodiorite containing apatite and zircon.
702961 - mineral separate, biotite separate containing apatite and zircon inclusions
BR = bomb run.
Chondrite values from Taylor & Gorton (1977).

solutions containing high concentrations of Ba (>500 μg). Eby (1972) noted a correlation between low chemical yields and high Ba contents. A black residue may form after step 25. This appears to be of organic derivation; however, tests showed that it does not contain REE.

Other points For most rocks 1-2 g samples will contain sufficient REE for a good analysis and still not exceed the 500 μg total on the ion-exchange papers. The technique is flexible and larger or smaller sample sizes may be sufficient, depending on their REE content. With large sample sizes it may be difficult to keep large quantities of cations in solution prior to ion exchange. Care must be taken not to exceed the capacity on the resin or ion-exchange paper. Fractionation of LREE and HREE on the columns may occur if too much sample is used. This will not always be easily detected because the yield correction uses Tm which behaves essentially as a HREE. Eby avoided this problem by use of selected radionuclides and this is intrinsically a better method for yield correction, however it may be costly. Careful analysis of the wet chemistry and ion exchange procedures will avoid many of the difficulties.

The resin will lose its exchange capability with time. As a rule of thumb, we suggest no more than 20 analyses per column in the same resin. Repacking of the columns after each run is optional, however it is probably a wise procedure to adopt.

Be careful to replace the glass wool as this will disintegrate with use and the resin may be lost.

4. CONCLUSIONS

The IE-XRF technique is a valuable geochemical technique which is easily applicable to a wide range of rock types, especially those with REE abundances greater than 10-20 x chondrites.

The technique must be treated with a great deal of care, however it is one which is readily taught to students and researchers who have a basic knowledge of chemistry.

The advantages of this techniques are numerous however the following are notable:

1. It is relatively quick and inexpensive;
2. Large numbers of samples can be processed which allows one to do reconnaissance studies on potentially interesting problems; and
3. "Generalist" geology departments can afford to develop the technique without major costs (presuming an XRF is available).

ACKNOWLEDGEMENTS

We are indebted to Dr Brian Fryer of Memorial University of Newfoundland for his demonstration of the technique to N.H. and G.A.J. He has also answered our many questions and at an early stage donated ion-exchange papers which were otherwise scarce.

Ross Taylor was instrumental in providing SMSS analyses of internal standard rocks without which we would have been severely handicapped.

Scott McLennan and Helen Waldron provided REE analyses for comparative purposes.

Professor D.H. Green and Dr M. Solomon funded the purchase of glassware, chemicals, etc. We are also indebted to the Geology Department as a whole, since they provided the funds to automate the XRF.

REFERENCES

Croudace, I.W., 1980: A possible error source in silicate wet chemistry caused by insoluble fluorides. *Chem. Geol. 31*, 153-155.

Eby, G.N., 1972: Determination of rare-earth, yttrium and scandium abundances in rocks and minerals by an ion exchange X-ray fluorescence procedure. *Anal. Chem. 44*, 2137-2143.

Fryer, B.J., 1977: Rare earth evidence in iron-formations for changing Precambrian oxidation states. *Geochim. Cosmochim. Acta 41*, 361-367.

Fryer, B.J., and Jenner, G.A., 1978: Geochemistry and origin of the Archean Prince Albert Group volcanics, western Melville Peninsula, Northwest Territories, Canada. *Geochim. Cosmochim. Acta 42*, 1645-1654.

Graf, J.L., Jr., 1977: REE as hydrothermal tracers during the formation of massive sulphide deposits in volcanic rocks. *Econ. Geol. 72*, 527-548.

Higgins, N.C., 1980: The genesis of the Grey River Tungsten Prospect: a fluid inclusion, geochemical and isotopic study. Ph.D. thesis, Memorial University of Newfoundland. 540pp.

Jenner, G.A., Fryer, B.J., and McLennan, S.M., 1979: Geochemistry of the Archaean Yellowknife Supergroup. *Geochim. Cosmochim. Acta 45*, 1111-1129.

Kerrich, R., and Fryer, B.J., 1979: Archaean precious metal hydrothermal systems, Dome Mine, Abitibi Greenstone belt. Part 2: REE and oxygen isotope studies. *Can. J. Earth Sci. 16*, 440-458.

McLennan, S.M., and Taylor, S.R., 1979: REE mobility associated with uranium mineralization. *Nature 282*, 247-250.

McLennan, S.M., and Taylor, S.R., 1980: Geochemical standards for sedimentary rocks: trace-element data for U.S.G.S. standards SCo-1, MAG-1 and SGR-1. *Chem. Geol. 29*, 333-343.

Nance, W.B., and Taylor, S.R., 1976: REE patterns and crustal evolution - I. Australian post-Archean sedimentary rocks. *Geochim. Cosmochim. Acta 40*, 1539-1551.

Strelow, F.W.E., and Jackson, P.F.S., 1974: Determination of trace and ultra-trace quantities of REE by ion exchange chromatography-mass spectrography. *Anal. Chem. 46*, 1481-1486.

Taylor, R.P., and Fryer, B.J., 1980: Multiple-stage hydrothermal alteration in porphyry copper systems in northern Turkey: the temporal interplay of potassic, propylitic and phyllic fluids. *Can. J. Earth Sci. 17*, 901-926.

Taylor, R.P., and Fryer, B.J., 1980b: Rare earth element geochemistry as an aid to interpreting hydrothermal ore deposits. *In* A. Evans (ed.), vol.4. John Wiley & Sons, Chichester, England.

Taylor, S.R., and Gorton, M.P., 1977: Geochemical application of spark source mass spectrography, III - Element sensitivity, precision and accuracy. *Geochim. Cosmochim. Acta 41*, 1375-1380.

REFERENCES

Allègre, C.J., Bréva t, O., Dupré, B., and Minster, J.F., 1980: Isotopic and chemical effects produced in a continuously differentiating convecting Earth mantle. *Trans. Roy. Soc. Lond. A. 297*, 447-477.

Anderson, R.L., De Long, S.E., and Schwarz, W.M., 1978: Thermal model for subduction with dehydration in the downgoing slab. *J. Geol. 86*, 731-739.

Anderson, R.N., Uyeda, S., and Miyashiro, M., 1976: Geophysical and geochemical constraints at converging plate boundaries, I, Dehydration in the downgoing slab. *Geophys. J. Roy, Astron. Soc. 44*, 333-357.

Anastasiou, P., and Seifert, F., 1972: Solid solubility of Al_2O_3 in enstatite at high temperatures and 1-5 kb water pressure. *Contrib. Mineral. Petrol. 34*, 272-287.

Arculus, R.J., 1976: Geology and geochemistry of the alkali basalt-andesite association of Grenada, Lesser Antilles island arc. *Bull. Geol. Soc. Amer. 87*, 612-624.

Arculus, R.J., 1978: Mineralogy and petrology of Grenada, Lesser Antilles island arc. *Contrib. Mineral. Petrol. 65*, 413-424.

Arth, J.G., 1976: Behaviour of trace elements during magmatic processes - a summary of theoretical models and their application. *J. Res. U.S. Geol. Surv. 4*, 41-47.

Atlas, L., 1952: The polymorphism of $MgSiO_3$ and solid-state equilibria in the system $MgSiO_3$-$CaMgSi_2O_6$. *J. Geology 60*, 125-147.

Beccaluva, L., Macciotta, G., Savelli, C., Serri, G., and Zeda, O., 1980: Geochemistry and K/Ar ages of volcanics dredged in the Philippine Sea (Mariana, Yap and Palau Trenches and Parece Vela Basin). *In* D.E. Hayes (ed.), *The Tectonic and Geologic Evolution of Southeast Asian Seas and Islands*. 247-268. Am. Geophys. Union, Washington, D.C., Monogr. 23.

Berry, R.F., 1981: Petrology of the Hili Manu lherzolite, East Timor. *J. Geol. Soc. Aust. 28*, 453-469.

Biggar, G.M., 1977: Some disadvantages of $Pt_{95}Au_5$ as a container for molten silicates. *Min. Mag. 41*, 555-556.

Bloomer, S., Melchior, J., Poreda, R., and Hawkins, J., 1979: Mariana arc-trench studies: petrology of boninites and evidence for a "boninite series". *EOS 60*, 968 (abstract).

Boettcher, A.L., and O'Neil, J.R., 1980: Stable isotope, chemical and petrographic studies of high-pressure amphiboles and micas: evidence for metasomatism in the mantle source regions of alkali basalts and kimberlites. *Am. J. Sci. 280-A*, 594-621.

Brown, A.V., Rubenach, M.J., and Varne, R., 1980: Geological environment, petrology and tectonic significance of the Tasmanian Cambrian ophiolitic and ultramafic complexes. *In* A. Panayiotou (ed.), *Ophiolites: Proceedings of International Ophiolite Symposium, Cyprus*. 649-659. Min. Agric. Nat. Resour., Nicosia.

Boyd, F.R., and Schairer, J.F., 1964: The system $MgSiO_3$-$CaMgSi_2O_6$. *J. Petrol. 5*, 275-309.

Brown, G.M., Holland, J.G., Sigurdssom, H., Tomblin, J.F., and Arculus, R.J., 1977: Geochemistry of the Lesser Antilles volcanic island arc. *Geochim. Cosmichim. Acta 41*, 785-801.

Bultitude, R.J., Johnson, R.W., and Chappell, B.W., 1978: Andesites of Bagana volcano, Papua New Guinea: chemical stratigraphy, and a reference andesite composition. *BMR J. Aust. Geol. Geophys. 3*, 281-295.

Burnham, C.W., 1967: Hydrothermal fluids at the magmatic stage. *In* H.L. Barnes (ed.), *Geochemistry of Hydrothermal Ore Deposits*. 34-76. Holt, Rinehart & Winston, New York.

Cameron, W.E., 1980: Comments on: Role of multistage melting in the formation of oceanic crust. *Geology 8*, 562.

Cameron, W.E., Nisbet, E.G., and Dietrich, V., 1979: Boninites, komatiites and ophiolitic basalts. *Nature 280*, 550-553.

Cameron, W.E., Nisbet, E.G., and Dietrich, V.J., 1980: Petrographic dissimilarites between ophiolitic and ocean-floor basalts. *In* A. Panayiotou (ed.), *Ophiolites: Proceedings of International Ophiolite Symposium, Cyprus*. 182-192. Min. Agric. Nat. Resour. Nicosia.

Carlson, R.W., Macdougall, J.D., and Lugmair, G.W., 1978: Differential Sm/Nd evolution in oceanic basalts. *Geophys. Res. Lett. 5*, 229-232.

Carmichael, I.S.E., 1979: Glass and the glassy rocks. *In* H.S. Yoder, Jr. (ed.), *The Evolution of the Igneous Rocks*. 233-244. Princeton University Press, Princeton, New Jersey.

Cawthorn, R.G., Biggar, G.M., Graham, C.M., Graham, G., Ford, C.E., Sharpe, M.R., and Davies, G., 1981: Experimental petrological data on the parental magmas to the Bushveld complex. *Contrib. Mineral. Petrol.* (submitted).

Clague, D.A., and Frey, F.A., 1981: Petrology and trace element geochemistry of the Honolulu volcanic series, Oahu: implications for the oceanic mantle below Hawaii. *J. Petrol.* (submitted).

Coish, R.A., 1977: Ocean floor metamorphism in the Betts Cove ophiolite, Newfoundland. *Contrib. Mineral. Petrol. 60*, 255-270.

Coish, R.A., and Church, W.R., 1979: Igneous geochemistry of mafic rocks in the Betts Cove ophiolite, Newfoundland. *Contrib. Mineral. Petrol. 70*, 29-39.

Cox, K.G., 1978: Komatiites and other high-magnesia lavas: some problems. *Phil. Trans. R. Soc. Lond. A 288*, 599-609.

Crawford, A.J., 1980: A clinoenstatite-bearing cumulate olivine pyroxenite from Howqua, Victoria. *Contrib. Mineral. Petrol. 75*, 353-367.

Crawford, A.J., Beccaluva, L., and Serri, G., 1981: Tectono-magmatic evolution of the West Philippine-Mariana Region and the origin of boninites. *Earth Planet. Sci. Lett. 54*, 346-356.

Dallwitz, W.B., 1968: Chemical composition and genesis of clinoenstatite-bearing volcanic rocks from Cape Vogel, Papua: a discussion. *23rd Int. Geol. Congr. 2*, 229-242.

Dallwitz, W.B., Green, D.H., and Thompson, J.E., 1966: Clinoenstatite in a volcanic rock from Cape Vogel area, Papua. *J. Petrol. 7*, 375-403.

Davies, G., Cawthorn, R.G., Barton, J.M., and Morton, M., 1980: Parental magma to the Bushveld Complex. *Nature 287*, 33-35.

Delaney, J.M., and Helgeson, H.C., 1978: Calculations of the thermodynamic consequences of dehydration in subducting oceanic crust to 100 kbar and >800°C. *Am. J. Sci. 278*, 638-686.

De Paolo, D.J., 1980: Crustal growth and mantle evolution: inferences from models of element transport and Nd and Sr isotopes. *Geochim. Cosmochim. Acta 44*, 1185-1196.

De Paolo, D.J., 1981: Nd isotopic studies: some new perspectives on Earth structure and evolution. *Trans. Am. Geophys. Union (EOS) 62*, 137-140.

De Paolo, D.J., and Johnson, R.W., 1979: Magma genesis in the New Britain island-arc: constraints from Nd and Sr isotopes and trace element patterns. *Contrib. Mineral. Petrol. 70*, 367-379.

De Paolo, D.J., and Wasserburg, G.J., 1976: Nd isotopic variations and petrogenetic models. *Geophys. Res. Lett. 3*, 249-252.

De Paolo, D.J., and Wasserburg, G.J., 1977: The sources of island arcs as indicated by Nd and Sr isotopic studies. *Geophys. Res, Lett. 4*, 465-468.

Dietrich, V., Emmerman, R., Obechanski, R., and Puchlet, H., 1978: Geochemistry of basaltic and gabbroic rocks from the West Mariana basin and the Mariana Trench. *Earth Planet. Sci. Lett. 39*, 127-144.

Duncan, R.A., and Green, D.H., 1980: Role of multistage melting in the formation of oceanic crust. *Geology 8*, 22-26.

Duncan, R.A., and Green, D.H., 1980b: Reply to comments on role of multistage melting in the formation of oceanic crust. *Geology 8*, 562-563.

Dupré, B., and Allègre, C.J., 1980: Pb-Sr-Nd isotopic correlation and chemistry of the North Atlantic mantle. *Nature 286*, 17-22.

Ewart, A., 1976: Mineralogy and chemistry of modern orogenic lavas - some statistics and complications. *Earth Planet. Sci. Lett. 31*, 417-432.

Ewart, A., Brothers, R.N., and Mateen, A., 1977: Mineralogical and chemical evolution of the Tonga-Kermadec-New Zealand island arc. *J. Volcanol. Geotherm. Res. 2*, 205-250.

Foden, J.D., and Varne, R., 1980: The petrology and tectonic setting of Quaternary-Recent volcanic centres of Lombok and Sumbawa, Sunda arc. *Chem. Geol. 30*, 201-226.

Ford, C.E., 1978: Pt-Fe alloy sample containers for melting experiments on Fe-bearing rocks, minerals and related systems. *Min. Mag. 42*, 271-275.

Frey, F.A., and Green, D.H., 1974: The mineralogy, geochemistry and origin of lherzolite inclusions in Victorian basanites. *Geochim. Cosmochim. Acta 38*, 1023-1059.

Frey, F.A., Bryan, W.B., and Thompson, G., 1974: Atlantic Ocean floor: geochemistry of basalts from Legs 2 and 3 of the DSDP. *J. Geophys. Res. 79*, 5507-5527.

Frey, F.A., Green, D.H., and Roy, S.D., 1978: Integrated models of basalt petrogenesis: a study of quartz tholeiites to olivine melilitites from south eastern Australia utilizing geochemical and experimental petrological data. *J. Petrol. 19*, 463-513.

Fyfe, W.S., and McBirney, A.R., 1975: Subduction and the structure of andesitic volcanic belts. *Am. J. Sci. 275-A*, 285-297.

Gast, P.W., 1968: Trace element fractionation and the origin of tholeiitic and alkaline magma types. *Geochim. Cosmochim. Acta 32*, 1057-1086.

Gill, J.B., 1970: Geochemistry of Viti Levu, Fiji, and its evolution as an island arc. *Contrib. Mineral. Petrol. 27*, 179-203.

Gill, J.B., 1976: Composition and age of Lau Basin and Ridge volcanic rocks: implications for evolution of an interarc basin and remnant arc. *Bull. Geol. Soc. Amer. 87*, 1384-1395.

Gill, J.B., 1981: *Orogenic Andesites and Plate Tectonics*. Springer-Verlag, Berlin, Heidelberg, New York. 390pp.

Gill, R.C.O., 1979: Comparative petrogenesis of some Archean and modern low-K tholeiites: a critical review of some geochemical aspects. *Phys. Chem. Earth 11*, 431-447.

Green, D.H., 1970: The origin of basaltic and nephelenitic magmas. *Trans. Leicester Lit. Phil. Soc. 64*, 26-54.

Green, D.H., 1971: Composition of basaltic magmas as indicators of conditions of origin: application to oceanic volcanism. *Phil. Trans. Roy. Soc. Lond. A 268*, 707-725.

Green, D.H., 1973: Experimental melting studies on a model upper mantle composition at high pressure under water saturated and water under-saturated conditions. *Earth Planet. Sci. Lett. 19*, 37-53.

Green, D.H., 1973b: Contrasted melting relations in a pyrolite upper mantle under mid-oceanic ridge, stable crust and island arc environments. *Tectonophysics 17*, 285-297.

Green, D.H., 1976: Experimental testing of "equilibrium" partial melting of peridotite under water-saturated, high pressure conditions. *Can. Mineral. 14*, 225-268.

Green, D.H., 1981: Petrogenesis of Archaran ultramafic magmas and implications for Archaean tectonics. *In* A. Kroner (ed.), *Precambrian Plate Tectonics*. 469-489. Elsevier, Amsterdam.

Green, D.H., and Ringwood, A.E., 1967: The genesis of basaltic magmas. *Contrib. Mineral. Petrol. 15*, 103-190.

Green, D.H., Hibberson, W.O., and Jaques, A.L., 1979: Petrogenesis of mid-ocean ridge basalts. *In* M.W. McElhinny (ed.), *The Earth: Its Origin, Structure and Evolution*. 283-297. Academic Press, London.

Green, T.H., 1980: Island arc and continent-building magmatism - a review of petrogenetic models based on experimental petrology and geochemistry. *Tectonophysics 63*, 367-385.

Griffin, B.J., 1979: Energy dispersive analysis system calibration and operation with TAS-SUEDS, an advanced interactive data reduction package. *Univ. of Tasmania, Dept of Geology Publ. 343*.

Hart, S.R., 1969: K, Rb, Cs contents and K/Rb, K/Cs ratios of fresh and altered submarine basalts. *Earth Planet. Sci. Lett. 6*, 295-303.

Hart, S.R., 1971: K, Rb, Cs, Sr and Ba contents and Sr isotope ratios of ocean floor basalts. *Phil. Trans. Roy. Soc. Lond. A269*, 573-587.

Hart, S.R., and Davis, K.E., 1978: Nickel partitioning between olivine and silicate melt. *Earth Planet. Sci. Lett. 40*, 203-219.

Hart, S.R., Erlank, A.J., and Kable, E.J.D., 1974: Sea floor basalt alteration: some chemical and isotopic effects. *Contrib. Mineral. Petrol. 44*, 219-230.

Haskin, L.A., Haskin, M.A., Frey, F.A., and Waldeman, T.R., 1968: Relative and absolute terrestrial abundances of the rare earths. *In* L.H. Ahrens (ed.), *Origin and Distribution of the Elements*. 889-912. Pergamon Press, New York.

Hawkesworth, C.J., 1979: $^{143}Nd/^{144}Nd$, $^{87}Sr/^{86}Sr$ and trace element characteristics of magmas along destructive plate margins. *In* M.P. Atherton and J. Tarney (eds), *Origin of Granite Batholiths*. 76-89. Shiva, Cheshire.

Hawkesworth, C.J., O'Nions, R.K., Pankhurst, R.J., Hamilton, R.J., and Evensen, N.M., 1977: A geochemical study of island-arc and back-arc tholeiites from the Scotia Sea. *Earth Planet. Sci. Lett. 36*, 253-262.

Hawkesworth, C.J., O'Nions, R.K., and Arculus, R.J., 1979: Nd and Sr isotope geochemistry of island arc volcanics, Grenada, Lesser Antilles. *Earth Planet. Sci. Lett. 45*, 237-248.

Hawkesworth, C.J., and Powell, M., 1980: Magma genesis on the Lesser Antilles island arc. *Earth Planet. Sci. Lett. 51*, 297-308.

Hawkins, J.W., Bloomer, S., Evans, C., and Melchior, J., 1979: Mariana arc-trench system: petrology of the inner trench wall. *EOS 60*, 968.

Hellman, P.L., Smith, R.E., and Henderson, P., 1979: The mobility of the rare earth elements: evidence and implications from selected terrains affected by burial metamorphism. *Contrib. Mineral. Petrol. 71*, 23-44.

Hickey, R., and Frey, F., 1981: Geochemical characteristics of boninite series volcanics: implications for their source. *Earth Planet. Sci. Lett.* (submitted).

Hickey, R., Frey, F.A., and Jenner, G., 1980: Trace element and isotopic characteristics of boninites: implications for their source. *EOS 61*, 1140 (abstract).

Hill, R.E.T., and Roedder, P.L., 1974: The crystallization of spinels from basaltic liquids as a function of oxygen pressure. *J. Geol. 82*, 709-729.

Huebner, J.S., 1980: Pyroxene phase equilibria at low pressure. *In* C.T. Drewett (ed.), *Reviews in Mineralogy: Pyroxenes*. 213-288. Mineral. Soc. Amer., Washington, D.C.

Huebner, J.S., and Turnock, A.C., 1980: The melting relations at 1 bar of pyroxenes composed largely of Ca-, Mg-, and Fe-bearing components. *Am. Mineral. 65*, 225-271.

Humphris, S.E., and Thompson, G., 1978: Trace element mobility during hydrothermal alteration of oceanic basalts. *Geochim. Cosmochim. Acta 42*, 127-136.

Hussong, D. *et al.*, 1978: Leg 60 ends in Guam. *Geotimes, October*, 19-22.

Irvine, T.N., 1967: Chromian spinel as a petrogenetic indicator. Part 2. Petrologic applications. *Can. J. Earth Sci. 4*, 71-103.

Jacobsen, S.B., and Wasserburg, G.J., 1979a: The mean age of mantle and crustal reservoirs. *J. Geophys. Res. 84*, 7411-7427.

Jacobsen, S.B., and Wasserburg, G.J., 1979b: Nd and Sr isotopic study of the Bay of Islands ophiolite complex and the evolution of the source of mid-ocean ridge basalts. *J. Geophys. Res. 84*, 7429-7445.

Jaques, A.L., 1980: Petrologic and experimental studies on the petrogenesis of Papua New Guinea ophiolites. Univ. of Tasmania, Hobart. Unpublished Ph.D. dissert. 251pp.

Jaques, A.L., 1981: Petrology and petrogenesis of cumulate peridotites and gabbros from the Marum Ophiolite Complex, northern Papua New Guinea. *J. Petrol. 22*, 1-40.

Jaques, A.L., and Chappell, B.W., 1980: Petrology and trace element geochemistry of the Papuan ultramafic belt. *Contrib. Mineral. Petrol. 75*, 55-70.

Jaques, A.L., and Green, D.H., 1979: Determination of liquid composition in high pressure melting of peridotite. *Am. Mineral. 64*, 1312-1321.

Jaques, A.L., and Green, D.H., 1980: Anhydrous melting of peridotite at 0-15 kb pressure and the genesis of tholeiitic basalts. *Contrib. Mineral. Petrol. 73*, 287-310.

Jakěs, P., and Gill, J., 1970: Rare earth elements and the island arc tholeiitic series. *Earth Planet. Sci. Lett. 9*, 17-28.

Jenner, G.A., 1981: Geochemistry of high-Mg andesites from Cape Vogel, PNG. *Chem. Geol. 33*, 307-332.

Jenner, G.A., and Fryer, B.J., 1980: Geochemistry of the upper Snooks Arm Group basalts, Burlington Peninsula, Newfoundland: evidence against formation in an island arc. *Can. J. Earth Sci. 17*, 888-900.

Jenner, G.A., and Fryer, B.J., 1981: Reply to a discussion of "Geochemistry of the upper Snooks Arm Group basalts, Burlington Peninsula, Newfoundland: evidence against formation in an island arc." *Can. J. Earth Sci.* (in press).

Jenner, G.A., and Green, D.H., 1981: High-Mg andesites: petrology and some constraints on their petrogenesis. *Contrib. Mineral. Petrol.* (submitted).

Jenner, G.A., and Varne, R., in prep. Boninites, high-Mg andesites and ophiolitic basalts: inter-relationships and significance for generation of ocean crust.

Johnson, R.W., Jaques, A.L., Hickey, R.L., McKee, C.O., and Chappell, B.W., 1981: Manam Island, Papua New Guinea: petrologic development of a basaltic island-arc volcano. *IAVCEI Symposium - Arc Volcanism, Abstracts,* 155-156.

Johnson, I.J., 1979: Partial fusion relationships in andesitic compositions. Manchester University, unpublished Ph.D. dissert. 185pp.

Karig, D.E., and Moore, G.F., 1975: Tectonic complexities in the Bonin Arc system. *Tectonophysics 27,* 97-118.

Kay, R.W., and Hubbard, N.J., 1978: Trace elements in ocean ridge basalts. *Earth Planet. Sci. Lett. 38,* 95-116.

Kay, R.W., and Senechal, R.G., 1976: The rare earth geochemistry of the Troodos Ophiolite Complex. *J. Geophys. Res. 81,* 964-970.

Komatsu, M., 1980: Clinoenstatite in volcanic rocks from the Bonin Islands. *Contrib. Mineral. Petrol. 74,* 329-338.

Kuroda, N., and Shiraki, K., 1975: Boninite and related rocks of Chichi-jima, Bonin Islands, Japan. *Sci. Rep. Shizuoka Univ. 10,* 145-155.

Kuroda, N., Shiraki, K., and Urano, H., 1978: Boninite as a possible calc-alkalic primary magma. *Bull. Volcanol. 41,* 563-575.

Kushiro, I., 1972: Effect of water on the composition of magmas formed at high pressures. *J. Petrol. 13,* 311-334.

Kushiro, I., 1972b: Determination of liquidus relations in synthetic silicate systems with electron probe analysis: the system forsterite-diopside-silica at 1 atmosphere. *Am. Mineral. 57,* 1260-1271.

Kushiro, I., 1973: Regularities in the shift of liquidus boundaries in silicate systems and their significance in magma genesis. *Carnegie Inst. Yr Book 72,* 497-502.

Kushiro, I., and Sato, H., 1978: Origin of some calc-alkaline andesites in the Japanese Islands. *Bull. Volcanol. 41,* 576-585.

Langmuir, C.H., Vorka, R.D., Hanson, G.N., and Hart, S.R., 1977: A general mixing equation applied to the petrogenesis of basalts from Iceland and Reykjanes Ridge. *Earth Planet. Sci. Lett. 37,* 380-392.

Longhi, J., and Boudreau, A.E., 1980: The orthoenstatite liquidus field in the system forsterite-diopside-silica at one atmosphere. *Am. Mineral. 65*, 563-573.

Maaloe, S., and Aoki, K., 1977: The major element composition of the upper mantle estimated from the composition of lherzolites. *Contrib. Mineral. Petrol. 63*, 161-173.

Marsh, B.D., 1979: Island-arc volcanism. *Am. Scient. 67*, 161-172.

Marsh, B.D., and Kantha, L.H., 1978: On the heat and mass transfer from an ascending magma. *Earth Planet. Sci. Lett. 39*, 435-443.

Matsuda, J.-I., Zashu, S., and Ozima, M., 1977: Sr isotopic studies of volcanic rocks from island arcs in the western Pacific. *Tectonophysics 37*, 141-151.

McLennan, S.M., and Taylor, S.R., 1981: Role of subducted sediments in island-arc magmatism: constraints from REE patterns. *Earth Planet. Sci. Lett. 54*, 423-430.

McReath, I., 1972: Petrogenesis in island arcs with particular reference to the Tonga and South Sandwich areas and Deception Island. University of Leeds, unpublished Ph.D. dissertation.

Meijer, A., 1980: Primitive arc volcanism and a boninite series: examples from western Pacific island arcs. *In* D.E. Hayes (ed.), *The Evolution of Southeast Asian Seas and Islands*. 269-279. Amer. Geophys. Union, Washington, D.C., Monograph 23.

Meijer, A., Anthony, E., and Reagan, M., 1981: Petrology of volcanic rocks from the forearc sites. *In* Initial Reports of the Deep-Sea Drilling Project, 60, U.S. Government Printing Office, Washington, D.C. (in press).

Meijer, A., and Hanan, B., 1981: Pb isotopic composition of boninite and related rocks from the Mariana and Bonin fore-arc regions. *EOS 62*, 408.

Miyashiro, A., 1974: Volcanic rock series in island arcs and active continental margins. *Am. J. Sci. 274*, 321-355.

Mori, T., and Green, D.H., 1975: Pyroxenes in the system $Mg_2Si_2O_6$-$CaMgSi_2O_6$ at high pressure. *Earth Planet. Sci. Lett. 26*, 277-286.

Morse, S.A., 1980: *Basalts and Phase Diagrams: An Introduction to the Quantitative Use of Phase Diagrams in Igneous Petrology*. Springer-Verlag, New York, 493pp.

Mrozowski, C.L., and Hayes, D.E., 1980: A seismic reflection study of faulting in the Mariana fore arc. *In* D.E. Hughes (ed.), *The Tectonic and Geologic Evolution of Southeast Asian Seas and Islands*. 223-234. Am. Geophys. Union, Washington, D.C., Monograph 23.

Mysen, B.O., and Boettcher, A.L., 1975: Melting of a hydrous mantle: I. Phase relations of natural peridotites at high pressures and temperatures with controlled activities of water, carbon dioxide and hydrogen. *J. Petrol. 16*, 520-548.

Nakamura, Y., 1971: Equilibrium relations in Mg-rich part of the pyroxene quadrilateral. *Mineral. J. 6*, 264-276.

Nesbitt, R.W., and Sun, S.S., 1980: Geochemical features of some Archaean and post-Archaean high-magnesian low-alkali liquids. *Phil. Trans. Roy. Soc. Lond. A297*, 365-381.

Nesbitt, R.W., Sun, S.S., and Purvis, A.C., 1979: Komatiites: geochemistry and genesis. *Can. Mineral. 17*, 165-186.

Nicholls, I.A., 1974: Liquids in equilibrium with peridotitic mineral assemblages at high water pressures. *Contrib. Mineral. Petrol. 45*, 289-316.

Nicholls, I.A., and Ringwood, A.E., 1974: A possible mantle origin for andesitic magmas. *Earth Planet. Sci. Lett. 21*, 221-229.

Nisbit, E.G., and Fowler, C.M.P., 1978: The Mid-Atlantic Ridge at 37° and 45°N: some geophysical and petrological constraints. *Geophys. J. R. Astronom. Soc. 54*, 631-660.

Nisbet, E.G., Bickle, M.J., and Martin, A., 1977: The mafic and ultramafic lavas of the Belingue Greenstone Belt, Rhodesia. *J. Petrol. 18*, 521-566.

Norrish, K., and Chappell, B.W., 1977: X-ray fluorescence spectrometry. *In* J. Zussman (ed.), *Physical Methods in Determinative Mineralogy*. 201-272. Academic Press, London, 2nd ed.

Norrish, K., and Hutton, J.T., 1969: An accurate X-ray spectrographic method for the analysis of a wide range of geologic samples. *Geochim. Cosmochim. Acta 33*, 431-451.

O'Nions, R.K., Hamilton, P.J., and Evensen, N.M., 1977: Variations in $^{143}Nd/^{144}Nd$ and $^{87}Sr/^{86}Sr$ ratios in oceanic basalts. *Earth Planet. Sci. Lett. 34*, 13-22.

O'Nions, R.K., Evensen, N.M., and Hamilton, P.J., 1979: Geochemical modelling of mantle differentiation and crustal growth. *J. Geophys. Res. 84*, 6091-6101.

Pearce, J.A., 1975: Basalt geochemistry used to investigate past tectonic environments on Cyprus. *Tectonophysics 25*, 41-67.

Pearce, J.A., and Norry, M.J., 1979: Petrogenetic implications of Ti, Zr, Y and Nb variations in volcanic rocks. *Contrib. Mineral. Petrol. 69*, 33-47.

Perfit, M.R., Gust, D.R., Bence, A.E., Arculus, R.J., and Taylor, S.R., 1980: Chemical characteristics of island-arc basalts: implications for mantle sources. *Chem. Geol. 30*, 227-256.

Poreda, R., and Craig, H., 1979: Helium and neon in oceanic volcanic rocks. *EOS 60*, 969 (abstract).

Rhodes, J.M., and Dungan, M.A., 1979: The evolution of ocean-floor basaltic magma. *In* M. Talwani, C.G. Harrison and D.E. Hayes (eds), *Deep Drilling Results in the Atlantic Ocean: Ocean Crust.* 262-272. Am. Geophys. Union, Washington, D.C.

Ringwood, A.E., 1966: The chemical composition and origin of the earth. *In* P.M. Hurley (ed.), *Advances in Earth Sciences*. 287-356. M.I.T. Press, Cambridge.

Ringwood, A.E., 1974: The petrological evolution of island arc systems. *J. Geol. Soc. Lond. 130*, 183-204.

Rodgers, K.A., 1973: Chrome-spinels from the Massif du Sud, southern New Caledonia. *Mineral. Mag. 39*, 326-339.

Roedder, P.L., and Emslie, R.F., 1970: Olivine-liquid equilibrium. *Contrib. Mineral. Petrol. 29*, 275-289.

Roedder, P.L., Campbell, I.H., and Jamieson, H.E., 1979: A re-evaluation of the olivine-spinel geothermometer. *Contrib. Mineral. Petrol. 68*, 325-334.

Sato, H., 1977: Nickel content of basaltic magmas: identification of primary magmas and a measure of the degree of olivine fractionation. *Lithos 10*, 113-120.

Sato, H., 1981: Origin of high magnesian andesites and associated volcanic rocks from the Tertiary Setouchi volcanic province, southwest Japan. *IAVCEI Symposium - Arc Volcanism, Abstracts, Tokyo*, 318-319.

Saunders, A.D., Tarney, J., Marsh, N.G., and Wood, D.A., 1980: Ophiolites as ocean crust or marginal basin crust: a geochemical approach. *In* A. Panayiotou (ed.), *Ophiolites: Proceedings International Ophiolite Symposium Cyprus*. 193-204. Min. Agric. Nat. Resour., Nicosia.

Saunders, A.D., Tarney, J., and Weaver, S.D., 1980b: Transverse geochemical variations across the Antarctic Peninsula: implications for the genesis of calc-alkaline magmas. *Earth Planet. Sci. Lett. 46*, 344-360.

Scott, R., and Kroenke, L., 1980: Evolution of back arc spreading and arc volcanism in the Philippine Sea: Interpretation of Leg 59 DSDP results. *In* D.E. Hayes (ed.), *The Tectonic and Geologic Evolution of Southeast Asian Seas and Islands*. 283-291. Am. Geophys. Union, Washington, D.C. Monogr. 23.

Sharaskin, A.Ya., Dibretsov, N.L., and Sobdev, N.V., 1980: Marianites: the clinoenstatite bearing pillow-lavas associated with the ophiolite assemblage of Mariana Trench. *In* A. Panayiotou (ed.), *Ophiolites: Proceedings International Ophiolites Symposium Cyprus*. 473-479. Min. Agric. Nat. Resour., Nicosia.

Shiraki, K., and Kuroda, N., 1977: The boninite revisited. *N.J. Geog. (Tokyo) 86*, 174-190.

Shiraki, K., Kuroda, N., Maruyama, S., and Urano, H., 1978: Evolution of the Tertiary volcanic rocks in the Izu-Mariana Arc. *Bull. Volcanol. 41*, 548-562.

Shiraki, K., Kuroda, N., Urano, H., and Maruyama, S., 1980: Clinoenstatite in boninites from the Bonin Islands, Japan. *Nature 285*, 31-32.

Sigurdsson, H., and Schilling, J.G., 1976: Spinels in mid-Atlantic ridge basalts: chemistry and occurrence. *Earth Planet. Sci. Lett. 29*, 7-20.

Simonian, K.O., and Gass, I.G., 1978: Arakapas fault belt, Cyprus: a fossil transform fault. *Bull. Geol. Soc. Am. 89*, 1220-1230.

Smith, I.E.M., 1976: Volcanic rocks from southeastern Papua. Australian National University, unpublished Ph.D. dissertation.

Smith, I.E.M., and Davies, H.L., 1976: Geology of the southeast Papua mainland. *Aust. Bur. Min. Resour. Bull. 165*.

Smyth, J.R., 1974: Experimental study on the polymorphism of enstatites. *Am. Mineral. 59*, 345-352.

Spera, F.J., 1980: Aspects of magma transport. *In* R.P. Hargraves (ed.), *Physics of Magmatic Processes*. 265-323. Princeton University Press, Princeton, New Jersey.

Stern, C.R., and Wyllie, P.J., 1975: Effects of iron adsorption by noble-metal capsules on phase boundaries in rock-melting experiments at 30 kilobars. *Amer. Mineral. 60*, 681-689.

Sun, S.-S., 1980: Lead isotopic study of young volcanic rocks from mid-ocean ridges, ocean islands and island arcs. *Phil. Trans. R. Soc. Lond. A297*, 409-445.

Sun, S.-S., and Nesbitt, R.W., 1977: Chemical heterogeneity of the Archaean mantle, composition of the Earth and mantle evolution. *Earth Planet. Sci. Lett. 35*, 429-448.

Sun, S.-S., and Nesbitt, R.W., 1978: Geochemical regularities and genetic significance of ophiolitic basalts. *Geology 6*, 689-693.

Sun, S.-S., and Nesbitt, R.W., 1978b: Petrogenesis of Archaean ultrabasic and basic volcanics: evidence from rare earth elements. *Contrib. Mineral. Petrol. 65*, 301-325.

Sun, S.-S., Nesbitt, R.W., and Sharaskin, A., 1979: Geochemical characteristics of mid-ocean ridge basalts. *Earth Planet. Sci. Lett. 44*, 119-138.

Takahashi, E., Kushiro, I., and Tatsumi, Y., 1981: Melting of a peridotite at high pressures and its bearing on island arc magmas. *IAVCEI Symposium - Arc Volcanism, Abstracts*, 365-366.

Takeuchi, Y., 1978: Tropochemical twinning: a mechanism of building complex structures. *Recent Prog. Nat. Sci. Japan 3*, 153-181.

Tatsumi, Y., 1981: Melting experiments on a high-magnesian andesite. *Earth Planet. Sci. Lett. 54*, 357-365.

Tatsumi, Y., and Ishizaka, K., 1981: Existence of andesitic primary magma: an example from southwest Japan. *Earth Planet. Sci. Lett. 53*, 124-130.

Tatsumi, Y., and Ishizaka, K., 1981b: Miocene Setouchi volcanic belt - volcanism of andesitic primary magmas. *IAVCEI Symposium - Arc Volcanism, Abstracts, Tokyo*, 373-374.

Tatsumi, Y., and Kushiro, I., 1981: Origin of high magnesian andesite. *IAVCEI Symposium - Arc Volcanism, Abstracts, Tokyo*, 375-376.

Taylor, S.R., 1977: Island arc models and the composition of the continental crust. *In* M. Talwani and W.L. Pitmann III (eds.), *Island Arcs and Deep Sea Trenches and Back-Arc Basins*. 325-336. Am. Geophys. Union, Washington, D.C.

Taylor, S.R., and Gorton, M.P., 1977: Geochemical application of spark source mass spectrography, III. Element sensitivity, precision and accuracy. *Geochim. Cosmochim. Acta 41*, 1375-1380.

Tilley, C.E., Yoder, H.S., Jr., and Schairer, J.F., 1964: New relations on melting of basalts. *Carnegie Inst. Wash. Yr Book 63*, 92-97.

Tohara, T., 1981: Origin of magnesian andesites from northwestern Shikoku, Japan. *IAVCEI Symposium - Arc Volcanism, Abstracts, Tokyo*, 365-366.

Ujike, O., 1972: Petrology of Tertiary calc-alkaline volcanic rock suite from northeastern Shikoku and Shodo-Shima Island, Japan. *Sci. Rep. Tohoku Univ. Ser. 3, 11*, 159-201.

Varne, R., and Brown, A.V., 1978: The geology and petrology of the Adamsfield ultramafic complex, Tasmania. *Contrib. Mineral. Petrol. 67,* 195-207.

Warner, R.D., 1975: New experimental data for the system CaO-MgO-SiO_2-H_2O and a synthesis of inferred phase relations. *Geochim. Cosmochim. Acta 39,* 1413-1421.

Warner, R.D., and Luth, W.C., 1974: The diopside-orthoenstatite two phase region in the system $CaMgSi_2O_6$-$Mg_2Si_2O_6$. *Am. Mineral. 59,* 98-109.

Wedepohl, K.H., and Muramatsu, Y., 1979: The chemical composition of kimberlites compared with the average composition of three basaltic magma types. *In* F.R. Boyd and H.O.A. Meyer (eds), *Kimberlites, Diatremes and Diamonds: Their Geology, Petrology and Ceochemistry*. 300-312. Am. Geophys. Union, Washington, D.C.

Wells, P.R.A., 1977: Pyroxene thermometery in simple and complex systems *Contrib. Mineral. Petrol. 62,* 129-139.

Whitford, O.J., Nicholls, I.A., and Taylor, S.R., 1979: Spatial variations in the geochemistry of Quaternary lavas across the Sunda arc in Java and Bali. *Contrib. Mineral. Petrol. 70,* 341-356.

Wood, C.P., 1980: Boninite at a continental margin. *Nature 288,* 692-694.

Wood, D.A., 1979: A variably veined suboceanic upper mantle-genetic significance for mid-ocean ridge basalts from geochemical evidence. *Geology 7,* 499-503.

Wright, T.L., and Doherty, P.L., 1970: A linear programming and least squares computer method for solving petrologic mixing problems. *Bull. Geol. Soc. Am. 81,* 1995-2007.

Yang, H.-Y., 1973: Crystallization of iron-free pigeonite in the system anorthite-diopside-enstatite-silica at atmospheric pressure. *Am. J. Sci. 273,* 488-497.

Yang, H.-Y., and Foster, W.R., 1972: Stability of iron-free pigeonite at atmospheric pressure. *Am. Mineral. 57,* 1232-1241.